MOULDED JOINING TECHNOLOGY WITH MODIFIED BONDED-IN RODS: DEVELOPED AND DESIGNED FOR MODULAR ROUNDWOOD TRUSSES

UNIVERSIDAD
DE GRANADA

Dissertation
In partial fulfilment of the requirements for the Degree of
Doctor of Engineering

submitted to the Doctoral Program in Civil Engineering
University of Granada, Spain

submitted by

Tarick Chahade M.Sc., April 2022

Directors:

Dr. Leandro Morillas Romero
Department of Structural Mechanics and Hydraulic Engineering
University of Granada
Plaza Campo del Principe S/N C.P. 18071, Granada, España
lmorillas@ugr.es

Prof. Dr.-Ing. Kay-Uwe Schober
Department of Civil Engineering
Mainz University of Applied Sciences
Holzstraße 36, D-55116 Mainz, Germany
schober@hs-mainz.de

Editor: Universidad de Granada. Tesis Doctorales
Autor: Tarick Chahade
ISBN: 978-84-1117-478-7
URI: https://hdl.handle.net/10481/76831

Tarick Chahade M.Sc.

PhD candidate at the University of Granada, Spain
Doctoral Program in Civil Engineering
Plaza Campo del Principe S/N C.P. 18071, Granada, España
chahade@para-metric.de

Researcher/Engineer at the Institute of Innovative Structures Mainz, Germany
Staff member at the Timber and Plastics Research Group
Department of Civil Engineering
Mainz University of Applied Sciences
Holzstraße 36, D-55116 Mainz, Germany
tarick.chahade@hs-mainz.de

https://www.researchgate.net/profile/Tarick-Chahade-2

ABSTRACT

Timber structures and buildings made from sustainable forestry might be the solution to today's ecological challenges when their renewable materials are locally processed with low energy consumption in production. The current market shows a dominance of rectangular cross-sections in engineered timber solutions. Roundwood – a traditional material in the past – is no longer common due to a lack of applications in modern structures, lost knowledge in handcraft skills and the high costs of digital manufacturing. However, solid timber with a circular cross-section outperforms other engineered wood products, such as glued laminated products, in terms of energy consumption and environmental aspects. To overcome restrictions in joint technologies and to increase the usability of roundwood in modern constructions, this doctoral thesis focuses on the development of a new joining technology for modular two dimensional trusses, adapted to the preferences of structural roundwood.

Part one of this thesis deals with the connection configuration in roundwood with experimental investigations on the pull-out strength of grouted threaded rods, bonded parallel to grain into timber. The adhesive bond between threaded rod and roundwood was achieved by polymer concrete and a much thicker bondline, compared to standardised glued-in rods. This new-type technique for joining timber members with threaded steel rods was investigated for Douglas fir roundwood specimens to assess (i) the characteristic and design connection capacity under different climate and service conditions, (ii) the influence of moisture induced damage and wood defect on the connection capacity and (iii) the slip modulus.

Part two of this thesis describes the development of digital fabricated moulded joints to connect roundwood members with grouted threaded rods in the nodes of modular two dimensional trusses. The investigations were split into four main focus areas and started with the assessment of the design principle and function of the moulded joints. The aim was to reach an efficient load transfer for tension and compression, and an easy (de-)assembly with no grouting process. After the form finding, a generative algorithm was developed with parametric engineering software to address and analyse massive amounts of data or truss variations and to automate the design for the digital joint fabrication. The structural analysis of the moulded joints was done with finite element software and served for the investigation of different applied composite materials (steel casting, polymer concrete, epoxy resin and cement based concrete). In the final step, a composite material composed of wood fibres and epoxy resin was developed, fabricated and tested to determine strength and stiffness parameter. After material testing, the composite material was adapted to a moulded joint prototype to investigate the manufacturability for complex 3D solid shapes.

ACKNOWLEDGEMENTS

Throughout the writing of this dissertation at the *Institute of Innovative Structure Mainz* in Germany (research institution of the Department of Civil Engineering at the Mainz University of Applied Sciences) I have received a great deal of support and assistance. I would like to take this opportunity to thank everyone at the Institute, who helped me with advice and support.

First and foremost I want to thank my mentor and supervisor Prof. Dr. Kay-Uwe Schober. It has been an honor to be his PhD student and to work as a staff member for him for almost 5 years. I appreciate all his contributions of time, ideas and funding to make my PhD experience productive. I am thankful that he gave me the opportunity to go the next step in my scientific career and that he always watched my back in case of turbulence, even during though times in the PhD pursuit. He is a person who looks out for his people and I cannot thank him enough for this.

I would like to thank my supervisor Dr. Leandro Morillas Romero for the opportunity to realise my PhD at the University of Granada in Spain and for all his time, patience and professional exchange, which helped to improve the quality of my work. Special thanks to all the other researchers, doctors and professors I got to know at the University of Granada, who have always given us a warm welcome and have taught us the Spanish way of life: *La siesta Española se ríe del sueño Americano*.

Parts of the presented doctoral thesis were funded by the German Federal Ministry for Economic Affairs and Energy according to a decision of the German Federal Parliament (Grant Agreement No. ZF4119606). This thesis would not have been possible without the financial support of the German Federal Ministry and the contributions of the two research partners *Modell- und Formenbau GmbH Sachsen-Anhalt* and *Sachverständigen-Ingenieurbüro Oppel*. Special thanks go to Jens Garlin and Michaela Götze.

In addition, I would like to thank my parents and family for their wise counsel and sympathetic ear. You are always there for me.

Mainz, 04.04.2022 Tarick Chahade

CONTENTS

SYMBOL DIRECTORY

ABBREVIATIONS

AOI	Area of interest for Digital Image Correlation measuring
BIM	Building Information Modelling
C	Cement based concrete
CAD	Computer Aided Design
CAM	Computer Aided Manufacturing
CNC	Computerised Numerical Control
DIC	Digital Image Correlation
EP	Epoxy resin
FE	Finite element
FEM	Finite element modelling
HPC	High performance concrete
i-SD^{BIM}	Interactive Structural Design algorithm for BIM applications
LVDT	Linear Variable Differential Transformer
MC	Moisture content
MoE	Modulus of Elasticity
NFC	Natural fibre composite
NFRP	Natural fibre-reinforced plastics
PC	Epoxy resin-bonded concrete, also known as polymer concrete
PU	Polyurethane
rH	Relative humidity
SC	Service class
SLS	Serviceability limit state
STD	Span to depth ratio of truss structure
STW	Strength to weight ratio of truss structure
UHPC	Ultra-high performance concrete
ULS	Ultimate limit state
Vic-3D®	Evaluation software of digital image correlation system
WFC	Wood-fibre composite

INDEXES

1. Index	Orientation of the reference surface (direction of the surface normal)
2. Index	Direction of stress/strain
r, t, l	Natural axes of wood: radial, tangential, longitudinal
R, φ, z	Cylindrical coordinate axes
x, y, z	Cartesian coordinate axes
1, 2, 3	Axes of spatial principle stresses
t, c, v, f	Tension, compression, shear, flexural
0, 90	In grain direction, perpendicular to grain direction
k, d	Characteristic value, design value
0.05	5%-fractile value
max	Maximum value
mean	Mean value
min	Minimum value
chord	Upper or lower chord members in truss structure
dh	Drill hole in roundwood for modified bonded-in rods
nut	Nut
purl	Purlin
r	Threaded steel rod
spa	Spanner
strut	Diagonal strut members in truss structure
was	Washer
w, s, pc	Roundwood (wood), steel, polymer concrete
E	Edge joint
F	Field joint
S	Support joint
Frame	Cast-steel frame structure
Mould	Moulded joint
HEA	Structural steel H section
UPE	Hot rolled steel channel

SYMBOLS

a_f	Distance between trusses in roof structure	m
c	Cast-steel frame structure dimension	mm
d	Diameter	mm
e	Inner dimension of cast-steel frame structure for washer support	mm
$f_{k,1}$	Characteristic adhesive joint strength of bonded-in rods	MPa
$f_{ct,PC,mean}$	Mean tensile strength of polymer concrete	MPa
f	Strength	MPa
	Max. deflection in loading direction for 3-point flexural tests	mm
g	Net weight	kN
		kN/m
h	Cross-section height	mm
h_{pitch}	Steel rod thread pitch	mm
i	Radius of gyration	mm
k	Approximate axis length of moulded joint	mm
k^*	Axis length of cast-steel frame structure	mm
k^{**}	Axis length of moulded joint for the field, edge and support joint	mm
k^{***}	Second axis length of moulded joint for the support joint	mm
k_c	Instability factor	-
$k_{d,k}$	Fractile factor for characteristic values	-
$k_{d,n}$	Fractile factor for design values	-
k_{def}	Deformation factor	-
k_{mod}	Modification factor for duration of load and moisture content	-
ℓ	Length	mm
ℓ_{ad}	Adhesive bonding length of bonded-in rods	mm
m_x	Average failure load or strength	kN
		MPa
n	Number of samples/test specimens	-
n_{joint}	Number of joints in truss structure	-
n_{uc}	Number of upper chord roundwood members in truss structure	-
n_w	Number of roundwood members in truss structure	-
o	Geometrical parameter to control the outer curvature of the edge joint between the chord and diagonal strut	mm
p	Designation of the used parameter in the design algorithm	-

q_{ULS}	Permissible line load on truss structure in ultimate limit state	kN/m
r	Radius	mm
s_x	Standard deviation	-
s_x^2	Variance	-
s_w	Wood strength class	-
t	Thickness	mm
t_d	Truss depth	m
$t_{d,static}$	Static truss depth	m
t_s	Truss span	m
u	Deformation in longitudinal or z- direction	mm
	Max. deformation in loading direction for compressive tests	mm
v	Drill hole diameter in moulded joint	mm
w	Cross-section width	mm
w_{m-p}	Width of moulded joint for purlin support	mm
w_{inst}	Instantaneous deflection excluding creep effect	mm
w_{fin}	Final deflection including creep effect	mm
x_i	Failure load of sample i	kN
	Strength of sample i	MPa
$\overline{x}$	Mean value (average)	-
A	Cross-section area	mm^2
E	Modulus of elasticity	MPa
F	Loading	kN
$F_{ax,Rk}$	Characteristic pull-out joint capacity of bonded-in rods	kN
$F_{cr,mean}^{PC}$	Mean value of load level for initial cracking in polymer concrete for modified bonded-in rods	kN
F_H	Resultant horizontal or radial forces in polymer concrete for modified bonded-in rods	kN
F_L	Applied load in longitudinal direction or in grain direction	kN
G	Shear module	MPa
H	Eaves height of truss roof structure	m
K_1	Stiffness of roundwood	kN/mm
K_3	Stiffness of threaded rod	kN/mm
K_{equiv}	Equivalent stiffness of strut member	kN/mm
K_{ser}	Slip modulus	kN/mm
L_w	Roundwood strut length	m
L_s	Threaded rod overhang length	m
L_{system}	Strut system length of strut members in truss structure	m

L_{cr}	Critical buckling length of strut members (stability design)	m
M	Bending moment	kNm
M_0	Ovendried mass	g
M_{24h}	Mass after 24h immersion time	g
$M_{absorp.}$	Water absorption	%
T	Temperature	°
V_x	Coefficient of variation	-
X_d	Design value (Load capacity) Design value (Strength)	kN MPa
X_k	Characteristic value (Load capacity) Characteristic value (Strength)	kN MPa
α	Chord-diagonal strut angle in truss structure	°
σ	stress	MPa
σ_1	Axis 1 of spatial principle stresses (tension)	MPa
σ_3	Axis 3 of spatial principle stresses (compression)	MPa
γ_M	Partial factor	-
ε	Strain	-
η	Factor of model uncertainties	-
θ	Angle of diagonal strut within polymer concrete for modified bonded-in rods	°
ρ	Density	g/cm^3
φ	Transformation angle from Cartesian to Cylindrical coordinate system	°
Δk	Manual adjustment of cast-steel frame structure and moulded joint axis length	mm
Δu_1	Relative deformation of roundwood in longitudinal direction	mm
Δu_2	Relative deformation of steel rod in longitudinal direction	mm
Δu_3	Corresponding relative deformation of the slip modulus	mm

1 INTRODUCTION

1.1 MOTIVATION

Environmental and energy aspects become more important with a strong influence on building materials and technologies. In this context, architects and engineers face important questions on how to build (with) our environment and how to meet the increased demand on renewable materials to improve the ecological footprint of the building sector. Today's forestry is the only available technology to extract carbon dioxide from the atmosphere. It is estimated that harvesting 1 kg of wood absorbs 1.47 kg of carbon dioxide and produces 1.07 kg of oxygen. In Germany, the 11 million hectare local forests sink 1.3 billion tons of greenhouse gas emissions (15% of total emissions).

Timber structures and buildings, made from sustainable forestry, might be the solution to today's ecological challenges when their renewable materials are locally processed with low energy consumption in production and transformation and low toxicity. Advantages of timber structure are their low specific weight, high compressive and tensile strengths in timber grain direction, reduced construction time, remarkable durability and the ability to recycle, reuse and compost structural components after deconstruction. Solid timber with round cross-sections (structural roundwood) outperforms other engineered wood products, such as glued laminated timber in terms of energy consumption and environmental aspects. The production of structural roundwood is simple and effective (Fig. 1-1) with an aesthetic appearance and texture of the circular cross-section.

Fig. 1-1 Logs (left) and structural roundwood (right)

The current market of timber products shows a clearly identifiable dominance of rectangular cross-sections in modern buildings. Structural roundwood, as traditional material in the past, is not common anymore due to missing applications in modern structures, lost knowledge in handcraft skills and high costs of CNC-based manufacturing. Existing standards are mostly designed for rectangular cross-sections, such as recommended minimum edge distances for mechanical fasteners. Architects and engineers will continue to ignore cylindrical cross-sections in structural design and will always refer back to standards with sawn timber (rectangular cross-section), unless there are no new ambitions to update the portfolio of roundwood joining technologies including new design methods. To overcome restrictions of existing connection methods and to increase the usability of structural roundwood in the timber building sectors, new joints for modular 2D truss structures have been developed: a digital fabricated moulded joining technology with modified bonded-in rods, which optimises the connection configuration in roundwood with an increased load bearing capacity and only uniaxial loading.

1.2 RESEARCH OBJECTIVES

This thesis focused on the development of a moulded joining technology for 2D trusses, adapted to the preferences of structural roundwood, to overcome restrictions of existing connection methods and, therefore, to increase the usability of roundwood in modern structural design. The following two objectives were pursued to achieve this aim:

Objective 1 – The development of roundwood joints with modified bonded-in rods, consisting of a single metal connector adhesively bonded into roundwood members in fibre direction, with a simple fabrication and full cross-section (Fig. 1-2, left). Glued-in threaded rods in the axial direction of strut members represent the basis of the connection technology and were developed further to increase the load bearing capacity and usability. Due to inconsistencies in design codes and geometrical restrictions of the bondline thickness of 'classic' glued-in rods, the load capacity to be achieved is far below the utilisation capacity of the roundwoods and the steel rods. The doctoral thesis strived for a more economical and efficient connection configuration in which the load bearing capacities do not deviate highly one from the other. The research approach was based on a substitution of the compound material of glued-in threaded rods by resin-bonded concrete, also known as polymer concrete. The concept relies on increasing the drill hole diameter and therefore contact surface between wood and polymer concrete for the load distribution. Moreover, glued-in connections perform with a low fabrication process reliability and are only allowed for inside constructions.

Objective 2 - The development of moulded joints to connect roundwood strut members in the nodes of 2D trusses with an easy assembly and the ability to transfer tensile and compressive loads (Fig. 1-2, right). The joining technology was developed according to (i) an assembly (and de-assembly) with no time-consuming grouting process, (ii) the possibility to substitute individuals components, (iii) a high degree of prefabrication and preassembly, (iv) an adaptation of the joint principle to different truss designs, (v) an efficient load transfer concept for tensile and compressive loads and (vi) a form-fitted architectural design.

1.3 RESEARCH QUESTIONS

The development of the joining technology had two main research topics: the connection design in roundwood with grouted rods (modified bonded-in rods) and the connection design in the intersection with moulded joints. The first research topic focused on experimental investigations on modified bonded-in rods to answer the following research questions:

- How does the connection structurally behave under different service conditions?
- How do the crack propagation and moisture induced damage in wood affect the connection capacity?
- What are the characteristic and design values of the single fastener capacity?
- What is the slip modulus?

The second research topic focused on parametric, numerical and experimental investigations on the moulded joint to answer the following research questions:

- How to define the material and structural composition of the joint to ensure an efficient load transfer for compression and tension, and an easy (de-)assembly with no grouting process?
- How to address massive amounts of data or truss variations?
- How to support the digital design and fabrication process of the joints?
- How do different moulding materials affect the load transfer?
- How to develop and apply a composite material based on wood fibers?

Fig. 1-2 Modified bonded-in rods (left) and model of moulded joining technology (right)

1.4 METHODOLOGY

Chapter 2 deals with an overview to existing connection methods for structural roundwood and summarises the literature research, background and theoretical framework for both main areas of work to illustrate the basis of the developed joining technology. This includes the connection design in roundwood (glued-in and modified bonded-in rods) and in the intersection (moulded joints composed of polymer concrete).

Chapter 3 defines the main objective of this work including development specifications of the joining technology to underline the innovative aspects of this thesis. To meet the defined main objective, the thesis needed to focus on an optimisation of the connection configuration in roundwood and in the intersection. The specific objectives for both areas of work are stated.

Chapter 4 covers experimental investigations on uniaxial tension tests with modified bonded-in (grouted) threaded rods in roundwood. All specimens were timber members with a diameter of 200 mm. One specific diameter and connection geometry was chosen for the experimental investigation to compare the test results with each other and to detect the climate exposure influence on the connection capacity. Digital Image Correlation systems were used for part of the samples to detect the structural behaviour of the connection. The failure behaviour and loads of the joints during testing were determined with an investigation of the influence of natural pre-cracks in wood. After completing, the test results of 27 samples were processed further in a statistic evaluation to calculate the characteristic and design load-carrying capacity, and other mechanical parameter, such as the slip modulus. In order to rate the structural performance of the developed connection, the test results were compared to design values of 'classic' glued-in rods and test results of other researchers on modified bonded-in threaded rods in squared timber.

Chapter 5 describes the development of the moulded joining technology in the intersection. The design concept envisaged a hybrid connection composed of an inner steel structure and an enveloping moulded joint with a coupled load distribution. To load each structural member according to its high material strengths, it was aimed that the moulded material or steel serve for the compressive or tensile load distribution.

The first part covered the assessment of the moulded joint design principle and function (form finding) with respect to an efficient load transfer concept for compression and tension, and an easy assembly and de-assembly of the 2D truss structure. The second part focused on the parametric development of the joints and investigated the application to the practical example of a roof truss structure. In order to analyse and design a high amount of different variations of 2D trusses, a design algorithm was developed. The algorithm created an interactive structural design workflow (i-SD^{BIM}) for local and global design processes in architecture and engineering. The third part focused on numerical investigations of the joints to

detect the impact of the moulded material Modulus of Elasticity on the structural behaviour. Based on the finite element modelling results, a suitable composite material, composed of wood fibres and epoxy resin, was fabricated and tested in compression and bending tests. Chapter 5 concludes with the production-related design of a moulded joint prototype. In chapter 6, this doctoral thesis ends with a summary and an outlook for further study.

2 THEORETICAL BACKGROUND

2.1 ROUNDWOOD AS STRUCTURAL MATERIAL

The central idea of this thesis is to build with wood in its naturaly grown round shape as old and new building material. The production of the building material roundwood is easy and efficient and the curved surface performs with an unique aesthetic appearance compared to existing wooden building materials with rectangular cross-sections, which clearly dominate the market today.

In December 1993, a Buddhist temple in the town of Ikaruga in Japan (Hōryū-ji) was declared a UNESCO World Heritage Site and placed under monument protection [WAD 2020]. In the justification of the UNESCO Committee, it is written that the oldest surviving wooden buildings in the world are located on this site, built in the year 607. The example is intended to underline the durability of wood, provided that the building material is correctly installed according to its unique material properties. Wood played a major role in constructions for thousands of years and nowadays more than 15 million m^3 of wood are processed for the German building sector each year. This quantity can be divided into three groups sawn (squared) timber, roundwood and wood-based materials.

RANTA-MAUNUS [RAN 1999] investigated the application of structural roundwood in the building sector with experimental studies on roundwood and sawn timber (squared timber) in order to compare both cross-section types with each other. 1400 specimens, composed of different softwood species, such as Scots Pine *(Pinus Sylvestris L.)* and Norway Spruce *(Picea Abies L. Karst.)*, were tested in this study to determine bending, compression and tension strength properties. The research results confirmed higher strength values for roundwood compared to sawn timber made from the same logs. The bending strengths for roundwood were observed with even double the value of sawn timber. The work of RANTA-MAUNUS [RAN 1999] confirmed the potential of roundwood in the building sector.

Especially the anatomy of roundwood shows a 'more homogenous' cross-section with the heartwood in the centre of the logs and increased load-carrying capacity compared to sawn timber with rectangular cross-sections and irregular distribution of heartwood and sapwood depending on the sawing pattern.

The product standard EN 338, strength and stiffness parameter for structural timber, can be adapted to roundwood, but there is a lack of information on the issue (specific strength parameters). In direct comparison, the former German design code [DIN 1052] recommended a 20% increase of the tensile and bending strength for naturaly grown roundwood without bark and bast. Despite the benefits in structural performance, design rules for structural roundwood elements are missing and standards focus on sawn timber with rectangular cross-sections, such as EN 14081-1 for strength grading. The former German design code for visual strength grading [DIN 4074-1] refers only to rectangular cross-sections as well.

In order to use the logs quickly, drying chambers are used with the disadvantages of high energy consumption and uncontrollable cracks along the wooden surface. If the logs are air-dried without any technical drying process (naturaly dried logs) and then cylindrically milled to roundwood, the energy balance can be reduced up to 80% (Fig. 2-1). Costs can be reduced up to 50% by using naturaly grown roundwood with only removed barks and no cylindrical milling [RAN 1999]. The varying diameter along the roundwood performs with an interesting architectural appearance and high strengths [DIN 1052], but complicates the use in wood building constructions.

Roundwood was profusely used in the past, but today it represents a small portion of the timber building sector. Depending on the region, roundwood is differently used in traditional building designs. Probably the best-known example of roundwood being used in Europe is the log house in which roundwood is installed as columns, beams and surface elements. Other examples of applications can be found in bridge constructions as supporting structures or in buildings as decorative elements. In rural areas with a lot of forest, the logs are modified by hand with barely any machining and are immediately installed. Fig. 2-2 (traditional roundwood trusses in rural areas) underlines the complexity of roundwood connections, which require a high effort of manufacture, but also a significant amount of time and workload. In Europe, these skills have gradually been unlearned and are replaced by machine supported manufacturing processes today. Roundwood is rarely used in modern structural design, due to the fact that these fabrication processes have developed rather late and moreover, that not every business have these skills and competences.

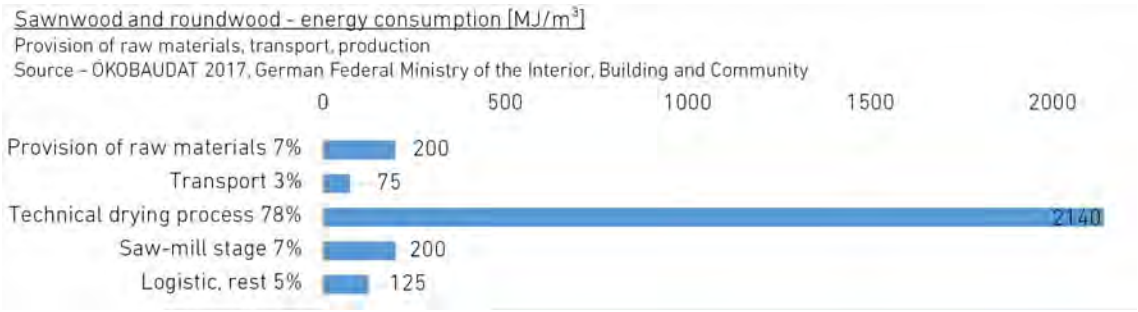

Fig. 2-1 Energy consumption for provision of raw material, transport and production

Fig. 2-2 Traditional roundwood trusses in rural areas

From today's perspective, artisanal fabrication methods of roundwood joints are replaced by machine support, which enables cost-effective mass productions. Despite new added production processes, there is still a subordinate focus on roundwood in the building sector due to a much higher value added for companies in case of extracting glued-laminated products with rectangular cross-section from the raw material. Both aspects, the geometrical restrictions and low value added, prevent the increased use of roundwood in truss systems. Due to missing ambitions in research and practice, existing standards for timber structures are mostly designed for rectangular cross-sections. The circular shape requires new efficient connection systems and design methods adapted to the preferences of architects, engineers and carpenters.

2.2 NON-GLUED CONNECTIONS IN ROUNDWOOD TRUSSES

Trusses are composed by chords and attached strut and tie members with a hinged connection. The member axis of an ideal truss is straight and only transverse loads acting on the end joints. Ideal trusses are very effective to carry high loads resulting in regularly distributed normal stresses in the entire structure matching the favourable material strengths of wood in fibre direction (Tab. 2-1).

The ideal truss is a hypothetical entity. In practice, continuous upper and lower chords are connected to diagonal struts and ties and, if necessary, vertical posts. These connections are usually not hinged and perform with a certain rotation stiffness depending on the chosen connection type. The load introduction is usually along the upper chord which leads to bending stresses in wood. In addition, the rigid connections or continuous chords transmit bending stresses to attached truss members.

Carpentry joints represent the oldest type of wood connections and serve only under compression. For tensile loading, the members need to be secured under shear loading with dowels. Those types of connections are not suitable for high tensile loads and require a complex carpentry work on the circular cross-section.

Tab. 2-1 Characteristic material strengths of softwood according to EN 338

Strength class		C22	C24	C27
Tensile strength in grain direction	[MPa]	13	14.5	16.5
Tensile strength perp. to grain direction		0.4	0.4	0.4
Compressive strength in grain direction		20	21	22
Compressive strength perp. to grain direction		2.4	2.5	2.5
Bending strength		22	24	27

Other ways to connect roundwood members are internal or external mechanical fasteners. The load transmission in those joints is achieved, e.g., by dowel-type wood or metal connectors and steel plates (Fig. 2-3). The load transmission from wood to metal plate is realised by a number of dowel-type connectors along the axis of the struts. The connection is able to distribute tensile loads, but they do have the disadvantages of a reduced cross-section, high embedding stresses around fasteners and a lack of design rules for the dowel distribution along the strut: Design rules for mechanical fasteners do not address roundwood in particular, e.g., in the definition of edge distances and only permit one dowel perpendicular to the roundwood grain direction resulting in uneconomic and large size connections. Those joint types are not suitable for roundwood design:

– because the circular section has to be modified in a complex and expensive fabrication process, practical only for computer-aided manufacturing,
– there are only limited design rules available,
– secondary bending stresses have to be considered and
– a weaker net section has to be taken into account including embedding stresses for dowel connections.

For the development of wooden strut structures in general, the structural design of the connection is usually decisive for the dimensioning of the strut members. The configuration of the connection between the diagonal struts and chords is especially critical to design due to an impact on the load situation in wood. Embedding stresses in the dowel-wood region and loading perpendicular to the grain direction must be avoided (Tab. 2-1). More suitable solutions should perform like in tree knots - with full cross-section and fibre parallel loading in wood. Different projects highlight the architectural and structural efficiency of structural roundwood in 2D trusses, for instance the pre-fabricated truss installation by WholeTrees® for the Festival Foods Grocery Store in Madison, WI (Fig. 2-3, right), where the truss members are loaded in axial tension and compression.

BLASS provided an overview of conventional joining methods for the realisation of 2D truss systems with rectangular cross-sections [BLA 2012]. The research contrasted the use of carpentry and metal plate joints including design approaches and final experimental investigations to determine the load bearing capacity on full-scale trusses. LOKAJ AND KLAYMONOVA investigated different types of

mechanical joints to underline selected problems in using roundwood in building structures [LOK 2014a-b, 2016]. The research studies focused on mechanical reinforcement possibilities of roundwood bolted joints with slotted steel plates. The specimens were tested under tension in grain direction. To increase the load bearing capacity, different reinforcements were applied to the specimens: steel band, screws and surrounding plates. The reinforced samples performed with an increased load bearing capacity of approximate 20%. Subsequent research studies investigated static and multicycle dynamic loadings with additional tests on sawn timber with rectangular cross-section to compare both building materials. The test results suggested values of resistance for circular cross-sections, which were similar to European design rules.

GORMAN AND KRETSCHMANN investigated three types of roundwood connections with structural screws, gussets and metal plates [GOR 2012]. The results showed that all connections exceeded the anticipated design load with significant differences between the ductility and deflection capacity of the joint types.

BRITO AND JUNIOR provided an overview of roundwood joint types used in Brazil [BRI 2012]. The research contrasted different types of connection configuration for the realisation of strut and surface structures in roundwood to promote a more efficient use in modern structural designs. First experimental investigation on a two piece connector, which requires only two drill holes in wood, were performed by ECKELMAN AND SENFT [ECK 1995]. A metal pin with a female threaded hole in the centre (dowel nut) was placed through a drill hole transversal to the strut axis, in the first step. Subsequently, a threaded rod was placed through a drill hole in longitudinal direction, which fits with the diameter of the threaded hole in the metal pin. Yellow poplar *(liriodendron tulipifera)* with an approximate diameter of 200 mm was investigated in this research with the result of strongly varying failure loads. The results were strongly affected by the natural pre-crack pattern in the wood, what prevented a practical application of the connection in practice. All presented connection types showed a splitting failure mechanism in which either tensile strengths perpendicular to the timber grain direction or embedding strengths of wood in the bolt region were exceeded. The challenge for wood connections is to avoid both unfavourable effects.

Fig. 2-3 Dowel-type connectors with steel plates for structural roundwood
[*with permission of the owners/authors of the pictures*]

2.3 GLUED-IN RODS

Glued-in threaded rods as single connector for timber members in grain direction have been investigated extensive over the past years and can be adapted to roundwood with the advantage of a simple fabrication process, no modification of the circular cross-section and no weakening by fasteners. The binder between steel rod and wood, provides a rigid connection with no embedding stresses in the rod-wood region taken into account. Glued-in rods became famous in timber engineering due to the high stiffness and fire-resistance and the good aesthetic appearance. Besides the advantages, the applied adhesives in the joints tend to limited gap-filling qualities, strength-reducing effects during the initial hardening time and sensitivity to increasing temperature and moisture content change [TLU 2011].

In case of a uniaxial tensile load application, the load is transmitted first by tension through the steel rod, then transferred from steel to wood by the adhesive. Fig. 2-4 shows the general load distribution and failure types tensile failure in steel, pull-out joint failure along the rod and tensile failure in timber. One further potential failure type is not shown, which may occur when the installation of the rod in wood is inaccurate with cavities and eccentricities.

The pull-out joint capacity (Fig. 2-4) of single glued-in threaded rods in fibre direction is defined in the German Annex of EN 1995-1-1/NA by the adhesive joint strength $f_{k,1}$, the nominal diameter of the steel rod and the embedment length. The load transmission is assumed as constant along the rod with an adhesive joint strength of 4 MPa [EN 1995-1-1/NA/Table 12] for bonding lengths smaller than 250 mm, matching the timber shear strength according to EN 338 for strength classes larger than or equal to C24. For larger bonding lengths, the adhesive joint strength is reduced to take an increased inhomogeneous load distribution into account. The characteristic pull-out joint failure along the rod can be calculated with Eq. 2.1 according to EN 1995-1-1/NA, Eq. 155.

The envelope surface in Fig. 2-5 shows the design pull-out joint capacity for single glued-in rods as a function of the adhesive bonding length and nominal rod diameter with a reduced adhesive joint strength for bonding lengths larger than 250 mm. The design connection capacity of the steel rod for tension is illustrated as polyline and is calculated according to EN 1995-1-1/NA and European design rules for mechanical fasteners [EN 1993-1-8]. The steel rod property class is set to 4.6 to determine the lower bond limit of the load bearing capacity in steel. Timber takes a modification factor of 0.8 [EN 1995-1-1] into account for the design values. Tension failure in wood (Fig. 2-4) is almost independent from the connection design and exceeds the pull-out joint capacity. For instance, roundwood members, investigated in this study, have a diameter of 200 mm, are assigned to strength class C24 (tensile strength 14.5 MPa) and can be utilised up to 290 kN (design value) for axial tensile loading.

$$F_{ax,Rk} = f_{k,1} \cdot \pi \cdot d_r \cdot \ell_{ad}$$

with

$F_{ax,Rk}$	*Characteristic pull-out joint capacity along the rod*
$f_{k,1}$	*Characteristic adhesive joint strength*
d_r	*Nominal diameter of the steel bar*
ℓ_{ad}	*Adhesive bonding length*

(Eq. 2.1)

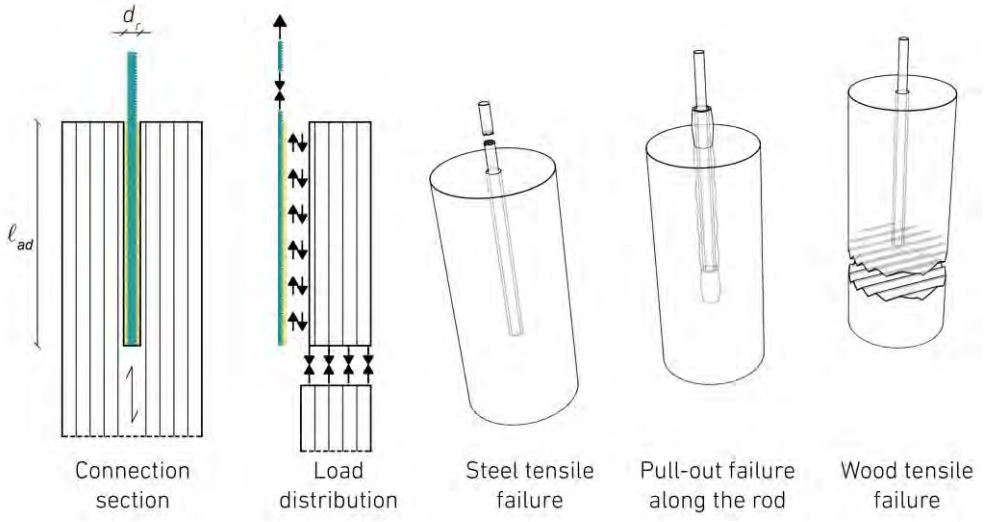

Fig. 2-4 Section, load distribution and failure types of glued-in rods in wood

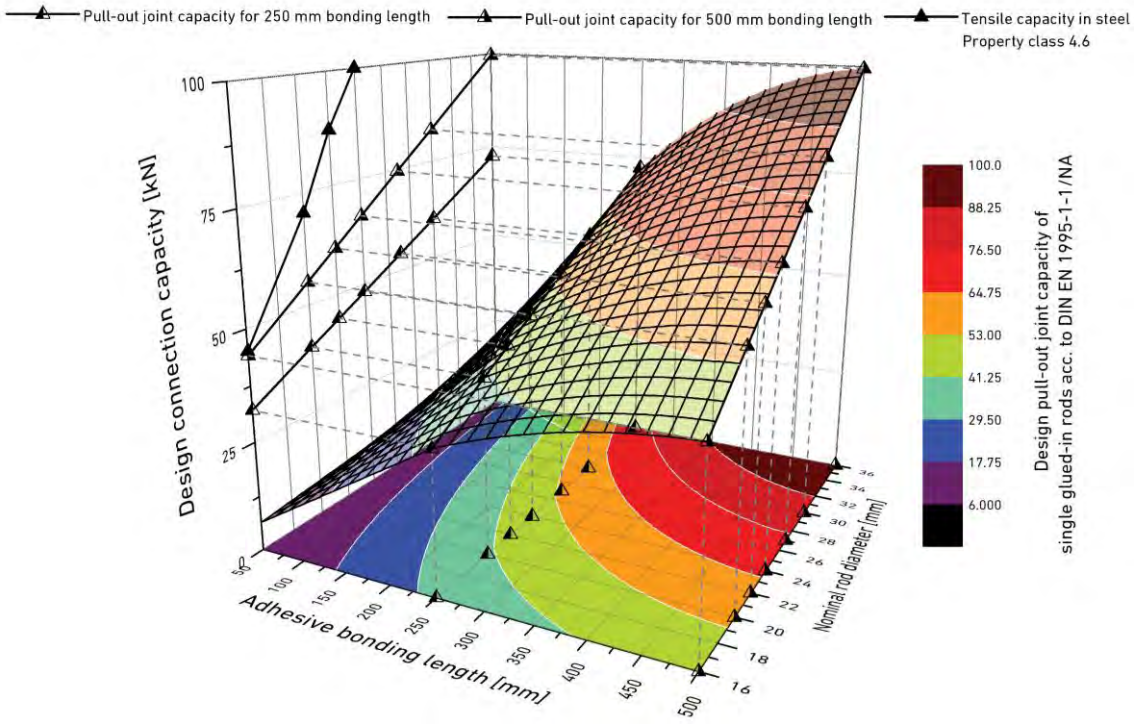

Fig. 2-5 Design pull-out joint capacity of single glued-in rods acc. to EN 1995-1-1/NA

The evaluation of the design connection capacity of glued-in threaded rods shows that pull-out along the rod yields the lower failure load, even if we reduce the steel property class to 4.6. The connection is not able to take full advantage of the steel tensile strength with a maximum design shear failure load in timber of approximate 100 kN for a bonding length of 500 mm and a rod diameter of 36 mm. Next to structural performance aspects, the connection is not allowed to be used in outdoor exposure and due to the thin adhesive joint, there is no possibility of an easy quality control of the bonding process.

Research on glued-in threaded rods in timber has a long history and started in the 1980s. MOEHLER AND LAUTENSCHLAEGER were the first researchers in Germany who investigated the structural behaviour of glued-in rods in glulam or in timber engineering in general [MOE 1978, 1981]. The first design proposal was developed and published by RIBERHOLT [RIB 1988]. The publication of STEIGER AND SERRANO [STE 2015] summarises the most important research done in regard to connections and reinforcement with glued-in threaded rods. Different types of adhesives were tested in research studies, such as phenol-resorcinol, epoxies or polyurethanes. A general statement about the best suited adhesive for glued-in rods cannot be made, because many different adhesives of each type exist today with strongly varying material properties [AIC 2003]. Next to the adhesive, the used timber species and specification (e.g. softwood, hardwood, and glulam) have also an impact on the structural behaviour of the connection [HAR 2000].

SERRANO presented a test method to determine the strength and the fracture characteristics of the bond of glued-in rods in wood [SER 2001]. LIPPERT designed in the framework of his doctoral thesis rigid wooden frame corner with glued-in rods [LIP 2002], while LETTOW developed a finite element method to model glued-in rods in wood [LET 2006]. Interesting research studies represent the work of TLUSTOCHIWICZ AND SERRANO [TLU 2011] where the test set-up was varied to investigate the possible failure types for wood connections with glued-in rods. LING AND LIU [LIN 2015] adapted the joining technology to glued-laminated timber, while HUNGER AND STEPINAC [HUN 2016] investigated the application to different wood species. MORGADO AND DIAS [MOR 2013] performed first approaches on glued-in threaded rods in roundwood with multiple adhesively bonded rods in timber grain direction. For almost all specimens the failure occurred in steel. THELIN AND FELDT [THE 2018] developed a numerical model for glued-in rods in roundwood with the focus on the simulation of the pull-out joint failure along the rod. The behaviour of glued-in rods in cross-laminated timber was firstly investigated by AZINOVIC AND SERRANO [AZI 2018].

Previous research studies of other researchers focused on the application of adhesively bonded rods for different wooden type materials, such as solid timber or glulam. Compared to the research study, presented in this thesis, conventional adhesives were used. The fabricated drill hole diameter in timber was roughly equivalent to the diameter of the steel rod, which limited the load-carrying capacity to be achieved in the contact surface between steel and timber.

2.4 MODIFIED BONDED-IN RODS (GROUTED RODS)

The necessity of the bondline thickness enlargement and adhesive substitution results from the discrepancy to characterize the bonding behavior along the shear interface [BENG 2002, STE 2015]. In design guidelines for glued-in rods, the drill hole diameter is limited to the rod diameter plus 2 mm bondline. SCHOBER [SCH 2012, 2013] developed and investigated modified bonded-in rods for the first time with enlargement effects of the drill hole to achieve simple manufacturing, high quality control and a larger lateral surface for more efficient axial loading, followed by a substitution of polyurethane or epoxy resin based adhesives (conventional adhesives) by epoxy-bonded polymer concrete.

By analogy with the load distribution of glued-in threaded rods, the load is firstly transmitted by tension through the steel rod and then transferred through polymer concrete to the contact surface with wood. Compared to glued-in threaded rods, an additional tensile splitting failure type in polymer concrete and timber with radial oriented cracking has to be taken into account. The load is transmitted from the polymer concrete to the wood (Pull-out joint failure) and finally acts upon the wood with a pure tension load application (Fig. 2-6).

The drill hole enlargement and use of polymer concrete (PC) instead of adhesive enable a constructional design of the connection in which the load bearing capacities of the failure types tensile failure in steel, tensile splitting failure in PC and timber, pull-out joint failure and tensile failure in wood do not deviate highly one from the other. The diameter of the steel rod can be modified without affecting the pull-out joint capacity, on condition that there is a sufficient adhesion compound between steel, PC and wood. As a result of an optimised contact surface for the load distribution, the pull-out joint capacity increases.

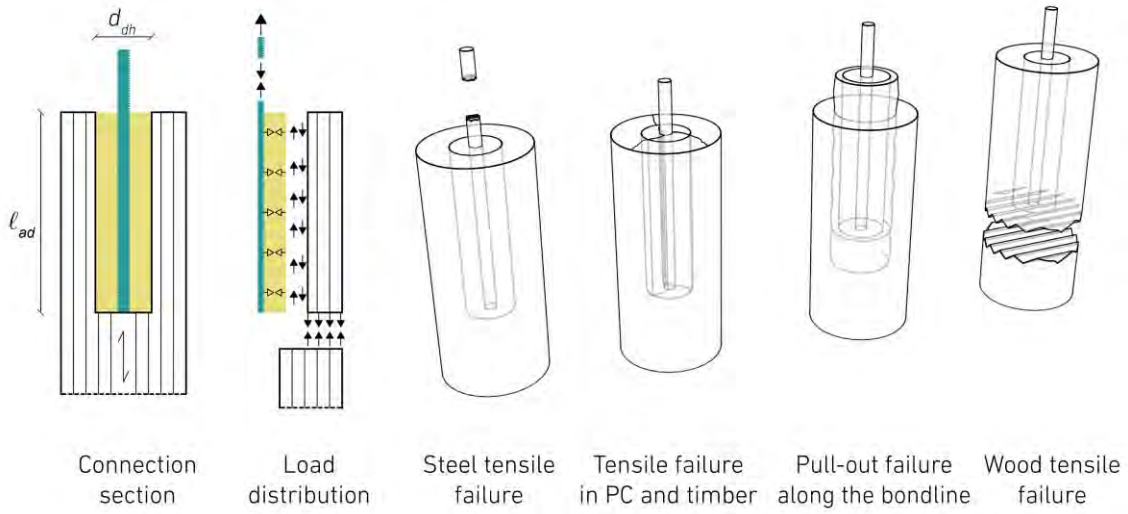

Fig. 2-6 Section, load distribution and failure types of grouted rods in wood

In the following, EN 1995-1-1/NA is adapted to modified bonded-in rods to discuss the adaptation of existing design rules for the determination of the pull-out joint capacity. The calculation is based (i) on the assumption of the same load bearing behaviour as for 'classic' glued-in rods and (ii) on experimental test results of JAHREIS [JAH 2018] for grouted rods, which showed a limited bonding length of 300 mm for the investigated connection geometries. The pull-out joint capacity of single grouted threaded rods is defined by the adhesive joint strength $f_{k,1}$, the diameter of the drill hole for the grouting material and the embedment length. The load transmission is assumed as constant along the joint with an adhesive joint strength of 4 MPa for embedment lengths smaller than 250 mm. The envelope surface in Fig. 2-7 shows the design pull-out joint capacity as a function of the adhesive bonding length and drill hole diameter. The timber strength class is set to C24 [EN 338] with a roundwood diameter of 200 mm and a modification factor k_{mod} of 0.8 [EN 1995-1-1].

Tensile failure in the reduced wood section (minus the PC section) is not addressed in Fig. 2-7 because it occurs at loads larger than 270 kN (design value) for the analysed connection geometries and describes the upper bond limit of the connection capacity to be achieved. Tensile failure in steel is also not addressed in the illustration, simply because rod diameter and strength class can be chosen freely with no effect on the pull-out joint capacity. Advantages, compared to 'classic' glued-in rods, are the increased pull-out joint capacity (Fig. 2.5 vs. 2.7) and the possibility to force steel failure, which is impossible for single glued-in rods in fibre direction today. For the practical application, the diameter and steel grade of the rod must be adjusted to achieve ductile tensile steel failure and to avoid brittle failure types, such as tensile splitting failure in PC and timber or pull-out joint failure.

Previous experimental research studies on threaded rods grouted into solid and glued-laminated specimen with PC were carried out by a small group of structural engineers [DRASS, JAHREIS, SCHOBER], where three types of pull-out joint failure were observed:

- Adhesive failure directly in the contact surface between wood and PC, leading to a pull out of the PC cone (Fig. 2-8a),
- shear failure in wood, leading to a pull out of the PC wood cone (Fig. 2-8b)
- and a mixed failure of both types (Fig. 2-8c).

The adhesion fracture is exactly in the PC-wood contact surface. This failure type, as well as the mixed failure, can be prevented by a visual inspection of the inner wood surface and the use of suitable PCs as compound material. In case of a good compound behaviour between PC and wood, the connections fail in wood (shear failure according to Fig. 2-8b).

$$F_{ax,Rk} = f_{k,1} \cdot \pi \cdot d_{dh} \cdot \ell_{ad}$$

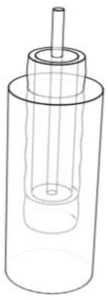

with

$F_{ax,Rk}$	*Characteristic pull-out joint capacity along the joint*
$f_{k,1}$	*Characteristic adhesive joint strength*
d_{dh}	*Drill hole diameter*
ℓ_{ad}	*Adhesive bonding length*

(Eq. 2.2)

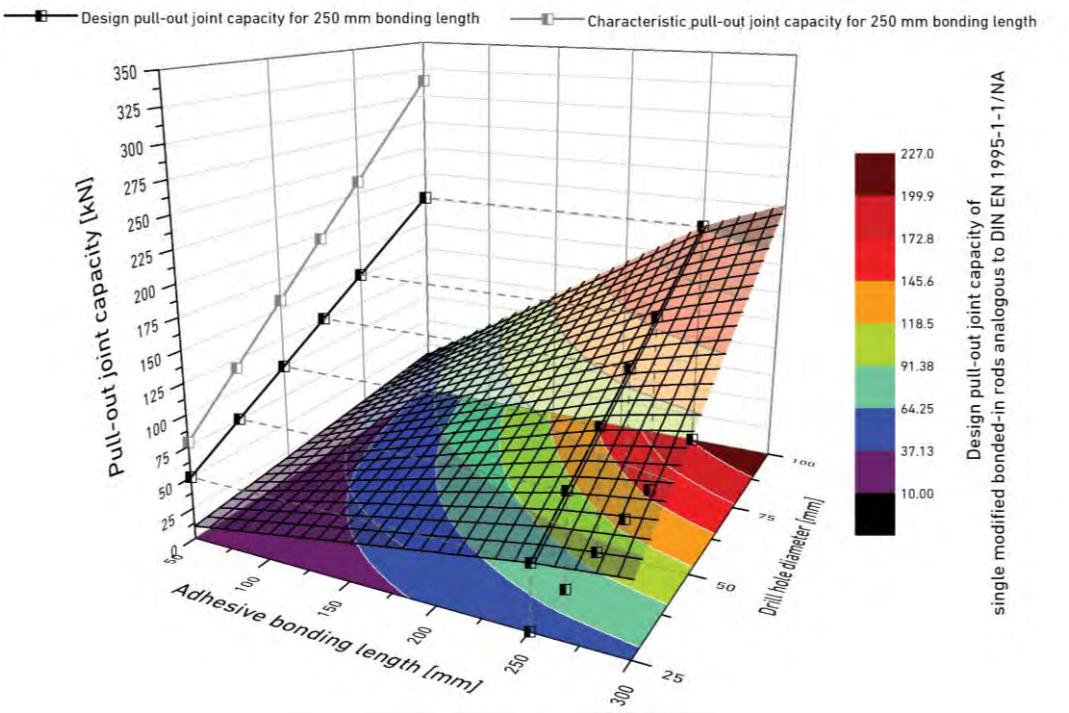

Fig. 2-7 Pull-out joint capacity of single grouted rods analogous to EN 1995-1-1/NA

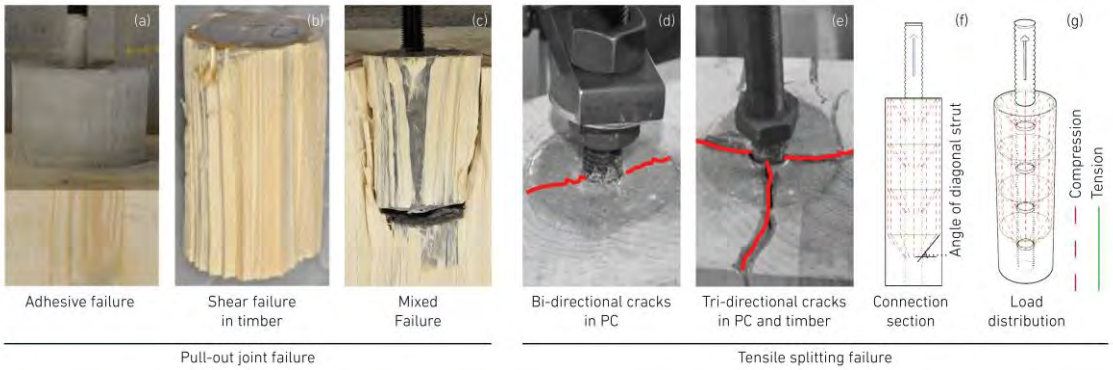

Fig. 2-8 Observed failure types of PC grouted rods in timber in experimental studies

Next to pull-out joint failure, tensile splitting failure in PC and timber (Fig. 2-8, d-g) were observed in experimental studies. The tensile load in the steel rod is transmitted by shear between the PC and the threaded rod. Due to the shape of the threaded rod, compressive loads are transmitted to the PC with resulting tensile ring stresses (Fig. 2-8g). The angle of diagonal strut (Fig. 2-8f) defines the loading portion for shear (longitudinal load component) and tension (horizontal or radial load component) for the load transmission in the contact surface between steel rod and PC. As a result of the ring tensile stresses in PC, first longitudinal cracks appear in the upper region of the connection near the steel rod. The initial cracking in PC is characterised through a bi-directional disruption within PC (Fig. 2-8d). This fracture pattern starts with the occurrence of micro-cracks near the steel rod, which regroup to near outer surface macro-cracks under a constant rate of loading. Those macro-cracks disrupt the PC cross-section over the full height. The PC wants to expand in the upper region of the connection, but it is confined by wood, which prevents it from splitting. The final tri-directional crack-fracture (Fig. 2-8e) occurs in the PC as well as in timber. An idealised structural model composed of tensile and compression trajectories is shown in Fig. 2-8, f-g.

To calculate the associated load for initial cracking in PC, the definition of the tangential stress is derived with the long term hydrostatic pressure resistance formula [DIN 8075] for thin-walled pipes under internal pressure load. The mathematical expression, shown in Eq. 2.3e, is determined by

– Eq. 2.3, a-c inserted into Eq. 2.3d,
– a substitution of the tangential strain by the tensile strength of PC and
– solving the equation for the applied load in longitudinal direction.

The used PC is a two-component epoxy-bound concrete with mineral aggregate. The resin is a stable crystallising low-molecular epoxy resin. The hardener adapted for the product is a fluid, colourless to light yellow at room temperature polyamine adduct, which holds an average reactivity for the interlacing of the fluid resin. The mineral additive is composed of well-graded gravel with a grain size of maximum 6 mm. A comparison with in constructions common used cement based concrete, strength class C25/30 [EN 206], is shown in Tab. 2-2. The high compressive strength of the PC results from the bonding behaviour of the polymer binder material and the mineral fillers, which leads to a high packing density and an ideal-elastic behaviour with a semi-ductile hardening rule. To determine the tensile strength of the implemented PC, tests were carried out. Relating to the results, the specimens performed with tensile strengths, $f_{ct,PC,mean}$, between 12 and 13 MPA. The same PC type and tensile strength range were applied and determined by LEUTBECHER [LEU 2008], SCHOBER [SCH 2012] and DRASS [DRA 2014] in previous studies (Eq. 2.3e).

Tab. 2-2 Mean strength comparison of polymer and cement based concrete

Strength	PC	C (C25/30)	PC/C
	[MPa]	[MPa]	-
Compression	116	33	3.5
Tension	13	2.6	6.2
Bending	30	5.5	5.4

$$F_H = F_L / \tan\theta \qquad \textit{(Eq. 2.3a)}$$

$$p = F_H / (\pi \cdot d_r \cdot \ell_{ad}) \qquad \textit{(Eq. 2.3b)}$$

$$t = 0.5 \cdot (d_{dh} - d_r) \qquad \textit{(Eq. 2.3c)}$$

$$\sigma_t = p \cdot (d_{dh}/2t) \qquad \textit{(Eq. 2.3d)}$$

$$F_{cr,mean}^{PC} = f_{ct,PC,mean} \cdot \tan\theta \cdot \ell_{ad} \cdot \pi \cdot d_r \cdot \frac{d_{dh} - d_r}{d_{dh}} \qquad \textit{(Eq. 2.3e)}$$

with

d_r *Steel rod diameter*
d_{dh} *Drill hole diameter*
$f_{ct,PC,mean}$ *PC tension strength*
ℓ_{ad} *Adhesive bonding length*
p *Inner pressure*
t *Thickness polymer concrete*
$F_{cr,mean}^{PC}$ *Initial cracking in PC*
F_H *Resultant horizontal or radial force*
F_L *Applied load in longitudinal direction*
σ_t *Tangential strain in polymer concrete*
θ *Angle of diagonal strut within polymer concrete*

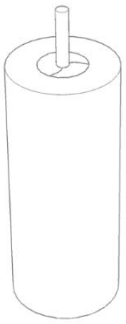

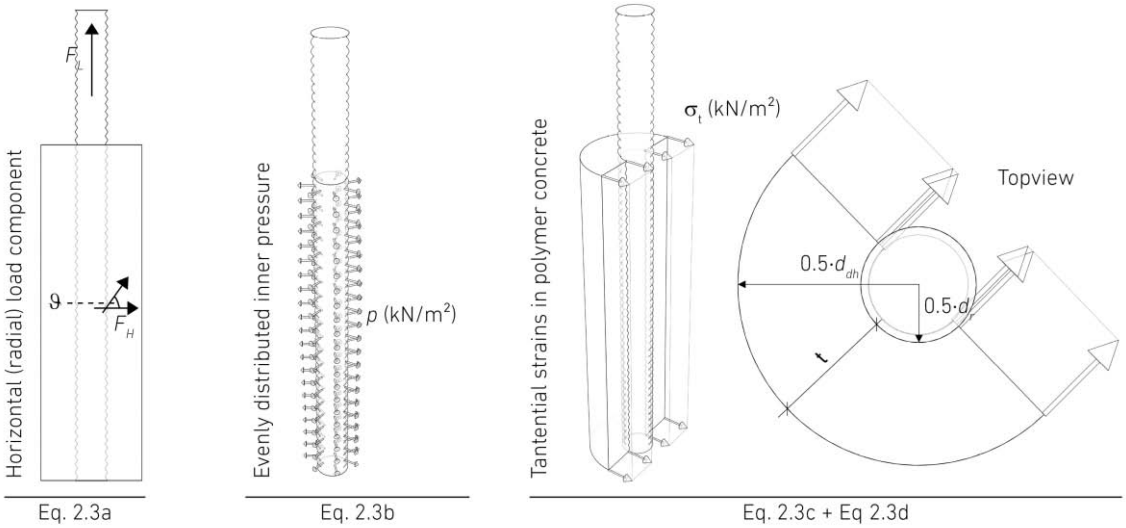

Fig. 2-9 Tangential strains in PC according to DIN 8075

The envelope surface in Fig. 2-10 shows the associated load (mean value) for initial cracking in PC as a function of the steel rod diameter and angle of diagonal strut for 250 mm bonding length and 75 mm drill hole diameter. Initial cracking in PC for M12, M24 and M36 threaded steel rods are illustrated as lines to highlight the delay in crack appearance for different steel bar geometries. The angle of diagonal strut has a big influence as well and was investigated by DRASS AND SCHOBER [DRA 2014] for squared solid timber and glulam with grouted M24 rods. A scale effect was taken into account by a variation of the drill hole diameter. The angle was determined analytically based on Eq. 2.3e and the observed loads for initial cracking in PC during testing. After testing, the specimens were opened to verify the calculated inclination angle of diagonal struts to the cross-section joint with observed angles between 34° and 40° along the embedment length.

After initial cracking in PC, the load-carrying capacity of the connection is dominated by adhesive bond and timber embedment stiffness. The PC expansion is restricted by the surrounded timber and the radial compressive strains lead into tangential tensile strains in wood. After exceeding the timber tensile strength, the ultimate load bearing capacity of the connection is reached (on the assumption that no pull-out joint failure occurs in the connection before) characterised by a radial oriented three-directional fracture in PC and timber (Fig. 2-8e).

Previous research studies on single threaded rods grouted into timber with PC were carried out by a small group of structural engineers [DRASS, JAHREIS, OPPEL, SCHOBER] covering experimental and numerical investigations. The research results are introduced in the following paragraphs.

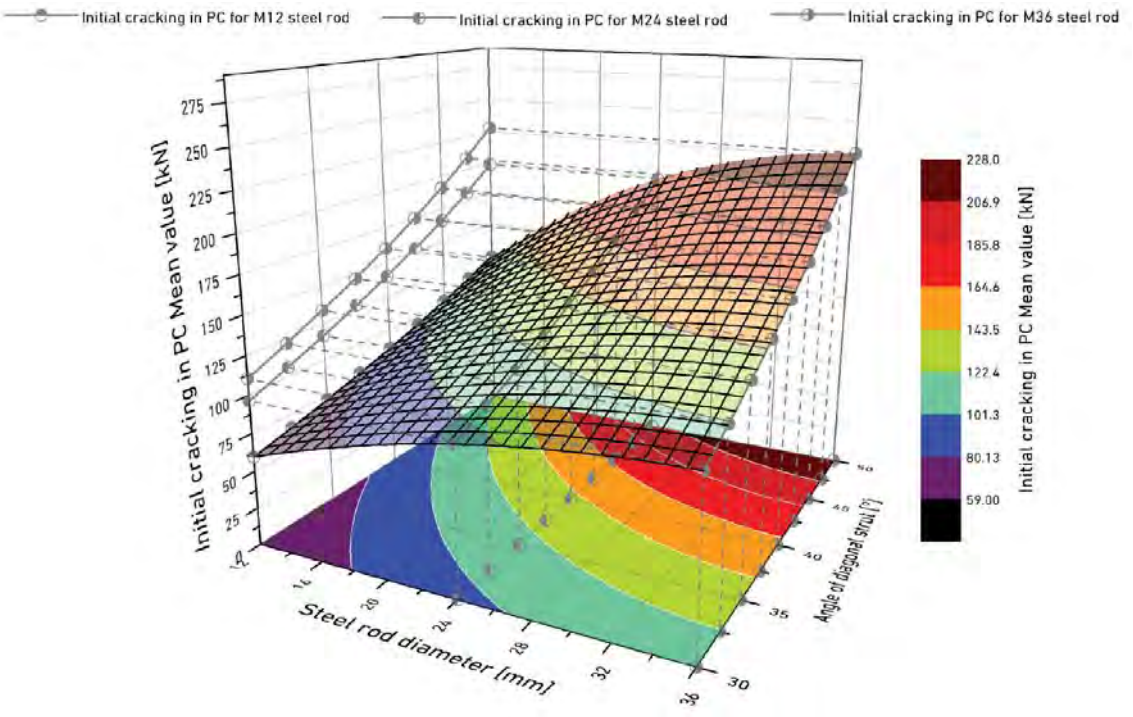

Fig. 2-10 Initial cracking in PC analogous to DIN 8075

PC grouted threaded rods in timber were developed first by SCHOBER [SCH 2012]. Threaded steel rods M12 10.9 or structural steel bars BSt 500 with equal diameter were embedded 120 mm in glued-laminated specimens made of GL 24h [EN 14080]. The specimen dimension was chosen to $w / h / \ell$ = 200 / 200 / 280 mm with a drill hole diameter of 50 or 75 mm and four investigated materials as binder: epoxy resin, mineral-bound mortar, PC (commercial name Compono® 100 S) and UHPC. The specimens were tested for loading parallel and perpendicular to the timber grain direction.

The experimental results identified PC as a suitable binder with high pull-out joint capacity (shear failure in wood according to Fig. 2-8b). The connection capacity increased up to 20% with larger drill hole diameter and showed an impact of the flank geometry and steel grade on the load bearing capacity: Threaded rods outperformed structural steel bars up to 15%. A reduced connection capacity for loading perpendicular to the grain direction was not observed in the experimental studies. Epoxy resin, mineral-bound mortar and UHPC specimens showed for larger drill holes an exothermic chemical reaction caused by the influence of the increased volume.

The mean values of each test series are summarised in Tab. 2-3 with information on the maximum applied tensile loads categorised by the drill hole diameter and steel rod type. The analytical approach for the pull-out joint capacity (Eq. 2.2: analogous to EN 1995-1-1/NA) is added to the table to discuss the adaptation and modification of existing European design rules for glued-in rods on grouted rods (Eq. 2.2). For Eq.2.2, a homogenous load distribution along the PC-wood contact surface is assumed with an adhesive joint strength of 4 MPa according to EN 1995-1-1/NA/Table 12. For a drill hole diameter of 50 mm, the mean failure load of the experiments matches with the analytical approach of EN 1995-1-1/NA adapted to grouted rods (Eq. 2.2), but are overrated for specimens with a larger drill hole. This indicates a variable adhesive joint strength depending on the drill hole diameter or connection geometry.

Tab. 2-3 SCHOBER [2012] - Test results of grouted steel bars in timber

Steel bar		M12 10.9	BSt 500	M12 10.9	BSt 500
Drill hole diameter	[mm]	50		75	
Bonding length	[mm]	120		120	
Epoxy resin	Pull-out joint capacity; mean value of each test series [kN]	22	23	12	10
Minder-bound mortar		20	20	15	16
Polymer concrete[1]		79	69	95	73
UHPC		5	7	10	10
Characteristic pull-out joint capacity[2] [kN]		75		113	

[1] Compono® 100 S (commercial name); [2] According to Eq. 2.2 (Adhesive joint strength of 4 MPa)

DRASS AND SCHOBER [DRA 2014] investigated the impact of the drill hole diameter on the connection capacity with experiments on PC grouted threaded rods in glued-laminated timber made of GL 24h [EN 14080]. The specimens were tested under tension in timber grain direction with an adhesive bonding length of 250 mm, a variation of the drill hole diameter and the use of the same PC type (Compono® 100 S) as in previous tests [SCH 2012]. Threaded rods (M20 10.9) were grouted in timber with a specimen dimension of 160 / 360 / 1000 mm *(w / h / ℓ)*.

In analogy to the investigation of SCHOBER in 2012, the European design approach for the pull-out joint capacity shows good correlation with the observed failure loads during testing for timber specimens with 50 mm drill hole. For wider drill holes, tensile splitting failure mostly occurred in PC and timber with no information on the adhesive joint strength in the PC-wood contact surface. DRASS [DRA 2014] confirmed an increased connection capacity for wider drill holes and investigated initial bi-directional cracking in PC in detail. Table 2-4 includes the observed loads for initial cracking in PC during testing, which exceeded the expected values according to the German design approach DIN 8075 for specimens with 75 and 100 mm drill holes. Here, cracking in PC appeared around 130 or 150 kN with tensile splitting failure in PC and timber around 180 or 200 kN.

After testing, the specimens were opened to investigate the inclination angle of diagonal struts to the cross-section joint with observed smaller strut angles for larger drill holes and therefore increased radial load distribution.

Tab. 2-4 DRASS [2014] - Test results of grouted threaded rods in timber

Steel bar		M20 10.9		
Drill hole diameter	[mm]	50	75	100
Bonding length[1]	[mm]	250		
Initial cracking in PC[2]	[kN]	100	130	153
Pull-out joint capacity[2]		169	175	
Tensile splitting joint capacity (polymer concrete and wood)[2]			182	204
Angle of diagonal strut in PC, measured after testing[2]		40	35	34
Characteristic pull-out joint capacity[3]		157	236	314
Initial cracking in PC Mean value[4]		102	104	110

[1] Compono® 100 S (binder polymer concrete commercial name),
[2] Mean value of each test series
[3] According to Eq. 2.2 (Adhesive joint strength of 4 MPa)
[4] According to Eq. 2.3e (polymer concrete tensile strength 13 MPa, Diagonal strut angle in PC measured after testing)

JAHREIS [JAH 2018] investigated the impact of the drill hole diameter and adhesive bonding length (varied from 30 to 60 mm and 100 to 300 mm) on the connection capacity of grouted threaded rods (M16 10.9) in glued-laminated specimen made of GL 24h [EN 14080]. 60 specimens with a dimension of 120 / 120 / 500 mm *(w / h / ℓ)* were tested under tension in timber grain direction with Compono® 100 S as binder for 20 different connection geometries.

The test results clarified an impact of the connection geometry on the adhesive joint strength (calculation based on the assumption of a homogenous load distribution along the full PC-wood contact surface). All specimens showed pull-out joint failure (shear failure in wood according to Fig. 2-8b) with increased adhesive joint strengths for specimens with smaller drill holes. This scale effect can be explained with the initial cracking or expansion of PC leading into radial oriented compressive stresses and an increased adhesive joint strength in the PC-wood contact surface. The adhesive joint strength is defined by the shear strength in timber and an additional strength portion caused by the radial expansion of PC (scale effect for grouted rods). A reduced drill hole results in less area for the shear load distribution, but increases the adhesive joint strength in the PC-wood contact surface at the same time. The determined mean failure loads for adhesive joint failure in the study of JAHREIS [JAH 2018] and associated numerical determination of the envelope surface for the experimental results [OPP 2017] are illustrated in Fig. 2-11. To rate the adaptation of existing European design approaches to grouted threaded rods, the characteristic pull-out joint capacities according to EN 1995-1-1/NA are highlighted as point clouds as well. OPPEL focused on the numerical investigation of grouted rods in glulam. In particular, a finite element model was developed to analyse the stresses and strains in the connection region. Preliminary experimental investigations served for verification to achieve a high quality of the model with all irregularities in the wood, such as fibre deviations or knots.

The envelope surface of OPPEL [OPP 2017] in Fig. 2-11 correlates well with the experimental results of JAHREIS [JAH 2018]. Based on the model, it can be stated that grouted rods show a loss of pull-out joint capacity for adhesive bonding lengths larger than 250 mm and almost no increase of capacity between 200 and 250 mm for the investigated connection geometries. The non-linear connection capacity distribution along the adhesive bonding length and drill hole diameter axes underlines the previous mentioned scale effect with varying adhesive joint strengths depending on the connection geometry. EN 1995-1-1/NA does not take this scale effect into account and assumes a constant adhesive joint strength of 4 MPa with a high deviation of the connection capacity to the test results of JAHREIS AND OPPEL (Fig. 2-11). OPPEL proposes a mathematical expression for the adhesive joint strength as a function of the drill hole diameter and adhesive bonding length to solve this problem (Eq. 2.4). The design proposal is in line with EN 1995-1-1/NA and substitutes only the adhesive joint strength.

$$f_{k,1} = f_{v,k} \cdot \frac{(-0.088 \cdot d_{dh} \cdot \ell_{ad}^{\,2} + 2.95 \cdot d_{dh} \cdot \ell_{ad} - 0.54 \cdot \ell_{ad}^{\,2} + 2.92 \cdot d_{dh} + 29 \cdot \ell_{ad} - 173)}{\pi \cdot d_{dh} \cdot \ell_{ad}}$$

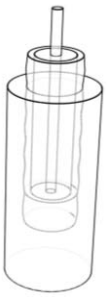

(Eq. 2.4)

with

$f_{k,1}$	*Characteristic adhesive joint strength*
$f_{v,k}$	*Characteristic timber shear strength*
d_{dh}	*Drill hole diameter*
ℓ_{ad}	*Adhesive bonding length*

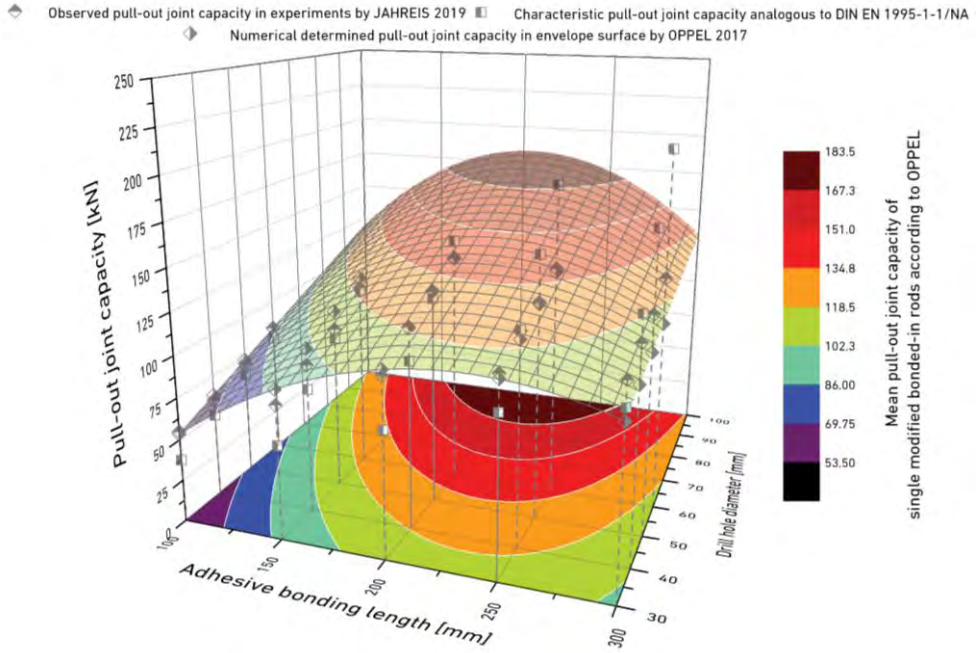

Fig. 2-11 Pull-out joint capacity of single grouted rods (JAHREIS & OPPEL)

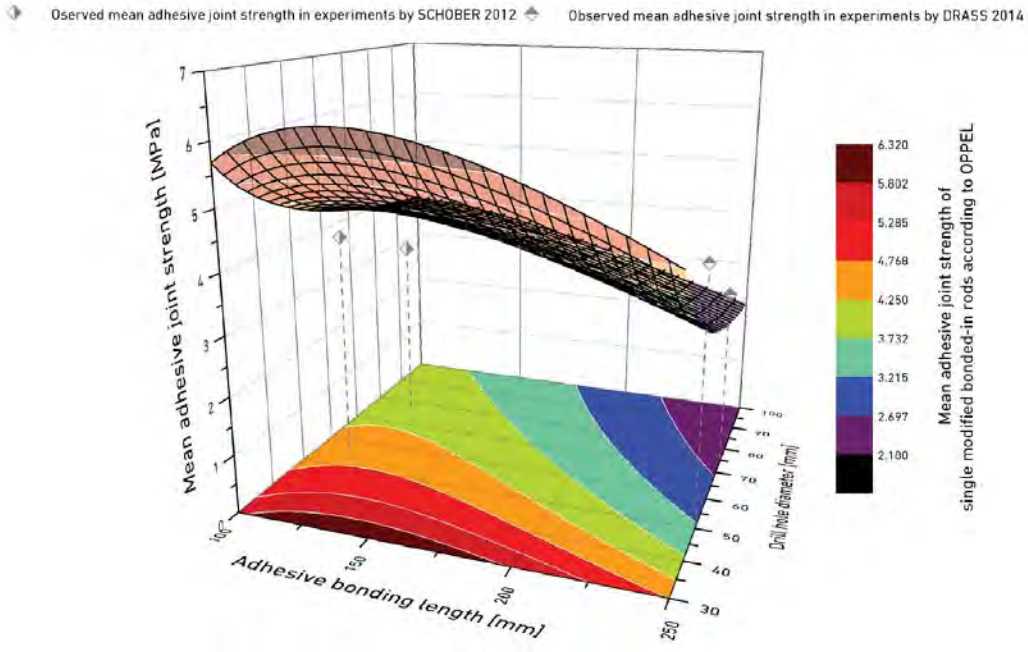

Fig. 2-12 Mean adhesive joint strength of single grouted rods (JAHREIS & OPPEL)

Fig. 2-12 shows the adhesive joint strength as a function of the bonding length and drill hole diameter according to Eq. 2.4 in comparison to the research results of SCHOBER [SCH 2012] and DRASS [DRA 2014]. Specimens with a drill hole of 30 mm performed with almost constant strengths of 6 MPa for the bonding length range 100 to 200 mm. Comparing the lower and upper bond limit, the adhesive joint strength tripled from approximate 2 MPa (drill hole diameter of 100 m and bonding length of 250 mm) to 6 MPa (drill hole diameter of 30 mm and bonding length smaller than 200 mm) confirming a scale effect for smaller drill holes. Here should be the noted, that the pull-out joint capacity increased for larger drill holes (Fig. 2-11) despite the reduced adhesive joint strength. Connection geometries with drill holes up to 50 mm performed with at least 4 MPa adhesive joint strength and were reduced to minimum 2.1 MPa for larger drill holes and bonding lengths. The investigation of JAHREIS AND OPPEL helped to answer important research questions on the adhesive joint strength for different connection geometries. The adhesive joint strength observed in the study of DRASS [DRA 2014] AND SCHOBER [SCH 2012] are highlighted in Fig. 2-12 with a clearly visible deviation to the proposed model of OPPEL.

Next to research studies on grouted rods in timber loaded under tension, JAHREIS [JAH 2018] and SCHOBER [SCH 2016a-b] focused on the development of coupling elements anchored in wood with PC for other structural purposes, such as grouted composite anchors or steel plates for uniaxial, tri-axial and column-beam connections, offering the possibility to transfer bending moments.

SCHOBER AND CHAHADE [SCH 2018] performed research studies on grouted rods (M20 10.9) conditions for glulam made of GL 24h exposed to surrounding climate with higher moisture contents. 15 specimens with a dimension of 160 / 360 / 1000 mm were tested under tension in timber grain direction with Compono® 100 S as binder. The drill hole diameter was set to 75 mm and the adhesive bonding length to 250 mm. The load carrying capacity of grouted timber joint exposed to outdoor climate in tension was determined with a 10% reduction compared to indoor climate. The failure type changed for outdoor specimens from tensile splitting failure in PC and wood to pull-out joint failure due to a reduction of the wood shear strength (shear failure in timber according to Fig. 2-8b). The observed pull-out joint and tensile splitting load capacities correlated with the experimental study of DRASS [DRA 2014] for specimens with the same connection geometry, but showed a deviation to the study of JAHREIS AND OPPEL.

Previous experimental research studies focused on the load bearing behaviour of grouted threaded rods embedded in squared timber. SCHOBER [SCH 2012] identified polymer concrete as a suitable binder in direct comparison to epoxy resin, minder-bound mortar and UHPC. DRASS [DRA 2014] varied the drill hole diameter for three test series and confirmed an increased load bearing capacity and reduced adhesive joint strength for larger drill holes. JAHREIS [JAH 2018] AND OPPEL [OPP 2017] determined the impact of the drill hole diameter and bonding length (scale effect) on the pull-out joint capacity and adhesive joint strength for a

wide range of connection geometries. The test results were further processed for the calculation of the adhesive joint strength with the outcome of the mathematical expression, presented in Eq. 2.4. SCHOBER [SCH 2018] determined a high load bearing capacity for grouted rods exposed to outdoor climate with a 10% reduction compared to indoor climate. The experimental investigations for outdoor exposure clarified the potential of modified bonded-in rods and gave the incentive to continue the research in this direction. Compared to the research study, presented in this thesis, mainly glulam or squared solid timber were used with a marginal focus on the adaptation to outdoor constructions and to other timber materials, such as structural roundwood.

2.5 MOULDED JOINTS COMPOSED OF POLYMER CONCRETE

The connection between roundwood members can be realised with (i) no mechanical fasteners, (ii) metal plates and mechanical fasteners perpendicular to grain direction, and (iii) mechanical fasteners in grain direction. In addition to mechanical fasteners, external joints can be used in the intersection with the advantage of redirecting the load distribution in the intersection from wood to the joint. The external joint substitutes the roundwood members in the intersection point. The load is following the longitudinal axes of the strut members with a load concentration and distribution in the external joint and almost only uniaxial loading in wood (Fig. 2-13).

External steel joints (Fig. 2-13, right) are commonly used in practice due to high strength parameter for the design in the ultimate limit state, high stiffness parameter for the design in the serviceability limit state and an easy and cost-effective fabrication. The disadvantageous of steel joints are the high density and energy consumption for production. The most known steel joint is the Mero-joint with a sphere or platonic form and implemented threaded nuts. Rods are embedded in the strut members and are connected to the nuts by rotation. First constructions composed of roundwood for 3D truss structures were developed by RUG [RUG 1990, 1995].

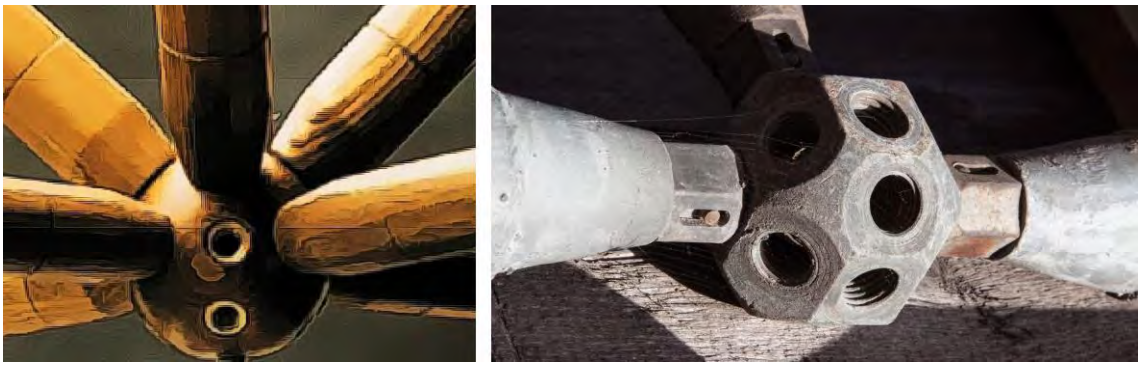

Fig. 2-13 Mero-joint in the intersection composed of wood (left) and steel (right)

A more recent development represents the granted patent by the University of Applied Sciences Trier, Germany [BEC 2018]. It describes a wooden strut construction comprising a first strut member and at least one second member. These members are force-locked together in an external moulded joint composed of PC (Figure 2-14). Analogous to the steel joint, the PC moulded joint substitutes the roundwood in the intersection with the result of partly reduced transversal stresses in the strut member.

From an environmental perspective, the primary energy consumption for the steel joint production is far too high and does not match with the ecological aspects of wood as building material. In direct comparison, the primary energy consumption for the PC joint production is reduced compared to steel joints. From an architectural point of view, the PC joints perform with an aesthetic appearance following the shape and direction of roundwood. Due to high PC material strengths (Tab. 2-2), this innovative approach has changed the way joints and constructions are designed in the timber building sector today.

The use of PC has a long tradition in the mechanical engineering sector and was firstly adapted to joints for timber constructions by SCHOBER [SCH 2014a]. Fig. 2-14a shows the first type of PC joint for 2D trusses, which is adapted to the shape of the strut members and is placed between chord and diagonal strut members. A single glued-in threaded rod is embedded in the diagonal strut member in fibre direction and is connected to the moulded joint. The fitted shape of the joint helps to keep the roundwood manufacturing effort in the connection region as low as possible. From a structural point of view, the joint takes over load-carrying functions for compressive loads. A screw connects the moulded joint with the chord in order to transfer tensile loads. The tensile and compressive load transmission is decoupled from each other with no structural functionality of the moulded material for tensile loads. The connection causes transversal stresses in the chord members, but enables an easy assembly of the truss structure.

Fig. 2-14 Moulded joints composed of polymer concrete

SCHOBER AND BECKER [SCH 2014b, BEC 2016a-b] further developed the connection design for 3D structures (Fig. 2-14, b-c) with single glued-in threaded rods in fibre direction for all roundwood members. The PC moulded joint eliminates high embedding stresses compared to mechanical fasteners connections and is able to transmit large compressive loads with comparatively low tensile strengths (Tab. 2-2). Therefore, this connection shall be used for primarily compression loaded structures, such as arc or tree construction.

Next to structural performance aspects, the joint type is not suitable for the design of modular trusses with an easy assembly. To connect strut and joint members by rotation analogous to the Mero-joint (Fig. 2-13), single glued-in threaded rods are embedded in roundwood in fibre direction, while nuts are grouted in the moulded joint. Due to the typology of the truss structure, it is practically impossible to assemble the construction in the factory and on site without grouting process at some point resulting in time consuming and expensive workloads. The construction has to be factory assembled, while the degree of pre-assembly is limited by the maximum allowable transport dimension. The rotation and grouting process represent weaknesses that are undesirable for the design of modular systems.

The PC moulded joint is designed in a monolithic arrangement and does not offer the possibility to substitute individual components in case of decay. A decisive point is that components of the coupled system cannot be developed and fabricated independently by one another. A modification of the global system affects the design, manufacturing and assembly process differently with no uniform solution and therefore increasing costs and workloads.

PC moulded joints represent an unexplored research field today. Especially in regard to roundwood, the *Holzkompetenzzentrum Trier* and the *Institute of Innovative Structures Mainz* are strongly represented in this field. The *Holzkompetenzzentrum Trier* is focusing on the implementation of the joining technologies shown in Fig. 2-14 in practice. This includes material investigations on PC by LAMBERT [LAM 2021].

Previous research studies of other researchers focused on the development of PC joints for truss and tree structures. Compared to research study presented in this thesis, the joints are developed in a monolithic arrangement with polymer concrete as moulded material with no structural functions for tensile loads.

3 OBJECTIVES

3.1 DEVELOPMENT SPECIFICATIONS

This thesis focuses on the development of moulded joints with modified bonded-in rods for modular trusses, adapted to the preferences of structural roundwood. The defined development specifications are introduced in the following to underline the innovative aspects of the new joining technology with the focus on the connection design in roundwood (modified bonded-in rods) and in the intersection (moulded joints).

From an architectural point of view, the joining technology should perform with

- an aesthetic appearance to provide an incentive effect for architects to build with the joining technology in timber building design.
- the possibility to adapt the joint principle to a variety of strut arrangements in the intersection to expand the number of designs to be realised in practice.
- the possibility to use cylindrical milled roundwood (constant diameter along the strut axis) and natural grown roundwood (only removed bark and bast layers) as strut members.

From a structural point of view,

- the roundwood members should only be loaded under tension and compression in fibre direction (favourable loading along strong main axis with high strengths) to keep the timber material usage as low as possible. The idea is to resemble the idea of an ideal truss in praxis as much as possible.
- the connection in roundwood should perform with a high load bearing capacity and an exposure to different climate conditions.
- the moulded joint should serve for the compressive and tensile load distribution.

– the moulded joint should be composed of a composite material based on wood fibres and epoxy resin to reduce the weight, to improve the architectural appearance and to optimise the ecological footprint.

From a manufacturing point of view,

– the roundwood fabrication should be as simple as possible with no modification of the circular cross-section and no computer-aided support.

– the moulded joint design and fabrication should be supported by a generative algorithm, which automates and optimises the design process.

The modularity of the connection is defined by

– a construction system, composed of roundwood members with modified bonded-in rods and moulded joints, with a simple pre-assembly, assembly and deconstruction. This reduces the construction time and allows an adaptation of the technology to permanent and temporary buildings.

– an easy container transport with strut lengths smaller than six meters.

– a low mass of the moulded joints to improve the handling and optimise the strength to weight ratio of the trusses.

– an adaptation of the same joint to different truss spans.

3.2 SPECIFIC OBJECTIVES

To reach the main objective of this thesis and the defined development specifications, the first research topic focuses on experimental investigations on modified bonded-in rods in roundwood. Previous research studies on threaded rods grouted into solid and glued laminated specimen with polymer concrete were carried out by a small group of structural engineers covering experimental and numerical investigations. The research results showed an increased load-carrying capacity compared to glued-in rods. The usability of the connection for outdoor construction was only investigated in own research studies on glulam [SCH 2018]. The research work presented in this thesis is based on those studies with an adaptation to structural roundwood. Pull-out tests have been carried out to answer important research questions in regard to the connection capacity. The specific research objectives are defined as follows:

- Assessment of the connection capacity of modified bonded-in rods in roundwood under different climate or service conditions.
- Assessment of crack propagation, moisture induced damage and wood defect influence on the connection capacity.
- Assessment of the slip modulus and single fastener capacity (characteristic and design values).

The second research topic focuses on parametric, numerical and experimental investigations on the moulded joints in the intersection. The aforementioned polymer concrete joints for 3D trusses (section 2.5) represent the basis of the new connection technology and were developed further to serve for the design of modular 2D trusses with an easy (de-)assembly and the ability to transfer compressive and tensile loads. The specific objectives for the development of the moulded joining technology are defined as follows:

- Assessment of the design principle and function of the moulded joints with an efficient load transfer concept for tension and compression, and an easy (de-)assembly with no grouting process (form finding).
- Development of a generative algorithm to address massive amounts of data or truss variations and to automate the design process for the digital joint fabrication (Parametric Design).
- Assessment of the structural behaviour of the joints for different applied composite materials (Structural Analysis).
- Fabrication and testing of a composite material based on wood fibres and epoxy resin (experimental investigations).
- Fabrication of a moulded joint prototype.

3.3 SWOT-ANALYSIS

Tab. 3-1 shows the SWOT-Analysis to underline the strengths, weaknesses, opportunities and threats of the joining technology for structural roundwood. The analysis was done in the beginning of the research studies.

Tab. 3-1 Joining technology SWOT-analysis

Strengths	Weakness
Aesthetic and environmentally-friendly building material (roundwood production is simple and effective)	Expensive moulded joint: Architects and engineers may refer back to simple and low cost connections such as metal plates
Aesthetic and form-fitted joint design	Dominance of rectangular cross-section
No embedding stresses in bolt- timber region and no reduced cross-section	Volatile timber costs (variable supply and demand and therefore raw material prices)
Adaptation to constructions loaded under tension and compression	Joint fabrication is not profitable in case of a low number of connections
Modularity, standardised components and the possibility of a non-destructive disassembly	Authorisation procedure needed in advance of the technology launch
High degree of prefabrication and -assembly, easy assembly (no casting on site)	Lack of control over ethical and environmental supply chain (wooden raw material)
High potential of the new developed moulded material based on wood fibres and epoxy resin for the building sector in general	
Supported by a cost-efficient generative design algorithm	
Opportunities	**Threats**
Long-term timber market expansion for circular cross-sections	Development specification (3.1) and specific objectives (3.2) cannot be reached
Short-term expansion of aesthetic roundwood 2D trusses	Usability for outdoor constructions is not guaranteed
Alternatives to rectangular wooden trusses	Successful authorisation procedure is not guaranteed
Elimination of geometrical joint restrictions for circular cross-sections	Large amount of tests may delay the investigations and increase the final cost of the technology
Supporting ecological and architectural trends	An automatisation of the design algorithm may not be achieved due to a too complex network of parameter to be taken into account
Local supplies and workforce	

EXPERIMENTAL INVESTIGATIONS ON MODIFIED BONDED-IN RODS 4

4.1 MATERIALS AND METHODS

This chapter presents experimental investigations serving for axial connectors in roundwood truss structures. Single glued-in threaded rods, bonded parallel to grain into softwood, represent the basis of the investigations. To increase the load-carrying capacity and usability of this connection technique in roundwood, a resin-bonded polymer concrete with an increased bondline thickness and contact surface to timber was investigated. The connection capacity and slip modulus of the modified bonded-in rod connection was studied on Douglas fir roundwood specimen exposed to different service conditions. The study investigated also the influence of wood defects on the connection capacity. The specific objectives are defined in section 3.2.

4.1.1 Test specimens

Polymer concrete (PC) is increasingly used since the 1920s. The main difference to conventional concrete is the type of binder: conventional concrete consists of cement, water and aggregates such as gravel or sand. In PC reactive resins are used instead of cement. Polyurethane resin-based PCs are more ductile, while those based on epoxy resins (used in this study) are more resistant to tensile and bending stresses. PC is lighter than cement-based concretes caused by the finer plastic matrix that binds the aggregates. The mixing ratio between the masses of the aggregates and the reactive resin including hardener varies between 1:4 and 1:13. Several polymer concrete types were studied and analysed in preliminary work by DRASS [DRA 2014] and SCHOBER [SCH 2008] to identify a suitable compound material for grouted threaded steel rods into timber, e.g. Compono® 100 S. The polymer concrete is composed by a two component epoxy resin adhesive (resin and curing agent) and gravel as aggregate. The resin is low-molecular and based on Bisphenol A.

The hardener is a polyamine adduct, which holds an average reactivity for the interlacing of the fluid resin. The aggregate consists of well-graded gravel with a grain size of maximum 6 mm. The mixing ratio between the aggregates and the reactive resin including hardener was 1:5 by weight and based on experiences of previous material studies. The material properties are summarised in Table 4-1 and are described by SCHOBER [SCH 2008] as well as in the German Technical Approval [DIBt Z-10.7-282]. The adhesive connection achieves around 70% of the final strength after one day and is considered to reach the final strength after seven days.

Tab. 4-1 Material properties of used PC (Compono® 100 S) for modified bonded-in rods

Material properties of Compono® 100 S	Unit	Value[1]	References
Density	[g/cm³]	1.96	SCH 2008
Dynamic MoE	[MPa]	22,800	SCH 2008
Static MoE		18,000	Z-10.7-282
Tensile strength		13.0	SCH 2008
Bending strength		30.0	SCH 2008
Compressive strength (cube specimen)		116.0	SCH 2008
Compressive strength (prism specimen)		98.2	SCH 2008
Compressive strength (prism specimen)		81.0	Z-10.7-282
Shear strength		4.0 – 5.0	Z-10.7-282
Shear modulus		9,300	Z-10.7-282
Coefficient of thermal expansion	[10-6/K]	20.5	SCH 2008

[1] Mean values

All 27 tested timber specimen consisted of Douglas fir *(Pseudotsuga menziesii)* roundwood, sample length 1.0 m, outer diameter 200 mm, with a central drill hole, diameter 75 mm and length 250 mm (Fig. 4-1). The natural crack and annual ring pattern of each roundwood specimen were inspected visually before grouting and testing to determine the influence on the connection capacity later on (section A.1.1). Existing design rules for strength grading [EN 14081-1 and DIN 4074-1] refer to squared timber and do not cover roundwood cross-sections. In this study, visual strength grading was used to determine strength classes according to EN 1912, which defines the assignment of visual strength grading aspects into strength classes depending on species. European strength class C24 could be assigned for all specimen in relation to the visual attributes according to DIN 4074-1 (e.g. fibre inclination below 12%, annual ring width lower than 8 mm etc.) and EN 1912. The efficiency of the chosen method for grading roundwood can be rated in different ways: On the one hand, the approach is not precise enough with the consequence that the results of the experimental investigations cannot be reproduced. On the other hand, the strength class is secondary and not important for the evaluation of the tests in case of tensile splitting failure. Even if pull-out

failure or shear failure appear in wood along the bondline, EN 338 indicates a constant shear strength of 4 MPa for strength classes greater than or equal to C24. EN 1995-1-1/NA indicates the same strength for bonding lengths smaller than or equal to 250 mm. Under this assumption, the exact strength state of the roundwood members plays a subordinate role for the experimental evaluation.

As connector, threaded steel rods, M24-10.9 [DIN 976-1], ISO metric thread, flank angle 60° were chosen with a yield strength of 900 MPa in order to prevent premature yielding of the rod. The threaded rods were placed centered with distance holders into the air pressure cleaned drill hole of the timber samples. To minimise lateral loads due to inclination, a 30 mm deep recess was fabricated at the bottom of the grouting chamber to centre the steel rods (Fig. 4-1a). After placing the rods the grouting chamber was filled with the adhesive, in this case a two-component epoxy polymer concrete, commercial name Compono® 100 S.

When processing polymer concrete, it is necessary to pay attention to the safety and health instructions. Polymer concrete is highly allergic. In addition, fumes are generated when the resin reacts with the hardener. This is why an adequate ventilation must be provided during manufacture. It is important to wear appropriate protective clothing, because the components are toxic during the chemical reaction. In addition to safety glasses and mouth guards, nitrile gloves should be used. Failure to comply with the safety and health instructions (see unsupervised students in Fig. 4-1c) will lead to allergic reactions such as skin irritation and acne.

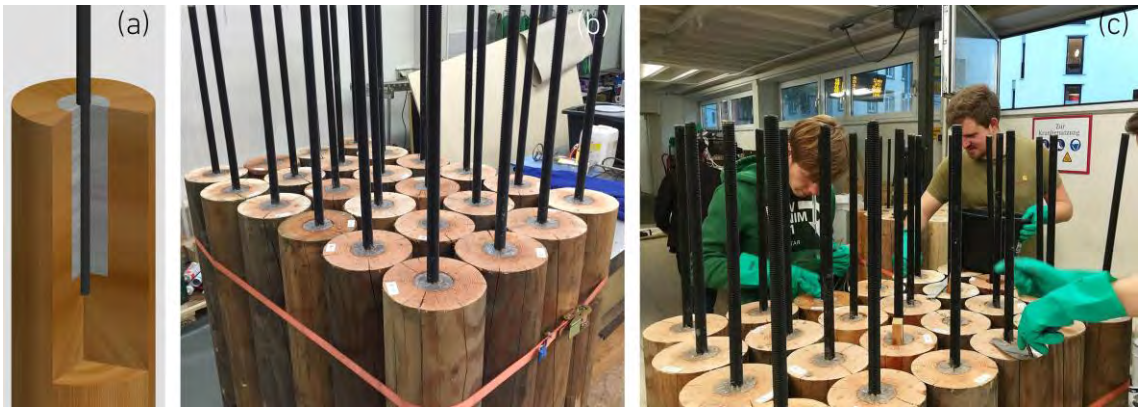

Fig. 4-1 Modified bonded-in threaded rods: longitudinal section sketch (a), cross-section view (b) and fabrication of test specimens (c)

The total number of prepared composite specimens (27) were split into three series with nine specimens per series to consider the environmental conditions of the three service classes according to EN 1995-1-1. The first series was tested exactly after seven days with climate conditions according to service class 1 (SC 1), which is characterised by an average moisture content in most softwoods of maximum 12%, corresponding to a temperature of 20°C and a relative humidity 65% in the surrounding air (only exceeded for a few weeks per year, e.g. normative indoor climate). To simulate the environmental conditions of the other two service

classes and test series, the specimens were stored with a climate exposure of three years in total. SC 2 describes a higher moisture exposure and is characterised by an average moisture content in most softwoods by 20% corresponding to $T = 20°C$ (temperature), rH = 85% (relative humidity), exceeded only a few weeks per year. SC 3 is characterised by climatic conditions leading to higher moisture contents than in SC 2 (outdoor climate in Europe). Therefore, SC 2 specimens were covered to avoid direct weathering, while SC 3 specimens were directly exposed to weathering. After three years climate exposure, the specimens of service class 2 and 3 were tested directly in the lab (indoor, SC 1) with no further interim storage. Tab. A-1 (section A.1.1) summarises all important parameter including test date, room temperature, air humidity, and so on.

4.1.2 Test set-up, instrumentation and data acquisition

The load application was done by Zwick Roell Z250 test machine, maximum load application 240 kN. The load cell of the test machine was used to determine the loading during the experimental procedure. The load application was done first within the elastic range, force controlled, speed 20 kN/mm to eliminate the impact of slippage and settlement in the clamping device. Thereafter, the testing changed to a displacement controlled load application, speed 0.35 mm/min until the ultimate load was reached. Fig. 4-2 shows the tensile load distribution as a function of the time for sample 2, SC 3. In this case, there was no failure in the connection with a maximum load distribution of 240 kN for approximate five minutes. This test setup was applied to all specimens. To connect the specimen with the base, a clamping device for circular cross-sections was designed and fabricated (Fig. 4-3). The threaded rod was attached to a long nut above the crossbeam of the test machine in order to introduce uniaxial tensile loads into the connection generated by an elevation change of the crossbeam. Inductive and laser supported displacement sensors were used to record displacements in longitudinal and radial direction for SC 1 specimens. To measure the longitudinal displacement on the outer surface, aluminium brackets were attached in 0°/120°/240° position around the circumference and distributed over the height into four levels (Fig. 4-3).

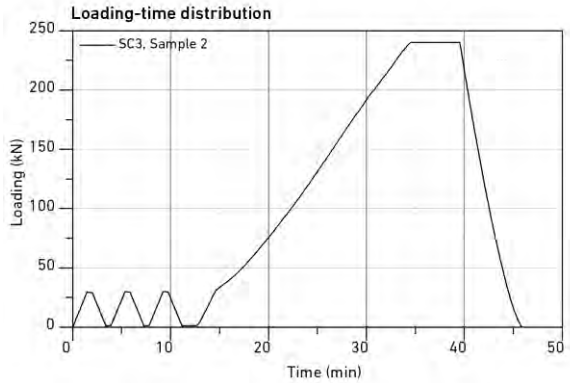

Fig. 4-2 Loading-time distribution for modified bonded-in rods

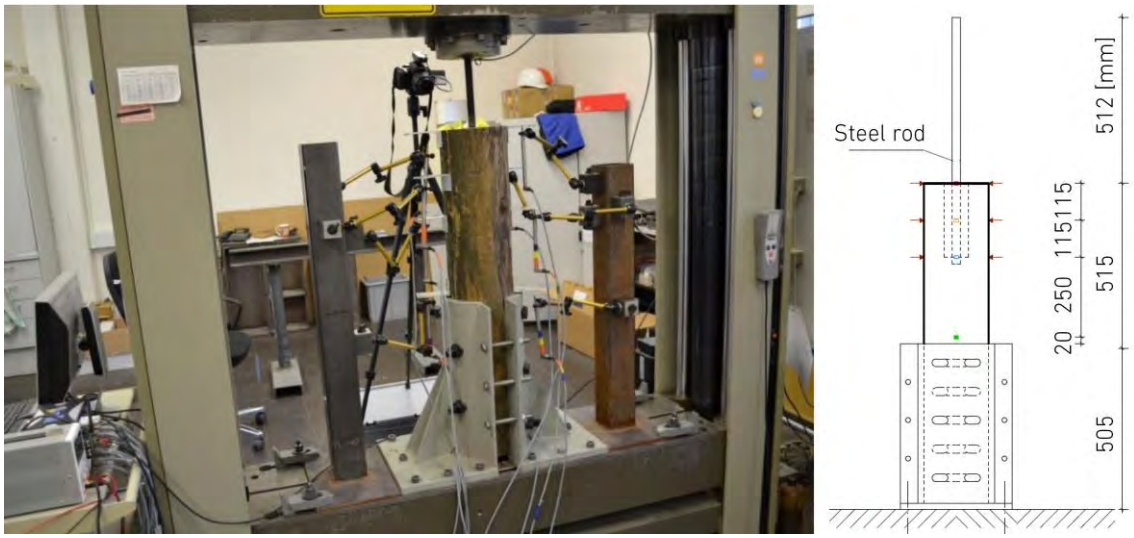

Fig. 4-3 Test set-up and hold down (left), specimen geometry (right)

For the experimental investigations in SC 2 and SC 3, Digital Image Correlation (DIC) was used. DIC is an optical method that employs tracking and image registration techniques for accurate 2D and 3D measurements of changes in images almost independently of the specimens material. It is a contactless process in which digital optical recordings in the undeformed and deformed state are captured to calculate displacements and strains in all directions by software analysis. The DIC measurement system helped to answer research questions regarding the crack arrangement in polymer concrete, the structural behavior of the connection along the bondline and the displacement of the steel rod near the polymer concrete.

Surface displacements were measured optically by three camera pairs with a subsequent numerical calculation of the corresponding strain fields. The surface displacement measurement was done two- and three-dimensional. Two camera pairs detected the displacements (Fig. 4-4 and 4-5, left), covering the full cross-section surface of the timber end grain, the polymer concrete and the threaded rod with an image resolution of 4000 x 3000 px, 25 mm lens and a stereo angle of approximately 32.5°. One further camera pair recorded displacements at the curved timber surface (Fig. 4-4 and 4-5, right). The same camera types were used in this case with a 50 mm lens caused by an increased distance to the specimen. The stereo angle was approximately 20.5°.

A black coloured pattern (speckle image) was applied to the surface. The specimens were sanded first to achieve a preferably smooth surface with no irregularities. In the next step, timber, PC and steel were primed white to create a better contrast with a subsequent application of the speckle image by the airbrush technique .The DIC system tracked the displacement of each speckle and evaluated displacements with the integrated software Vic-3D®-system from Correlated Solutions, Inc.

Fig. 4-4 Camera and spotlight setting for SC 2 and SC 3 specimens

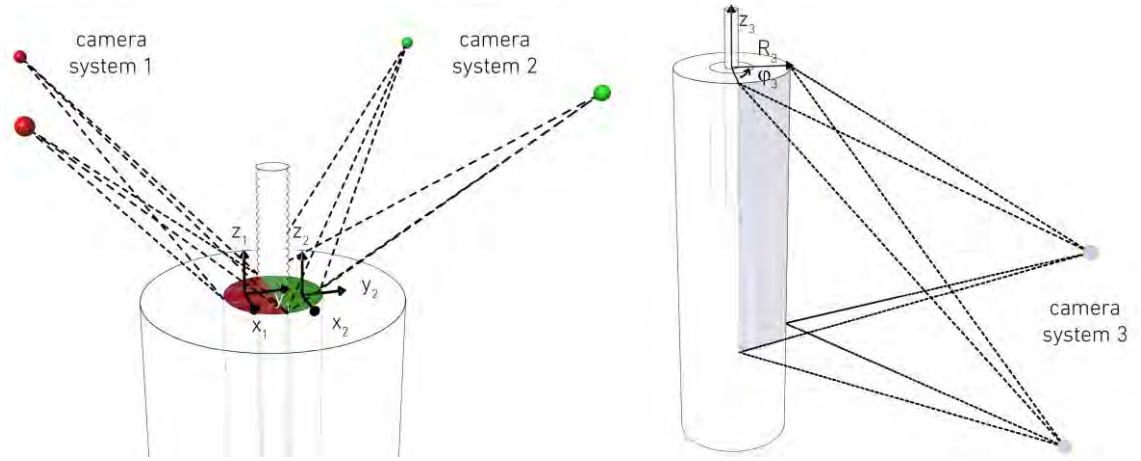

Fig. 4-5 Areas of interest and coordinate systems of the three camera pairs in Vic-3D®

Once the alignment of the specimen and the connection to the test machine was done, the camera systems were adjusted or configured. All test specimens had the same nominal dimensions, but it cannot be excluded that little variations in the specimens geometry or small displacements of the camera position during the exchange of the specimens lead to false test results. This is why the procedure of the connection configuration was repeated for each specimen to guarantee a high precision and accuracy of the measurement.

In the beginning of the camera configuration the aperture of each camera was closed slowly until the required depth of field was achieved. Subsequently, the light exposure time needed to be increased to compensate the reduced brightness of the partly-closed aperture. The focus function in Vic-3D® was used to optimise the camera configuration. The software visualised coloured markings on the specimen rating the efficiency of the chosen camera configuration. Via Vic-3D® the live images were transferred to the computer screen. As soon as the test folder was created for the specimen, a table file was automatically generated with information on the SC, sample number, time and loading (input signal from the test machine loading cell) for each image.

Camera system 1 and 2 recorded displacements in the polymer concrete surface (Fig. 4-5, left). A Cartesian coordinate system was generated with an integrated Vic-3D® plug-in (plane fit) for each camera pair with the *z*-axis perpendicular to the

analysed surface, the *x*-axis parallel to the camera pair in the polymer concrete surface and the *y*-axis perpendicular to the *x*-axis. The origin of the coordinate system was placed randomly in one point of the analysed surface. Camera system 3 captured displacements in the roundwood outer surface. In this case, a further plug-in of Vic-3D® was used to convert an initially created Cartesian coordinate system into a cylindrical coordinate system with the *z*-axis in loading or longitudinal direction (Fig. 4-5, right).

Comparable to the functionality of the human eye, a stereo system is required to record measurements in 3D space with a pair of cameras aligned to the same surface from two perspectives (Fig. 4-6, left). It is a method of photogrammetry for the simultaneous determination of the positions of the observing camera pair and points in the common field of view by measured angular relationships.

After configuration of the camera systems, both cameras of a pair were calibrated. For the calibration process, panels in different scales were used to cover the entire area of interest as much as possible (Fig. 4-6, right). Approximately 50 images with varied positions and inclinations of the panel were taken and edited with Vic-3D® for an improved result of the calibration. Here should be noted that uneven, rough or reflective surfaces and also shadows on the panel needed to be avoided to reach a high quality of the calibration.

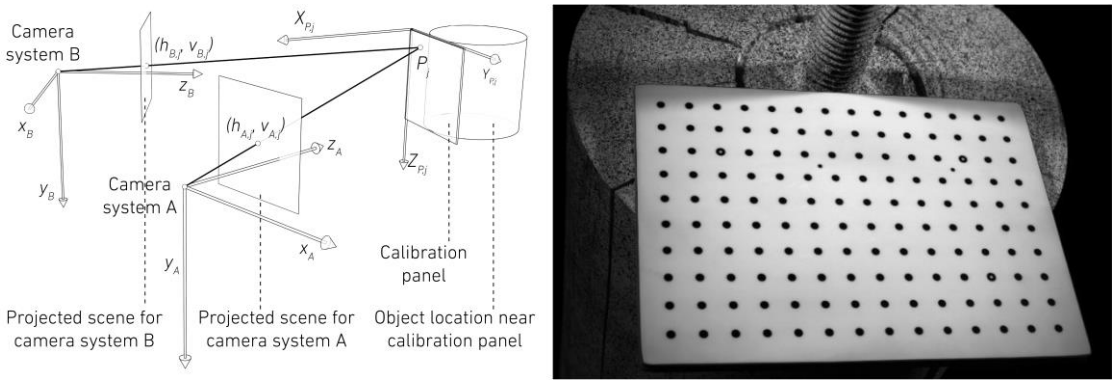

Fig. 4-6 Scheme of stereo camera system calibration (left) and calibration panel (right)

Vic-3D® provided an output of the measurement tolerances to verify the camera configuration and calibration. Fig. 4-7 shows the sensitivity of the DIC system for longitudinal or tangential strains in roundwood or polymer concrete (Fig. 4-8) in the unloaded state without error source and with a placed spotlight (error source) under the camera pairs. The evaluation clarified an approximate tripling of the measured strains for the test setup with spotlight, but also negligibly small values compared to the measured strains in roundwood and polymer concrete during testing. The measurement tolerances of Vic-3D® were smaller than 0.05‰ and could be neglected for the evaluation.

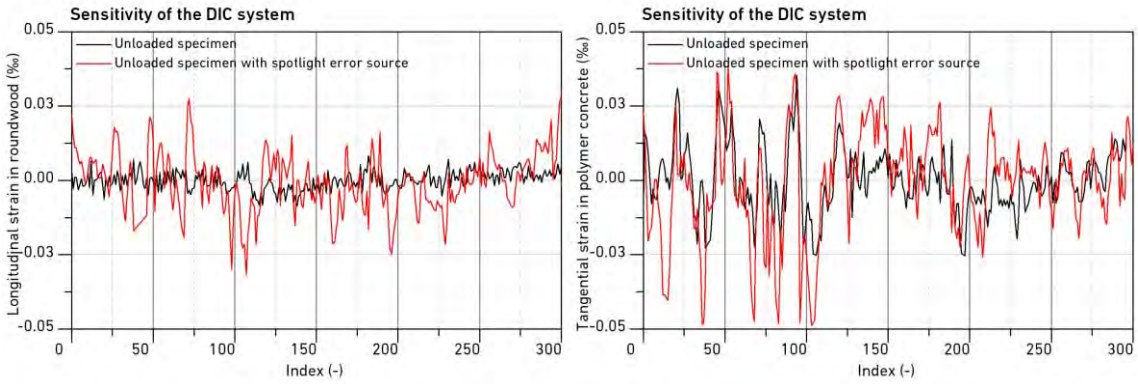

Fig. 4-7 Sensitivity of the DIC system (measurement tolerances)

4.1.3 Data processing

The target parameters in the data processing were longitudinal strains in the roundwood outer surface, tangential strains in the polymer concrete and the displacement of the steel rod in longitudinal direction in the corresponding coordinate system (Fig. 4-8). Vic-3D® provided a direct output of longitudinal strains in roundwood with the integrated coordinate system transformation from Cartesian to cylindrical coordinates. In this case, the *z*-axis is aligned in longitudinal or loading direction (Fig. 4.5, right). The tangential strains in polymer concrete could not be calculated directly with Vic-3D® and required a further data processing of the Cartesian oriented strain field (Fig. 4-5, left) in external software (Grasshopper® for McNeel Rhinoceros®).

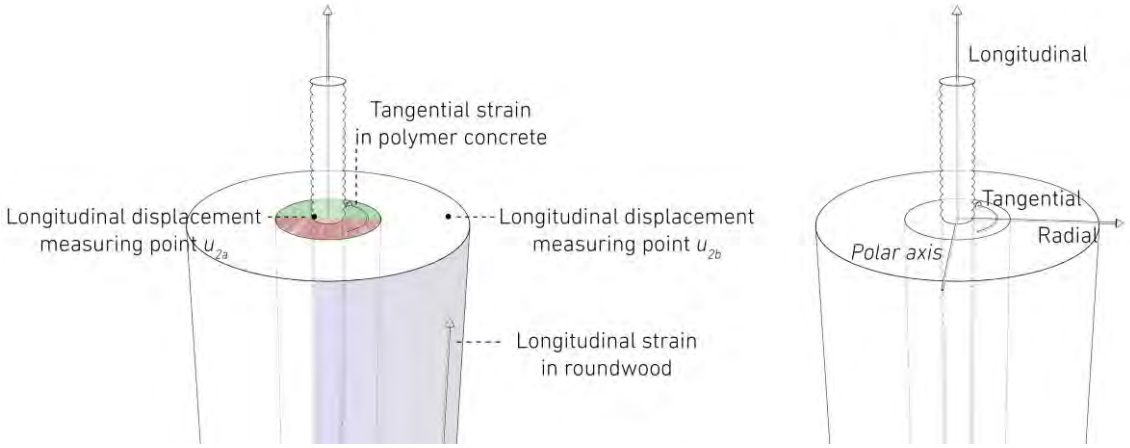

Fig. 4-8 Target parameter (left) and target coordinate system (right) of the DIC system

The data processing started with the import of the calibration file and the corresponding speckle images. The first speckle image, which was taken in the unloaded state, served as reference. Here, the regions to be correlated or analysed (Fig. 4-8, left) were marked with an AOI (area of interest). To provide the software with references for measuring the displacements of the speckle points, so-called subsets (subareas) were placed over the speckle pattern (Fig. 4-9, left). The size of the subset was selected manually and controlled the area of the image that was

used to track the displacement between images. The subset size had to be large enough to provide a contrast and distinctive pattern for the calculation (correlation) in the investigated area. The displacements of the speckle point pixels were compared with the unloaded original image (reference image). Based on information of Correlated Solutions ®, there should be approximately four speckles in a subset.

Next to the definition of the subset, the size of the sub step (step size) needed to be defined and configured the number of pixels to be analysed (Fig. 4-9, right). Generally, a step size of one defines a calculation (correlation) at ever pixel. For a step size of three, every third pixel is analysed, and so on. The computing time increases with the square of the step size, due to the two-dimensional surface and pixel orientation in two directions. The subset should be as large as possible for safe calculation and at the same time as low as possible for high resolution. As a guideline for sufficient resolution, the step size should not exceed one third of the subset size. The displacements of the pixels for different steps were evaluated and compared to each other to reach safe calculation and high resolution at the same time. The sub step was set between 20 and 25 pixel for all specimens.

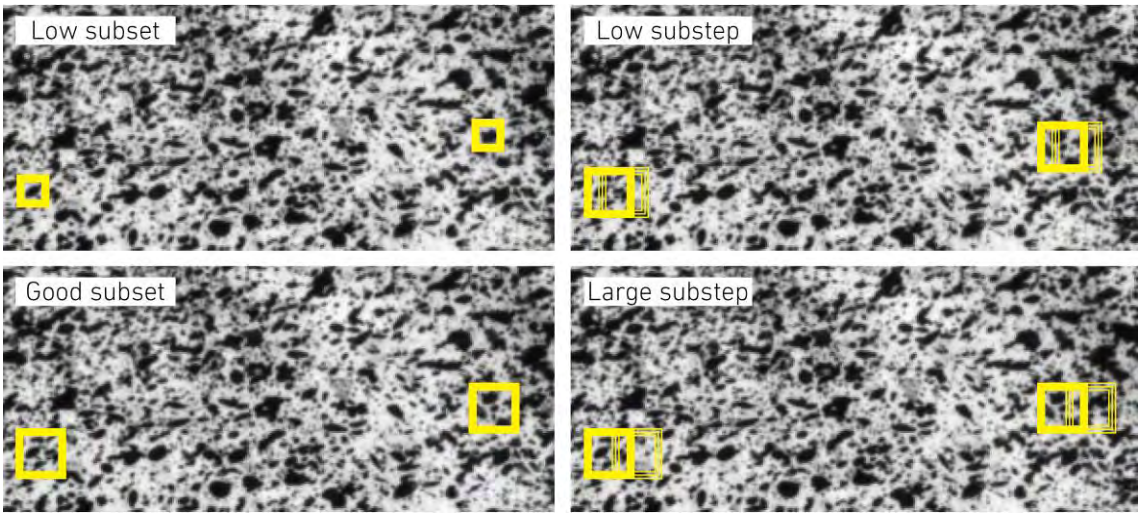

Fig. 4-9 Subset (left) and substep (right) in polymer concrete surface in Vic-3D®

After image correlation, various results were displayed in Vic-3D® and exported as text document for further evaluation. Based on the generated colour scale of the strain field in Vic-3D® (Fig. 4-10), the plausibility of the results was checked, for instance along existing cracks. In case of strongly scattering results, it was also possible to smooth data over the surface or time with an average calculation for manually selected subsets or images. The strain visualisation in Fig. 4-10 is captured for 200 kN loading.

The roundwood outer surface was divided into two sections for the evaluation: the joint section from 0 mm to 250 mm and the timber section below from 250 mm to 400 mm bonding length (Fig. 4-11). Six measuring boxes were captured for each section with H1 to H6 for the joint section and H7 to H12 for the timber section. The strains in the area of each measuring box (rectangle) were calculated with a

subsequent determination of the average value, representing one measuring point in the centre of the box. The following parameter were exported for each measuring box as text file for further processing in Microsoft Excel®:

– position along the bondline (Fig. 4-11, left),
– longitudinal strain (Fig. 4-8, left) and
– loading.

The final layout (Fig. 4-11, right) shows the strain-bonding length distribution with associated curves representing different loading ranges. Section A.1.3 summarises the results for the test specimens.

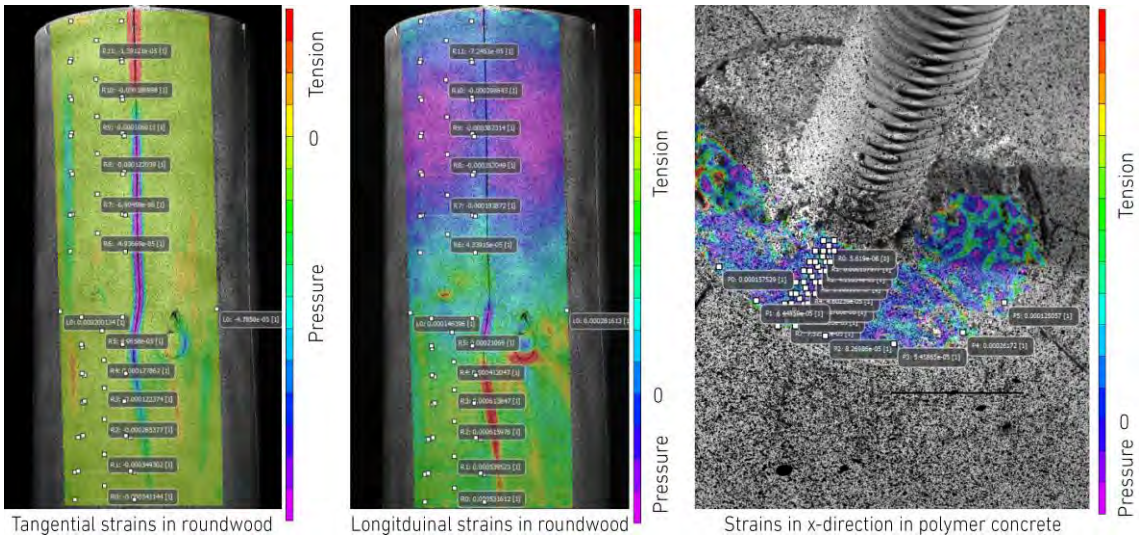

Fig. 4-10 Strain field visualisation in Vic-3D®

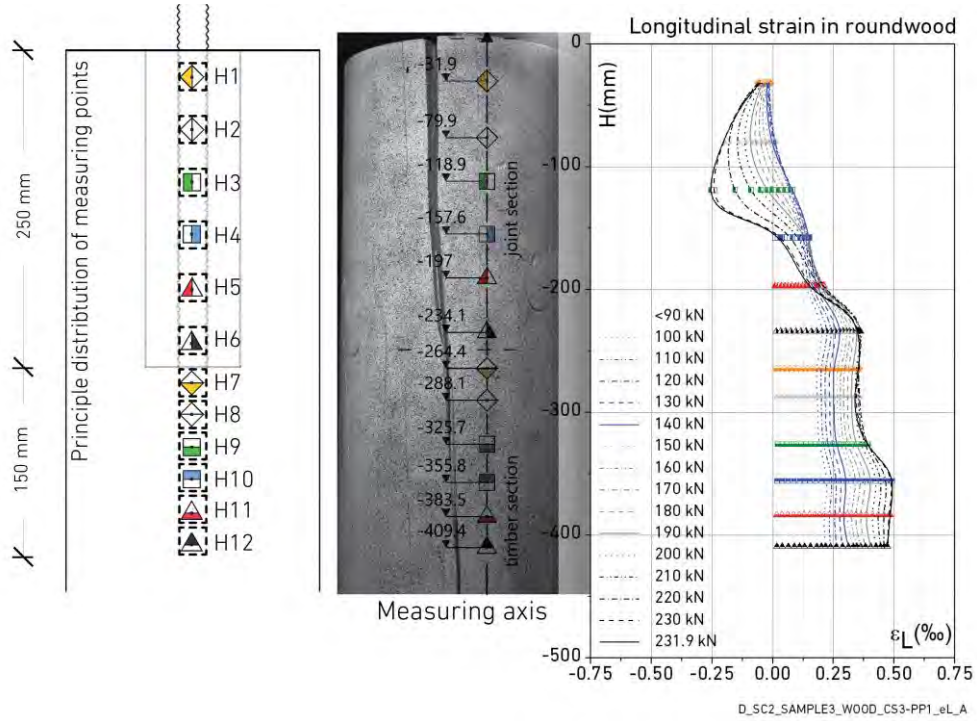

Fig. 4-11 Longitudinal strains in roundwood outer surface for sample 3, service class 2

Cartesian strains in the polymer concrete (Fig. 4-5, left) were calculated in Vic-3D® and required a further transformation with external software. The measuring boxes or points were distributed along a radial axis in polymer concrete (Fig. 4-10, right). For each specimen, five axes (Fig. 4-13, left) were analysed in total: three axes along cracks (axes a, b and c) and two in between (axes A and B). Axes were distributed along cracks to identify the associated load for each forming fracture in PC. The following parameter were exported for each measuring box in a table file for further processing in Grasshopper® for McNeel Rhinoceros® according to the coordinate system defined in Fig. 4-5, left:

– metrical position along *x*- and *y*- axis,
– loading, strains in *x*- and *y*- direction, shear strains and
– metrical position of additional orientation points along *x*- and *y*- axis.

Parametric design software with integrated graphical operators (Grasshopper®) were used to transform the metrical oriented strains into tangential and radial components. The scheme of the post processing steps is shown in Fig. 4-12 with a visualisation of the Vic-3D ® output parameter in the first step (Fig. 4-12, 1). Orientation points were defined along the outer circular edge of the polymer concrete (see also Fig. 4-10, right) to identify the metrical position of the connection centroid in x- and y direction. This was done with a circle fit through the orientation points (graphical operator) and a subsequent determination of the centre (Fig. 4-12, 1). Step 2 describes the offset of all geometric objects from the connection centroid to the coordinate system origin. In order to transform the metrical oriented strains into tangential and radial components, the transformation angle φ for each measuring box was determined with graphical operators in step 3. This was done by an angle calculation between the *x*-axis and eight extension lines from the coordinate system origin to the centres of the measuring boxes (Fig. 4-12, 3). Eq. 4.1 shows the determination of the tangential strains. Fig. 4-12, step 4, illustrates the final cylindrical coordinate system with tangential and radial oriented strains in PC.

$$\varepsilon_t = 0.5 \cdot \left(\varepsilon_{xx} + \varepsilon_{yy}\right) + 0.5 \cdot \left(\varepsilon_{xx} - \varepsilon_{yy}\right) \cdot cos(2\varphi) + \varepsilon_{xy} \cdot sin(2\varphi) \qquad \textit{(Eq. 4.1)}$$

with

ε_t	*Tangential strain*
ε_{xx}	*Direction of surface normal and strain in x-direction*
ε_{yy}	*Direction of surface normal and strain in y-direction*
ε_{xy}	*Direction of surface normal in x-direction, strain in y-direction* ($\varepsilon_{xy} = \varepsilon_{yx}$)
φ	*Transformation angle*

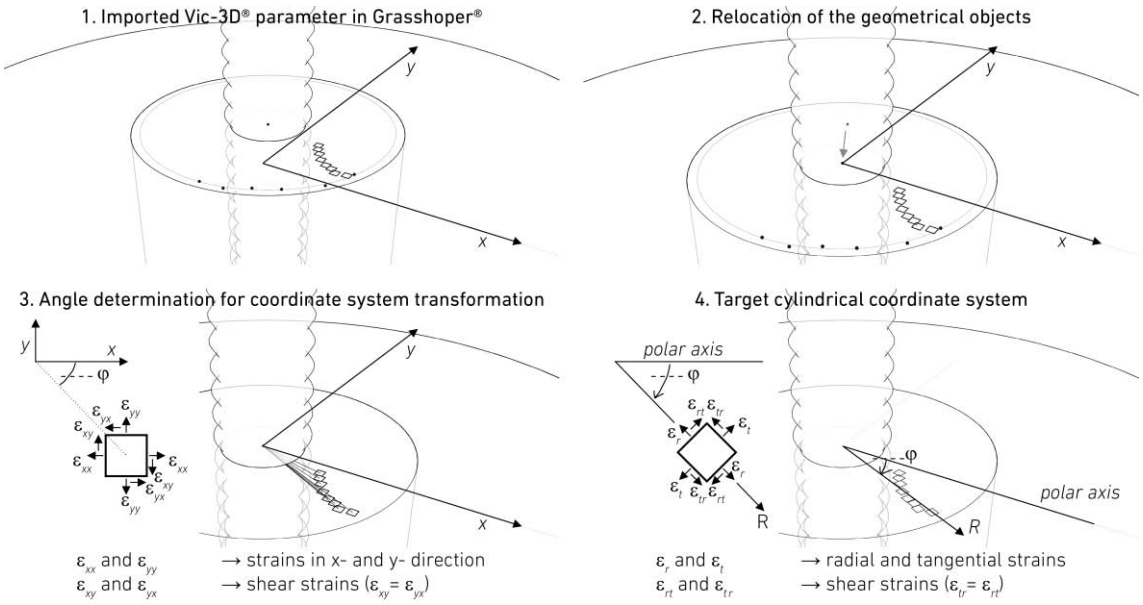

Fig. 4-12 Scheme of post processing and coordinate transformation in Grasshopper®

The final layout (Fig. 4-13, bottom) shows the tangential strain-load distribution with associated curves representing the measuring boxes R1 to R8. In case of missing measuring boxes, the image correlation failed in this area caused by irregularities in the uneven polymer concrete surface. Section A.1.2 summarises the results for the test specimens. The displacement of the measuring points u_{2a} and u_{2b} (Fig. 4-8, left) in longitudinal direction were captured with camera system 1 or 2 and are evaluated and discussed in the end of section 4.2.

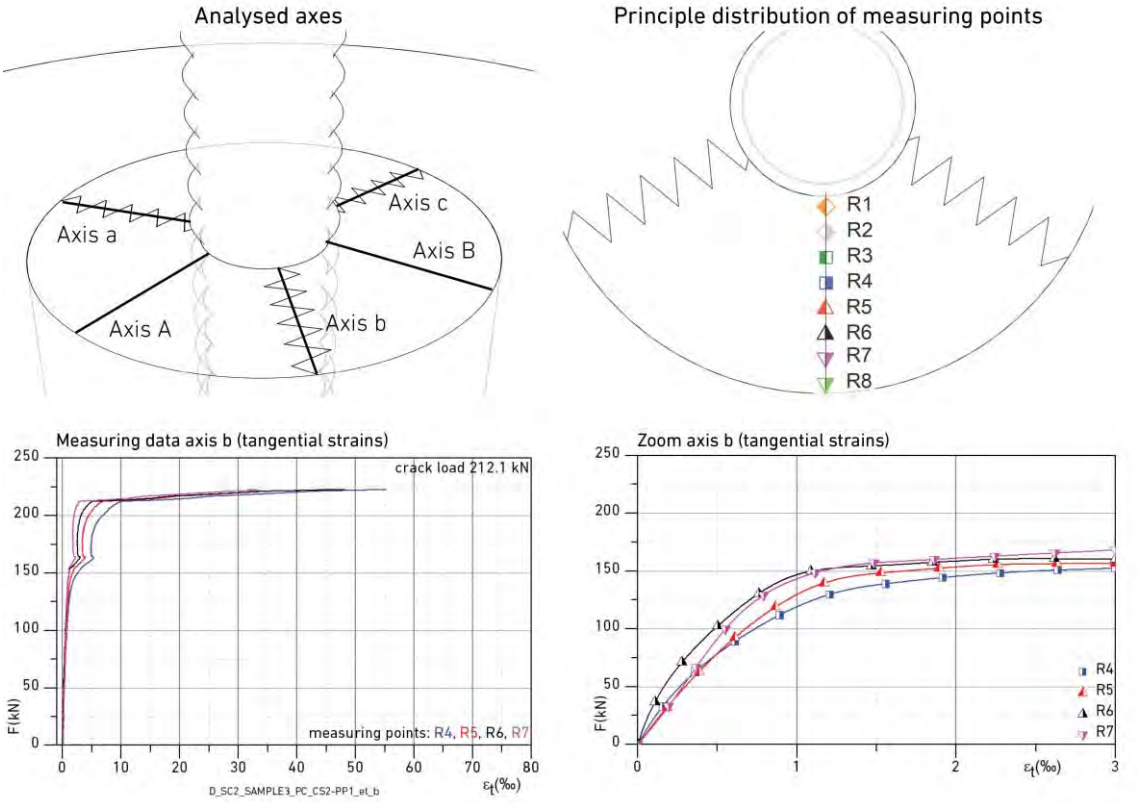

Fig. 4-13 Tangential strains in polymer concrete for sample 3, service class 2

4.2 RESULTS AND DISCUSSION

4.2.1 Failure behaviour of the joint during testing

The LVDT sensor measurement displayed for SC 1 specimens did not record the displacements sufficiently, caused by (i) the circular cross-section of roundwood, (ii) the inhomogeneous behaviour of timber and (iii) eccentricities in the experimental setup.

Tab. 4-2 summarises the failure loads for the test series including nine specimens for each service class. SC 1 specimens failed between 191 kN and 230 kN as a result of a tensile splitting fracture in PC and timber (Fig. 4-14a). All specimens showed the same brittle failure type. The threaded rods embedded in the PC (Fig. 4-14b) showed fracture in the lower part of the connection caused by radial expansion and tensile splitting at the loaded end.

After testing, the specimens were opened to investigate the inclination angle of diagonal struts to the cross-section and the load transfer peak in the grouted joint. For all test specimens in SC 1, a small strut angle of 35° was observed at the loaded end zone, increasing over the embedment length up to 40°. There, shear failure in PC appeared (Fig. 4-14b) caused by radial expansion and tensile splitting at the loaded end (Figure 6, left). The detected strut angles are compliant with the experimental results of DRASS [DRA 2014].

Further test series comparing the influence of climate conditions on the structural behaviour were performed in SC 2 and 3 with the same test setup and material configuration.

SC 2 specimens showed the same tensile splitting failure in PC and timber as in SC 1. Eight of nine specimens failed by tri-axial cracking in PC and timber with a crack distribution of about 120° around the circumference. A slightly different behaviour was observed for sample no. 3, where four cracks in a 90° distribution around the circumference appeared.

The test series in SC 3 confirmed similar tri-axial fracture behaviour for six specimens. Due to a much higher moisture influence on the shear stiffness, the fracture behaviour changed from PC and timber cracking to pull-out joint failure along the bondline (Fig. 4-14c). The overall load-carrying capacity of the connection was not affected by pull-out failure.

Tab. 4-2 summarises the average mean value of the ultimate loads obtained from the experimental testing for each SC to discuss the impact of different climate conditions in the following. The table also provides information on the failure type of each test specimen.

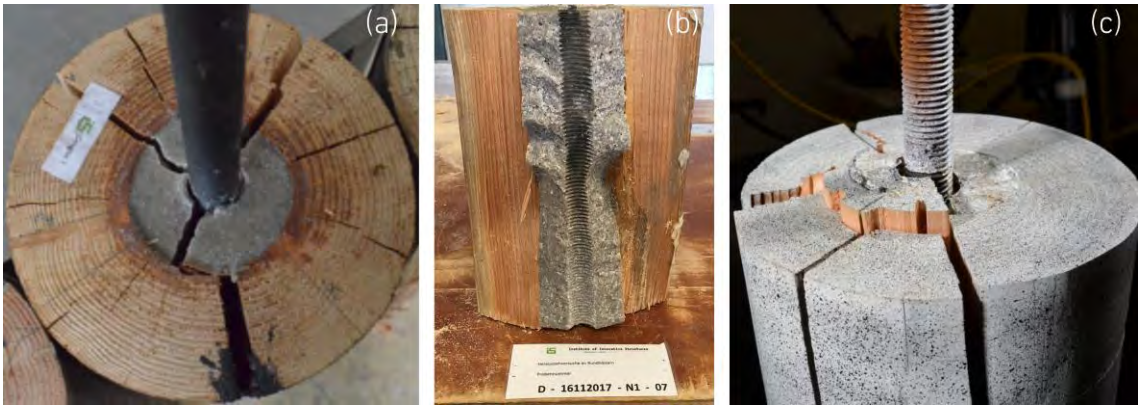

Fig. 4-14 Tensile failure in PC and timber (a), shear fracture in PC (b) and pull-out failure along the bondline

Tab. 4-2 Load-carrying capacity and failure type of test specimens

Service Class	1									
Sample No.	1	2	3	4	5	6	7	8	9	$\bar{x}$
Failure load [kN]	230	205	218	218	209	209	191	206	230	213
Tensile splitting failure	✓	✓	✓	✓	✓	✓	✓	✓	✓	
Service Class	2									
Sample No.	1	2	3	4	5	6	7	8	9	$\bar{x}$
Failure load [kN]	210	X	232	X	240	236	237	215	240	232
Tensile splitting failure	✓	✓	✓	✓	✓	✓	✓	✓	✓	
Service Class	3									
Sample No.	1	2	3	4	5	6	7	8	9	$\bar{x}$
Failure load [kN]	217	X	231	227	231	236	216	239	223	229
Tensile splitting failure	✓	✓	✓	✓		✓	✓			
Pull-out failure					✓			✓	✓	

X – without failure due to the limited capacity of the testing machine (load application of 240 kN for 5 min.)

4.2.2 Investigations on the climate exposure influence

DIC measurement was used to evaluate the crack arrangement in the PC. Ten specimens were fully evaluated, while eight specimens could not be analysed due to irregularities (unevenness) in the polymer concrete surface. Tab. 4-3 shows the crack arrangement in PC with the associated load level for each of the ten specimens, including SC 2 and 3.

The results indicate an impact of the SC on the associated load for each crack (crack 1, 2, 3). The direct exposure to weathering for SC 3, reduced the tensile strength of PC with the result of earlier appearing cracks but with no impact on the failure load of the connection: the cracks occurred in a very small loading range

between approximate 125 and 145 kN for SC 3, except for specimen 2. The earlier occurrence of cracks does not affect the load-carrying capacity of the connection due to the surrounded roundwood, which took over major structural functions in the load distribution as soon as the cracks appear in PC.

In total, three different types of crack arrangement were observed: (i) A simultaneous bi directional fracture followed by one or two further cracks, (ii) a simultaneous tri directional fracture and (iii) a fracture pattern with cracks, which appear one after the other. The first two cracks (initial bi-directional fracture in PC) were fully formed for the mean load of 140 kN for SC 2 and SC 3 specimens with tangential strains between 1‰ and 2‰. The mean load of 140 kN is in line with Eq. 2.3e, presented in chapter 2, for a PC tensile strength of 13 MPa, diagonal strut angle of 40°, bonding length of 250 mm, and rod and drill hole diameter of 24 and 75 mm.

The diversity of the crack arrangement is caused by the inhomogeneous timber material properties with natural pre-cracks in roundwood and an offset of the heartwood. The impact of the wooden irregularities on the crack arrangement in PC is discussed in section 4.2.4. Section A.1.2 provides information on the tangential strains in PC for each evaluated test specimen.

Tab. 4-3 Crack arrangement in polymer concrete for service class 2 and 3 specimens

Service Class		2					
Sample No.		3	4	5	6	7	$\bar{x}$
Load level on first crack	[kN]	143	137	120	137	150	137
Load level on 2nd crack		149	137	134	138	157	143
Load level on 3rd crack		212	162	179	145	165	173
Failure load		232	X	240	236	237	Tab. 4-2
Service Class		3					
Sample No.		2	3	4	7	8	$\bar{x}$
Load level on first crack	[kN]	144	126	111	128	122	126
Load level on 2nd crack		160	132	124	133	131	136
Load level on 3rd crack		183	144	133	137	143	143
Failure load		X	231	227	216	239	Tab. 4-2

X – without failure due to the limited capacity of the testing machine (load application of 240 kN for 5 min.)

For example, the results of sample 5 (SC 2) is used in the following for discussion. Tangential strains were evaluated for multiple axis defined along and between the cracks: Axis b was defined along a radial crack in the PC (Fig. 4-15). The measuring points R2-R6 were arranged outward from the center (see also Fig. 4-13). First cracks appeared at 120 kN, followed by a further crack at 134 kN loading in measure point R6 due to the increase of tangential tensile strains without any

further increase in loading for crack axis b (Fig. 4-16, left). The third crack appeared around 179 kN (Tab. 4-3). Axis B was defined between two radial cracks (Fig. 4-15) to obtain the tangential strain development in the PC. A significant strain drop from approximate 1.25 to 0.5‰ could be observed around 120 kN loading (Fig. 4-16, right). The tensile strain in the PC decreased and remained constant until the specimen failed.

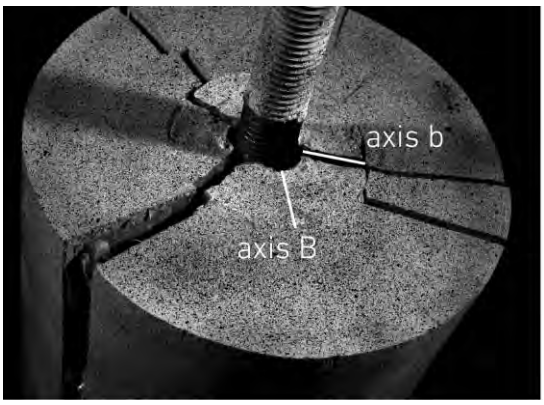

Fig. 4-15 Axes location b and B for tangential strain evaluation in PC (SC 2, sample 5)

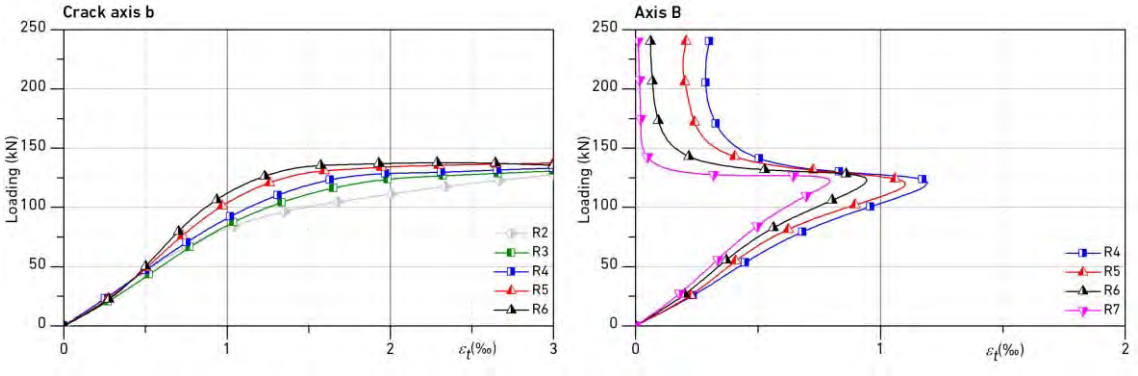

Fig. 4-16 Load-tangential strain behaviour in PC (SC 2, sample 5, axes b and B)

The tensile load-carrying capacity of modified bonded-in threaded rods exposed to outdoor climate in tension was calculated with an increase of approximately 9% compared to indoor climate. In direct comparison, own previous research studies on glulam [SCH 2018] showed a decrease in load-carrying capacity of approximately 10% compared to SC 1 members caused by a reduction in stiffness and strength for specimens exposed to outdoor conditions.

The increase in the load-carrying capacity can be explained by the material properties of PC and roundwood. The specimens for SC 1 were tested one week after the fabrication of the grouted joints in roundwood. According to the product specifications of Compono® 100 S, this time period should be sufficient to reach the full strengths in PC. One reason for the decreased load carrying capacity for SC 1 specimens could be that those information are wrong and the period between fabrication and testing was not long enough to reach full strengths in PC.

In regard to the material properties of roundwood, the specimens for SC 1 and thereafter those for SC 2 and SC 3 were ordered from different suppliers and therefore wood growing and harvesting processes lead to scattering material strengths.

A reduced load-carrying capacity of the connection could not be observed in SC 2 and 3 with multiple failure types in SC 3 test series (tensile fracture in PC and timber, and pull-out joint failure along the bondline). Referring to the application to different climate conditions, no softening of the timber properties could be observed for SC 2 specimens.

4.2.3 Investigations on the embedment influence

After initial cracking in polymer concrete (load level on 2nd crack according to Tab. 4-3), the load-carrying capacity of the connection was dominated by adhesive bond and timber embedment stiffness. The PC expansion was restricted by the surrounded roundwood and the radial compressive strains led into tangential tensile strains in roundwood. After exceeding the tensile strength, cracking occurred in radial direction (sudden brittle failure). Fig. 4-17 shows the evaluation of the longitudinal strain on the timber outer surface, covering the 250 mm embedment length of the grouted joint and the timber section below. Compression strains could be observed in the upper third of the embedment length with 0.4‰, while the lower two thirds showed tensile strains up to 0.6‰. Particular attention shall be paid to the compressive stresses. The crack propagation appeared at the loaded end first and disrupted the cone in opposite direction. The crack increased with the loading. The disrupted PC cone part expanded in radial direction, while timber embedment prevented it from failing. The aforementioned radial strains in timber caused a local bending of wood resulting in compressive strains in the upper third of the bonded zone (Fig. 4-17, strain range -0.5‰ to 0‰), where radial peak stresses appeared at 60 mm embedment length. Section A.1.3 provides information on the longitudinal strains in roundwood for each test specimen.

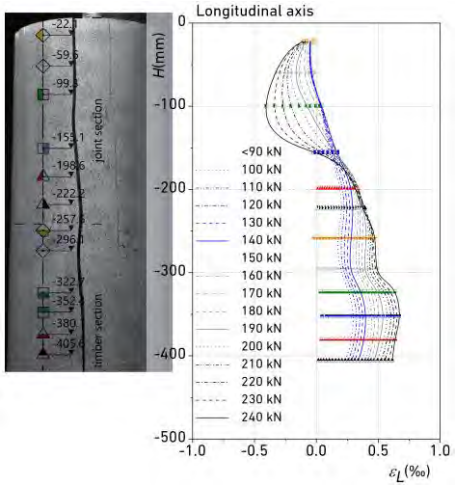

Fig. 4-17 Axis location (left), load-longitudinal strain-behaviour in wood (SC 2, sample 5)

The position of the minimum compressive stresses along the embedment length of the ten analysed specimens (including SC 2 and SC 3) varied from (i) 60 mm to 80 mm (average 67.5 mm) for a load application up to 200 kN, (ii) 60 mm to 95 mm (average 75 mm) for 220 kN loading and (iii) 60 mm to 120 mm (average 90 mm) for 240 kN. At 60 mm embedment length measured from end grain, the maximum load transfer could be observed (Fig. 4-17). Above, the connection did not participate in the load distribution. The load was introduced at 60 mm first, and decreased longitudinally in the direction of the unloaded end.

The longitudinal strains increased between 60 mm and 200 mm embedment for loading up to 150 kN. Thereafter, the strain state was almost constant, indicating that the load transfer to roundwood took place between 60 mm and 200 mm embedment length from the loaded end. For higher stress states with loading larger than 200 kN, the longitudinal strains increased between 60 mm and 250 mm, indicating an enlarged area along the bondline for the load transfer to roundwood.

OPPEL [OPP 2017] and JAHREIS [JAH 2019] investigated the maximum effective bond length of threaded rod in glulam with numerical and experimental models and confirmed an offset of the load introduction in the upper area of 60 mm and an effective embedment length of 200 mm, which is in line with the observed behavior in this study for loading up to 150 kN and also the normative recommendation of bonding lengths.

4.2.4 Investigations on the influence of natural pre-cracks in wood

An important parameter for the usability of the connection is the influence of natural pre-cracks in wood on the load-carrying capacity and the crack arrangement in PC. Pre-cracks had an impact on the radial load transfer from PC to timber (Fig. 4-18, left). They highlight the region with a minimum radial load transfer. The crack pattern started for the majority of the specimens with two cracks (bi-directional crack pattern marked with integer 1 in Fig. 4-18, left). After the bi-directional disruption of the PC, either one or two cracks (marked with integer 2) started to evolve in order to rebalance and align the acting loads. Fig. 4-18 shows four idealised variations of pre-cracks in wood and their effect on the crack arrangement in PC on the assumption of homogenous material properties of the wood, no eccentricity of the rod and no offset of the heartwood. The blue dashed curve shows the radial load transfer in the polymer concrete and timber contact surface. Fig. 4-18 does not include specimens from SC 3. The direct climate exposure led to a much higher degree of pre-cracks in roundwood (section A.1.1: Fig. A-6 vs. A-7), which made the replication of the crack arrangement in PC much more complicated. This confirms the previous stated recommendation to use the connection only in SC 1 and SC 2 conditions, although the load-carrying capacity of the joint was not affected by SC 3 conditions (Tab. 4-2).

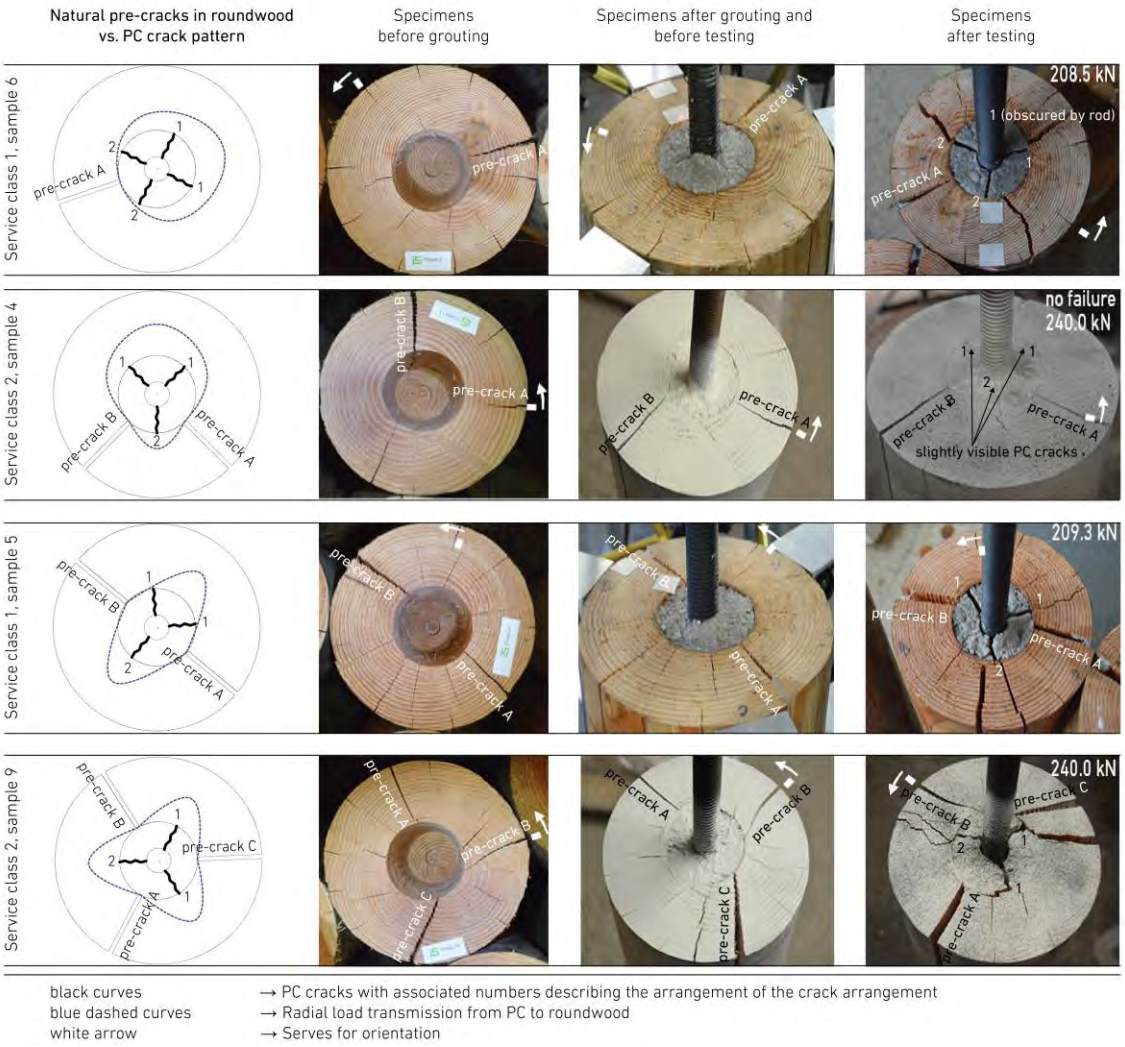

Fig. 4-18 Influence of the pre-cracks in roundwood on the crack arrangement in PC

In total, three parameters were identified in the experimental investigations impacting the crack arrangement in the PC: (i) Inclined position of the rod, (ii) pre-cracks in the wood and (iii) an offset of the heartwood from the center of the log element. The first two cracks in PC appeared on one side of the test specimen next to each other. The next one or two cracks formed on the opposite side of the two initial cracks in order to balance the loads after splitting. An offset of the heartwood from the center of the log affected the load transfer from timber to PC, due to a variation of strength and stiffness parameter along the bondline in the PC-wood contact surface.

All parameters had an influence on the crack arrangement, while the strongly varying material properties within one roundwood specimen made a precise statement about the crack arrangement practically impossible if there was no visual inspection of the specimens before testing. It must be ensured that (i) the pre-cracks in roundwood are limited according to the variations presented in Fig. 4-18 and (ii) the heartwood is located in the drill hole and not outside. The inclination of the steel rod had an impact on the direction of the first two cracks, but had no marked impact on the connection capacity.

4.2.5 Characteristic and design connection capacity for tensile failure

Based on the experimental study on modified (grouted) bonded-in rods, characteristic and design values were calculated according to EN 1990. The approach covers the investigated connection geometry and relies on a statistic evaluation of the tensile splitting failure load in PC and roundwood for 24 specimens (Tab. 4-2). Three out of 27 specimens showed pull-out failure along the bondline and are excluded from the calculation.

s_x^2	$= \frac{1}{n-1}\sum_1^{24}\left(x_i - m_x\right)^2$	*Annex D, eq. D.2*[1]	*(Eq. 4.2a)*
V_x	$= s_x / m_x$	*Annex D, eq. D.3*[1]	*(Eq. 4.2b)*
X_d	$= \eta \times m_x \times \left(1 - k_{d,n} \times V_x\right)$	*Annex D, eq. D.4*[1]	*(Eq. 4.2c)*
X_k	$= \eta \times m_x \times \left(1 - k_{d,k} \times V_x\right)$	*Annex D, eq. D.1*[1]	*(Eq. 4.2d)*

with

s_x^2	*Variance*	200.72	
s_x	*Standard deviation*	14.17	
n	*Number of samples*	24	
V_x	*Coefficient of variation*	0.06	
x_i	*Failure load of sample i*	*Tab. 4-2*	[kN]
m_x	*Average failure load*	223.90	[kN]
X_d	*Design value*	149.91	[kN]
X_k	*Characteristic value*	173.08	[kN]
η	*Factor for model uncertainties*	0.87	*SCH 2012*
$k_{d,n}$	*Design fractile factor*	3.64	*Table D.2*[1]
$k_{d,k}$	*Characteristic fractile factor*	1.76	*Table D.1*[1]

[1] DIN EN 1990:2002 + A1:2005 + A1:2005/AC:2010

Eq. 4.2a and 4.2b show the determination of the variance and coefficient of variation, which are used to calculate the characteristic and design (Eq. 4.2c) value for the load-carrying capacity. The design approach covers model uncertainties, such as scale, volume, material properties or human impact in fabrication with a reduction factor $\eta = 0.87$. This assumption is based on the results of previous research studies [SCH 2012] in which almost homogenous material properties were observed for time shifted PC fabrication processes. The capacity for connection design of the tested specimens (material properties) was calculated to 153 kN (design value) and 174 kN (characteristic value) serving for further analytical design models.

4.2.6 Characteristic and design pull-out capacity along the bondline

Based on the experimental study on modified (grouted) bonded-in rods, characteristic and design values were calculated according to EN 1990. The approach covers the investigated connection geometry and relies on a statistic evaluation of the pull-out joint capacity along the bondline for 3 specimens in SC 3 (Tab. 4-2).

s_x^2	$= \frac{1}{n-1}\sum_1^3 (x_i - m_x)^2$	*Annex D, eq. D.2*[1]	*(Eq. 4.2a)*
V_x	$= s_x / m_x$	*Annex D, eq. D.3*[1]	*(Eq. 4.2b)*
X_d	$= \eta \cdot m_x \cdot (1 - k_{d,n} \cdot V_x)$	*Annex D, eq. D.4*[1]	*(Eq. 4.2c)*
X_k	$= \eta \cdot m_x \cdot (1 - k_{d,k} \cdot V_x)$	*Annex D, eq. D.1*[1]	*(Eq. 4.2d)*

with

s_x^2	*Variance*	64.00	
s_x	*Standard deviation*	8.00	
n	*Number of samples*	3	
V_x	*Coefficient of variation*	0.03	
x_i	*Failure load of sample i*	*Tab. 4-2*	[kN]
m_x	*Average failure load*	231.00	[kN]
X_d	*Design value*	121.63	[kN]
X_k	*Characteristic value*	177.51	[kN]
η	*Factor for model uncertainties*	0.87	*SCH 2012*
$k_{d,n}$	*Design fractile factor*	11.4	*Table D.2*[1]
$k_{d,k}$	*Characteristic fractile factor*	3.37	*Table D.1*[1]

[1] DIN EN 1990:2002 + A1:2005 + A1:2005/AC:2010

Eq. 4.2a and 4.2b show the determination of the variance and coefficient of variation, which are used to calculate the characteristic (Eq. 4.2d) and design (Eq. 4.2c) value for the load-carrying capacity. The design approach covers model uncertainties, such as scale, volume, material properties or human impact in fabrication with a reduction factor $\eta = 0.87$. This assumption is based on the results of previous research studies [SCH 2012] in which almost homogenous material properties were observed for time shifted PC fabrication processes. The capacity for connection design of the tested specimens (material properties) was calculated to 120 kN (design value) and 178 kN (characteristic value). The low design connection capacity underlines the previous stated recommendation to use the connection only for SC1 and SC2 specimens. Here should be noted, that the low design connection capacity is mainly caused by the low number of samples, resulting in an increased design fractile factor.

4.2.7 Comparison of test results with European design rules and previous studies on glulam

Existing design rules of glued-in rods [EN 1995-1-1/NA] were adapted to this study on modified bonded-in rods according to Eq. 2.2. For the following calculation, a modification factor of k_{mod} = 0.8 and partial factor of γ_M = 1.3 were applied covering SC 1 and 2 specimens and a medium load-duration class. In EN 1995-1-1/NA, the connection capacity of a single glued-in threaded rod is defined by the adhesive joint strength $f_{k,1}$, the diameter of the steel rod and the embedment length (Eq. 2.1). The load transfer is assumed as constant along the embedment length with an adhesive joint strength of 4 MPa [EN 1995-1-1/NA/Table 12] matching the timber shear strength according to EN 338 for strength classes larger than or equal to C24. For Eq. 2.2, the diameter of the steel rod was substituted by the polymer concrete cone diameter.

Tab. 4-4 Test results of grouted rods in roundwood vs. EN 1995-1-1/NA

Test results on roundwood specimens[1]		$\bar{x}$	Characteristic	Design
Pull-out failure load	[kN]	231	178	122
Tensile splitting failure load		224	173	150
European Design Rules[1]		-	Characteristic	Design
Pull-out failure load acc. to Eq. 2.2 (grouted rods)	[kN]	-	236	145
Pull-out failure load acc. to Eq. 2.1 (glued-in rods)		-	75	46

[1] Bonding length 250 mm, steel rod diameter 24 mm, drill hole diameter 75 mm, adhesive joint strength 4 MPa

The design value of the pull-out load of 145 kN, calculated according to the German annex of Eurocode 5, exceeds the design value calculated from the test results presented in this study with a difference of approximate 20 %. The results indicate that design rules for glued-in threaded rods cannot be adapted to modified bonded-in rods. In analogy to the research study of JAHREIS [JAH 2019], further experimental investigations with an increased number of test specimens and also varying connection geometries are necessary to conclusively clarify the adaptation of existing design rules on modified bonded-in rods with a modification of the adhesive joint strength as a function of the drill hole diameter and bonding length. The characteristic pull-out load of 236 kN overestimates the characteristic value calculated from the test results as well with a difference of approximately 33%.

Tab. 4-5 summarises the mean ultimate load for pull-out and tensile splitting failure in comparison to previous investigations on glulam with the same connection geometry (diameter, bonding length and polymer concrete type as binder) as in this study. The evaluation clarifies an increased pull-out joint capacity for roundwood members between 30% and 50% compared to DRASS [DRA 2014], OPPEL [OPP 2017] and SCHOBER [SCH 2018]. The load bearing capacity for tensile

splitting failure in timber and PC increases up to 20%. The comparison of the research results for roundwood and glulam members indicate an optimisation of the load bearing capacity for circular cross-sections caused by the 'more homogenous' cross-section with the heartwood in the centre of the logs and regular distribution of heartwood and sapwood.

Tab. 4-5 Test results of grouted rods in roundwood vs. previous studies

Pull-out failure load[1]		Test results	DRASS 2014	OPPEL 2017	SCHOBER 2018
$\bar{x}$	[kN]	231	175	150	156
Tensile splitting failure load[1]		Test results	DRASS 2014	-	SCHOBER 2018
$\bar{x}$	[kN]	224	182	-	189

[1] Bonding length 250 mm, drill hole diameter 75 mm, adhesive joint strength 4 MPa

4.2.8 Slip modulus and equivalent strut stiffness

The description of the non-linearity of the load-displacement behaviour of connections is highly complex and is determined in this section based on the test results of the DIC system. From the load-displacement curve in longitudinal direction, the corresponding slip modulus of the modified bonded-in rods in roundwood (K_{ser}) could be derived as the load divided by the corresponding displacement (Δu_2 in Fig. 4-19). This relative displacement covered the slip in the contact surface between steel rod and PC, and PC and wood. Furthermore, the central load introduction of the applied tensile loads into the roundwood specimens led to a warping displacement of the timber end grain. The displacement (Δu_2) was captured for twelve specimens in SC 2 and 3 with the DIC system, based on the displacement difference in longitudinal direction between measuring point u_{2a} (in the centre) and u_{2b} (in the edge), shown in Fig. 4 8, left.

In order to rate the scale or dimension of the relative displacement Δu_2, displacements of the roundwood (Δu_1) and steel rod (Δu_3) in longitudinal direction were calculated according to Hooke's law for reference lengths of 400 and 500 mm (Fig. 4-19) and are added to the evaluation for direct comparison in section A.1.4.

Fig. 4-20 shows the evaluation of the relative displacement Δu_2 and slip modulus $K_{ser,mean}$ for SC 2 and SC 3 specimens. The slip modulus was calculated for the average load-displacement distribution with reduced values for SC 3 specimens by approximate 10% for the loading range 150 to 200 kN. For lower loading, a decreased stiffness could be observed. Regardless of the SC, the load-displacement behaviour became approximately linear for load of up to 100 kN. At higher load levels the load-displacement behaviour became softer with a non-linear distribution.

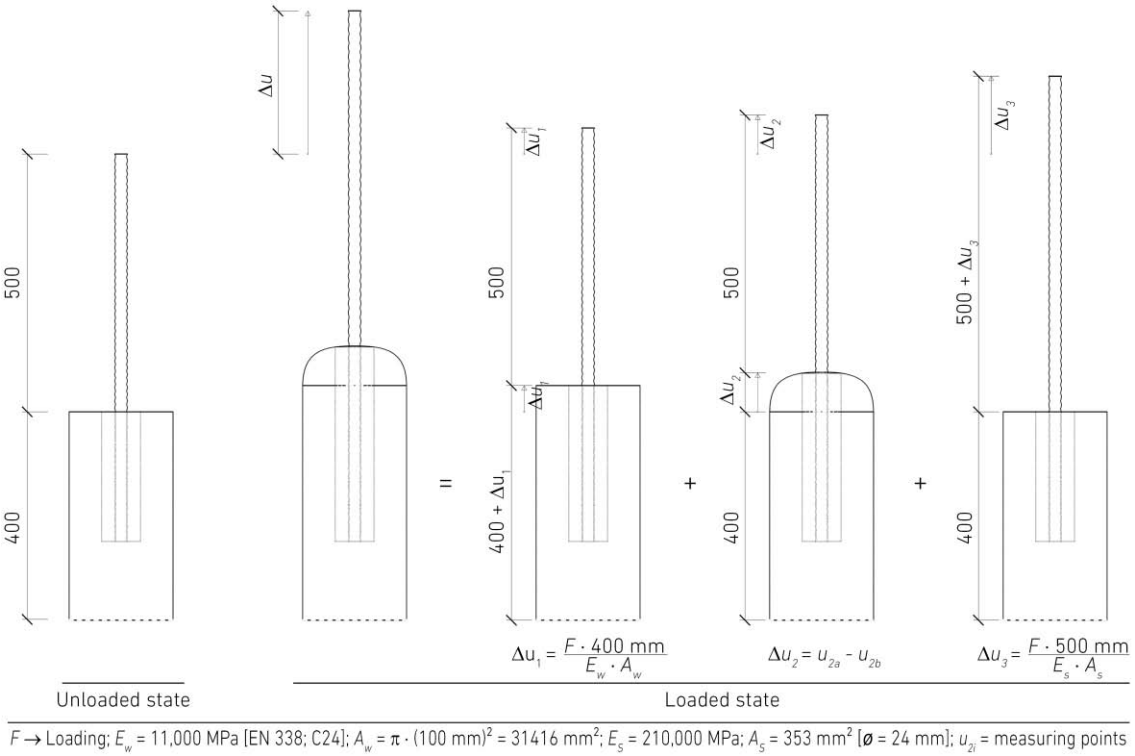

Fig. 4-19 Superposition of relative displacements in modified bonded-in rods for tension

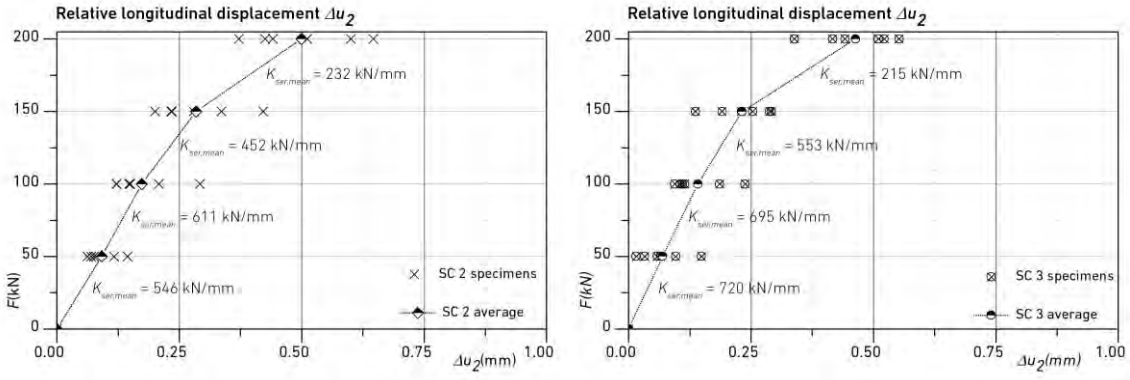

Fig. 4-20 Relative displacement and slip modulus

In the following, the slip modulus was calculated according to the regulations of EN 1380: The test standard defines the determination of the displacement characteristics of connectors with mechanical fasteners in the serviceability limit state and specifies the calculation of the slip modulus for the associated displacement between 10% (23 kN) and 40% (92 kN) of the maximum applied or ultimate load (230 kN). The use of mean values is not recommended in the following because of the high variability in results (Fig. 4-20). Instead, the design with the maximum relative displacement or minimum slip modulus for SC 2 is proposed. SC 3 specimens were excluded due to the fact, that the connection is not used for constructions directly exposed to weathering. Fig. 4-21 shows the evaluation of the minimum, maximum and mean slip modulus for SC 2 specimens according to EN 1380.

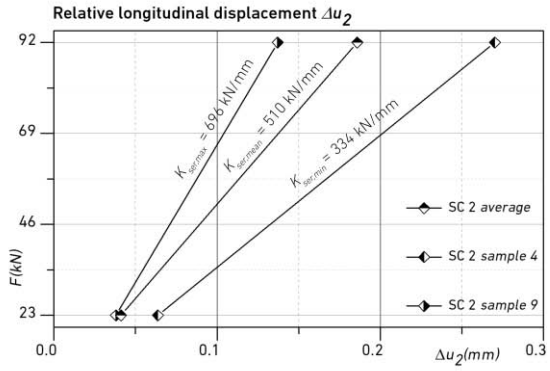

Fig. 4-21 Minimum, maximum and mean slip modulus for SC 2 specimens

The calculated mean, minimum and maximum slip moduli were adapted to roundwood members with grouted rods in both strut ends (Fig. 4-22) to discuss the impact of K_{ser} on the strut member stiffness. The diameter and strength class of wood and steel were chosen according to the investigated specimens in section 4.1.1 with a variation of the roundwood length and overhang length of the rod. The roundwood and rod stiffness, as well as slip modulus were considered as springs connected in series with a superposition of the relative displacements according to Fig. 4-22. The equivalent stiffness was calculated according to Eq. 4.3c. Four cases are evaluated in the following to determine the impact of the slip moduli on the equivalent stiffness of the strut members: (i) $K_{ser} = \infty$, (ii) $K_{ser} = K_{ser,max}$, (iii) $K_{ser} = K_{ser,mean}$ and (iv) $K_{ser} = K_{ser,min}$.

$$K_1 = \frac{E_w \cdot A_w}{L_w} \qquad \textit{(Eq. 4.3a)}$$

$$K_3 = \frac{E_s \cdot A_s}{L_s} \qquad \textit{(Eq. 4.3b)}$$

$$K_{equiv} = \frac{1}{\left(\frac{1}{K_1} + \frac{1}{2 \cdot K_{ser}} + \frac{1}{2 \cdot K_3}\right)} \qquad \textit{(Eq. 4.3c)}$$

with

K_1	*Stiffness of roundwood*	
K_3	*Stiffness of threaded rod*	
K_{ser}	*Slip modulus*	
K_{equiv}	*Equivalent stiffness of strut member*	
L_w	*Roundwood strut length*	*Parameter 1*
L_s	*Threaded rod overhang length*	*Parameter 2*
E_w	*Timber modulus of elasticity [EN 338, C24]*	11,000 MPa
E_s	*Steel modulus of elasticity*	210,000 MPa
A_w	*Roundwood cross-section area*	31416 mm^2
A_w	*Threaded rod cross-section area*	353 mm^2

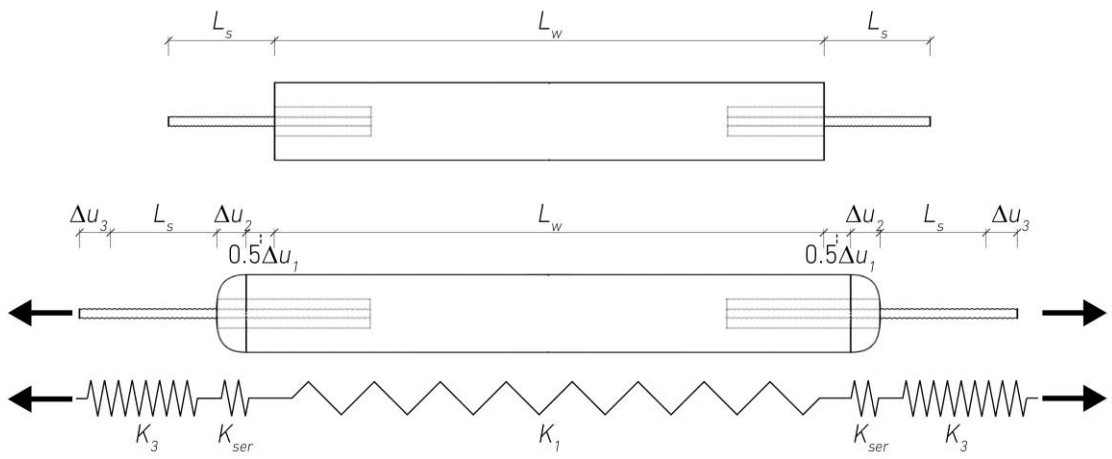

Fig. 4-22 Calculation of the strut member equivalent stiffness

Fig. 4-27 shows the equivalent stiffness comparison or ratio for the maximum and minimum determined slip moduli with a deviation of approximate 10% for roundwood strut lengths smaller than or equal to 3000 mm. For larger strut lengths, the impact of the slip moduli on the equivalent stiffness was strongly reduced to 5% or even less. Roundwood strut lengths between 1000 mm and 2000 mm with rod overhang lengths smaller than 300 mm had to take an increase of approximate 15% into account. For the upcoming design of the truss structure in the serviceability limit state, the minimum slip modulus will be applied to ensure a safe calculation and to avoid an underestimation of the overall truss displacement.

Fig. 4-28 clarifies the enormous impact of the slip modulus on the equivalent stiffness (or deformability) and describes the ratio for strut members with $K_{ser,\infty}$ and $K_{ser,min}$. The evaluation takes the stiffness of the wood and the steel in the connection into account for different applied roundwood strut member and rod overhang lengths. Roundwood strut members with lengths between 2000 and 3000 mm showed an increased ratio between 12 and 24% percent. Further information for other roundwood or steel lengths can be obtained from Fig. 4-23 - Fig. 4-28. The evaluation underlines that for the upcoming application of the joining technology in 2D truss structures, it is important to take the slip modulus and therefore decreased equivalent strut member stiffness into account.

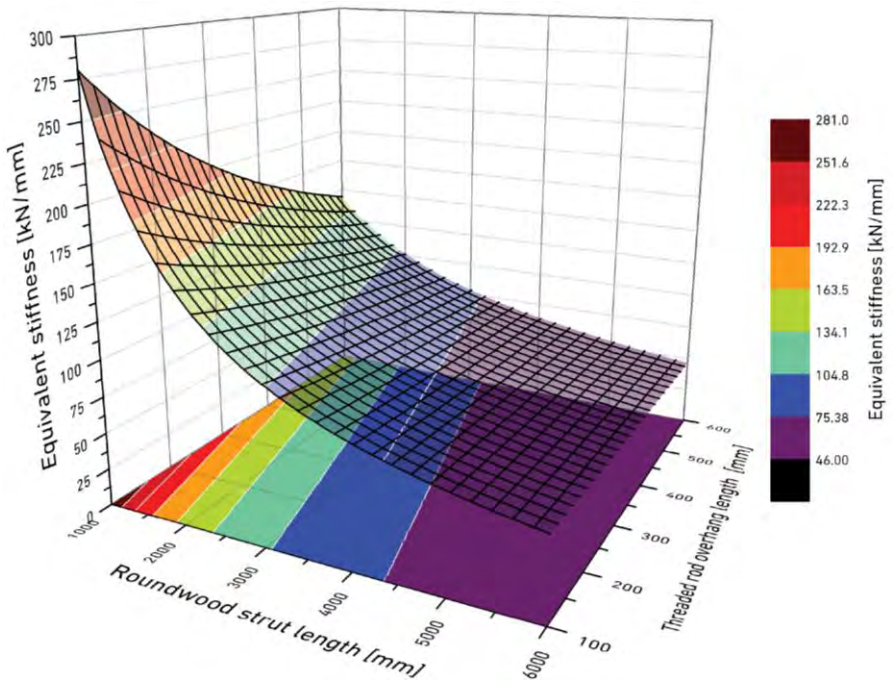

Fig. 4-23 Equivalent stiffness of roundwood strut members with grouted rods for $K_{ser,\infty}$

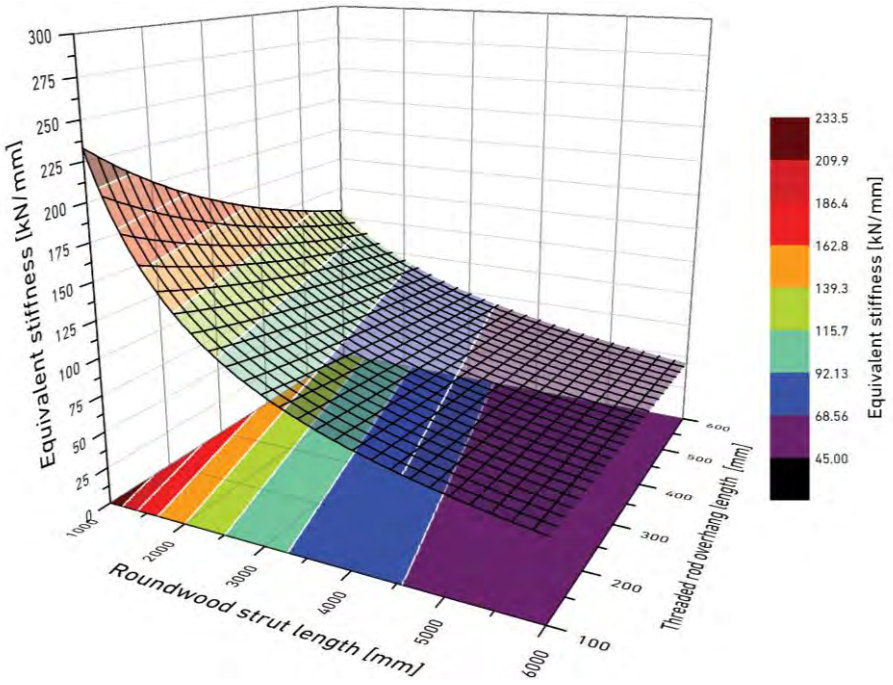

Fig. 4-24 Equivalent stiffness of roundwood strut members with grouted rods for $K_{ser,max}$

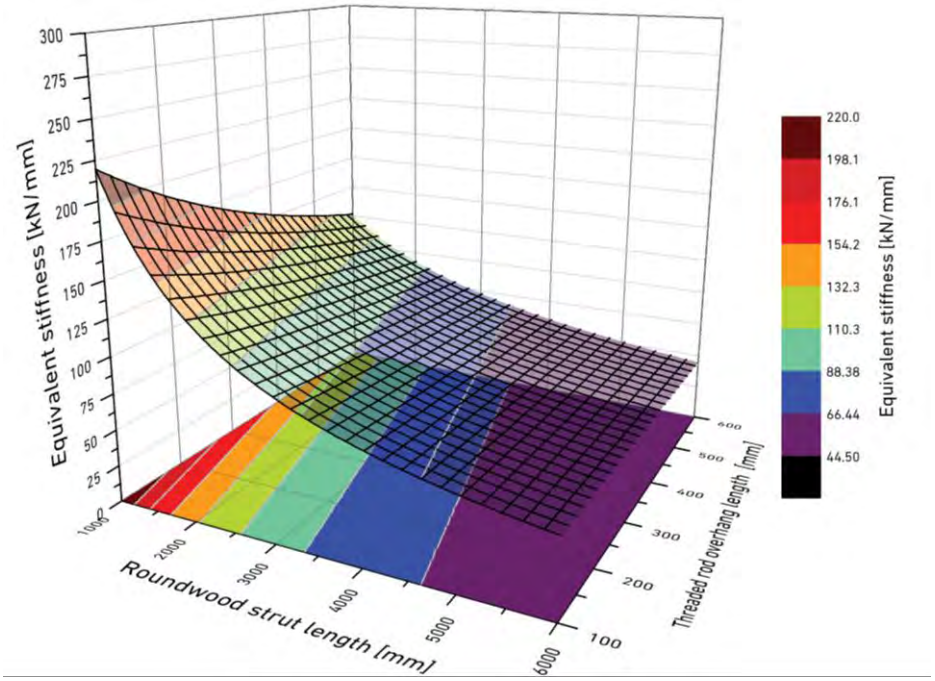

Fig. 4-25 Equivalent stiffness of roundwood strut members with grouted rods for $K_{ser,mean}$

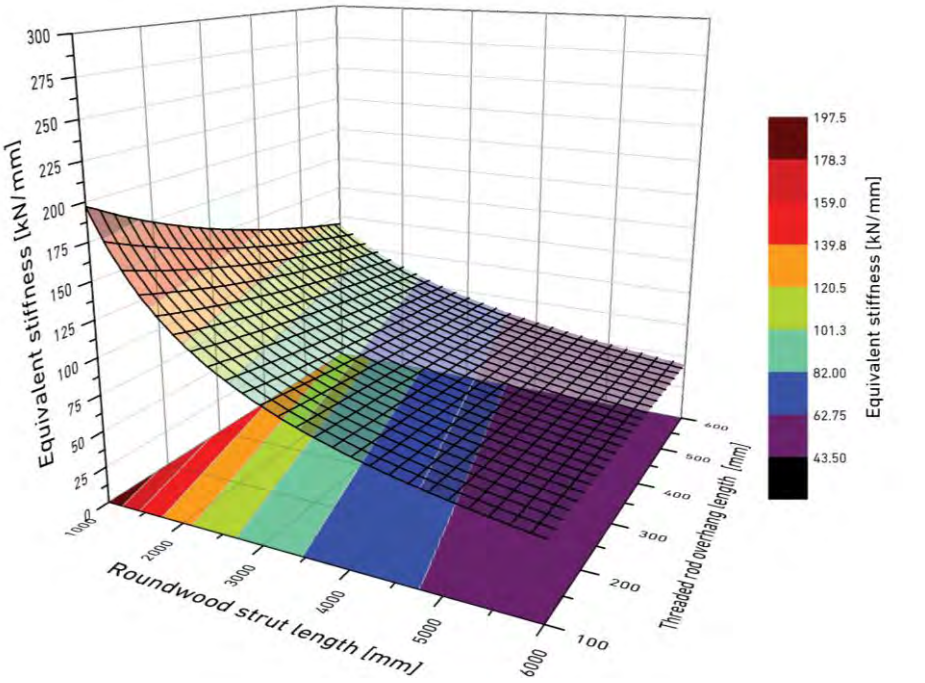

Fig. 4-26 Equivalent stiffness of roundwood strut members with grouted rods for $K_{ser,min}$

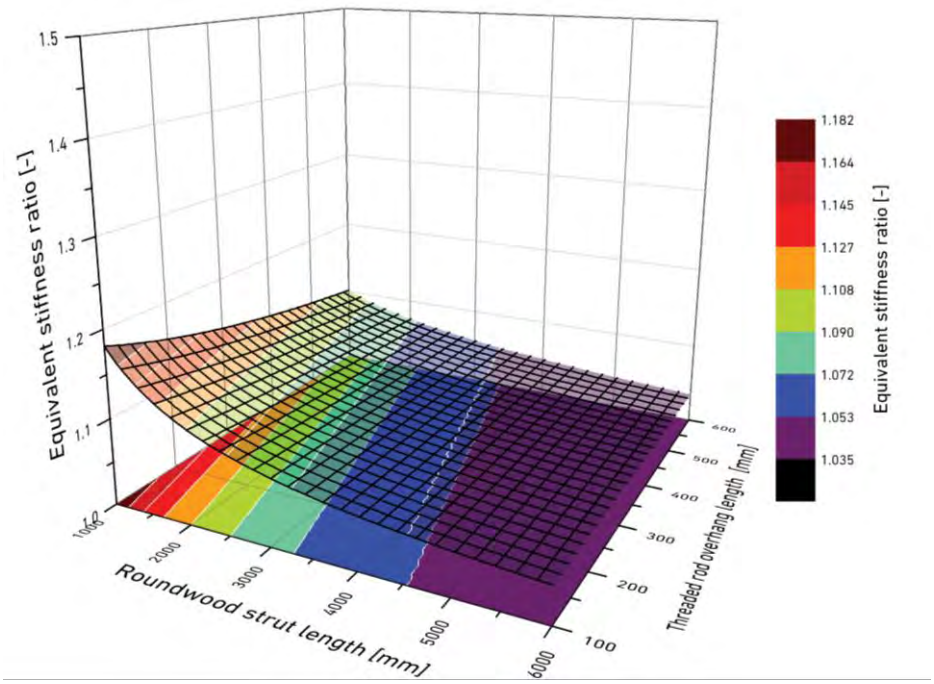

Fig. 4-27 Equivalent stiffness ratio between $K_{ser,max}$ and $K_{ser,min}$

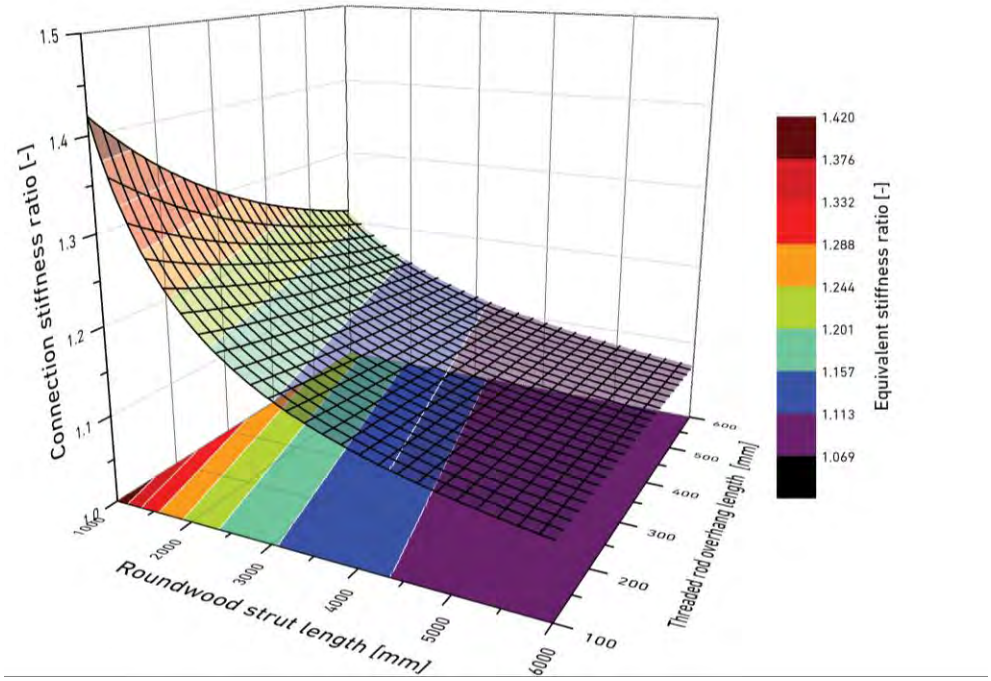

Fig. 4-28 Equivalent stiffness ratio between $K_{ser,\infty}$ and $K_{ser,min}$

4.2.9 Conclusions

Objective of the experimental investigation on the pull-out strength of modified bonded-in rods was the structural assessment of this new technique under different service conditions for structural roundwood. In contrast to 'classic' glued-in rods, the adhesive bond between threaded rod and wood was achieved by a much larger bondline thickness and polymer concrete as adhesive. The design load of the connection capacity of ~150 kN has been calculated from the test results and triples the connection capacity on the design level of glued-in rods, which can be calculated to ~46 kN (for the same steel rod diameter, strength class and bonding length). The normative tensile design load parallel to grain of C24 roundwood members (diameter 200 mm) can be calculated to 280 kN, which is 1.85-times the connection capacity of the test specimens. Therefore, the connection reveals potential for optimisation in further studies.

Referring to the application to different climate conditions, no degradation of the timber properties was observed for SC 2. An uniform or predictable failure mode is essential for the implementation of the technology in practice. For this reason, the connection should only be applied to SC 1 and SC 2 structural members. The variation in failure modes for SC 3 samples showed the complexity of timber structures exposed to direct climate conditions. In direct comparison, 'classic' glued-in rods are only allowed for SC 1 conditions. From the conclusions of this thesis, exposure to SC 3 is not recommended and must be investigated in further research.

Based on the experimental investigations, natural pre-cracks in roundwood for SC 1 and 2 do not affect the functionality or the load-carrying capacity under tensile loading. A visual inspection of each specimens should be done before grouting with (i) natural pre-cracks in roundwood limited according to the variations presented in Fig.4- 18 and (ii) a heartwood location within the drill hole area. The maximum stress peaks were observed at 60 mm embedment length from the loaded end. There, steel sleeves will be attached in further studies for confining the roundwood members and to take over the tensile loads in tangential direction analogous to the structural function of ring reinforcements. This modified approach might be the solution for increasing the load bearing capacity up to the tensile design load parallel to grain.

Grouted rods ensure a simple roundwood fabrication with no modification of the circular cross-section and no computer-aided support. The connection requires only one drill hole in the timber end grain with the additional benefit of using either cylindrical milled roundwood (constant diameter along the strut axis) or natural grown roundwood (only removed bark and bast layers) as strut members. The easy fabrication enables an access for traditional craft businesses, even without computer-aided competences. The determined equivalent stiffness of roundwood strut members and load bearing capacity for SC 1 and SC 2 specimens serve for the design of the truss structures in the following chapter.

MOULDED JOINING TECHNOLOGY IN 2D TRUSSES

5

The main objective of this thesis was the development of moulded joints for 2D trusses with modified bonded in rods in roundwood, presented in chapter 4. So far, the investigated connection in roundwood ensures (i) an aesthetic appearance with no visible drill holes, (ii) a high load bearing capacity compared to 'classic' glued-in rods and (iii) an exposure to service class 1 and 2 climate conditions with no impact of natural pre-cracks in roundwood on the load bearing capacity. The next step was the development of moulded joints in the intersection. The specific objectives for the joint and truss design are illustrated in Fig. 5-1.

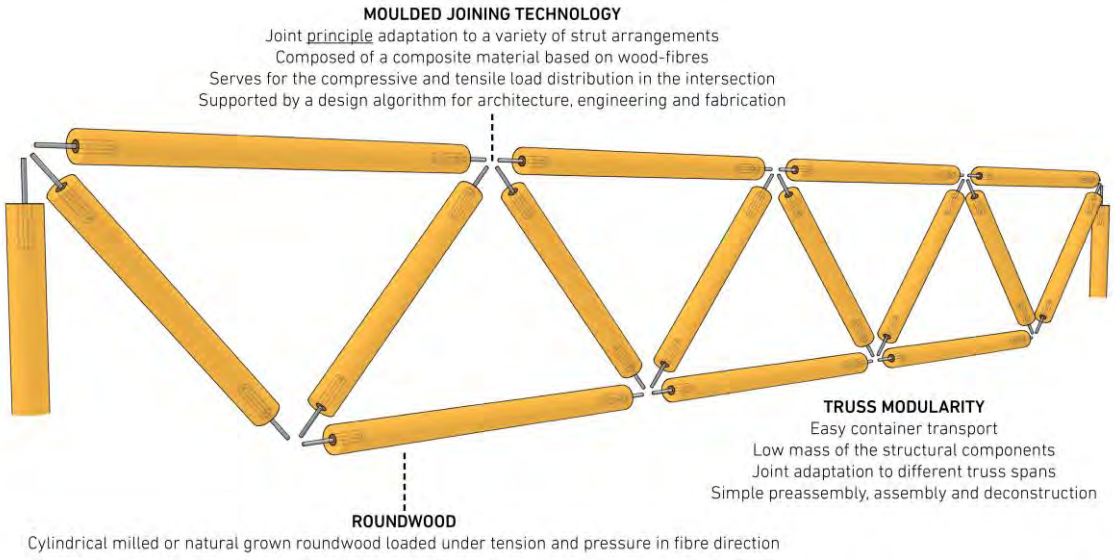

Fig. 5-1 Specific objectives for the moulded joint and truss design

The aforementioned joints for 3D trusses (section 2.5) represent the basis of the new joining technology and were developed further in structure and materiality to serve for modular 2D trusses. The structure of this chapter provides

- the design principle/function assessment of the joints (form finding),
- the development of a generative design algorithm for the digitally manufactured joining technology and truss structure (Parametric Design),

– the assessment of the structural behaviour of the joints for different applied composite materials (Structural Analysis) and
– the development of a composite material based on wood fibres and epoxy resin, including experimental investigations and the fabrication of a joint prototype.

5.1 FORM FINDING AND DESIGN ALGORITHM

5.1.1 Methods

The first part of this section covers the form finding process and algorithm development for modular 2D trusses including the design of moulded joints in the intersection. In this context, the design principle and function assessment of the joints had to focus on how to transmit compressive and tensile loads in the intersection and how to ensure an easy pre-assembly, assembly and deconstruction with no grouting process. The second part of this section focuses on the design of a design algorithm for modular 2D trusses in flat roof structures with modified bonded-in rods in roundwood and moulded joints in the intersection. The aim was to eliminate disadvantages of conventional design methods, such as iterative workflows, erroneous pre-designs, non-optimised structural performance capacities or high workloads with the creation of an automated digital value-chain for multiple CAD- and FEM-ready solutions. Considering the design of the joints in the intersection, parameter related to architecture, structural performance and assembly needed to be controlled and developed interdependently from each other. For this reason, the developed algorithm aimed to provide

– an automated architectural and structural design of joint and truss variations
– and an efficient design optimisation.

Preliminary research studies in the field of parametric design algorithm for 2D truss systems were performed by plenty of researchers, e.g., BENNETT [BEN 1978], KAWAMURA [KAW 2002], or RICHARDSON [RIC2012]. They developed algorithms focusing on a truss topology optimisation based on an interaction of architecture and engineering. The research studies were strongly limited to form finding processes of global truss designs depending on different load combinations. The first parametric design algorithm for polymer concrete moulded joints was developed by WEBER [WEB 2016]. In this case, a parametric CAD model was created to design the architectural shape of the joints with no implementation of structural performance. First parametric algorithms, combining local and global design processes in architecture and engineering were introduced in own preliminary work for the *World Conference on Timber Engineering* and further publications [CHA 2018 & 2022a]. The algorithm, named Interactive Structural Design algorithm (i-SD^{BIM}), was adapted to hyperbolic grid shell structures composed of roundwood strut members and spatial moulded joints.

Structural design has changed over the decades. In the 19th century, master builders merged the responsibilities of engineers and architects. During that period, both fields progressed with the focus on art and technique. Moreover, the present digitalisation of our environment has shifted the profession once again and has created the field of Parametric Design and Engineering, where engineers adapt the main themes of architecture and computer science. Contemporary software technologies will change the way of structural design, as well as the possibility for engineers to build smarter, cheaper and more efficiently.

Parametric modelling

Compared to general available Computer Aided Design (CAD) software, parametric methods do not define or design fixed geometries. They rather create a dynamic model with different types of parameters. Changing those parameters results in a different structure. An alternative appearance can be generated immediately without setting up a new structural model. The parametric software Grasshopper® was used in this thesis for the design of modular 2D trusses with the possibility to link topology, shape and structural behaviour by implemented finite element tools, e.g., Karamba3D®. Grasshopper® is a visual programming language and environment for the CAD application Rhinoceros®. Fig. 5-2 shows the interfaces of Grasshopper® (left) for programming and Rhinoceros® (right) for visualisation.

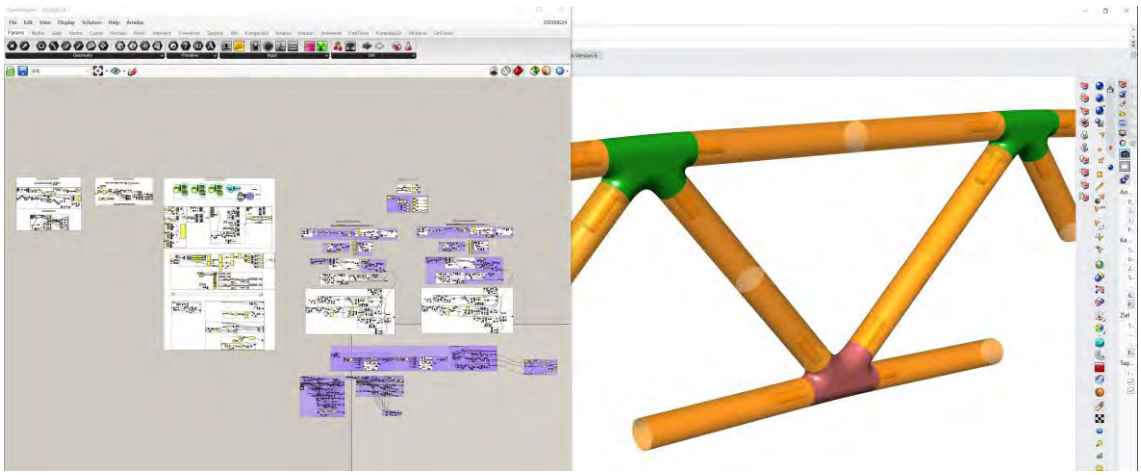

Fig. 5-2 Used software: Interfaces of Grasshopper® (left) and Rhinoceros® (right)

The modelling in Grasshopper® is done by drag and drop of components onto the canvas, which provide inputs and outputs for the connection of previous and subsequent components. Karamba3D® is a parametric structural engineering tool for the analyse of spatial trusses, frames, and shell structures. Karamba3D® is fully integrated into the parametric design environment of Grasshopper®. This facilitates the combination of parameterised geometric models, Structural Analysis and optimisation. Compared to existing BIM applications with the focus on an optimisation of information exchange, parametric modelling merges different design steps of architects and engineers in one common interface.

Workflow in parametric modelling (generative design)

Generative design is an iterative design process in which a program creates a set of outputs that meet certain constraints, and a designer fine-tunes the feasible region by selecting specific outputs or modifying input values and ranges. It is a method for exploring design possibilities that is used in multiple design fields, including art, architecture, communication design, and product design. The use of digital computers, coupled with the ability to explore a large number of options, allows designers to generate and test new options, beyond what a human alone could achieve, to arrive at an optimal design.

With new programming environments and scripting capabilities, it has become relatively easy for designers with little or no programming experience to implement their ideas via generative design. With respect to the profession of architects and engineers, generative design allows the potential of exploring a much broader solution space of typologies, shapes and characteristics related to the structural behaviour, fabrication and assembly of constructions. As the design processes in architecture and engineering are often incomplete, difficult to define, and interdependent, solving problems calls for a deep understanding of the involved parameter. Generative design can solve and address design problems efficiently, by defined rules to generate complex solutions. A specific example related to modified bonded-in rods in roundwood (chapter 4) is the variable equivalent strut member stiffness depending on the roundwood and overhang threaded rod length. Generative design enables to program or define the strut stiffness depending on the truss typology and is automatically adjusted for each iterative process and each strut member without manual readjustment.

The iterative process provided by computer software allows the trial-and-error approach in design and involves architects and engineers in the optimisation process. A 'classic' example of a precedent work is the Sagrada Familia, which was designed by the Catalan architect Antoni Gaudí and used rule-based geometrical shapes for structures [HER 2006]. Other examples include Foster and Partners' Queen Elizabeth II Great Court, where the tessellated glass roof was designed using a geometrical schema that defined hierarchical relationships, and then the generated solution was optimised to meet the geometric and structural requirements [WIL 2011].

Fig. 5-3 shows the general workflow in parametric modelling, starting with the idea to link or network different design steps in one common interface in order to create a powerful digital value chain for the design of modular 2D trusses in roundwood. The strategy describes a sketch, simply on a piece of paper, with information on the content and scheme of the algorithm (What's the algorithm supposed to do?). The most important and complex part is the formalisation of the source code including all operators, parameters and especially the determination of the parameters dependencies to each other. After finalisation, the feedback in form of a live image simulation needs to be evaluated and optimised by the designer

(architect and engineer). In case of no functionality of the algorithm, the strategy has to be changed. In case of minor failures, the source code needs to be adapted to reach full functionality of the algorithm. After successful completion, the designer can start with the optimisation of the structure by changing parameter step by step (iterative) and an evaluation of the results based on the feedback. The modelling is done after full optimisation by the designer. In summary, generative modelling means that the computer and designer work hand in hand: the computer is the driving force and generates a number of construction variants in no time, while the designer evaluates the feedback, optimises the results and chooses from the plenty construction variants the 'best' one.

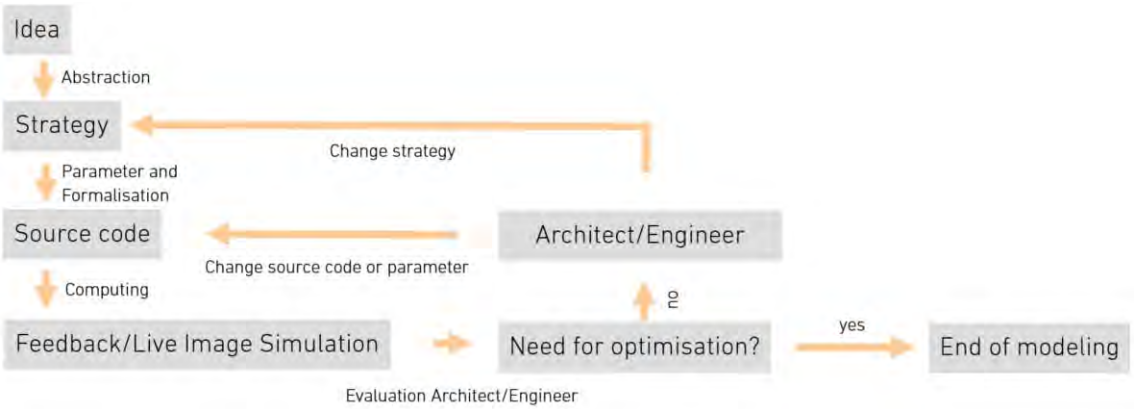

Fig. 5-3 Workflow in parametric modelling (generative design)

Idea, strategy and parameter

The idea of the algorithm focused on the creation of a digital value chain for the architectural and structural design of the digitally manufactured joining technology and modular 2D truss structure. The challenge here was to merge several design fields in one common interface, taking account of all the relevant parameters and their dependencies to each other, and to model and optimise different variations by mouse-click. The algorithm should not be only considered as an innovative feature next to the physical developed joining technology. In fact, it was necessary to develop the joining technology this way in order to control the high amount of parameters, covering architectural, structural and assembly dependencies in local and global.

The strategy was based on the creation of a merged design interface covering (i) the architectural design of the truss roof structure, (ii) the structural design of the truss structure and (iii) the architectural design of the moulded joints in the intersection serving for further export to FEM (section 5.2) and CAM (section 5.4) processes. The interaction was done in module 4 and provided a dynamic digital plan (live image simulation of architecture and engineering) with all information needed for the designer. Hereby, it was important that all information were visible at a glance in one plan, such as the results of the FE modelling or information

related to the assembly space. The strategy and parameters related to the truss design are shown in Fig. 5-4. Parameter dependencies as well as parameter of the moulded joints are addressed in section 5.1.2 in full. The materiality and geometry of the investigated roundwood test specimens with grouted rods (chapter 4) were adapted to the design algorithm in order to detect the application possibilities in 2D trusses. Other geometries were neglected due to missing information on the load bearing capacity of the modified bonded-in rods.

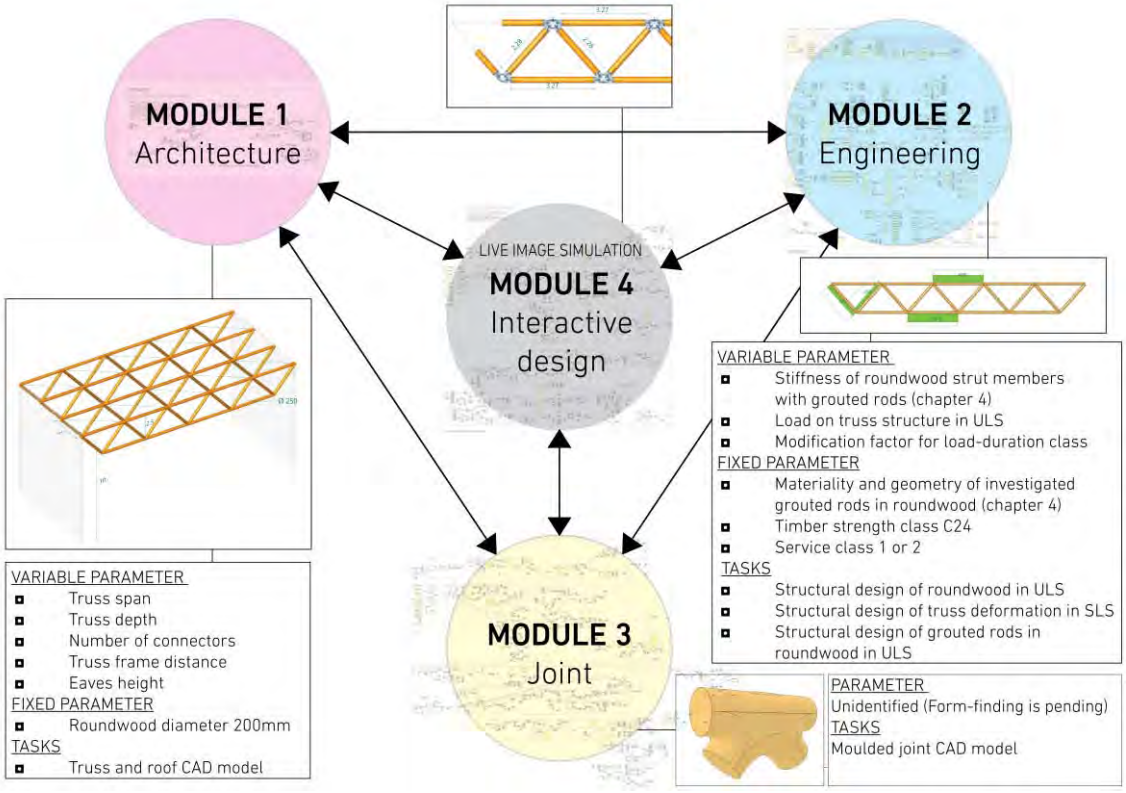

Fig. 5-4 Algorithm strategy and parameter

Next to the definition of the parameter dependencies and the source code, the algorithm should provide information on fitness parameter for the optimisation process and on truss mutations for excluding unwanted results from the large number of design options. The mass of roundwood and moulded joints should describe the fitness parameter in the design process and should reach a minimum in order to optimise the ecological footprint of the new joining technology. To avoid truss mutations, an integrated algorithm-penalty for architecture, structural performance and assembly should be taken into account with a visual error message in the live image simulation. From an architectural point of view, the roundwood strut members including embedded rods should not exceed six meters to ensure an easy container transport. In regard to the structural performance all structural design requirements for local and global truss members should be taken into account with an exclusion of truss mutations, which were not withstanding the actions on the structure. This included the design of roundwood strut members and the connection design in roundwood (modified bonded-in rods).

5.1.2 Results and discussion

Assessment of the joint design principle and function

The moulded joint was developed and designed in regard to an efficient load distribution (for tension and compression) and an easy pre-assembly, assembly and de-assembly. From a structural point of view, the solution had to perform a balancing act to reconcile the needs of the load distribution with those of the assembly process. The design approach envisaged a hybrid connection composed of an inner steel structure and an enveloping moulded material with a coupled load distribution. To load each structural member according to its high material strengths, it was aimed that the moulded material served for the compressive load distribution and that the inner steel structure served for the tensile load distribution.

A truss typology with only diagonal struts between the chord members was chosen for the design in this thesis to keep the material mass of the moulded joint as low as possible. The volume of the joints increases with decreasing angle between the roundwood members in the intersection. Therefore, variations with vertical posts in addition to diagonal struts were not investigated. However, the design principle should ensure an adaptation to any strut arrangement in the intersection.

Modified bonded-in rods in roundwood can only transfer compressive and tensile loads in timber fibre direction. In order to guarantee this and to avoid bending moments in the upper chord, the loads had to be introduced into the joints with no load introduction along the circular cross-section of the roundwoods.

Different types of moulded joints composed of an inner steel structure and enveloping moulded material were designed and compared with the defined objectives. The field joint with four strut members serves as example for the form finding process in the following.

Type 1 (Fig. 5-5a) describes a connection with eye terminals at the ends of the modified bonded-in rods, which are joined to a steel plate with bolts. To provide access for assembly, the joint is split into two parts, wherein the steel plate is casted into one of the moulded joint parts. The half-section, including steel plate, is connected to the eye terminals by bolts and is subsequently covered with the second section. The system offers an easy assembly and accessibility. Due to the fact, that the outer moulded joint is only used as a non-load-bearing cover, type 1 was neglected for further study.

Type 2 (Fig. 5-5b) describes a connection of fork terminals at the ends of the modified bonded-in rods, which are joined with a bolt in the centre of the moulded joint. The connection design provides for efficient load distribution in the intersection with no offset of the acting strut loads to the centre of gravity and therefore without bending moments. The inner steel structure consists of different steel components, does not allow an adjustment in the assembled state and requires large dimensioned fork terminals and bolts due to the high embedding

stresses in the contact region between bolt and forks. The moulded joint is divided also here into two parts to provide accessibility for assembly and serves only as a non-load-bearing cover. Type 2 was neglected for further study.

Type 3 (Fig. 5-5c) consists of eye terminals or nuts in the chord or diagonal strut members. The eye terminals and nuts are joined to a turnbuckle with holding bridge in the centre of the joint. The one-piece moulded joint has a side opening for the assembly of the strut members. For this purpose, a mounting rod can be inserted through the opening into the turnbuckle in the first step. Subsequently, the entire steel structure can be pre-stressed by a rotation around the gravity axis of the mounting rod. Tensile loads in the lower chord members are directly transmitted by the inner steel structure. In case of acting compressive loads, the moulded material takes over the load distribution. Disadvantages are non-standardised steel components and a limited load bearing capacity for transversal loads in the turnbuckle. In order to guarantee a coupled load distribution for compression and tension, the side opening must be grouted after assembly, thereby preventing a de-assembly of the structure. For these reasons, type 3 was neglected for further study.

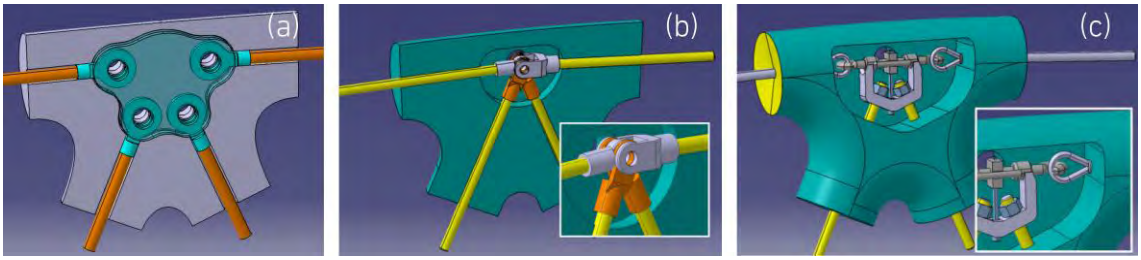

Fig. 5-5 Discarded moulded joint types (form finding process)

Type 4 (Fig. 5-6a) shows the design of a one-piece moulded joint with side opening and an inner frame structure, which is grouted into the outer moulded joint with a coupled load distribution and separate load introduction mechanisms for compression and tension. The modified bonded-in rods in roundwood are placed through the front sides of the moulded joint, while the final assembly occurs via the side opening. For this purpose, only washer and nuts are required to connect the strut and joint elements. The frame structure and enveloping moulded material are loaded according to their high material strengths: In case of compressive loads, the threaded rods including the nuts move towards the centre of the joint and the load introduction appears in the intersection surface between the front sides of the outer moulded joint and the end grain of the roundwood (Fig. 5-6b), whereby the moulded material is mostly loaded under compression. In case of tensile loads, the load is applied into the frame structure, stressed on bending (Fig. 5-6c). For a practical implementation, the dimension of the frame structure must be large enough to enable an assembly of the nuts with spanners. On the other hand and from a structural point of view, the dimension must be minimised as much as possible to reduce bending moments in the frame structure.

The joints in the upper chord provide an even support area for the purlins, such as steel profiles (Fig. 5-6a). The load introduction here follows the idea of an ideal truss resulting into normal forces without bending in the strut members. The shifted purlin support from the roundwood members in the upper chord to the joint eliminates the assembly problem from flat to circular and enables also varying diameters along the strut axis, common for natural grown roundwood.

Type 4 was chosen for the final joint design, due to an efficient load introduction for compressive and tensile loads, standardised and low-cost steel components (steel rods, nuts, washers) and an easy assembly and de-assembly through the side opening.

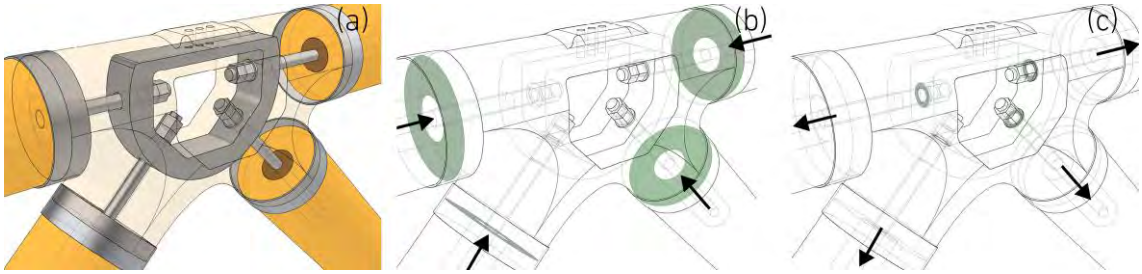

Fig. 5-6 Moulded joint (a) and load introduction for compression (b) and tension (c)

Three different moulded joint types needed to be developed for the illustrated truss typology in Fig. 5-1 depending on the strut arrangement in the intersection:

– The field joint in the upper and lower chord (Fig. 5-6) to join two diagonal strut members and two chord members.

– The edge joint in the lower chord (Fig. 5-7) to join two diagonal strut members and single chord members.

– The support joint in the upper chord (Fig. 5-8b) to join the truss structure with the column (boundary support of the truss structure).

The assembly concept of the modular truss structure aims to keep the degree of pre-assembly as high as possible with triangular modules to reduce the construction time on site. Construction components are initially positioned with an offset to the triangle centre of gravity (Fig. 5-7a) and are simultaneously moved to the gravity centre. To simplify the assembly, the components can be stored on rolling boards, assembled and fixed horizontally before placing the whole truss into the final position (Fig. 5-7d).

Pre-assembled triangular modules, single roundwood members and moulded joints are transported to the site. Roundwood members with bonded-in rods (chapter 4) and moulded joints are joined to the triangular modules according to Fig. 5-8a. Before the truss can be finalised, prefabricated roundwood members with grouted sockets are connected to the joints with a single rod, nuts and washers (Fig. 5-8b). The assembly process does not require any grouting process on site and is done by (i) a rotation of the single rod into prefabricated roundwood

members with grouted sockets and (ii) securing the position of the rod with nuts and washers. Due to the fact that the load bearing capacity of prefabricated grouted socket rods in roundwood was not determined with experimental testing in this thesis, the roundwood members should only be placed in strut or chord members loaded under compression. The assembly concept for truss systems with a decreased or increased number of joints are presented in the next section of this thesis after the determination of the final modular truss variations.

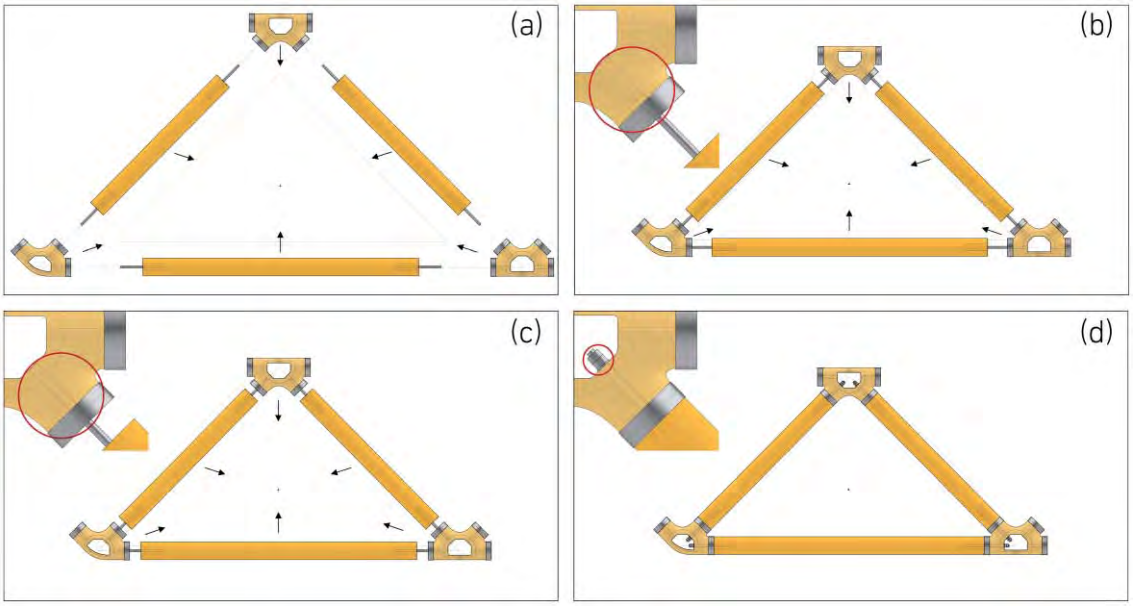

Fig. 5-7 Pre-assembly concept

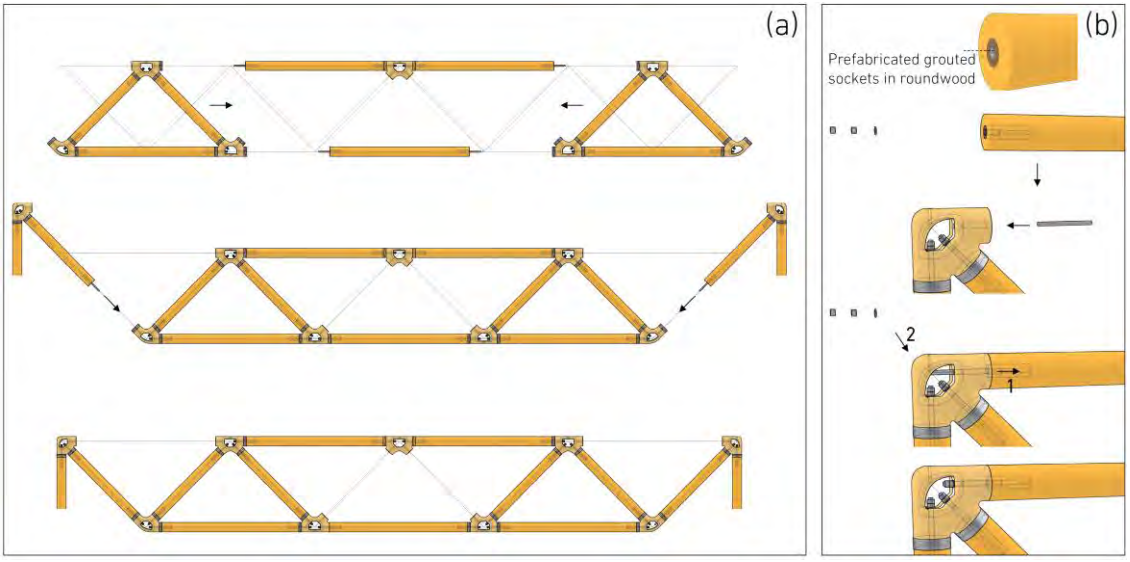

Fig. 5-8 Assembly concept on site

Architectural and structural truss design

The roundwood truss design was adapted to a flat roof structure with varying spans. The roundwood members consisted of Douglas fir *(Pseudotsuga menziesii)*, European strength class C24 [EN 338]. The diameter of the cylindrical milled roundwood was chosen to 200 mm with a casting compound diameter of 75 mm and bonding length of 250 mm. The threaded rod had a diameter of 24 mm and a strength class of 10.9 [DIN 976-1]. Material and geometrical properties were in line with the experimental tests and analytical investigations in chapter 4.

The design algorithm is composed of 4 modules as shown in Fig. 5-4. Module 1 of the design algorithm served for the global architecture of the truss and roof structure for multiple geometries. The source code of the algorithm needed to differentiate between several types of variables. The first variety 'I-parameters' were defined as geometrical input parameters of the roof truss structure with

$p_1 \rightarrow$	t_d	$\rightarrow$	*Truss depth,*
$p_2 \rightarrow$	t_s	$\rightarrow$	*Truss span,*
$p_3 \rightarrow$	n_{uc}	$\rightarrow$	*Number of upper chord members,*
$p_4 \rightarrow$	d_w	$\rightarrow$	*Roundwood diameter,*
$p_5 \rightarrow$	a_f	$\rightarrow$	*Distance between trusses in roof structure,*
$p_6 \rightarrow$	H	$\rightarrow$	*Eaves height.*

The truss was defined by parameter 1-4. To complete the roof structure, the frame distance and eaves height were added to the parameter cloud. The input parameter were either calibrated by the designer or determined in the optimisation process after completion of the algorithm. The static truss depth, chord-diagonal strut angle and strut system lengths were calculated by the input parameter. These kinds of variables were defined as dependent parameters or 'D-parameter' in the design process (marked with dashed lines in Fig. 5-9). Geometrical objects, mathematical formulas and transformations (translation, rotation, duplication) were used as operators or tools in module 1.

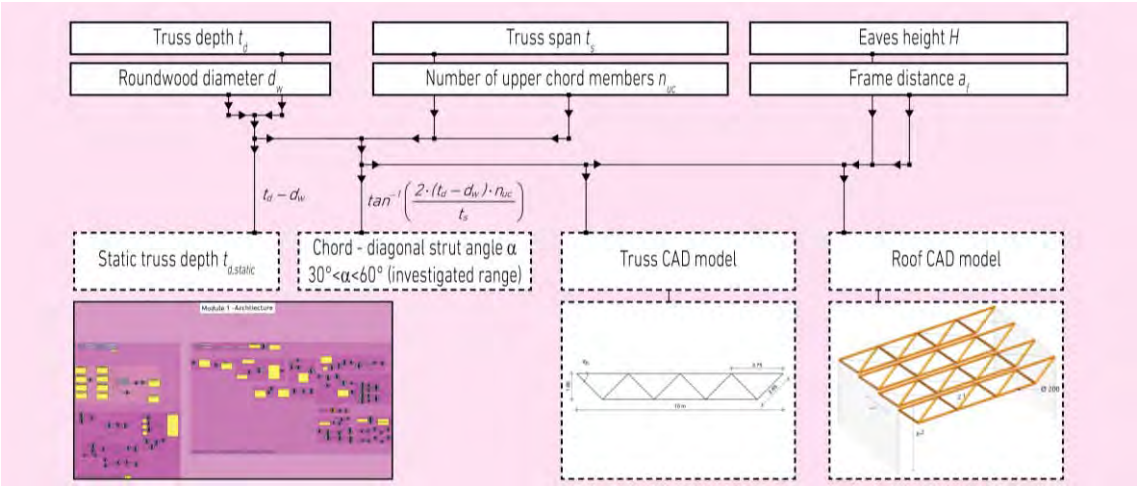

Fig. 5-9 Design algorithm module 1 - Architectural design of the truss roof structure

Module 2 of the algorithm served for the structural performance capacity in ULS of roundwood members [EN 1995-1-1] and modified bonded-in rods according to the results of the experimental investigations (max. applied design load ~150 kN). The load bearing capacity of the moulded joint was not determined with the design algorithm caused by a limitation of the finite element tool (Karamba3D®) to strut, slab, wall and shell structure. The moulded joint will be analysed by extern FE based programs in section 5.2.

Module 2 imported the results of the architectural findings and served for the finite element model. Based on the architectural model, the Finite Element discretisation occurred automatically and divided each strut member into two elements. Due to the fact that an ideal truss system was realised with a point load introduction into the joints in the upper chord and minimum negligible moments caused by the roundwood self-weight, a division into two elements was sufficient for the detection of normal forces in the strut members. The strut members were connected to each other by hinged joints, while the supports were defined in the end nodes of the upper chord. To ensure a static determined system without inner constraints, monovalent and bivalent supports were modelled separately for each node.

For the definition of the timber material properties, such as stiffness and strength parameter, EN 338 was implemented as design library with all required information for each timber strength class to choose from. For the design of the truss structure, the wood strength class was fixed to C24 analogous to the tested specimens in chapter 4. A ULS line load (I-parameter) was applied to the upper chord with an automated division into point loads acting on the joints in the upper chords. Based on the truss geometry, cross-section, material properties, ULS line load, boundary support and joint definition, the FE model was assembled with a subsequent calculation of the inner normal forces in the upper chord (compression), lower chord (tension) and diagonal struts (compression and tension). Due to the use of the equivalent member method for stability design, a calculation for second order theory was not necessary according to EN 1995-1-1.

The design in the serviceability limit state (global truss displacement) could not be implemented before the joint design (module 3) due to missing information on the roundwood and steel rod overhang lengths, which were necessary to calculate the equivalent stiffness for each strut member. To ensure no structural failure in modified bonded-in rods, tensile loads in the strut members were limited to 150 kN (algorithm-penalty) according to section 4.2.5.

Two different design requirements were applied for tensile and compressive stressed beam members. The lower chord and tensile stressed diagonal struts were calculated by the normal forces divided by the roundwood cross-section area. The design timber tensile strength was determined with the characteristic timber tensile strength value multiplied by the modification factor k_{mod} (I-parameter) of 0.9 and divided by the partial safety factor of 1.3 for solid timber. The final stress utilisation was calculated by the existing tensile stresses in roundwood divided by

the design timber tensile strength. The calculation covered timber structures for service class 1 and 2 and a short-term load duration class. Varying modification factors can be applied to the presented results by linear interpolation.

The stability design was applied to the upper chord and compressive stressed diagonal struts according to the equivalent member method for stability design [EN 1995-1-1]. The beam length was imported from module 1 with a reduction of the length based on an approximate model of the moulded joint dimension in module 2. Euler case 2 was adapted to the design approval. Therefore, the calculated roundwood beam length corresponded to the critical buckling length for stability design. The area coverage radius was calculated by the roundwood diameter. The critical buckling length divided by the area coverage radius resulted in the slenderness of the beam members. The relative slenderness was calculated by the slenderness, the 5%-fractile Modulus of Elasticity and characteristic compressive strength in timber. The relative slenderness was used to detect the instability factor k_c for stability design. The final stress utilisation was calculated by the maximum compressive load, the cross-section area, the design compressive strength along the grain and the instability factor k_c.

In module 2, the source code contained three 'I-parameter' with the applied line load in ULS on the upper chord, the modification factor for duration of load and the wood strength class C24 with associated material properties:

$p_7 \rightarrow$	q_{ULS}	$\rightarrow$	*Line load in ULS,*
$p_8 \rightarrow$	k_{mod}	$\rightarrow$	*Modification factor for duration of load and moisture content,*
$p_9 \rightarrow$	s_w	$\rightarrow$	*Wood strength class.*

The evaluation of the architectural and structural design of the truss structure is attached in section A.2.1 with information on 25 modular truss variations composed of chord-strut angles of 30°, 45° and 60° and truss spans between 10 m and 20 m. For each truss variation, the permissible line load in ULS was evaluated with information on the inner normal forces serving for the subsequent FE analysis of the moulded joints in section 5.2.

The third illustration (section A.2.1) serves for the ULS design of the roundwood members (stress utilisation) loaded under tension and compression in grain direction according to EN 1995-1-1. Truss variations with truss depths larger than 4 m, roundwood strut lengths smaller than 2 m and permissible line loads smaller than 4 kN/m were discarded from the evaluation (algorithm-penalties).

Tab. 5-1 summarises all 25 variations including information on the truss span, depth, number of total joints, chord-diagonal strut angle and permissible uniform distributed line load on the upper chord.

Tab. 5-1 Load table for 25 modular truss variations according to A.2.1

Truss No.	Truss span	Truss depth	Number of joints	Chord-diagonal strut angle α	Permissible uniform distributed line load in ULS[1]
-	[m]	[m]	-	[°]	[kN/m] - truss weight included
1	10	0.92	9	30	8.68
2	10	1.16	7	30	13.00
3	10	1.45	9	45	15.02
4	10	1.64	5	30	17.32
5	10	1.87	7	45	22.50
6	10	2.37	9	60	25.91
7	10	2.7	5	45	30.10
8	10	3.09	7	60	38.91
9	15	1.07	11	30	4.83
10	15	1.28	9	30	5.77
11	15	1.64	7	30	8.67
12	15	1.70	11	45	8.34
13	15	2.08	9	45	10.01
14	15	2.37	5	30	11.58
15	15	2.70	7	45	15.05
16	15	2.80	11	60	14.45
17	15	3.45	9	60	17.31
18	15	3.95	5	45	20.03
19	20	1.64	9	30	4.34
20	20	2.12	7	30	4.62
21	20	2.20	11	45	6.26
22	20	2.70	9	45	7.51
23	20	3.09	5	30	5.59
24	20	3.53	7	45	7.47
25	20	3.66	11	60	10.80

[1] The calculation covers timber structures for service class 1 and 2 and a short term load duration class

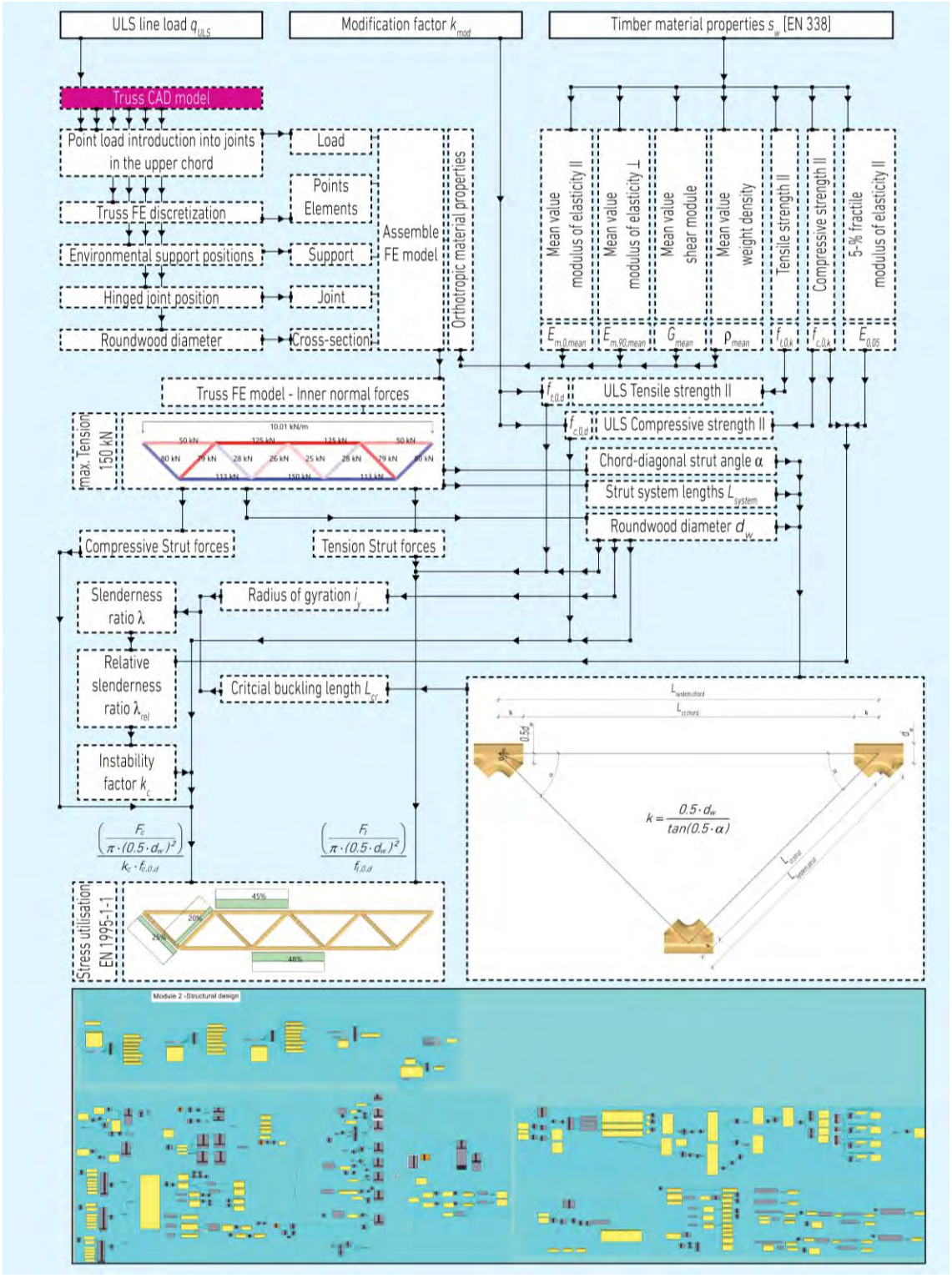

Fig. 5-10 Design algorithm module 2 - Structural truss design

Joint design

After the architectural and structural design of the truss structure, the algorithm served for the local design of the joints. Three joint types were developed in total for the (i) field joint in the lower and upper chord, (ii) edge joint in the lower chord and (iii) support joint in the upper chord to connect the truss structure with the column.

Based on the rod diameter for the connection design in roundwood (modified bonded-in rods) and additional rods to join the purlins with the joints in the upper chord, an integrated design library provided information on geometrical parameter for metric threads [DIN 13-1], washers [EN ISO 7089], nuts [EN ISO 4032] and spanners or ratchets. An exact model of the threads, washers and nuts was necessary to determine the minimum required dimension of the inner frame structure, while the visualisation of the ratchets helped to detect the assembly place and rotation angle for fastening or loosening the nuts.

A second design library served with information on HEA [EN 10034] and UPE [EN 10279] steel profiles (used as purlins) with an automated determination of the profile dimension for each truss variation based on a comparison of the plastic moment resistance of the profiles and acting moment stresses in ULS, which were calculated with the permissible uniform distributed line load (module 2), frame distance (module 1) and strut system length of the chord members (module 1). UPE profiles were used for the support joint in order to guarantee a load introduction into the joint with no eccentricities to the centre of gravity. HEA profiles were used for the field joint. Steel grade S 355 was chosen for both profile types in order to reduce the dimension of the purlins. Here should be noted, that steel profiles were preferred compared to wooden purlins due to the slim dimension and the simple connection along the flange.

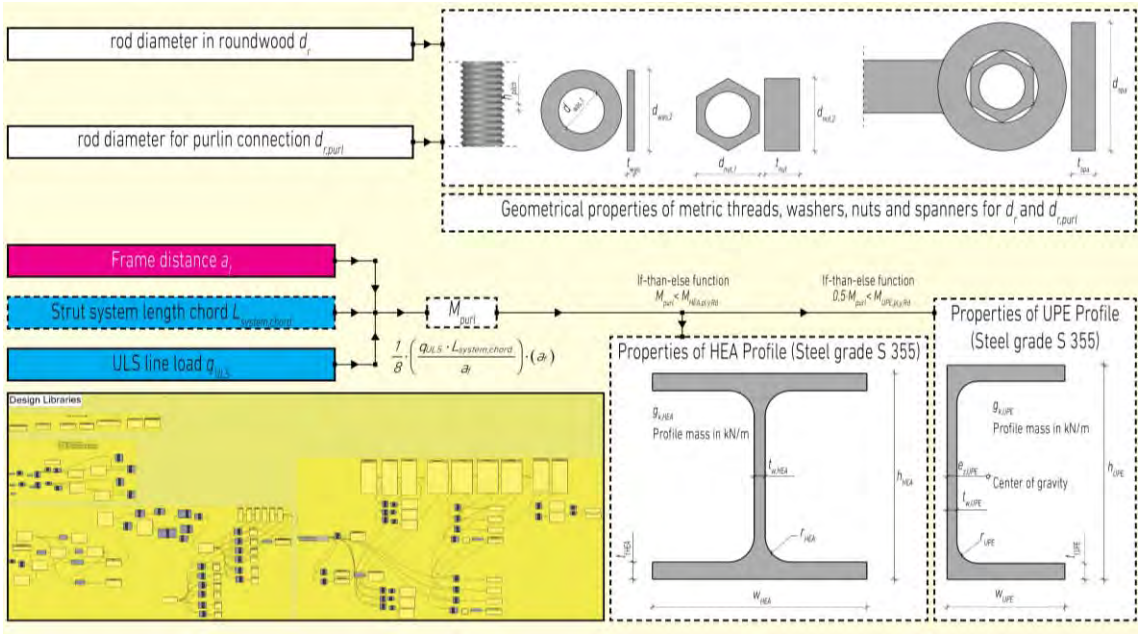

Fig. 5-11 Design algorithm module 3 - Library for steel components

The design library in module 3 provided two 'I-parameter': The rod diameter for the connection design in roundwood with 24 mm (according to the experimental investigations in this thesis with M24-10.9) and the diameter for additional rods to join the purlin with the joint. These rods secured the position of the purlin in horizontal direction and were fixed to M12-10.9:

$p_{10} \rightarrow$	d_r	$\rightarrow$ *Threaded rod diameter in roundwood,*
$p_{11} \rightarrow$	$d_{r,purl}$	$\rightarrow$ *Threaded rod diameter to interconnect purlins.*

For the design of the planar load introduction area for the purlin support, the required steel profiles, according to Fig. 5-11, were determined by the algorithm for a defined maximum frame distance of 5 m. Tab. 5-2 summarises the applied HEA and UPE profiles for each modular truss variation, presented in Tab. 5-1.

Tab. 5-2 Purlin steel profiles for 25 modular truss variations according to A.2.1

Truss No.	α	HEA	UPE	Truss No.	α	HEA	UPE	Truss No.	α	HEA	UPE
	[°]				[°]				[°]		
1	30	100	100	9	30	100	100	19	30	100	100
2	30	100	100	10	30	100	100	20	30	100	100
3	45	100	100	11	30	100	100	21	45	100	100
4	30	140	140	12	45	100	100	22	45	100	100
5	45	140	140	13	45	100	100	23	30	120	120
6	60	120	120	14	30	140	140	24	45	140	140
7	45	180	180	15	45	140	140	25	60	100	100
8	60	160	160	16	60	100	100				
				17	60	120	120				
				18	45	180	180				

The schematic process of the frame structure design is shown in Fig. 5-12 and required information on the geometrical properties of metric threads, washers, nuts and spanners. The axis length depended on the geometrical properties of the used steel components as well as the chord-diagonal strut angle. The axis length increased with smaller chord-strut angle due to the required assembly place for fastening and loosening the nuts according to the equation shown in Fig. 5-12. The implementation of geometrical dependencies was elementary for the functionality of the algorithm. The first variety 'I-parameter' for the frame structure was the manual adjustment of the axis length for each joint type with

$p^i_{12} \rightarrow$	Δk^i_{Frame}	$\rightarrow$ *Manual adjustment of frame structure axis length,*
	i	$\rightarrow$ *F = Field, E = Edge, S = Support.*

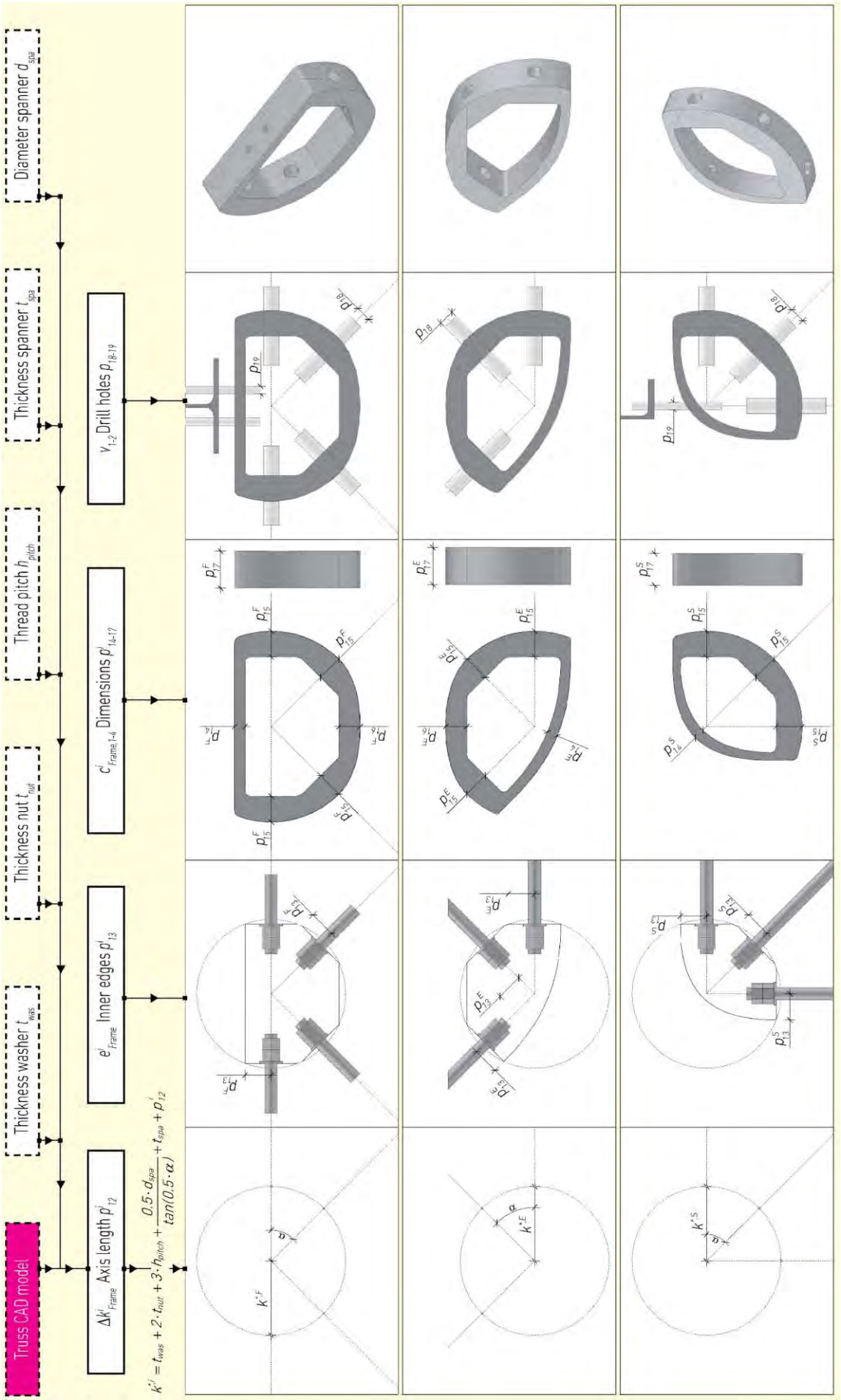

Fig. 5-12 Design algorithm module 3 - Frame structure design

To finalise the frame structure, the inner edges and dimensions (widths and thickness) of each joint type needed to be defined. Drill holes were taken into account with additional slips to facilitate the assembly and to decouple the frictional connection along the shell surface of the rods. The position of the drill holes were in line with the used steel profiles (Tab. 5-2) and ensured a frictional connection between frame structure and UPE or HEA profile with no collision for all 25 modular truss variations. The variety 'I-parameter' were defined as

p^{i}_{13}	→	e^{i}_{Frame}	→ *Inner edge dimension for washer support,*
p^{i}_{14-16}	→	$c^{i}_{Frame,1-3}$	→ *Frame structure widths,*
p^{i}_{17}	→	$c^{i}_{Frame,4}$	→ *Frame structure thickness,*
		i	→ *F = Field, E = Edge, S = Support,*
p_{18}	→	v_1	→ *Drill hole diameter for strut members,*
p_{19}	→	v_2	→ *Drill hole diameter for purlin support.*

The design of the outer moulded joint part started with the definition of the axis length of each joint type, which was calculated with the mathematical expression shown in Fig. 5-13 as a function of the chord-diagonal strut angle, the roundwood diameter and an additional parameter for manual adjustment. In the next step, the upper parts of the field and support joints were modelled with a flat support area for the steel purlins. The depth of the support area was defined as constant with 90 mm independent on the chord-diagonal strut angle or joint type. The width was determined automatically based on the design library for steel components and the evaluation of the required UPE or HEA profiles according to Tab. 5-2. The solid model of the outer moulded joint was designed for the field and support joints with no additional required parameter and were adapted to the shape and direction of the roundwood strut members. For the design of the edge joint, an integrated parameter controlled the curvature or shape between the chord and diagonal strut member according to Fig. 5-13. Drill holes for the connection of the strut members and purlins were taken into account analogous to the frame structure. The last variety 'I-parameter' of the algorithm were

p^{j}_{20}	→	Δk^{j}_{Mould}	→ *Manual adjustment of moulded part axis length,*
		i	→ *F = Field, E = Edge, S = Support,*
p^{j}_{21}	→	w^{j}_{m-p}	→ *Width of moulded joint for purlin support,*
		j	→ *F = Field, S = Support,*
p_{22}	→	o_{Edge}	→ *Curvature edge connector.*

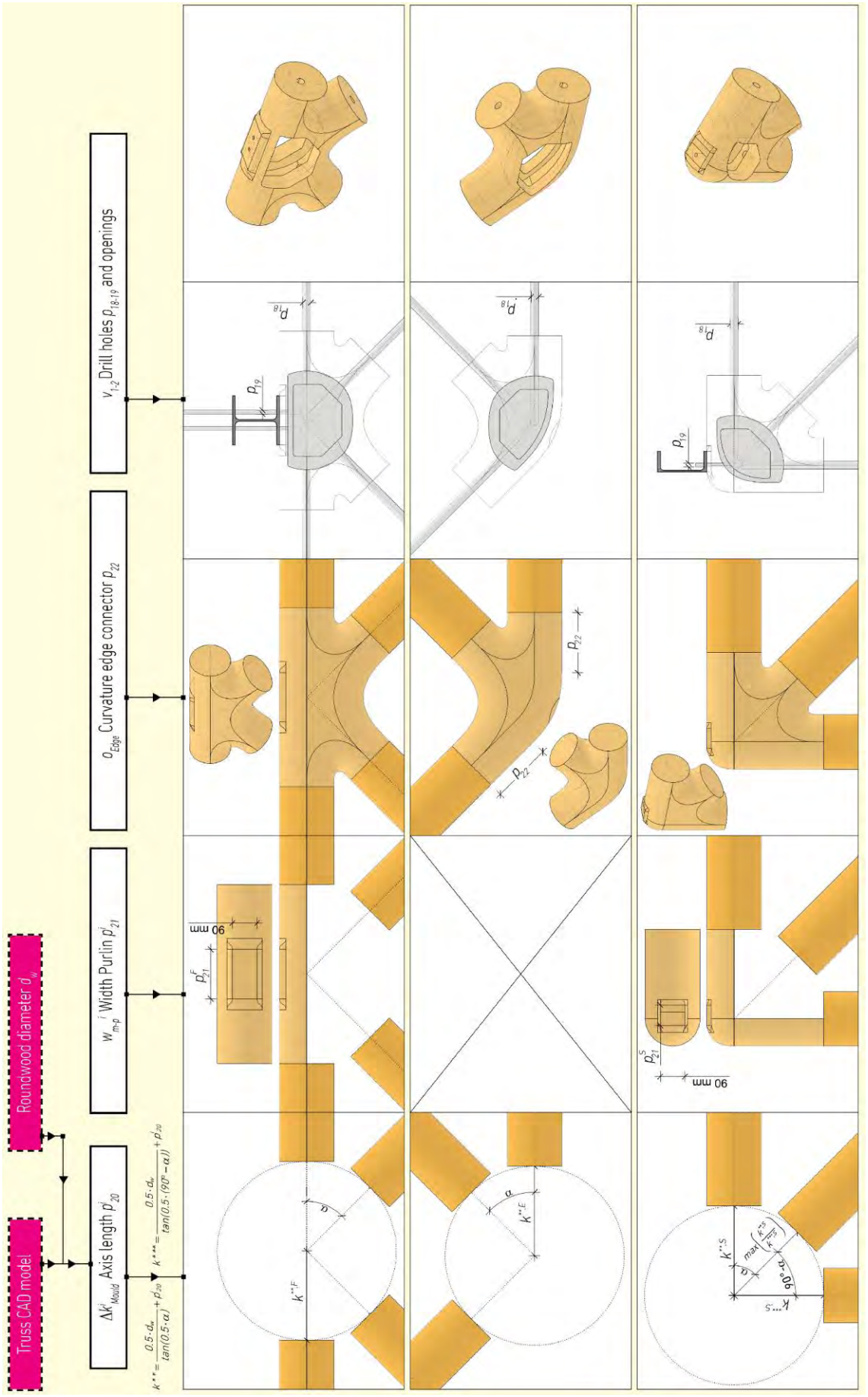

Fig. 5-13 Design algorithm module 3 - Outer moulded joint design

Interaction

Module 4 created a dynamic model by networking module 1-3. Fig. 5-14 shows the developed algorithm in Grasshopper® software. By networking several types of modules, a circular process was created, which enabled an interaction between the architectural, engineering and joint part of the design process. On this occasion, no limits were set to the creation of the subject areas.

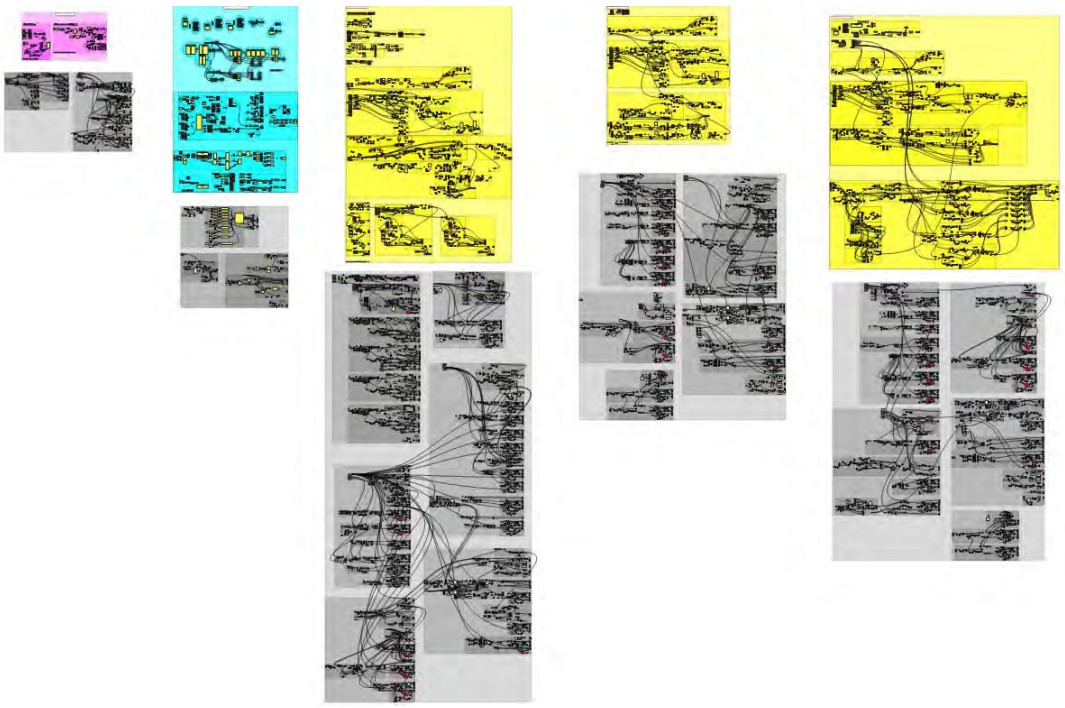

Fig. 5-14 Design algorithm source code in Grasshopper® (digital value chain)

The algorithm provided a live image simulations interface (Fig. 5-15) with all important information for the designer. To avoid truss mutations, integrated algorithm-penalties were taken into account. The algorithm penalties covered structural and assembly characteristics. The strut lengths of the roundwood members including the grouted rods should not exceed six meters to ensure an easy container transport and to avoid a lack of supply for roundwood members with longer component lengths. In regard to the structural performance all structural design requirements for truss members were taken into account. To ensure an easy assembly of the truss structure, the assembly space and rotation angle for the spanner was evaluated and visualised for the designer. Next to the live image simulation, the module served for a detailed 3D model of the truss structure including all structural components to calculate the total mass of the joints and truss structures, which was used to determine the strength to weight ratio for all 25 modular truss variations and therefore to rate the efficiency in direct comparison. A structural component list was created with the possibility to link costs and live material libraries from different suppliers after successful implementation of the joining technology in practice. The joint CAD models serve for the subsequent FEM (section 5.2) and CAM processes (section 5.4).

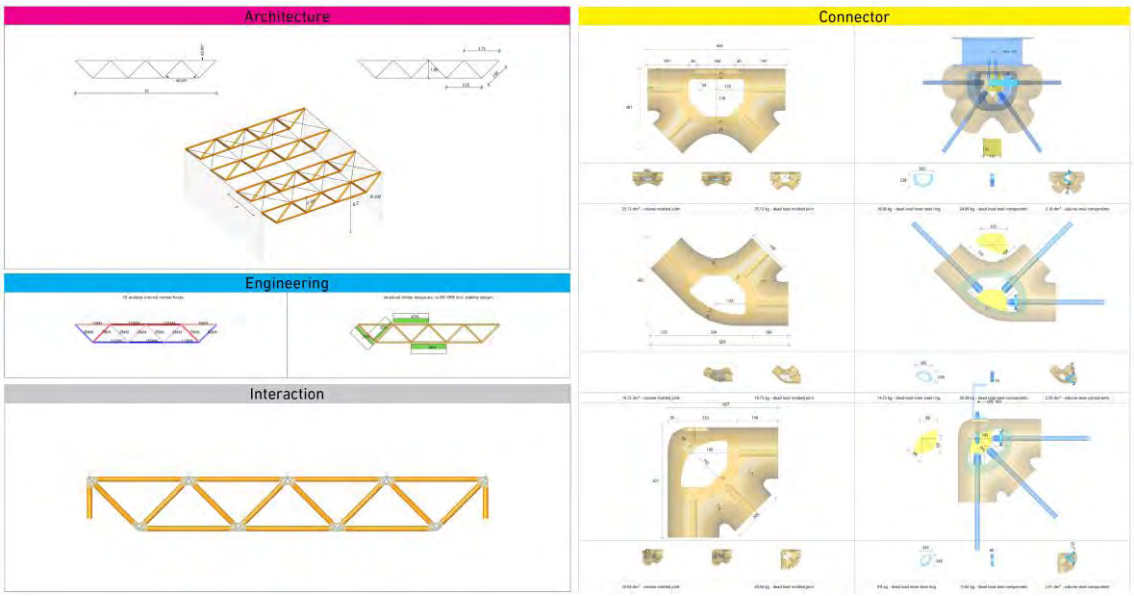

Fig. 5-15 Design algorithm live image simulation in Rhinoceros®

The geometrical parameter of all nine developed joints for the field, edge and support and three different chord-diagonal strut angles (30°, 45°, 60°) are attached in section A.2.2 with additional information on the connection configuration of the purlins as well as information on the assembly space for loosening and fastening the nuts. Section A.2.3 serves with the final 3D models of all 25 truss variations including the roundwood strut lengths with and without grouted rods in both sides of the strut members. Five truss types (T14, T18, T20, T23 and T24) exceeded the strut length of 6 m and do not allow an easy container transport.

Based on the final model and information on the roundwood length and overhang length of the threaded rod, the algorithm served for the structural design of the truss displacement in the serviceability limit state according to EN 1995-1-1. Chapter 4 derived the formula for the calculation of the equivalent strut stiffness for the tested specimens (Eq. 4.3c) and was implemented into the algorithm in order to create a FE model close-to-reality. In this context, the roundwood and rod stiffness, as well as slip modulus were considered as springs connected in series with a superposition of the relative displacements. The calculation of the equivalent strut stiffness for the lower chord members and diagonal strut members loaded under tension took the minimum determined slip modulus into account (Fig. 4-26) to provide an additional level of security for the calculation. For compression, the loads are introduced evenly in the contact surface between the timber end grain and the front sides of the joint (Fig. 5-6b) with no structural function of the threaded rod. This is why the calculation of the equivalent stiffness for the upper chord and diagonal strut members loaded under compression took an infinitely large or practically no slip displacement into account (Fig. 4-23).

The equivalent strut stiffness was transformed for the FE model into an equivalent strut Modulus of Elasticity for each strut member as a function of the roundwood cross-section area and strut system length with a subsequent determination of the

global truss displacement, representing the instantaneous deflection w_{inst}. The applied loads were considered as permanent for the worst case scenario. Two design requirements with (w_{fin}) and without (w_{inst}) creep effect were implemented into the design algorithm, where the displacement factor k_{def} and the deflection limit follow the guidelines of EC 5:

- the deflection factor was set to 0.8, covering solid timber for service class 1 and 2 specimens according to EN 1995-1-1/Table 3.2,
- the deflection limit was set to three hundredth of the span for the instantaneous displacement according to EN 1995-1-1/NA/Table 13,
- and the deflection limit was set to two hundredth of the span for the final displacement according to EN 1995-1-1/NA/Table 13.

Tab. 5-3 Max. global displacement in SLS for truss variations according to A.2.1

Truss No.	w_{inst}	w_{fin}	Truss No.	w_{inst}	w_{fin}	Truss No.	w_{inst}	w_{fin}
	[cm]	[cm]		[cm]	[cm]		[cm]	[cm]
1	1.02	1.83	9	2.11	3.80	19	2.36	4.24
2	0.88	1.58	10	1.65	2.97	20	1.72	3.10
3	0.66	1.18	11	1.42	2.56	21	1.73	3.11
4	0.63	1.14	12	1.21	2.17	22	1.44	2.59
5	0.59	1.06	13	1.00	1.80	23	2.78	5.00
6	0.51	0.91	14	1.46	2.63	24	1.18	2.13
7	0.48	0.87	15	0.97	1.74	25	1.19	2.14
8	0.51	0.92	16	0.85	1.53			
			17	0.76	1.37			
			18	1.18	2.13			
Limit	3.33	5.00	Limit	5.00	7.50	Limit	6.66	10.0

The truss assembly process was visualised in the last step, covering four cases in total depending on the number of upper chord members, and was carried out in three steps analogous to Fig. 5-7 and 5-8 with (i) the pre-assembly of triangular modules, (ii) the assembly of joints and roundwood members with grouted rods and (iii) the completion of the assembly with roundwood members with grouted sockets. Here should be noted, that roundwood members with grouted sockets needed to be inserted in strut members loaded under compression, due to missing tests in this thesis on the load bearing capacity for tension. Fig. 5-16 shows the assembly process with a colour highlighting of the three steps (step 1 in black, step 2 in grey and step 3 in brown) with information on the inner normal forces (compression in red, tension in blue) to identify strut members loaded under compression.

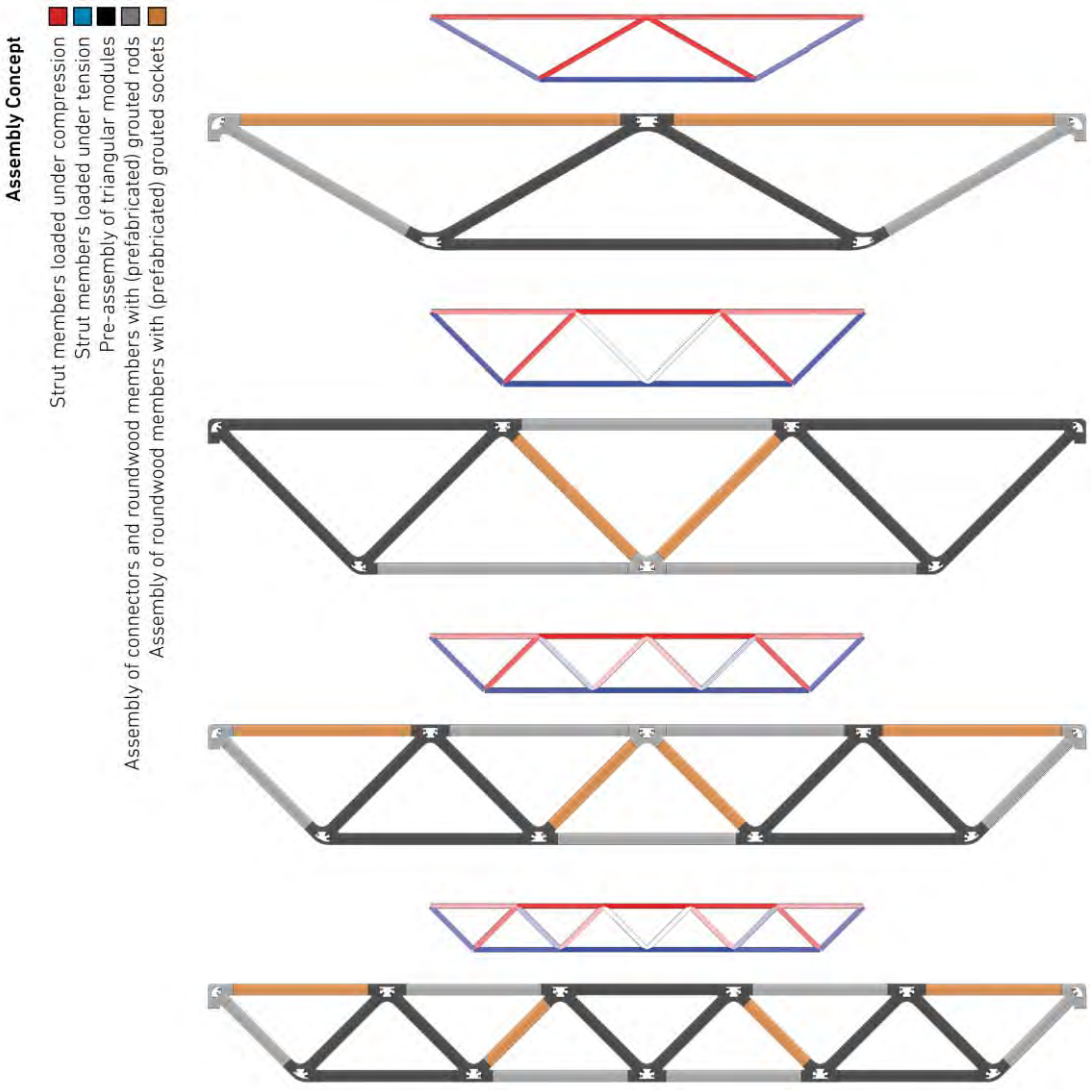

Fig. 5-16 Assembly concept of modular trusses analogous to Fig. 5-7 and 5-8

Comparison of different chord-strut angles and truss variations

The comparisons of the nine developed joints (section A.2.2) and 25 truss variations (section A.2.3) are discussed in the following paragraphs. The first part of the evaluation covered the determination of the joint masses including the inner frame structure, loose steel components and outer moulded joint for different chord-diagonal strut angles and joint types in order to illustrate how easy or difficult the structural components can be lifted during the assembly. Due to the fact that the applied material for the outer moulded joint is discussed in the next section and is not defined so far, the subsequent calculations covered densities of 1 g/cm^3 and 2 g/cm^3. The density for the inner steel frame structure and the loose steel components was set to 7.85 g/cm^3. Tab. 5-4 summarises the results with a clear identifiable impact of the outer moulded material density on the total mass of the joints. The mass of the field and edge joints decreased with increasing chord-diagonal strut angle. For the support joint, an angle α of 45° performed with the lowest mass.

Tab. 5-4 Joint masses according to A.2.2

Field joint	Outer moulded material mass	Inner frame structure mass	Total mass of joint	Loose steel components mass[1]
α	[kg] for ρ = 1 g/cm^3	[kg] for ρ = 7.8 g/cm^3	[kg]	[kg] for ρ = 7.8 g/cm^3
30°	36.30	21.40	57.70	9.15
45°	25.10	16.95	42.05	8.03
60°	18.25	15.14	33.39	7.35
α	[kg] for ρ = 2 g/cm^3	[kg] for ρ = 7.8 g/cm^3	[kg]	[kg] for ρ = 7.8 g/cm^3
30°	72.60	21.40	94.00	9.15
45°	50.20	16.95	67.15	8.03
60°	36.50	15.14	51.64	7.35
Edge joint	Outer moulded material mass	Inner frame structure mass	Total mass of joint	Loose steel components mass[1]
α	[kg] for ρ = 1 g/cm^3	[kg] for ρ = 7.8 g/cm^3	[kg]	[kg] for ρ = 7.8 g/cm^3
30°	28.20	19.00	47.20	6.90
45°	19.70	14.40	34.10	6.00
60°	14.10	12.20	26.30	5.60
α	[kg] for ρ = 2 g/cm^3	[kg] for ρ = 7.8 g/cm^3	[kg]	[kg] for ρ = 7.8 g/cm^3
30°	56.40	19.00	75.40	6.90
45°	39.40	14.40	53.80	6.00
60°	28.20	12.20	40.40	5.60
Support joint	Outer moulded material mass	Inner frame structure mass	Total mass of joint	Loose steel components mass[1]
α	[kg] for ρ = 1 g/cm^3	[kg] for ρ = 7.8 g/cm^3	[kg]	[kg] for ρ = 7.8 g/cm^3
30°	28.60	12.30	40.90	6.50
45°	20.00	9.80	29.80	6.10
60°	28.60	11.40	40.00	6.70
α	[kg] for ρ = 2 g/cm^3	[kg] for ρ = 7.8 g/cm^3	[kg]	[kg] for ρ = 7.8 g/cm^3
30°	57.20	12.30	69.50	6.50
45°	40.00	9.80	49.80	6.10
60°	57.20	11.40	68.60	6.70

[1] Threaded rods, nuts and washers (UPE and HEA profiles excluded)

After the mass evaluation of the joint types, the mass of the truss structures was calculated including the number and total mass of roundwood strut members for each truss variation. Tab. 5-5 summarises the results with additional information on the number and total mass of the joints for the applied moulded material densities of 1 g/cm^3 and 2 g/cm^3.

Tab. 5-5 Truss masses for 25 modular truss variations according to A.2.1-A.2.3

Truss No.	α	n_{joint}[4]	Total mass joints[1]	Total mass joints[2]	n_w[5]	Total mass roundwood[3]	Truss mass[1]	Truss mass[2]
-	[°]	-	[kg]	[kg]	-	[kg]	[kg]	[kg]
1	30	9	537	833	15	202	739	1034
2	30	7	404	626	11	239	643	865
3	45	9	403	608	15	288	690	896
4	30	5	270	420	7	265	536	685
5	45	7	302	457	11	312	614	769
6	60	9	361	538	15	361	722	898
7	45	5	202	307	7	324	526	631
8	60	7	279	420	11	385	665	805
9	30	11	671	1039	19	355	1026	1394
10	30	9	537	833	15	393	931	1226
11	30	7	404	626	11	425	829	1051
12	45	11	503	758	19	472	975	1230
13	45	9	403	608	15	497	899	1104
14	30	5	270	420	7	441	711	861
15	45	7	302	457	11	515	817	972
16	60	11	442	656	19	582	1025	1238
17	60	9	361	538	15	608	969	1146
18	45	5	202	307	7	516	718	823
19	30	9	537	833	15	585	1122	1417
20	30	7	404	626	11	611	1015	1238
21	45	11	503	758	19	684	1187	1442
22	45	9	403	608	15	705	1108	1313
23	30	5	270	420	7	616	886	1036
24	45	7	302	457	11	718	1020	1175
25	60	11	442	656	19	833	1275	1489

[1] Applied moulded material density of 1 g/cm^3 (mass includes frame structure and loose steel components)
[2] Applied moulded material density of 2 g/cm^3 (mass includes frame structure and loose steel components)
[3] Applied timber density of 0.42 g/cm^3 (mean value according to DIN EN 338)
[4] Number of joints in truss structure
[5] Number of roundwood strut members in truss structure

Based on the results of Tab. 5-5, Tab. 5-1 was further processed to provide a pure overview of the permissible uniform distributed line loads on the upper chord under exclusion of the truss masses. For this purpose, the values of the truss masses from Tab. 5-5 were converted into design value loads in ULS by a multiplication with the partial factor 1.35 for permanent actions. Analogous to the evaluation in Tab. 5-4 and 5-5, the moulded material densities were also set here to 1 g/cm^3 and 2 g/cm^3.

Tab. 5-6 Load table 2 for 25 modular truss variations according to A.2.1-A.2.3

Truss No.	Truss span	Truss depth	n_{joint}[3]	α	Truss weight[2]	Permissible uniform distributed line load[2]
-	[m]	[m]	-	[°]	[kN]	[kN/m] - truss weight excluded
1	10	0.92	9	30	13.96	7.28
2	10	1.16	7	30	11.68	11.83
3	10	1.45	9	45	12.09	13.81
4	10	1.64	5	30	9.25	16.39
5	10	1.87	7	45	10.38	21.46
6	10	2.37	9	60	12.13	24.70
7	10	2.7	5	45	8.52	29.25
8	10	3.09	7	60	10.87	37.82
9	15	1.07	11	30	18.81	3.58
10	15	1.28	9	30	16.55	4.67
11	15	1.64	7	30	14.19	7.72
12	15	1.70	11	45	16.61	7.24
13	15	2.08	9	45	14.91	9.02
14	15	2.37	5	30	11.62	10.81
15	15	2.70	7	45	13.12	14.18
16	15	2.80	11	60	16.71	13.33
17	15	3.45	9	60	15.47	16.28
18	15	3.95	5	45	11.11	19.29
19	20	1.64	9	30	19.14	3.38
20	20	2.12	7	30	16.71	3.79
21	20	2.20	11	45	19.47	5.29
22	20	2.70	9	45	17.73	6.62
23	20	3.09	5	30	13.98	4.89
24	20	3.53	7	45	15.87	6.68
25	20	3.66	11	60	20.10	9.80

Timber structures for service class 1 and 2 and a short term load duration class
[1] Applied moulded material density of 1 g/cm^3, design values in ULS
[2] Applied moulded material density of 2 g/cm^3, design values in ULS
[3] Number of joints in truss structure

In order to rate the efficiency of the developed truss structures in direct comparison, three parameters were evaluated and are discussed in the following, starting with the strength to weight ratio (STW), which was determined in Tab. 5-7 by dividing the maximum loads carried in ULS by the weight of the trusses. The ratio should reach a maximum, described the capability of the truss structure to carry x times its self-weight and served for evaluation of the structural performance capacity with regards to the material consumption. The second parameter described the span to depth ratio (STD), which is defined around 10 for traditional and efficient timber trusses with metal connectors and steel plates.

Here should be noted that the design process of the truss structures started in design module 1 (algorithm) with the determination of different truss typologies based on predefined truss spans of 10, 15 and 20 m, chord-diagonal strut angles of 30, 45 and 60°, and varying number of upper chord members. Based on these specifications, 25 modular variations were modelled with non-adjustable truss depths and associated permissible line loads, which were mostly limited by the maximum applied design tensile load of 150 kN in the lower chord (limited failure load for modified bonded-in rods). Next to the strength to weight and span to depth ratios, the ratio between the total mass of the joints and the truss mass (joint mass ratio) was evaluated as final parameter, to include an indicator for the costs. Fig. 5-17 summarises the dependencies of the three ratios for all 25 truss variations with a separate evaluation of the two investigated moulded material densities.

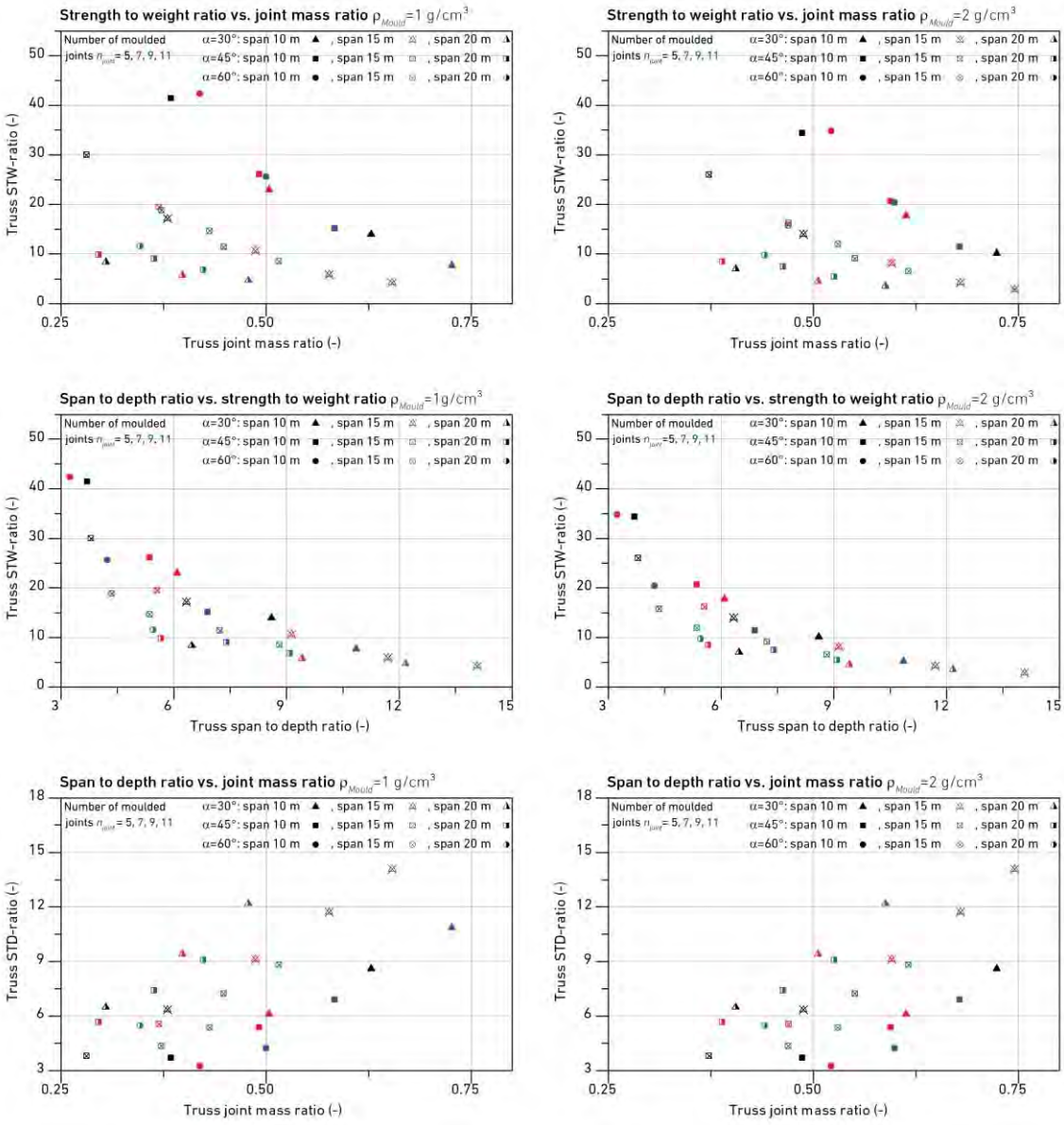

Fig. 5-17 Span to depth, strength to weight and joints mass ratios

Tab. 5-7 Strength to weight ratio for 25 modular truss variations according to A.2.1-A.2.3

Truss No.	Truss depth	Truss weight[1]	Permissible resultant load[1]	STW ratio[1]	Truss weight[2]	Permissible resultant load[2]	STW ratio[2]
-	[m]	[kN]	[kN] - truss excluded	-	[kN]	[kN] - truss excluded	-
1	0.92	9.98	76.83	7.70	13.96	72.84	5.22
2	1.16	8.68	121.32	13.98	11.68	118.32	10.13
3	1.45	9.32	140.88	15.11	12.09	138.11	11.42
4	1.64	7.23	165.97	22.96	9.25	163.95	17.72
5	1.87	8.29	216.71	26.15	10.38	214.62	20.68
6	2.37	9.74	249.36	25.60	12.13	246.97	20.37
7	2.7	7.10	293.95	41.38	8.52	292.53	34.35
8	3.09	8.97	380.09	42.36	10.87	378.20	34.81
9	1.07	13.85	58.65	4.24	18.81	53.68	2.85
10	1.28	12.56	73.98	5.89	16.55	69.99	4.23
11	1.64	11.19	118.85	10.62	14.19	115.84	8.16
12	1.70	13.16	112.00	8.51	16.61	108.55	6.54
13	2.08	12.14	138.06	11.37	14.91	135.29	9.07
14	2.37	9.59	164.14	17.11	11.62	162.12	13.95
15	2.70	11.03	214.73	19.47	13.12	212.64	16.20
16	2.80	13.83	202.90	14.67	16.71	200.02	11.97
17	3.45	13.08	246.59	18.85	15.47	244.20	15.79
18	3.95	9.70	290.70	29.97	11.11	289.29	26.04
19	1.64	15.15	71.58	4.72	19.14	67.60	3.53
20	2.12	13.70	78.74	5.75	16.71	75.74	4.53
21	2.20	16.02	109.19	6.81	19.47	105.75	5.43
22	2.70	14.96	135.18	9.04	17.73	132.41	7.47
23	3.09	11.96	99.81	8.35	13.98	97.78	6.99
24	3.53	13.77	135.69	9.85	15.87	133.60	8.42
25	3.66	17.22	198.84	11.55	20.10	195.96	9.75

All calculations cover timber structures for service class 1 and 2 and a short term load duration class
[1] Applied moulded material density of 1 g/cm^3, design values in ULS
[2] Applied moulded material density of 2 g/cm^3, design values in ULS

Conclusions

The main objective of this section was the assessment of the design principle/function of the joints and the subsequent development of a generative algorithm for the digitally manufactured joining technology and truss design.

For the form finding and structural design of modular truss structures and moulded joints, a generative design algorithm has been developed succesfuly in the beginning of this thesis. In relation to the predefined aims, it can be stated that the algorithm proved its functionality and is suitable for the automated design of truss structures and moulded joints, which can be further processed for the FEM and CAM process.

The algorithm was used to design and optimise nine different moulded joint types for 25 modular truss variations. Furthermore, the truss and joint masses were determined with the algorithm to detect the impact of the outer moulded material density on the STW, STD and joint mass ratios. Tab. 5-4 highlights the problem of the adaptation of materials with a high density with resulting joint masses up to 94 kg. A direct comparison of the lower (1 g/cm^3) and upper limits (2 g/cm^3) showed that decreased density of the moulded material (100%) resulted in

an increase of the STW ratio

– by 33% (mean value) for α = 30°,

– by 23% (mean value) for α = 45°,

– by 21% (mean value) for α = 60°,

– by 30% (mean value) for truss spans of 10 m,

– by 27% (mean value) for truss spans of 15 m and

– by 23% (mean value) for truss spans of 20 m.

a decrease of the joint mass ratio

– by 17% (mean value) for α = 30°,

– by 20% (mean value) for α = 45° and α = 60°,

– by 16% (mean value) for truss spans of 10 m,

– by 19% (mean value) for truss spans of 15 m and

– by 22% (mean value) for truss spans of 20 m.

For the truss variations, it could be stated that a chord-diagonal strut angle of 30° led to less efficient trusses than 45° or 60° (Fig. 5-17, middle) caused by the reduced depth and increased self-weight of the joints for smaller angles (Tab. 5-4). This explained also the general trend for less capacity or reduced STW ratio (Fig. 5-17, top) as the mass ratio of the joints increased under same conditions (truss span and number of joints). The trusses performed with a remarkably large

STW ratio in the range of 20-40 times their self-weight for a span to depth ratio lower than 6. Trusses with a span to depth ratio in the range of 6 to 10 showed a stable STW ratio of about 10. More slender trusses were less efficient, with a linear decrease in the STW ratio.

The algorithm in combination with the advantages of roundwood truss structures and the developed joining technology form the basis for a competitive, ecological and economic position in the building sector. The new design algorithm is crucial for the competiveness of the joining technology to save workloads and to compete against other more favourable joining technologies, such as mechanical fastener connections.

Based on the results of the joint and truss mass evaluation, section 5.3 aims to develop a suitable moulded material with a density of approximate 1 g/cm^3 to improve the STW ratio of the truss systems. Further required material properties are defined in section 5.2 after completion of the Structural Analysis of the moulded joint for different applied composite or building materials.

5.2 STRUCTURAL ANALYSIS

5.2.1 Materials and methods

Idealised FE model and material characteristics

This section is devoted to the analysis of the moulded joints in the intersection covering the 25 modular truss variations presented in section 5.1. In total, three different joint types (field, edge and support) were investigated for chord-strut angles of 30°, 45° and 60° (section A.2.2). Especially for the field joints, multiple load states (sub-models) were taken into account for the use of the same joint in different positions of the truss structures. The goal was to confirm the use of the developed joints in all 25 modular truss variations and to determine the structural behaviour for different applied composite materials for the outer moulded joint. After completion, suitable materials were defined for the inner steel frame structure and outer moulded joint. The commercial finite element package Ansys Mechanical 19.1® was used to create an idealised solid model of the joint and to simulate the interactive structural behaviour of the inner steel frame structure and outer moulded joint for analysing strength, stress and elasticity parameter.

The idealised solid model of the joints used Solid187 3D finite elements with higher order, ten-node elements with quadratic displacement behaviour, which are well suited for irregular meshes produced from CAD model imports. The Structural Analysis covered the materials epoxy resin, polymer concrete and non-reinforced normal and high performance concrete for the outer moulded joint, which were modelled with linear elastic material properties (idealised FE model) to provide an added level of security for the design. The properties of the chosen material types including commercial name are summarised in Tab. 5-8 with information on the stiffness (Modulus of Elasticity), density and strengths for compression and tension. The data sheets of the analysed materials epoxy resin and polymer concrete types are attached in the beginning of section A.2.4. The Modulus of Elasticity of the moulded material was defined as a variable parameter in the Structural Analysis, in the range 2.5 GPa (lower limit for epoxy resin) to 40 GPa (upper limit for non-reinforced high performance concrete).

The steel frame structure was modelled with ideal plastic material properties. Here, the MoE was set to 200 GPa with a yield strength of 0.5 GPa and tangency module of 1.45 GPa. Due to the complex shape of the frame structure, the fabrication will be realised with a cast steel. According to the calculated stresses in the frame structure, a suitable type was chosen after the FE analyse based on EN 1034, which defines certified or permitted steel castings for structural uses in Germany (Fig. A-55). The dimensions (parameter $p^{i}_{14\text{-}17}$) of the frame structures, shown in Fig. A38-46, were determined in an iterative calculation process under consideration of the FE results (stress-strength-stiffness-dependencies). This iterative approach is not documented to reduce the number of presented

sub-models. Therefore, the following investigations refer to the final joint geometries to be realised in practice.

The FE model took large displacement into account according to Theory III. order, used an iterative solver type to provide an effective convergence and calculated with the Newton Raphson method for the non-linear deformation. The Poisson's ratio was set for all analysis to 0.35.

Tab. 5-8 Investigated materials for the outer moulded joint according to Fig. A-55 - A-57

Parameter[1]	Unit	Biresin® LS	Compono® 100 S	Epument® 140/5AR	C 25/30[2]	C 70/85[2]
		Epoxy resin	Polymer concrete	Polymer concrete	Normal concrete	HPC
Density	[g/cm³]	1.2	2.0	2.3	2.3	2.3
MoE	[GPa]	2.5	20	35	30	40
Compressive strength	[MPa]	100	81	140	33	78
Tensile strength	[MPa]	69	13	25	2.6	4.6

[1] Mean values of density, MoE and strengths
[2] EN 206:2021-06 [EN 206]

Analysed sub-models

A frictional stiffness between the cast steel part and the outer moulded part was taken into account under compression, with material separation under tensile stresses. Contact elements 174 (applied to the contact surfaces of the outer moulded part) and target elements 170 (applied to the target surfaces of the inner cast steel part) were chosen for the model with generated contacts through the Gaussian points (detection methods). The contact and target elements were connected according to the Augmented Lagrange method, which describes a combination between the Penalty and Lagrange method. The stiffness-based method determined the contact load according to the penalty method and applied an additional load according to the Lagrange method in case of too large penetrations between the solid elements. The iterative method repeated several times until the penetration was small enough. One advantage of this method is that the contact zone between the inner and outer joint part could be precisely evaluated without irregularities. The analysis was done for standard climate conditions (T = 20°C, rH=65%) to prove the structural functionality of the joint for service class 1. Follow-up research will focus on other service classes or the influence of temperature after completion of the material development for the outer moulded joint (see also section 5.3).

The load application and boundary support are attached in A.2.4 for each calculated sub-model. The analysis took different positions in the truss structures into account, which were classified according to the joint type to be analysed

(field, edge, support) and the load application. The edge and support joints were analysed for chord-strut angles of 30°, 45° and 60° and covered six sub-models or stress states in total. In direct comparison, the number of sub-models for the field joint for chord-strut angles of 30°, 45° and 60° increased up to 26 due to the use of the joints in different positions of the truss structures. The analysed sub-models are summarised in Fig. 5-18 and 5-19 with

– sub-models A (field joint) in the upper chord with a symmetrical compressive load application,
– sub-models B (field joint) in the upper chord with compression in the chord members and in one diagonal strut member as well as one zero-force member,
– sub-models C (field joint) in the upper chord with compression in the chord members, and compression and tension in the diagonal strut members,
– sub-models D (field joint) in the lower chord with tension in the chord members and zero-force members in the diagonal struts,
– sub-models E (field joint) in the lower chord with tension in the chord members, and compression and tension in the diagonal strut members,
– sub-models F (edge joint) in the lower chord with tension in the chord member, and compression and tension in the diagonal strut members and
– sub-models G (support joint) in the upper chord with compression in the chord member, tension in the diagonal strut member and compression in the column.

The static analysis served for the determination of a suitable MoE range for the outer moulded material and for the localisation of stress peak regions in the inner frame structure and outer material. The following parameter were determined within the simulation in order to answer questions regarding to the stress states and displacements:

– Main tensile and compressive stresses in the inner frame structure to describe the structural behaviour and to identify high-stressed regions
– Van misses stresses in the inner frame structure to determine suitable cast steel materials.
– Main tensile and compressive stresses in the outer joint material to describe the structural behaviour, to determine high-stressed regions and to evaluate if epoxy resin, polymer concrete, normal concrete or HPC are suitable as moulded materials.
– Local displacements within the drill hole of the outer moulded joint to investigate if there is a collision with the inserted threaded rods.

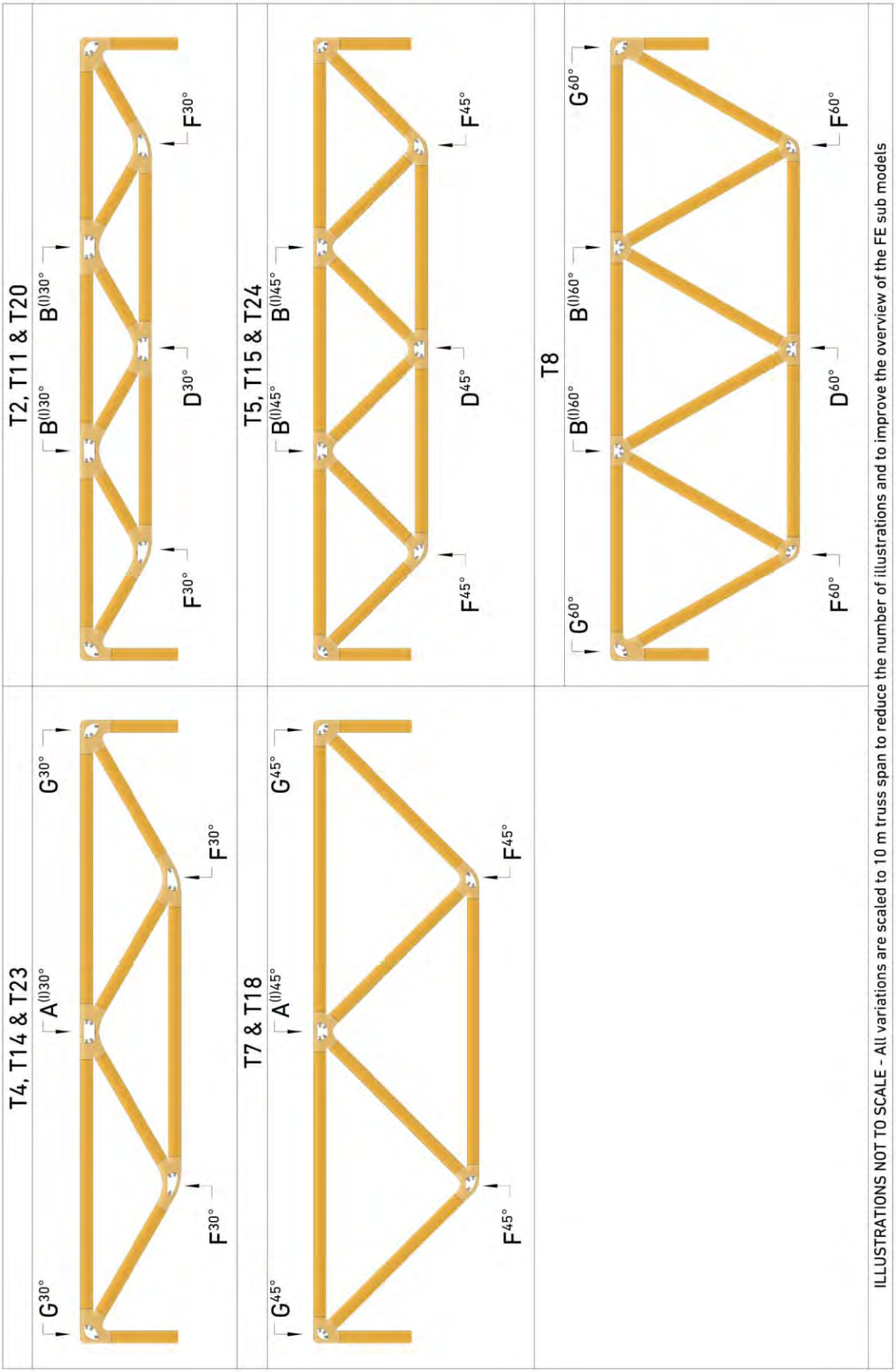

Fig. 5-18 Analysed sub-models part 1

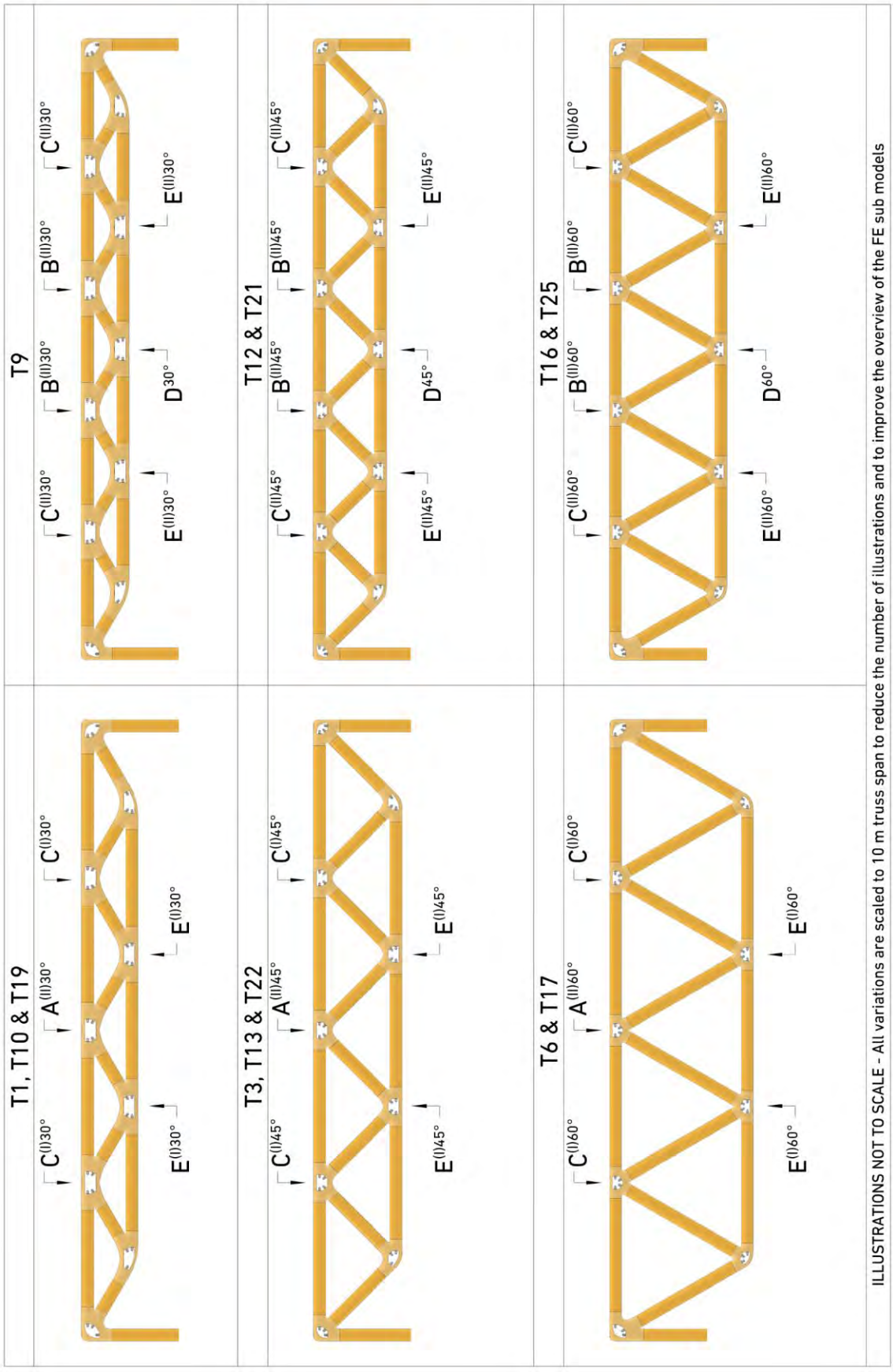

Fig. 5-19 Analysed sub-models part 2

5.2.2 Results and discussion

Field joint in the upper chord (sub-models A-C)

Sub-models A focused on the analysis of the field joints in the upper chord with a symmetrical compressive load distribution. Depending on the number of joints in the truss structure, two load stress states were classified with ($A^{(I)}$) increased vertical loads from the purlin and ($A^{(III)}$) increased compressive loads in the chord members. Both sub-models are discussed in the following.

The dependence of the maximum spatial stresses in the joint on the stiffness (MoE) of the moulded material for sub-models $A^{(I)}$ is illustrated in Fig. 5-20, with a separate evaluation of the inner frame structure (Fig. 5-20, left) and the outer moulded joint (Fig. 5-20, right). The full evaluation is attached in A.2.4 (Fig. A59-60) and includes truss variations with chord-diagonal strut angles of 30° and 45° (see also Fig. 5-18).

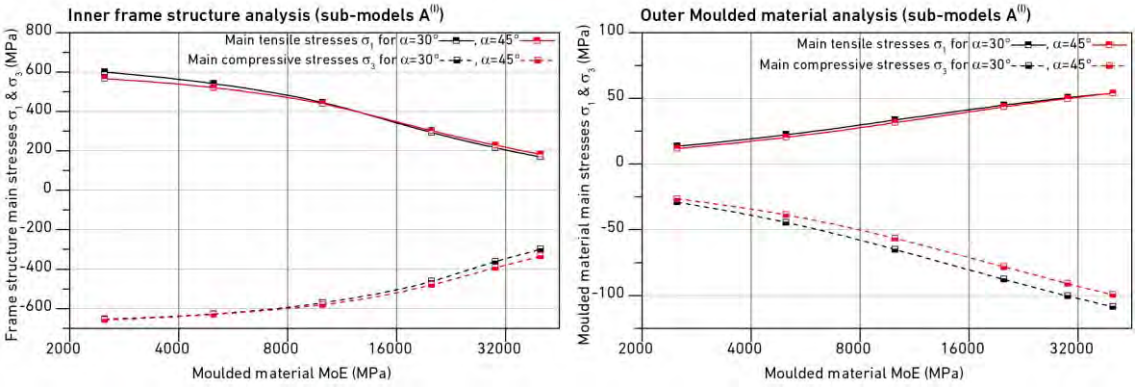

Fig. 5-20 FE analysis field joint - sub-models $A^{(I)}$

The maximum spatial stresses were located in the (assembly caused) slim frame structure 'bridge' above the side opening. As a result of the large load introduction from the purlin, the 'bridge' section bended in *z*- direction (see defined coordinate system in Fig. A-59 and following) with resulting maximum tensile and compressive stresses in this region. The evaluation of the main compressive and tensile stresses (Fig. 5-20, left) showed nearly no difference between the two analysed chord-diagonal strut angles despite different applied loads from the purlins. The closely match can be explained by the same product for the multiplication of the purlin load and the square of the 'bridge' length for α = 30° and 45°. High-stressed regions in the outer joint were observed in the moulded 'bridge' above the side opening. The trajectories of principle stresses are attached in Fig. A59-60.

As anticipated, the spatial stresses in the frame structure were found to increase with a reduction in the MoE of the surrounding moulded material. A direct comparison of the lower and upper limits of the MoE shows that reduced stiffness of the moulded material (>90%) resulted in redistribution and

– increase of main tensile stresses in the frame structure by min. 210%,

– increase of main compressive stresses in the frame structure by min. 97%,

– decrease of main tensile stresses in the outer joint by min. 75% and

– decrease of main compressive stresses in the outer joint by min. 73%.

The dependence of the maximum spatial stresses in the joint on the stiffness (MoE) of the moulded material for sub-models $A^{(II)}$ is illustrated in Fig. 5-21. The full evaluation is attached in A.2.4 (Fig. A61-63).

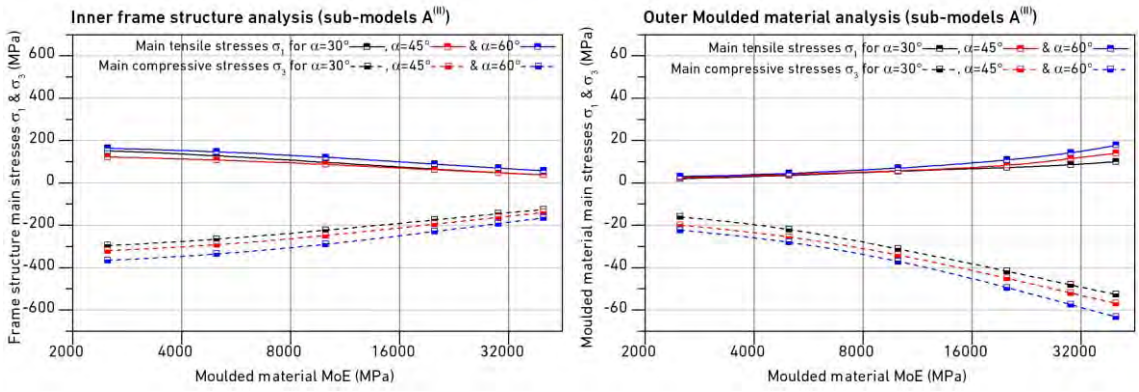

Fig. 5-21 FE analysis field joint - sub-models $A^{(II)}$

The maximum spatial stresses were located in the inner edge of the frame structure near the chord axis for α = 30°. In this case, the compressive loads in the chords and the horizontal compressive load portions in the diagonal strut members were dominating and caused bending of the frame structure in *x*-direction (see defined coordinate system in Fig. A-61 and following). The evaluation of the main compressive and tensile stresses (Fig. 5-21, left) showed an enlargement of the spatial stresses for α = 45° and 60° caused by increased purlin loads and relocated stress peaks in the frame structure 'bridge'.

High-stressed regions for tension and compression in the outer joint were observed in the moulded 'bridge' as well. For all investigated cases, sub-models $A^{(I)}$ were crucial for the design with increased stresses in the inner and outer joint part independent of the analysed moulded material MoE.

A direct comparison of the lower and upper limits of the MoE shows that reduced stiffness of the moulded material (>90%) resulted in a redistribution and

– increase of main tensile stresses in the frame structure by min. 183%,

– increase of main compressive stresses in the frame structure by min. 121%,

– decrease of main tensile stresses in the outer joint by min. 80% and

– decrease of main compressive stresses in the outer joint by min. 65%.

Sub-models B focused on the analysis of the field joints with asymmetrical compressive loads in the upper chord, compression in one diagonal strut member and one zero-force member. Depending on the number of joints in the truss structure, two load stress states were classified with ($B^{(I)}$) increased vertical loads from the purlin and ($B^{(II)}$) increased compressive loads in the chord members. Both sub-models are discussed in the following.

The dependence of the maximum spatial stresses in the joint on the stiffness (MoE) of the moulded material for sub-models $B^{(I)}$ is illustrated in Fig. 5-22. The full evaluation is attached in the appendix (Fig. A64-66).

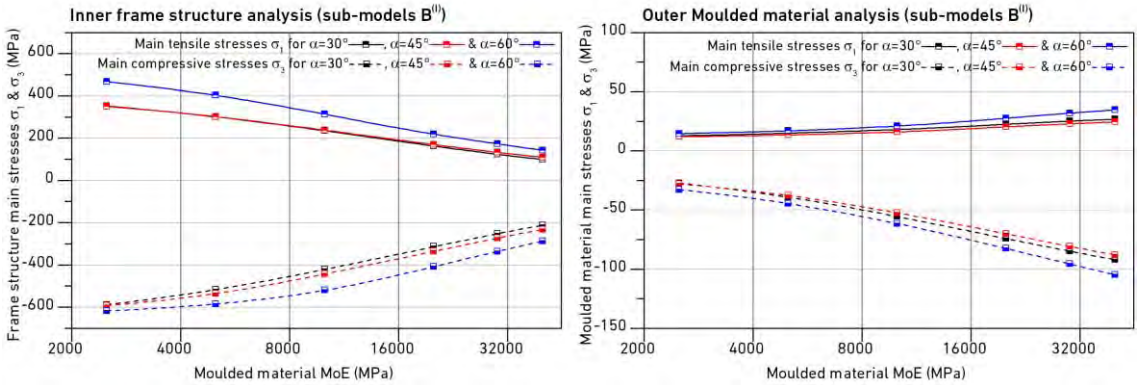

Fig. 5-22 FE analysis field joint - sub-models $B^{(I)}$

The maximum spatial stresses were observed in the (assembly caused) slim 'bridge' for the inner frame structure and outer moulded part, caused by the large load introduction from the purlin. The evaluation of the main compressive and tensile stresses (Fig. 5-22) showed also here nearly no difference between α = 30° and 45° with reduced stresses compared to 60°, independent of the investigated moulded material MoE. This tendency was observed for previous analysed sub-models as well and can be explained by the high enlargement of loads in the purlins and diagonal strut for α = 60°. The stress values for the inner and outer joint part were almost the same as for sub-models $A^{(I)}$, with additional high-stressed regions in the compressive load axis of the diagonal struts.

A direct comparison of the lower and upper limits of the MoE shows that reduced stiffness of the moulded material (>90%) resulted in a redistribution and

– increase of main tensile stresses in the frame structure by min. 221%,

– increase of main compressive stresses in the frame structure by min. 115%,

– decrease of main tensile stresses in the outer joint by min. 50% and

– decrease of main compressive stresses in the outer joint by min. 68%.

The dependence of the maximum spatial stresses in the joint on the stiffness (MoE) of the moulded material for sub-models $B^{(II)}$ is illustrated in Fig. 5-23. The full evaluation is attached in the appendix (Fig. A67-69).

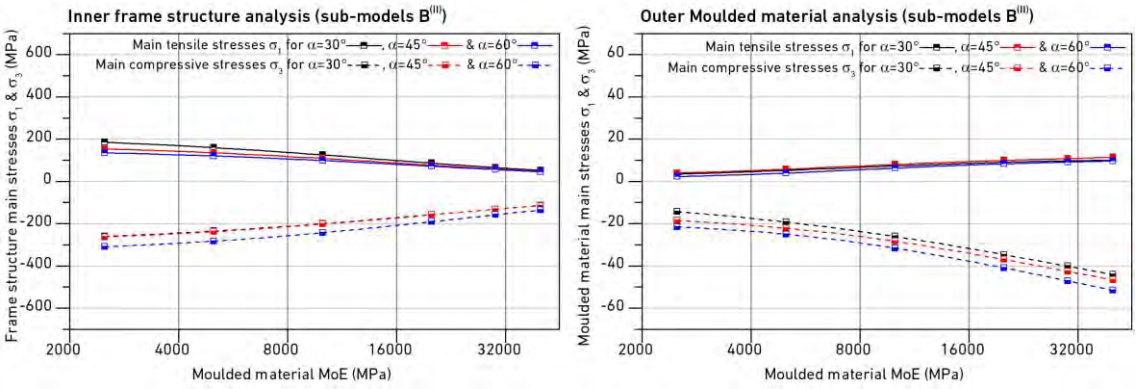

Fig. 5-23 FE analysis field joint - sub-models $B^{(II)}$

The maximum spatial stresses for tension were located in the inner edge of the frame structure near the chord axis for α = 30° and 45°. In these cases, the compressive loads in the chords and the horizontal compressive load portions in the diagonal strut members were dominating and caused bending of the frame structure in *x*-direction. For 60°, the stress peaks were observed in the frame structure 'bridge' caused by the increased purlin loads and bending in *z*-direction. The evaluation of the main tensile stresses (Fig. 5-23, left) showed a small reduction of the stresses for α = 45° and 60°, caused by the increased purlin loads, which helped to reduce the bending in the frame structure in *x*-direction near the chord axis. The main compressive stresses were observed in the (assembly caused) slim frame structure 'bridge' as a result of the purlin loads, independent of the analysed angle α or moulded material MoE.

High-stressed regions in the outer joint appeared in the moulded 'bridge'. For tension, the stress peaks were observed near the frame structure contact surface in the chord axis. The comparison of the two sub-models $B^{(I)}$ and $B^{(II)}$ showed that $B^{(I)}$ was crucial for the design with increased stresses in the inner and outer joint part independent of the analysed moulded material MoE.

A direct comparison of the lower and upper limits of the MoE shows that reduced stiffness of the moulded material (>90%) resulted in a redistribution and

– increase of main tensile stresses in the frame structure by min. 194%,

– increase of main compressive stresses in the frame structure by min. 128%,

– decrease of main tensile stresses in the outer joint by min. 65% and

– decrease of main compressive stresses in the outer joint by min. 58%.

Sub-models C focused on the analysis of the field joints with asymmetrical compressive loads in the upper chord as well as compression and tension in the diagonal strut members. Depending on the number of joints in the truss structure, two load stress states were classified with ($C^{(I)}$) increased loads in the chord members and ($C^{(II)}$) increased tensile loads in the diagonal strut member. Both sub-models are discussed in the following.

The dependence of the maximum spatial stresses in the joint on the stiffness (MoE) of the moulded material for sub-models C(I) is illustrated in Fig. 5-24. The full evaluation is attached in the appendix (Fig. A70--72).

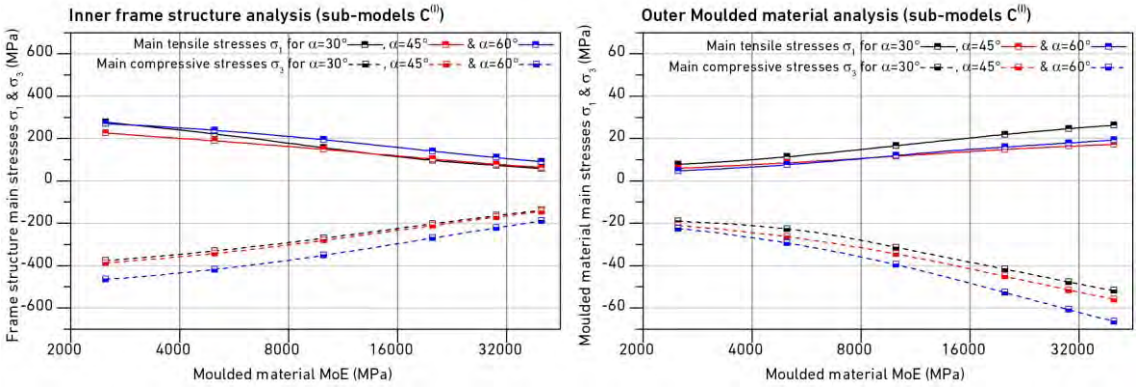

Fig. 5-24 FE analysis field joint - sub-models C(I)

The maximum spatial stresses were observed in the (assembly caused) slim 'bridge' of the inner frame structure caused by the load introduction from the purlin. The evaluation of moulded materials with a high MoE showed nearly no difference between α = 30° and 45° and increased results for 60° analogous to the previous analysed sub-models. For MoEs smaller than 10 GPa and α = 30°, the tensile stresses increased significantly with high-stressed regions in the inner edge of the frame structure near the diagonal compressive strut axis. This can be explained by softening of the surrounding material and therefore increased displacement of the frame structure in this zone.

High-stressed regions in the outer joint appeared in the moulded 'bridge' and increased significantly for α = 60°. For tension, the stress peaks were observed near the frame structure contact surface in the diagonal compressive strut axis with almost the same stress distribution for α = 45° and 60°, but increased stress values for 30°.

A direct comparison of the lower and upper limits of the MoE shows that reduced stiffness of the moulded material (>90%) resulted in a redistribution and

– increase of main tensile stresses in the frame structure by min. 198%,

– increase of main compressive stresses in the frame structure by min. 146%,

– decrease of main tensile stresses in the outer joint by min. 65% and

– decrease of main compressive stresses in the outer joint by min. 62%.

The dependence of the maximum spatial stresses in the joint on the stiffness (MoE) of the moulded material for sub-models C(II) is illustrated in Fig. 5-25. The full evaluation is attached in the appendix (Fig. A73-75).

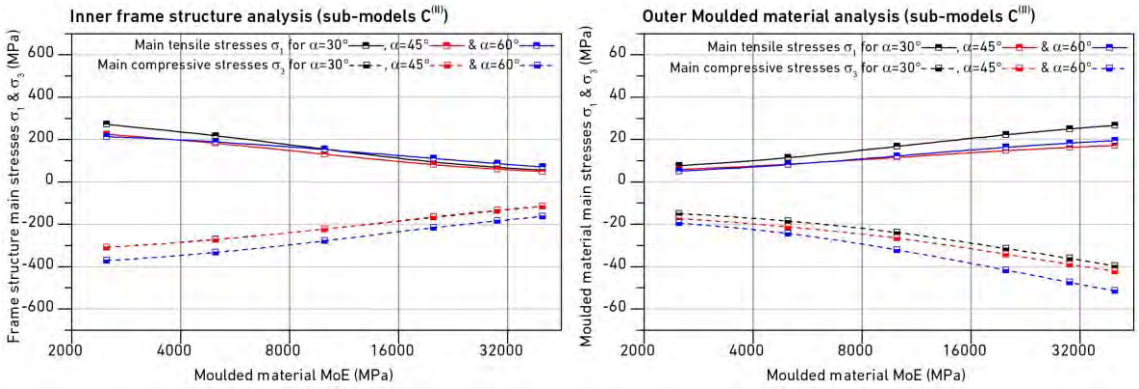

Fig. 5-25 FE analysis field joint - sub-models $C^{(II)}$

The maximum spatial stresses for tension were located in the inner edge of the frame structure near the diagonal compressive strut axis for α = 30° and 45°. For 60°, the stress peaks were observed in the frame structure 'bridge'. The evaluation of moulded materials with a high MoE showed nearly no difference between α = 30° and 45° and increased results for 60° analogous to the previous analysed sub-models. For MoEs smaller than 10 GPa and α = 30°, the tensile stresses increased significantly and were even higher than for α = 60°, caused by the low MoE of the surrounding material and therefore increased bending of the frame structure in the diagonal compressive strut axis. The main compressive stresses were observed in the (assembly caused) slim frame structure 'bridge' as a result of the purlin loads, independent of the analysed angle α or moulded material MoE.

High-stressed regions in the outer joint appeared in the moulded 'bridge'. Also here, the stresses increased significantly for α = 60°. For tension, the stress peaks were observed near the frame structure contact surface in the diagonal compressive strut axis with almost the same stress distribution for α = 45° and 60°, but increased stress values for 30°. The comparison of the two sub-models $C^{(I)}$ and $C^{(II)}$ showed that $C^{(I)}$ was crucial for the design with increased stresses in the inner and outer joint part independent of the analysed moulded material MoE.

A direct comparison of the lower and upper limits of the MoE shows that reduced stiffness of the moulded material (>90%) resulted in a redistribution and

– increase of main tensile stresses in the frame structure by min. 201%,

– increase of main compressive stresses in the frame structure by min. 128%,

– decrease of main tensile stresses in the outer joint by min. 65% and

– decrease of main compressive stresses in the outer joint by min. 58%.

Field joint in the lower chord (sub-models D-E)

Sub-models D focused on the analysis of the field joints with symmetrical tensile loads in the lower chords and zero-force members in the diagonal struts. The dependence of the maximum spatial stresses in the joint on the stiffness (MoE) of the moulded material for sub-models D is illustrated in Fig. 5-26. The full evaluation is attached in the appendix (Fig. A76-78).

The maximum spatial stresses were observed in the chord axis with high-stressed regions for tension and compression in the inner or outer edge of the frame structure. The use of the joint in the lower chord resulted in predominant stresses and a load transfer from chord to chord, which was mainly achieved by the inner frame structure. The applied load was 150 kN independent of the analysed angle α with decreasing stresses for α = 45° and 60°, caused by the smaller geometry of the frame structure.

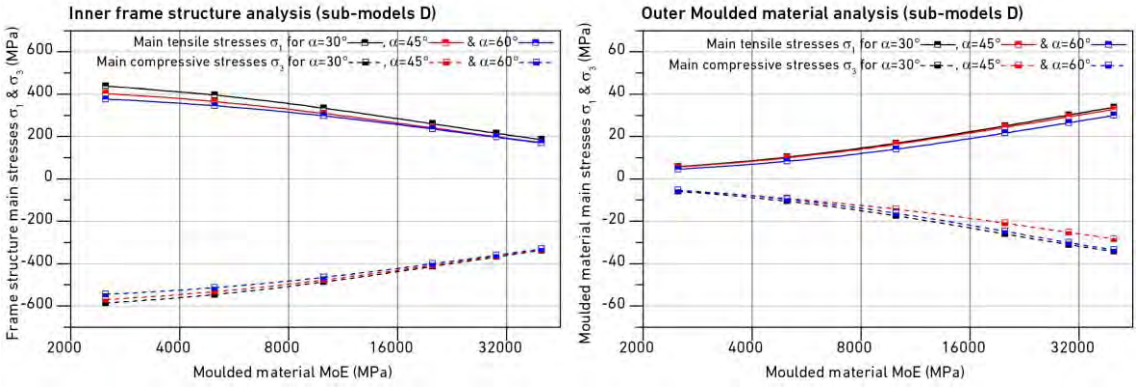

Fig. 5-26 FE analysis field joint - sub-models D

High-stressed regions in the moulded material resulted from the coupling of the chord members in the centre of the (assembly caused) slim 'bridge' section. High-stressed regions for tension and compression were observed in the moulded material contact surface to the inner frame structure in the chord axes.

A direct comparison of the lower and upper limits of the MoE shows that reduced stiffness of the moulded material (>90%) resulted in a redistribution and

- increase of main tensile stresses in the frame structure by min. 122%,
- increase of main compressive stresses in the frame structure by min. 64%,
- decrease of main tensile stresses in the outer joint by min. 82% and
- decrease of main compressive stresses in the outer joint by min. 80%.

Sub-models E focused on the analysis of the field joints with asymmetrical tensile loads in the lower chord as well as compression and tension in the diagonal strut members. Depending on the number of joints, two load stress states were classified with ($E^{(I)}$) increased loads in the chord and ($E^{(II)}$) increased loads in the diagonal strut members. Both sub-models are discussed in the following.

The dependence of the maximum spatial stresses in the joint on the stiffness (MoE) of the moulded material for sub-models $E^{(I)}$ is illustrated in Fig. 5-27. The full evaluation is attached in the appendix (Fig. A79-81).

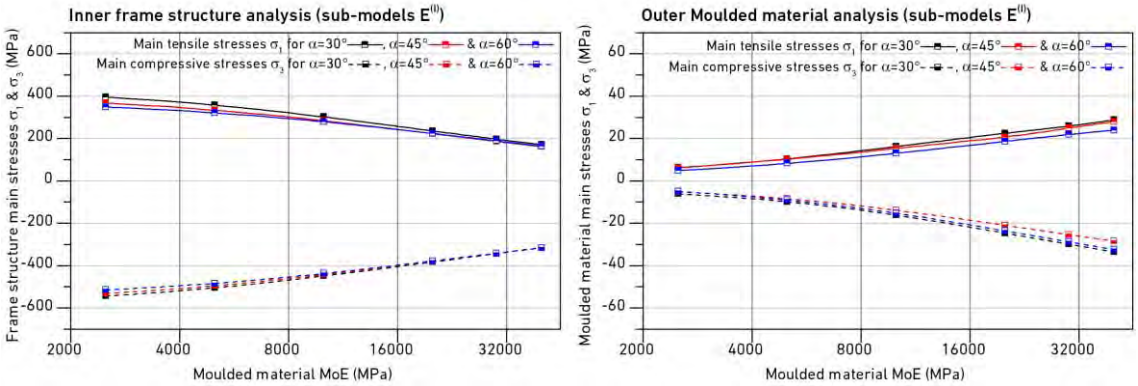

Fig. 5-27 FE analysis field joint - sub-models $E^{(I)}$

The maximum spatial stresses were observed in the chord axis with high-stressed regions in the inner or outer edge of the frame structure. Here should be noted, that the stress values were reduced a bit compared to sub-models D due to decreased forces in the lower chord members. The stress distribution of the spatial stresses in the frame structure (Fig. 5-27, left) showed a good convergence for all analysed chord-diagonal strut angles with a small stress reduction for α = 45° and 60°, caused by the smaller geometry of the frame structure.

High-stressed regions in the moulded material were observed in the contact surface to the inner frame structure analogous to sub-models D. High-stressed regions for tension resulted from the coupling of the tensile and compressive loads in the diagonal strut members.

A direct comparison of the lower and upper limits of the MoE shows that reduced stiffness of the moulded material (>90%) resulted in a redistribution and

– increase of main tensile stresses in the frame structure by min. 112%,

– increase of main compressive stresses in the frame structure by min. 63%,

– decrease of main tensile stresses in the outer joint by min. 77% and

– decrease of main compressive stresses in the outer joint by min. 81%.

The dependence of the maximum spatial stresses in the joint on the stiffness (MoE) of the moulded material for sub-models $E^{(II)}$ is illustrated in Fig. 5-28. The full evaluation is attached in the appendix (Fig. A82-84). The evaluation clarified hardly any influence on the spatial stresses in the moulded material and frame structure compared to sub-models D and $E^{(I)}$.

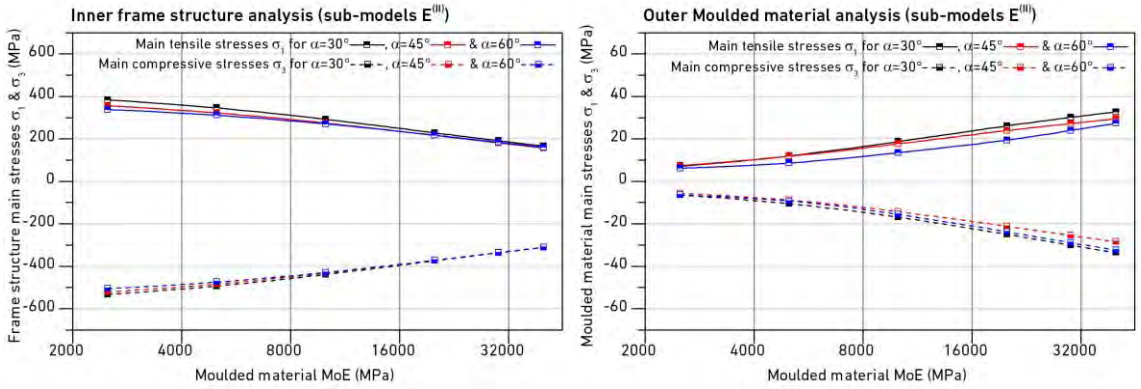

Fig. 5-28 FE analysis field joint - sub-models $E^{(II)}$

A direct comparison of the lower and upper limits of the MoE shows that reduced stiffness of the moulded material (>90%) resulted in a redistribution and

- increase of main tensile stresses in the frame structure by min. 111%,
- increase of main compressive stresses in the frame structure by min. 62%,
- decrease of main tensile stresses in the outer joint by min. 74% and
- decrease of main compressive stresses in the outer joint by min. 80%.

Edge joint (Sub-models F)

The edge joints were evaluated for three models (one sub-model for each chord-diagonal strut angle) with tension in the chord member, compression in the adjacent diagonal strut and tension in the second diagonal strut, which transmits the loads in the direction of the support joint.

The dependence of the maximum spatial stresses in the joint on the stiffness (MoE) of the moulded material is illustrated in Fig. 5-29. The full evaluation is attached in the appendix (Fig. A85-87).

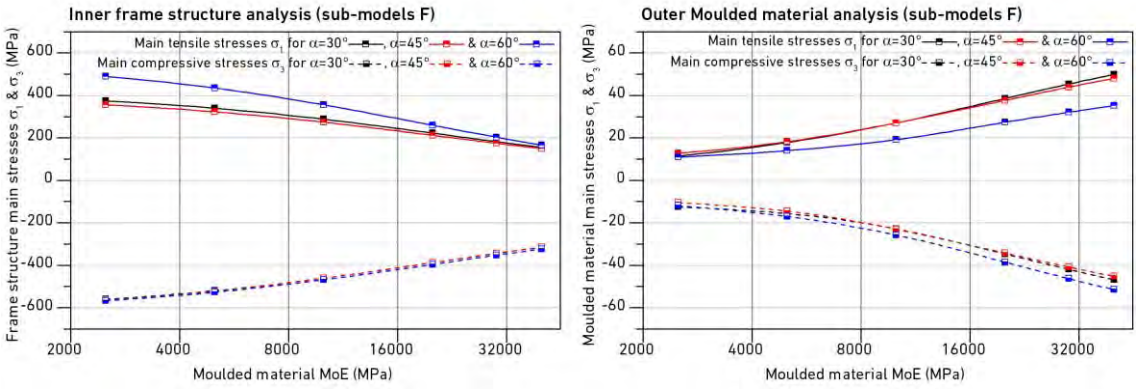

Fig. 5-29 FE-analysis edge joint - sub-models F

The evaluation of the main compressive stresses showed nearly no difference between the three analysed chord-diagonal strut angles caused by the uniform applied tensile load of 150 kN in the chord members. The main tensile stresses appeared in the outer edge of the frame structure for α = 30° and 45° with almost similar stress distribution. For 60°, the main tensile stresses increased and could be observed in the inner edge of the frame structure in the diagonal compressive strut axis, caused by the increased compressive load up to 150 kN.

The main compressive stresses in the moulded material showed nearly the same distribution for all analysed angles. For materials with a high MoE, the stress peaks resulted from the coupling of the tensile loads in the chord and diagonal strut members in the (assembly caused) slim 'bridge' section.

A direct comparison of the lower and upper limits of the MoE shows that reduced stiffness of the moulded material (>90%) resulted in a redistribution and

– increase of main tensile stresses in the frame structure by min. 138%,
– increase of main compressive stresses in the frame structure by min. 75%,
– decrease of main tensile stresses in the outer joint by min. 69% and
– decrease of main compressive stresses in the outer joint by min. 63%.

Support joint (Sub-models G)

The support joints were evaluated for three models (one sub-model for each chord-diagonal strut angle) with compression in the chord member, tension in the diagonal strut and compression in the direction of the column.

The dependence of the maximum spatial stresses in the joint on the stiffness (MoE) of the moulded material is illustrated in Fig. 5-30. The full evaluation is attached in the appendix (Fig. A88-90).

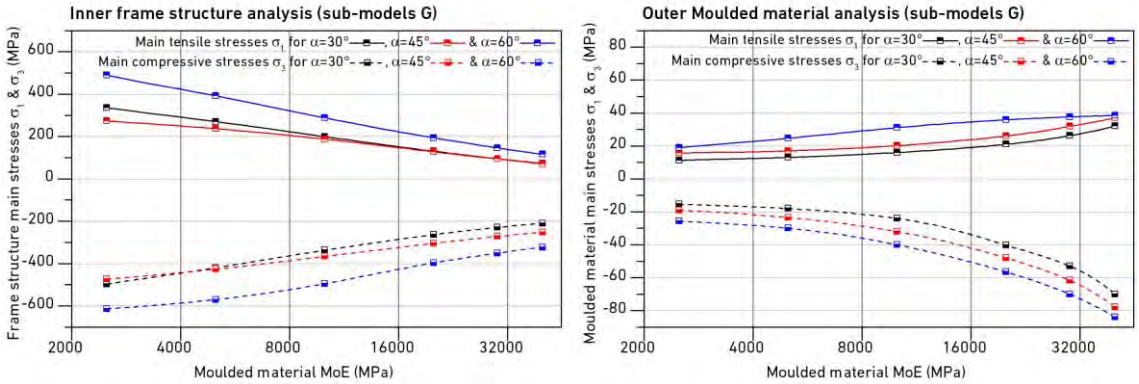

Fig. 5-30 FE analysis edge joint - sub-models G

The tensile loads in the diagonal strut were introduced in the inner edge of the frame structure with resulting stress peaks for compression in the inner edge of the frame structure. For 60°, the spatial stresses increased significantly caused by the enlargement of the applied tensile loads in the diagonal strut up to 150 kN.

High-stressed regions for compression in the moulded material were observed in the purlin load introduction area for materials with a low MoE. The deviation of the stresses for the three analysed chord-diagonal strut angles could be explained by different applied vertical loads as well as varying widths for the load introduction depending on the used UPE profile. High-stressed regions for tension resulted from the coupling of the compressive loads in the chord and column members in the (assembly caused) slim 'bridge' section. For 60°, the main tensile stresses increased significantly caused by an enlargement of compressive loads in the chord and column members.

A direct comparison of the lower and upper limits of the MoE shows that reduced stiffness of the moulded material (>90%) resulted in

– increase of main tensile stresses in the frame structure by min. 286%,

– increase of main compressive stresses in the frame structure by min. 88%,

– decrease of main tensile stresses in the outer joint by min. 50% and

– decrease of main compressive stresses in the outer joint by min. 69%.

Conclusions and discussion of suitable materials

To determine suitable materials for the outer moulded joint and inner frame structure, the results of the analysis for the joints types are discussed in the following paragraph by a comparison of the stress values with the strength parameter of the proposed materials in section 5.2.1. Here should be noted, that this section serves for a preliminary evaluation of the material properties of the outer moulded joint by a comparison of strength mean values (Tab. 5-8) with design values according to the results of the numerical analysis. The approach is sufficient to discuss possible materials with suitable stiffness and strength parameter. A comparison between design stress and strength values for the outer moulded part is added in section 5.3 after the experimental investigations on the finally applied composite material.

The application of the different materials was evaluated for each sub-model, followed by a final discussion on a uniform solution for the nine developed joints to guarantee the modular use in all 25 truss variations. Tab. 5-9 summarises the strength and stiffness parameter for normal concrete and illustrates the problem of moulded materials with a high MoE, which resulted in main tensile and compressive stresses in the moulded material far exceeding the tensile and compressive strengths (highlighted in red in Tab. 5-10). Unreinforced normal concrete is thus not suitable for use as the moulded material due to its high MoE and low strengths. Variations with reinforcement were discarded because of the complexity in the fabrication process, as well as different locations of the tensile stress peaks in the moulded material depending on the analysed sub-model.

Tab. 5-9 Results on the application possibility of unreinforced normal concrete

	Tension			Compression		
Unit	[MPa]					
Strength C 25/30[1]	2.6			-33.0		
Stresses[2] in sub-model	$\alpha = 30°$	$\alpha = 45°$	$\alpha = 60°$	$\alpha = 30°$	$\alpha = 45°$	$\alpha = 60°$
$A^{(I)}$	50.5	49.8	-	-100.4	-91.0	-
$A^{(II)}$	8.6	11.5	14.2	-48.2	-52.0	-57.5
$B^{(I)}$	25.1	22.8	31.8	-84.8	-80.8	-95.7
$B^{(II)}$	9.7	10.8	9.2	-40.2	-42.6	-47.1
$C^{(I)}$	24.7	16.3	17.9	-47.7	-51.5	-60.8
$C^{(II)}$	25.0	16.3	18.3	-36.1	-38.9	-47.5
D	30.2	29.3	26.5	-31.0	-25.3	-30.0
$E^{(I)}$	25.8	24.9	21.9	-29.9	-25.4	-28.8
$E^{(II)}$	30.1	27.2	24.0	-30.0	-25.5	-28.9
F	45.4	43.9	32.1	-41.9	-40.8	-46.3
G	26.3	31.8	37.6	-53.0	-61.7	-70.0

[1] Mean values, [2] Values in the ultimate limit state
Red values highlight ULS stresses exceeding the mean value strengths

Tab. 5-10 summarises the strength and stiffness parameter for high performance concrete and illustrates the problem of cement-based concretes in general. Despite the increased compressive strength and the ability to take over the compressive stresses for most of the analysed sub-models, the high MoE resulted in main tensile stresses in the moulded material far exceeding the tensile strengths. Unreinforced high performance concrete is thus not suitable for use as the moulded material due to its high MoE and low tensile strength. Also here, variations with reinforcement were discarded because of the complexity in the fabrication process.

Tab. 5-10 Results on the application possibility of unreinforced high performance concrete

	Tension			Compression		
Unit	[MPa]					
Strength C 70/85[1]	4.6			-78.0		
Stresses[2] in sub-model	$\alpha = 30°$	$\alpha = 45°$	$\alpha = 60°$	$\alpha = 30°$	$\alpha = 45°$	$\alpha = 60°$
$A^{(I)}$	53.8	53.8	-	-108.6	-99.5	-
$A^{(II)}$	10.1	14.0	17.8	-52.7	-57.0	-63.2
$B^{(I)}$	26.7	24.5	34.6	-91.9	-88.0	-104.8
$B^{(II)}$	10.0	11.4	9.6	-44.0	-46.6	-51.6
$C^{(I)}$	26.3	17.2	19.3	-51.8	-55.9	-66.3
$C^{(II)}$	26.3	17.2	19.5	-39.7	-42.2	-51.5
D	33.8	32.8	30.0	-34.3	-28.3	-33.5
$E^{(I)}$	28.8	28.0	24.0	-33.5	-28.4	-32.4
$E^{(II)}$	32.7	29.4	27.3	-33.6	-28.4	-32.4
F	49.8	48.0	35.2	-46.9	-45.2	-51.4
G	32.1	37.0	38.5	-70.0	-77.8	-84.0

[1] Mean values, [2] Values in the ultimate limit state
Red values highlight stresses in ULS exceeding the mean value strengths

The first investigated polymer concrete type, Epument® 140/5AR, performed with an higher compressive strength exceeding the main compressive stresses for all analysed sub-models (Tab. 5-11). Despite the good performance for compression, the high MoE of 35 GPa resulted in main tensile stresses in the moulded material far exceeding the tensile strength of 25 MPa for almost all analysed joint types. The second investigated polymer concrete type, Compono® 100 S, performed with reduced strengths (compression and tension), but reduced stiffness (20 GPa) in direct comparison to Epument® 140/5AR. Tab. 5-12 summarises the results with a good performance for compression, but with main tensile stresses in the moulded material far exceeding the tensile strength of 13 MPa analogous to the analysis of Epument® 140/5AR. For both polymer concrete types, variations with reinforcement were discarded because of the complexity in the fabrication process. In summary, both cement-based and polymer concrete are unsuitable as moulded materials due to their high MoE and low tensile strengths.

Tab. 5-11 Results on the application possibility of polymer concrete (Epument® 140/5AR)

	Tension			Compression		
Unit	[MPa]					
Strength Epument[1]	25.0			-140.0		
Stresses[2] in sub-model	$\alpha = 30°$	$\alpha = 45°$	$\alpha = 60°$	$\alpha = 30°$	$\alpha = 45°$	$\alpha = 60°$
$A^{(I)}$	52.4	52.1	-	-105.0	-95.8	-
$A^{(II)}$	9.3	12.9	16.0	-50.7	-54.8	-60.7
$B^{(I)}$	26.0	23.7	33.4	-88.8	-84.8	-100.8
$B^{(II)}$	9.9	11.2	9.5	-42.3	-44.8	-49.6
$C^{(I)}$	25.6	16.9	18.7	-50.0	-54.0	-63.9
$C^{(II)}$	26.0	16.8	19.0	-38.0	-40.8	-49.7
D	32.2	31.3	28.4	-32.9	-27.0	-32.0
$E^{(I)}$	27.5	26.6	23.1	-31.9	-27.1	-30.8
$E^{(II)}$	31.6	28.5	25.8	-32.0	-27.2	-30.9
F	47.9	46.2	33.8	-44.7	-43.3	-49.2
G	29.2	34.6	38.2	-60.8	-69.5	-77.1

[1] Mean values, [2] Values in the ultimate limit state
Red values highlight stresses in ULS exceeding the mean value strengths

Tab. 5-12 Results on the application possibility of polymer concrete (Compono® 100 S)

	Tension			Compression		
Unit	[MPa]					
Strength Compono[1]	13.0			-81.0		
Stresses[2] in sub-model	$\alpha = 30°$	$\alpha = 45°$	$\alpha = 60°$	$\alpha = 30°$	$\alpha = 45°$	$\alpha = 60°$
$A^{(I)}$	44.8	43.4	-	-87.8	-78.3	-
$A^{(II)}$	7.2	8.3	10.8	-41.7	-45.1	-49.5
$B^{(I)}$	22.5	20.3	27.6	-74.2	-70.1	-82.5
$B^{(II)}$	9.1	10.0	8.3	-34.7	-37.0	-41.0
$C^{(I)}$	22.0	14.8	16.0	-41.7	-45.1	-52.7
$C^{(II)}$	22.2	14.7	16.3	-31.5	-34.2	-41.6
D	25.0	24.4	21.6	-26.0	-20.9	-24.8
$E^{(I)}$	22.5	20.7	18.7	-24.6	-21.0	-23.6
$E^{(II)}$	26.2	23.9	19.4	-25.0	-21.2	-23.8
F	38.6	37.7	27.4	-34.7	-34.3	-38.6
G	21.0	26.0	35.9	-40.3	-48.0	-56.5

[1] Mean values, [2] Values in the ultimate limit state
Red values highlight stresses in ULS exceeding the mean value strengths

Tab. 5 13 summarises the results for epoxy resin (Biresin® LS) and illustrates the advantages of moulded materials with a low MoE (2.5 GPa), resulting in material strengths higher than the tensile and compressive stresses observed in the analyses. Epoxy resin is thus suitable for use as the moulded material, even without the installation of reinforcement to take over high tensile stresses.

Tab. 5-13 Results on the application possibility of epoxy resin (Biresin® LS)

	Tension			Compression		
Unit	[MPa]					
Strength Biresin[1]	69.0			-100.0		
Stresses[2] in sub-model	$\alpha = 30°$	$\alpha = 45°$	$\alpha = 60°$	$\alpha = 30°$	$\alpha = 45°$	$\alpha = 60°$
$A^{(I)}$	13.6	12.2	-	-29.1	-28.6	-
$A^{(II)}$	2.0	2.5	3.0	-16.0	-20.0	-22.4
$B^{(I)}$	12.9	12.0	14.6	-27.3	-28.0	-30.0
$B^{(II)}$	3.4	4.0	2.3	-14.4	-18.5	-21.6
$C^{(I)}$	7.7	6.0	4.8	-19.0	-21.0	-22.4
$C^{(II)}$	7.6	5.9	5.1	-15.0	-17.4	-19.4
D	5.8	5.6	4.6	-5.9	-5.4	-5.3
$E^{(I)}$	6.2	6.3	5.0	-6.2	-5.2	-5.0
$E^{(II)}$	7.1	7.4	6.1	-6.5	-5.7	-6.4
F	11.4	12.7	11.0	-12.5	-10.5	-12
G	11.3	15.8	17.0	-15.4	-19	-25.7

[1] Mean values, [2] Values in the ultimate limit state

The maximum spatial stresses in the cast steel frame structure of the field joints were observed for sub-models or positions $A^{(I)}$ and $B^{(I)}$, covering the use in the upper chord with an increased introduced load from the purlin. For positions F and G maximum spatial stresses were observed mostly in the contact surface between washer and frame structure (load introduction area of the tensile loads). The spatial stresses in the cast steel frame structure increased for all investigated sub-models with a reduction in the MoE of the surrounding moulded material. To be in line with the previous mentioned and required low MoE of the moulded material and therefore to ensure the structural functionality of the joint, the following evaluation of the frame structure stresses was done for a moulded material MoE of 2.5 GPa, matching the required stiffness in the joint. For the definition of a suitable material, the Van misses stresses were evaluated and compared with certified steel castings for structural uses in Germany [EN 1034]. Based on the results (Tab. 5-14), a suitable cast steel material was chosen: G18NiMoCr3-6 (Fig. A-58) with a tensile strength of 630 MPa and maximum allowable thickness of 150 mm.

Tab. 5-14 Results on the spatial and van misses stresses in the inner frame structure

Sub-model	Maximum tensile stresses[1]	Maximum compressive stresses[1]	Van misses stresses[1]
	[MPa]		
$A^{(I)\ 30°}$	598	-654	577
$A^{(I)\ 45°}$	566	-658	555
$B^{(I)\ 60°}$	468	-617	531
$F^{30°}$	374	560	489
$F^{45°}$	356	-564	491
$F^{60°}$	489	-566	494
$G^{30°}$	335	-497	450
$G^{45°}$	273	-473	418
$G^{60°}$	489	-613	531

[1] Values in the ultimate limit state for moulded material MoE of 2.5 GPa

The low MoE of epoxy resin resulted in increased local displacements of the joints, which were evaluated to determine a possible collision with the inserted threaded rods. Fig. 5-31 shows the local displacement parameters, using the example of a chord-diagonal strut angle of 45°. Instead of presenting the local displacements for each position, highlighted in blue in Fig. 5-31, the maximum displacement for each sub-model was evaluated (Tab. 5-15) and compared to the maximum allowable displacement defined by the slip between rod and drill hole in the outer moulded joint (2.5 mm according to parameter p_{10} and p_{18}). For all sub-models, the limit value of 2.5 mm was complied with.

Tab. 5-15 Results on the max. displacement in local z-direction (Biresin® LS)

	Maximum displacement		
Unit	[mm]		
Sub-model	$\alpha = 30°$	$\alpha = 45°$	$\alpha = 60°$
$A^{(I)}$	2.2	1.35	-
$A^{(II)}$	0.8	0.5	0.5
$B^{(I)}$	2.5	1.7	1.1
$B^{(II)}$	1.2	0.8	0.5
$C^{(I)}$	2.2	1.3	0.8
$C^{(II)}$	1.9	1.2	0.6
D	0.4	0.3	0.3
$E^{(I)}$	0.7	0.2	0.2
$E^{(II)}$	0.8	0.4	0.2
F	2.3	1.2	0.7
G	0.8	1.0	0.9

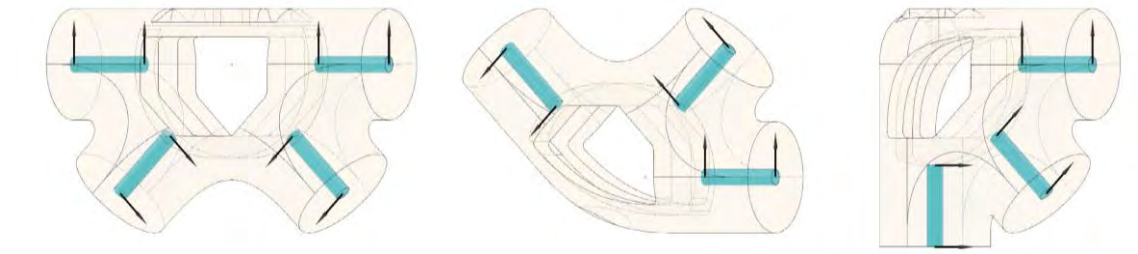

Fig. 5-31 Displacement of outer moulded joint drill hole surfaces in local z-direction

Based on the results of the FE analysis, the structural functionality was proved for the inner cast-steel frame structure (G18NiMoCr3-6) and outer joint for applied moulded materials with a low MoE, around 2.5 GPa. Polymer or cement-based concretes were found to be unsuitable because of their high MoE and resulting high tensile stresses in the moulded material.

Despite the advantages of epoxy resin, the use as pure outer moulded material did not match with the overall ecological concept of the developed joining technology for roundwood trusses. On this basis, the last research questions of this thesis were phrased on how to modify epoxy resin with

– renewable materials as fillers,
– a reduced density of approximate 1 g/cm^3 to improve the truss STW ratios,
– a ductile failure mechanism,
– a MoE of ~2.5 GPa analogous to Biresin® LS,
– a minimum design compressive strength of ~30 MPa (see also Tab. 5-13) and
– a minimum design tensile strength of ~17 MPa (see also Tab. 5-13).

Section 5.3 focused on these issues with experimental investigations on a moulded material composed of Biresin® LS and wood fibres, named wood-fibre composite.

5.3 EXPERIMENTAL INVESTIGATIONS ON WOOD-FIBRE COMPOSITE

5.3.1 Materials and methods

Wood plastic composites and associated fabrication methods

Due to the large amounts of waste generated by the construction industry, it has become crucial to explore renewable building materials that can be used in wider scope and more innovative ways in engineering. For classification of the investigated moulded material in this section, a short overview on natural fibre composites and reinforced plastics is introduced in the following paragraphs.

Natural fibre composites (NFCs) consist of cellulose, thermoplastics (polyethylene or polypropylene) and additives. Wood flour (and in some cases also wood chips) is used as a filling agent, whereby the ratio between filler and binder varies depending on the application. The advantages over traditional wood-based materials are the free, three-dimensional formability and the improved resistance to moisture. A disadvantage is the reduced breaking or fracture strength [STA 2008]. This is also why, NFCs are not suitable for load-bearing components and are currently used in minor structural tasks in the automotive and building industry [LAU 2018]. Due to increased environmental awareness and increasing awareness of the energy balance of materials, the demand for plastics made from renewable and biodegradable raw materials in NFCs is increasing.

Natural fibre-reinforced plastics (NFRPs) consist of a fossil- or bio-based plastic, the rigidity and strength of which is maintained through integrated natural fibres. NFRPs have some good properties, such as high stiffness, high tensile strength and low density. The majority of NFRPs are produced in a compression moulding process and are mainly used in the automotive and building industry as shell structures with a small wall thickness [GEN 2013]. One example describes the 'BioMat' research pavilion [DAH 2019] with a 3.6-metre-high shell structure and approximate 10-metre-span, located on the campus of the University of Stuttgart. What's special about this project is the modular construction of lightweight, single-curved elements forming a double-curved shell with individual segments of veneer-reinforced elastic bio composite cores.

Next to the compression moulding fabrication process, further methods are commonly used for NFCs and NFRPs, such as the resin injection method, also known as resin transfer moulding method, which creates high performance composite components by using a closed-mould [GAR 2022]. Moulds are typically made from matched metal tools into which a preform of dry fibres is inserted. After closing and clamping down the mould, resin is pumped into the tool cavity to thoroughly wet-out the fibres. Often the tool is heated to facilitate the curing of the resin. In addition, the closed-mould can be put under vacuum, which needs to be reduced during the filling process in order to inject or pump the epoxy resin system

into the mould. Due to the use of matched metal tools, parts have a good surface finish all over, requiring little finishing. If a suitable resin and a high injection pressure are used, the process can be extremely quick. Depending on the size of the part, cycles of just a few minutes are feasible. Despite the advantages, the fabrication method is mainly suitable for structures with a small wall thickness and does not guarantee a homogenous distribution of the mixture, resulting in undesired cavities and irregularities.

A further fabrication method involves vacuum resin infusion, where, analogous to resin transfer moulding, fibres are laid into the closed-mould before being subjected to vacuum pressure through the use of a composites vacuum pump. Once all the air has been removed from the mould and the fibres have been fully compressed under this pressure, epoxy resin is introduced through a pipe which then infuses through the fibres under the vacuum pressure. As soon as the resin has fully infused through the fibres, the resin supply is cut off using a pipe clamp and the resin is left to cure under vacuum pressure. During filling, the vacuum remains constantly. Resin infusion can produce parts with incredible strength and appearance quality, as well as an optimal resin-to-fibre ratio and void free composites, avoiding performance variations [SUM 2005]. In addition and in contrast to the resin transfer moulding method, the fibres can be pre-impregnated before being subjected to vacuum pressure. The disadvantage of this method is that a reserve of epoxy resin must be taken into account to avoid air, which is being drawn into the mould. As a result, the final product contains a reduced proportion of epoxy resin, but requires an increased proportion in comparison to the wasted resin in the manufacturing process. Also here, the fabrication method is mainly suitable for structures with a small wall thickness.

Vacuum pressed fabrication of test specimens

The development of the epoxy resin and wood fibre based composite material was based on the previously stated mechanical justifications (section 5.2) and the aim of using resource-efficient sources from an ecological point of view. With wood chips or fibres used as the filling material and resin as the only binder, WFC (wood-fibre composite) can be assigned to the class of NFRP materials. Although the composition of filler (wood fibres and chips) and binder (epoxy resin) is similar to the components of wood-based materials, such as Oriented Strand Boards or chipboards, the resin proportion (~50%) adapted to WFC is substantially higher so that the mechanical parameters, as well as the possible uses are not comparable.

The manufacturing method used to produce the test specimens combined the advantages of the resin injection and vacuum resin infusion methods, i.e. pre-impregnation of the wood fibres and compaction of fillers and binder by pressing under vacuum, which achieved an optimised homogenisation of the composite. The innovation is a WFC, which can be moulded and pressed under vacuum in the manufacturing process for producing 3D solid bodies.

The binder used for the test specimens was the epoxy resin type Biresin® LS presented in section 5.2 (product data sheet in Fig. A-55). The kind of wood chips or fibres used as fillers were derived from milling recycled pine wood. The thickness or dimension of the wood fibres varied as shown in Fig. 5-32 ranging in size from fine wood chips to coarse wood fibres of irregular dimensions. The final filler mix consisted of 50% fine wood chips and 50% coarse wood fibres.

Fig. 5-32 Filler mix for woof-fibre resin test specimens

The fabrication process (vacuum pressing) of WFC specimens for testing was carried out using a cylinder to compress pre-impregnated wood fibres under vacuum. The cylinder (Fig. 5-33) consisted of

– a steel pipe with welded flanges, an insertion opening and a vacuum port,

– an inner stamp for compressing the material and

– a threaded spindle as a lifter build up a defined pressure.

The filler and the epoxy resin were mixed (volume ratio 1:1) and placed in the insertion opening of the developed cylinder. The internal stamp with threaded spindle was used to compress the WFC with a applied pressure or compressive load of ~3.0 kN. The vacuum port on the opposite side was installed to guarantee a homogenous inner distribution of the WFC. In analogy to the vacuum resin infusion method, a reserve of epoxy resin was taken into account.

The pressed cylindrical specimens (12 batches) were post-processed into 14 cylindrical specimens (diameter 80 mm and height 140 mm) and 21 prism specimens (40 40 160 mm) for testing (Fig. 5-34). After processing, they were stored in controlled conditions (65% rH and 20 °C) for 2 weeks prior to testing. The sample labelling consisted of two numbers: the first represents the production batch and the second number indicates the specimen number.

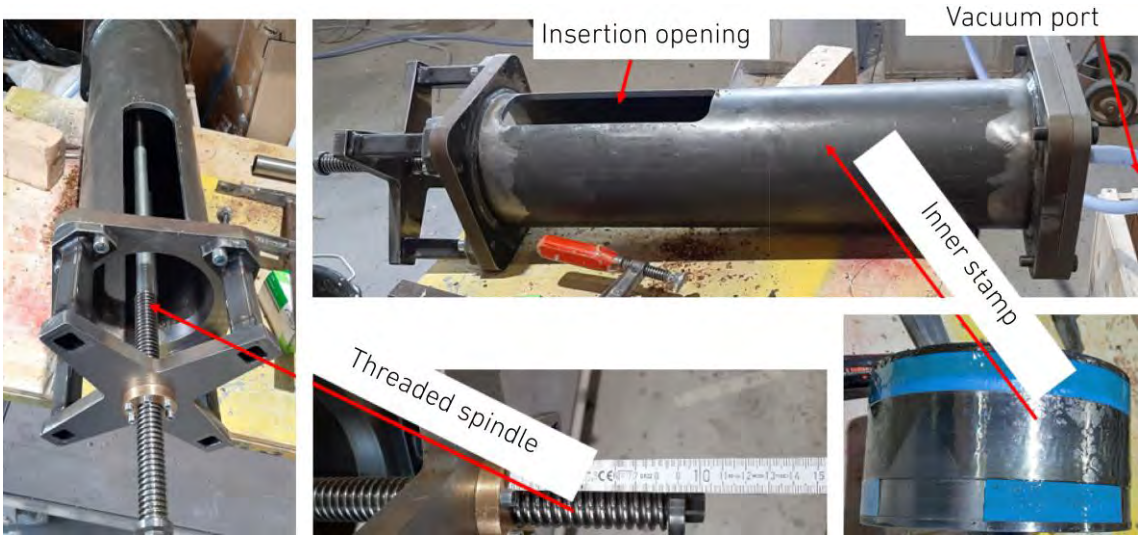

Fig. 5-33 Vacuum pressing fabrication process of wood-fibre composites

Fig. 5-34 Wood-fibre composite test specimens (production batches 1 - 12)

Test setup, instrumentation, data acquisition and processing

Compression tests were carried out on 14 cylindrical specimens to determine the MoE, yield strength, compressive strength and Poisson's ratio. Each specimen was equipped with two strain gauges to measure compressive strains in the loading or vertical direction and another strain gauge in the horizontal direction to detect the Poisson's ratio. The speed of the test machine cross-head was set to 2 mm/min. All tests were performed at room temperature (20 °C) and at constant relative humidity (65%).

Mechanical and physical properties of the prism specimens were evaluated in flexural tests, respectively, in three-point bending tests on 21 prismatic specimens to determine the flexural strengths after density measurements. The speed of the

test machine cross-head was set to 2 mm/min. The water absorption of WPCs was determined using the two-parted prism specimens after testing, which were dried at 100 °C for 24 hours and weighed after they were oven-dried. Following this, specimens were immersed in distilled water and their mass was measured after 24 hours.

Based on the obtained data for the flexural and compressive strengths, design values of the material strengths were calculated according to the EN 1990 and were compared to the previously stated mechanical justifications (section 5.2) for the moulded joint application.

5.3.2 Results and discussion

Compression tests on cylindrical test specimens

Tab. 5-16, Fig. 5-35 and 5-36 (strain–stress distribution in the loading direction) summarises the results of the compression tests. The MoE varied in the range 2.200–3.000 MPa and reached an ultimate strain up to 10% before failure (Fig. 5-35 and 5-36). The observed MoE range resulted primarily from the chosen epoxy resin type Biresin® LS with a MoE of ~2.400 MPa. Compressive stresses and strains were calculated according to Eq. 5.1.

The addition of wood fibres (filler) increased the MoE to 3.000 MPa (e.g. cylinder sample 14-1 in Tab. 5-16). In compression, the WFC material showed linear elastic behaviour up to 30 MPa (average yield strength), strain of ~1% and ultimate compressive strength in the range of 50–70 MPa. Poisson's ratio was determined to be 0.30, comparable with regular concrete or polymer concrete. The epoxy resin type Biresin® LS had a compressive strength up to 100 MPa. The WFC was found to have lower strength (50% to 70%) due to the addition of the wood fibres.

Specimens of the same fabrication batch showed different failure modes– ductile (Fig. 5-37, left) or brittle (Fig. 5-37, right) – and varying material properties. It is thought that brittle failure occurred due to an increased proportion of fine wood chips in the tested specimens. To solve this problem, in further research, quality control of the fabricated wood fibres must be done with regard to the distribution of the size and shape of the fibres. In general, the addition of fine wood chips and coarse wood fibres reduced the compressive strength of the WFC compared to the strength of the pure epoxy resin, but ensured for most of the specimens ductile failure at the same time –which is highly advisable for a composite material on a moulded joint or in the building sector in general.

$$\sigma_c = \frac{F}{\pi \cdot (40\,\text{mm})^2} \qquad \textit{(Eq. 5.1a)}$$

$$\varepsilon_c = \frac{u}{140\,\text{mm}} \qquad \textit{(Eq. 5.1b)}$$

with

σ_c	*Compressive stress*
ε_c	*Compressive strain*
F	*Applied load*
u	*Max. deformation in loading direction*

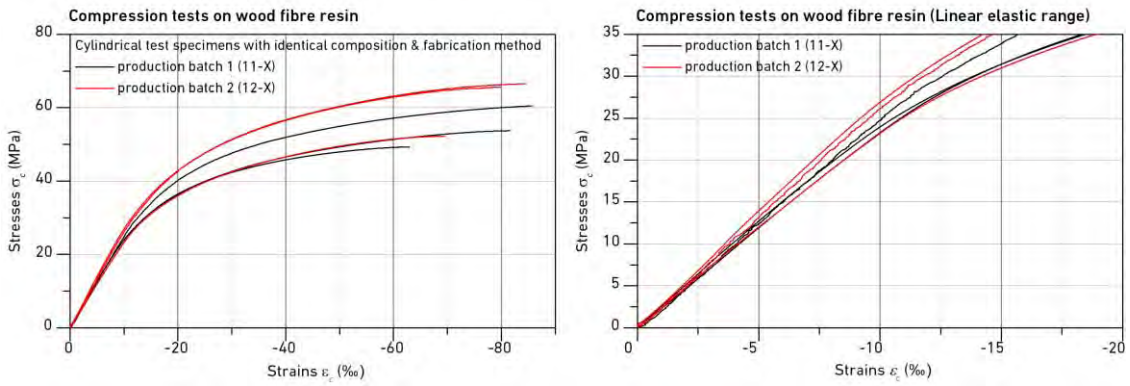

Fig. 5-35 Stress-strain distribution in cylindrical WFC specimens (production batches 1-2)

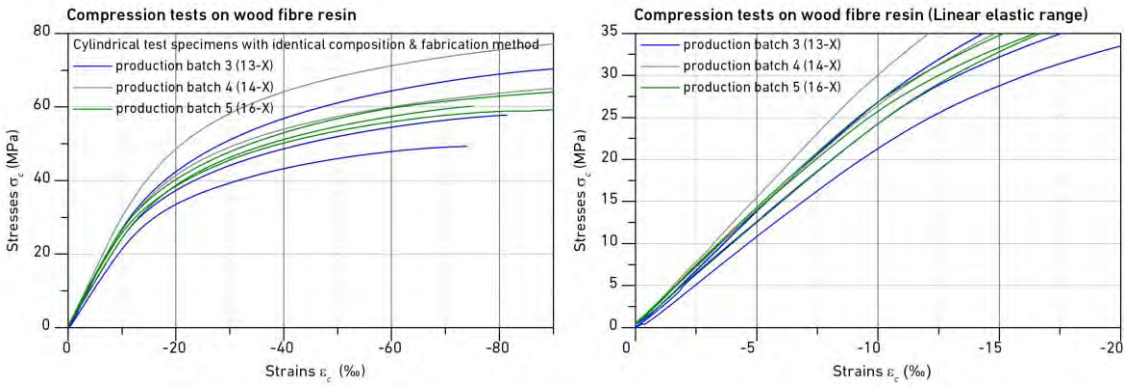

Fig. 5-36 Stress-strain distribution in cylindrical WFC specimens (production batches 3-5)

Fig. 5-37 Ductile (left) and sudden brittle (right) failure of cylindrical WFC specimens

Tab. 5-16 Compression tests on cylindrical wood-fibre composite specimens

Cylindrical sample	Production batch	MoE	Yield strength	Compressive strength	Poisson's ratio	Failure type
		[MPa]	[MPa]	[MPa]		
11-1	1	2.600	~30	60.4	0.30	Brittle
11-2	1	2.400	~30	49.2	0.34	Ductile
11-3	1	2.400	~25	53.7	0.30	Ductile
12-1	2	2.700	~30	66.5	0.31	Ductile
12-2	2	2.800	~30	65.6	0.30	Ductile
12-3	2	2.400	~25	52.6	0.30	Brittle
13-1	3	2.800	~30	70.5	0.30	Brittle
13-2	3	2.200	~25	49.6	0.28	Brittle
13-3	3	2.500	~25	57.7	0.25	Ductile
14-1	4	3.000	~30	78.4	0.27	Ductile
14-2	4	2.700	~35	66.5	0.34	Ductile
16-1	5	2.600	~30	60.2	0.30	Ductile
16-2	5	2.700	~35	65.1	0.30	Brittle
16-3	5	2.600	~35	59.4	0.34	Ductile
$\overline{x}$		2.600	~30	61.1	0.30	

Flexural tests on prismatic test specimens

The experimental set-up of the flexural tests is illustrated in Fig. 5-38. Compared with the compression test observations, the prismatic specimens showed for flexural tests linear elastic behaviour (Fig. 5-40 and 5-41) ,until final failure in the tension zone at a flexural strength of approximately ~35 MPa (Tab. 5-17). The observed fracture surface is shown in Fig. 5-39, using the example of test specimen 18-2. The WFC density was approximately 1.1 g/cm^3. The chosen epoxy resin type (Biresin® LS) had a density of 1.2 g/cm^3, representing a decrease of approximately 10% for the developed WFC due to the addition of fibres and air spaces in the specimens.

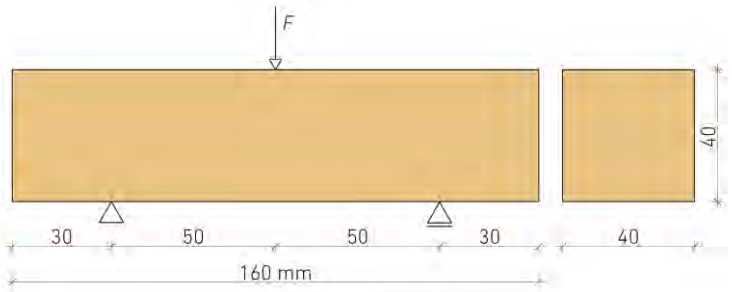

Fig. 5-38 Experimental set-up of flexural tests

$$\sigma_f = \frac{3 \cdot F \cdot 100\,\text{mm}}{2 \cdot (40\,\text{mm})^3} \qquad \textit{(Eq. 5.2a)}$$

$$\varepsilon_f = \frac{6 \cdot f \cdot 40\,\text{mm}}{(100\,\text{mm})^2} \qquad \textit{(Eq. 5.2b)}$$

with

σ_f	*Flexural stress*
ε_f	*Flexural strain*
F	*Applied load*
f	*Max. deflection in loading direction*

Fig. 5-40 and 5-41 illustrate the stress-strain distribution for the prismatic test specimens calculated according to Eq. 5.2. Even for specimens of the same production batch, an increased variance for the flexural strains and strengths were observed, caused by the inhomogeneous distribution of wood chips or fibres during the fabrication process. To solve this problem, in further study, also here quality control of the fabricated wood fibres must be done with a homogenisation of the wood fibres in both scale and ratio.

Tab. 5-17 Flexural tests on prismatic WFC[1] specimens and density measuring

Prism sample	Production batch	Flexural strength	Density
		[MPa]	[g/cm^3]
15-1	6	36.3	1.1
15-2	6	36.6	1.1
15-3	6	31.2	1.1
17-1	7	35.5	1.1
17-2	7	36.8	1.1
17-3	7	31.8	1.1
18-1	8	38.4	1.1
18-2	8	36.7	1.1
18-3	8	32.6	1.0
19-1	9	31.4	1.1
19-2	9	27.3	1.1
19-3	9	35.0	1.1
20-1	10	32.7	1.1
20-2	10	37.2	1.1
20-3	10	32.9	1.1
21-1	11	38.2	1.1
21-2	11	36.3	1.1
21-3	11	32.9	1.1
22-1	12	36.1	1.1
22-2	12	32.4	1.0
22-3	12	34.1	1.0
$\overline{x}$		34.4	1.1

[1] Wood-fibre composite

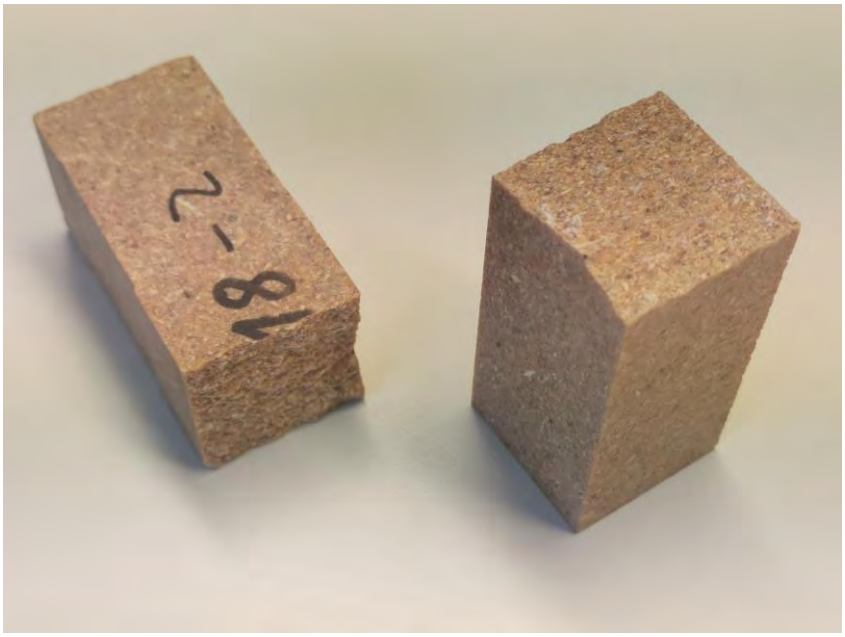

Fig. 5-39 Fracture surface of wood-fibre composite in flexural tests

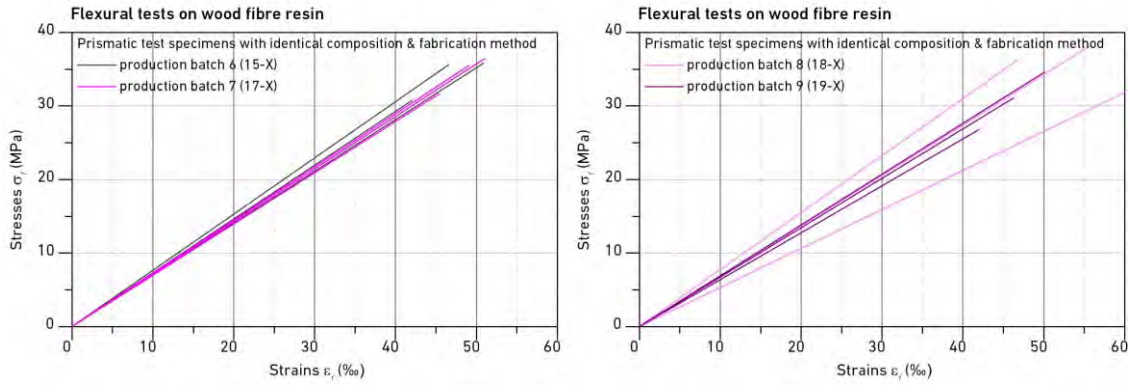

Fig. 5-40 Stress-strain distribution in prismatic WFC specimens (production batches 6-9)

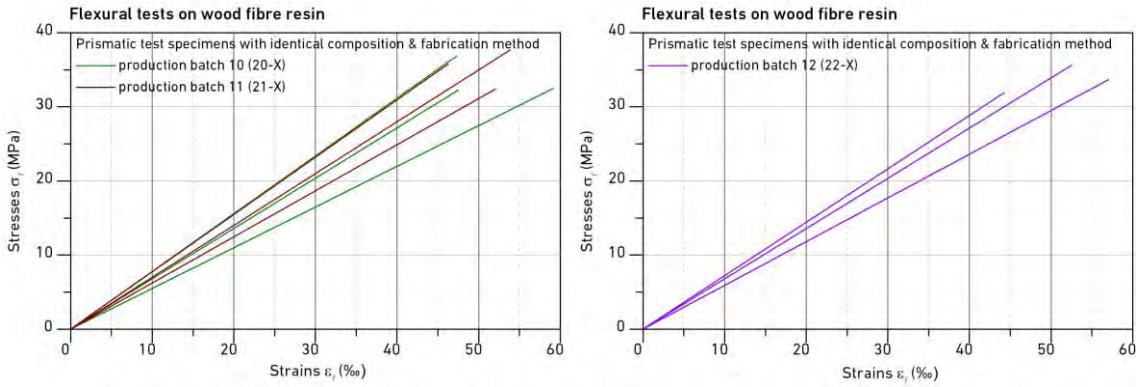

Fig. 5-41 Stress-strain distribution in prismatic WFC specimens (production batches 10-12)

Water saturation

The water absorption was calculated according to Eq. 5.3 and determined for two specimens of each prismatic production batch with results between 1.36% and 2.38% and an average value of 2.02% (Tab. 5-18).

$$M_{absorp.} = \frac{M_{24h} - M_0}{M_0} \cdot 100 \qquad (Eq.\ 5.3)$$

with

$M_{absorp.}$ *Water absporption*
M_0 *Oven – dried mass*
M_{24h} *Mass after 24h immersion time*

Tab. 5-18 Water absorption of prismatic wood-fibre composite specimens

Prism sample	Production batch	Oven-dried mass	Mass after 24h immersion time	Water absorption
		[g]	[g]	[%]
15-1	6	286.8	290.7	1.36
15-2	6	276.3	281.3	1.81
17-1	7	278.8	284.4	2.01
17-2	7	273.8	279.5	2.08
18-1	8	276.0	282.3	2.28
18-2	8	271.2	277.1	2.18
19-1	9	267.9	274.0	2.28
19-2	9	269.3	275.7	2.38
20-1	10	270.0	275.9	2.19
20-2	10	279.4	284.2	1.72
21-1	11	279.1	284.3	1.86
21-2	11	272.9	279.0	2.24
22-1	12	272.9	277.0	1.50
22-2	12	271.6	278.0	2.36
$\overline{x}$				2.02

Design values of the compressive and flexural strengths

Based on the results for the compressive strengths of the cylindrical test specimens, design values of the material properties were calculated according to EN 1990. The approach relies on a statistic evaluation and covered 14 specimens in total. Eq. 5.4a and 5.4b show the determination of the variance and coefficient of variation, which were used to calculate the design value for the compressive strength (Eq. 4.2c). The design approach defined the reduction factor η to 1.0 caused by multiple independent applied production processes and batches, which simulated model uncertainties, such as scale, volume, material properties or human impact, in praxis. The design compressive strength was calculated to approx. 26.5 MPa, by taking into account the statistical distribution of the tests results as shown in Tab. 5-16.

s_x^2	$= \frac{1}{n-1}\sum_1^{14}\left(x_i - m_x\right)^2$	*Annex D, eq. D.2*[1]	*(Eq.5.4a)*
V_x	$= s_x / m_x$	*Annex D, eq. D.3*[1]	*(Eq.5.4b)*
X_d	$= \eta \cdot m_x \cdot \left(1 - k_{d,n} \cdot V_x\right)$	*Annex D, eq. D.4*[1]	*(Eq.5.4c)*

with

s_x^2	*Variance*	69.14	
s_x	*Standard deviation*	8.32	
n	*Number of samples*	14	
V_x	*Coefficient of variation*	0.14	
x_i	*Compressive strength of sample i*	*Tab.*5 – 16	[MPa]
m_x	*Average compressive strength*	61.10	[MPa]
X_d	*Design value*	26.50	[MPa]
η	*Factor for model uncertainties*	1.0	
$k_{d,n}$	*Design fractile factor*	4.16	*Table D.2*[1]

[1] DIN EN 1990:2010-12 + A1:2005/AC:2010

Based on the results for the flexural strengths of the prismatic test specimens, design values of the material properties were calculated according to the EN 1990. The approach relies also here on a statistic evaluation and covered 21 specimens in total. The design flexural strength was calculated to approx. 24.2 MPa.

s_x^2	$= \frac{1}{n-1}\sum_1^{21}\left(x_i - m_x\right)^2$	*Annex D, eq. D.2*[1]	*(Eq. 5.4a)*
V_x	$= s_x / m_x$	*Annex D, eq. D.3*[1]	*(Eq. 5.4b)*
X_d	$= \eta \cdot m_x \cdot \left(1 - k_{d,n} \cdot V_x\right)$	*Annex D, eq. D.4*[1]	*(Eq. 5.4c)*

with

s_x^2	*Variance*	7.85	
s_x	*Standard deviation*	2.80	
n	*Number of samples*	21	
V_x	*Coefficient of variation*	0.08	
x_i	*Flexural strength of sample i*	*Tab. 5 – 17*	[MPa]
m_x	*Average flexural strength*	34.40	[MPa]
X_d	*Design value*	24.20	[MPa]
η	*Factor for model uncertainties*	1.0	
$k_{d,n}$	*Design fractile factor*	3.64	*Table D.2*[1]

[1] DIN EN 1990:2010-12 + A1:2005/AC:2010

Conclusions and comparison to polymer concrete

A material based on wood fibres and epoxy resin (WFC) was fabricated and tested to optimise the structural performance of the moulded joints (also with reduced mass for improving the truss STW ratio and good appearance). Pre-impregnation of the wood fibres and compaction of filer and binder by pressing under vacuum helped to achieve high material strengths of the WFC. Specimens were fabricated and tested under compression and bending with additional investigations on the density (1.1 g/cm^3) and water saturation (~2%).

The results confirmed the use of WFC as moulded material from a structural point of view due to the low MoE of 2.6 GPa and high strengths for compression and bending. The design compressive strength of 26.5 MPa is lower than the required 30 MPa in the previous numerical analysis (Tab 5-13). Follow up research on test series with an increased number of samples and a homogenisation of the filler proportions and dimensions should help to increase the design compressive strength to over 30 MPa. To estimate the design tensile strength of WFC, the ratio between the tensile and flexural strength (69/95) of the applied epoxy resin (see data sheet of Biresin® LS in Fig. A-55) was multiplied with the determined design flexural strength of WFC (24.2 MPa). Under the assumption that the ratio of tensile

to flexural strength is the same for Biresin® LS and WFC, the design tensile strength of WFC result to 17.6 MPa and thus overestimating the required 17 MPa in the previous numerical analysis (Tab. 5-13). The filler or wood fibre ratio of 50% improved the ecological footprint of the material with ductile failure mechanisms in 65% of the observed specimens (in compression tests).

A comparison to Biresin® LS showed almost the same MoE but strongly reduced strengths (~50%) for bending and compression as a result of the addition of wood fibres. The density could be reduced up to 10%.

Although the WFC was found to have a lower compressive strength than polymer concrete or high performance concrete (Tab. 5-19), it has advantages with regards to the structural behaviour of the moulded joint due to the enormous reduction in MoE and high tensile strength. The WFC density (approximately 1.1 g/cm^3) is up to ~60% lower than that of cement or polymer based concretes, enabling the realisation of light moulded joints for roundwood trusses.

The tests results illustrate the potential of the WFC for the lightweight construction sector. Here should be highlighted, that leading composite materials used in civil engineering have different material compositions and a different manufacturing process compared with WFCs. The high resin content of WFC is critical to discuss.

The following section covers the fabrication of the moulded joint prototype in order to verify if WFC is also capable for the design and fabrication of complex 3D shaped bodies.

Tab. 5-19 Wood-fibre composite vs. epoxy resin, polymer and high performance concrete

Parameter[1]	Unit	Biresin® LS	Compono® 100 S	Epument® 140/5AR	C 70/85[2]	WFC[3]
		Epoxy resin	Polymer concrete	Polymer concrete	HPC	
Density	[g/cm^3]	1.20	1.96	2.30	2.30	1.10
MoE	[GPa]	2.50	20	35	40	2.60
Compressive strength	[MPa]	100	81	140	78	61
Tensile strength	[MPa]	69	13	25	4.60	25

[1] Mean values of density, MoE and strengths
[2] EN 206:2021-06 [EN 206]
[3] Wood-fibre composite

5.4 PROTOTYPE FABRICATION

The fabrication technology and prototyping of solid WFC moulded joints was investigated after the material testing, using the example of the support joint. The design algorithm provided the CAD model of the inner cast-steel frame structure and outer moulded joint, which were further processed for the CAM process. Hereby, the first task described the fabrication of the frame structure, which was done by external firms with experience on the field of prefabricated cast-steel structural components. The CAD model of the inner cast-steel frame structure is shown in Fig. 5-42.

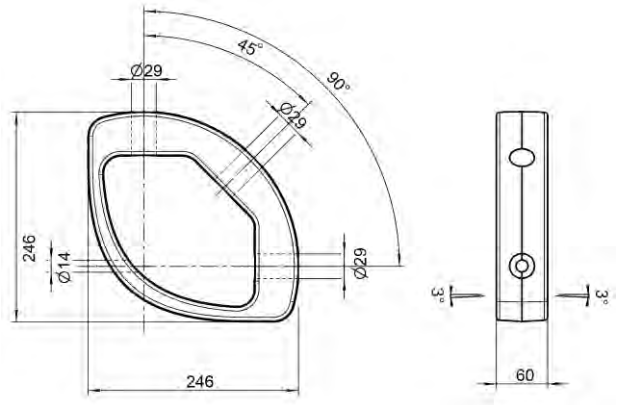

Fig. 5-42 Inner cast-steel frame structure (Prototype)

A two-part aluminium casting mould was milled (Fig. 5-43) with a core in the centre of the geometry to fix the cast-iron frame structure during the filling and compression of WFC into the casting mould. The fabrication of the casting mould was done by external firms.

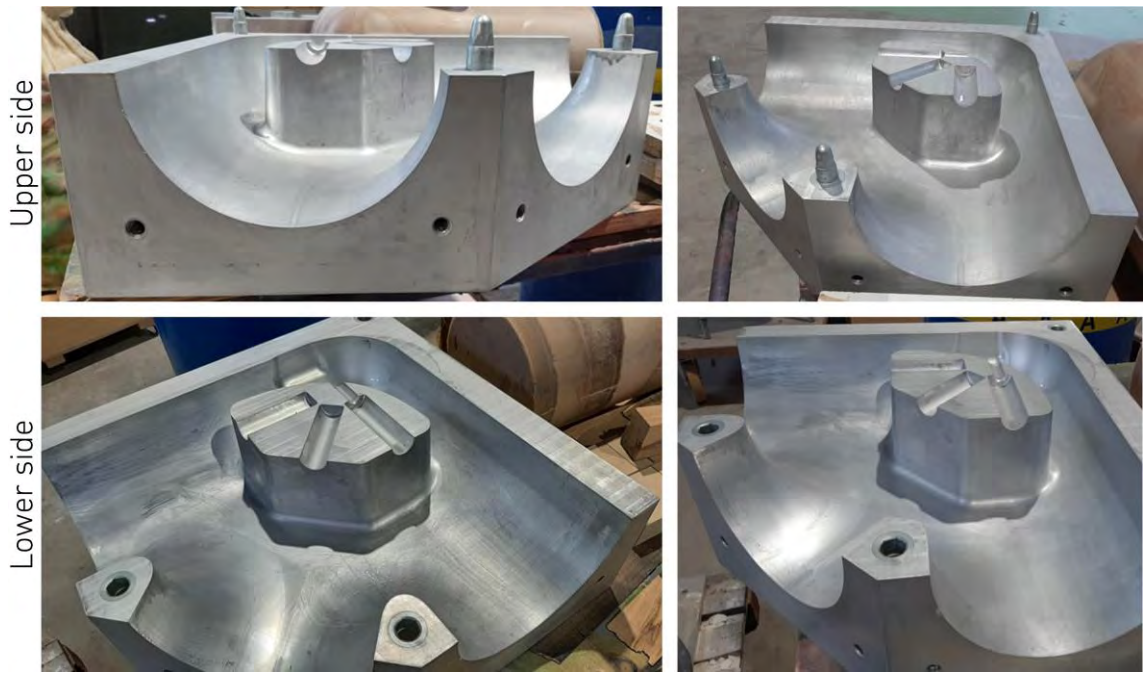

Fig. 5-43 Two-parted aluminium casting mould (Prototype)

The casting mould was connected to three fabricated cylinders (Fig. 5-33) in order to insert the WFC under vacuum (Fig. 5-44 and 5-45). Curing of the mixture was only carried out in the casting mould, which was highly polished to achieve a high surface quality directly after demoulding with no intense post-processing required.

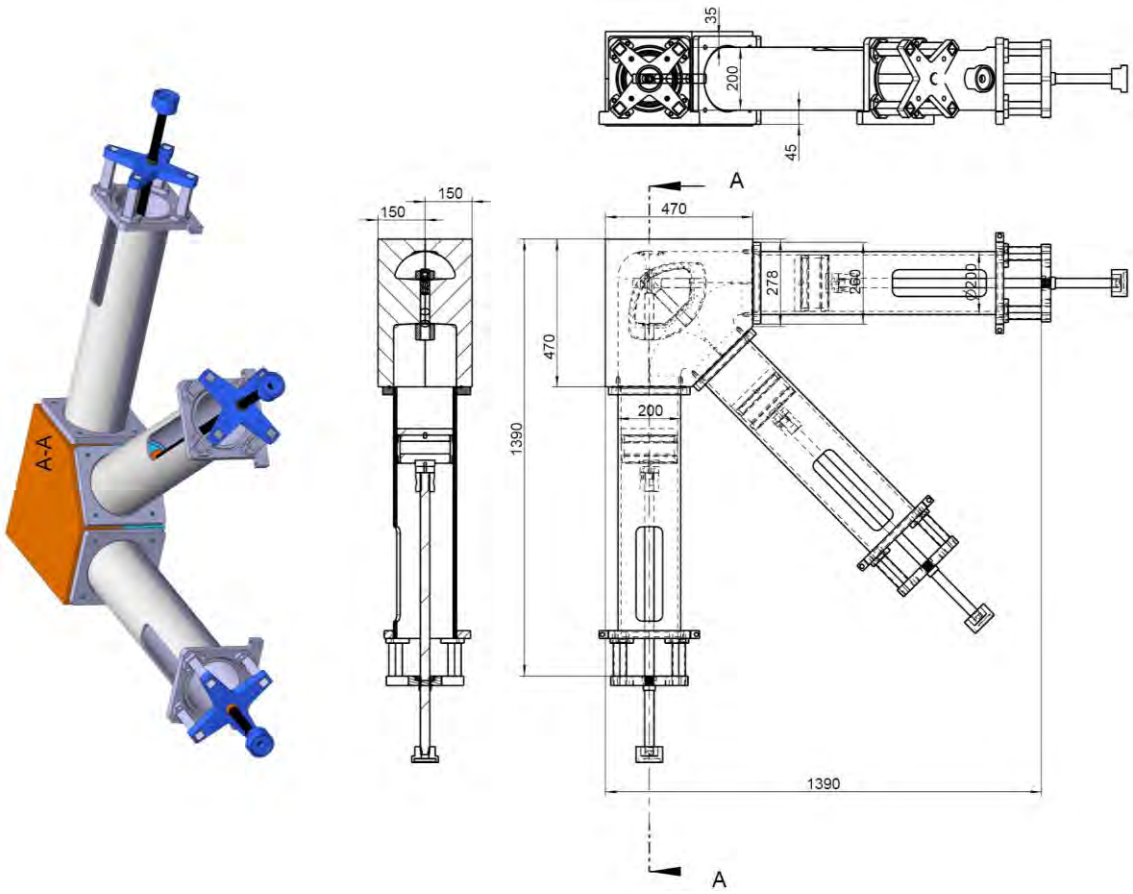

Fig. 5-44 Technical drawing of vacuum pressed fabrication of WFC joints (Prototype)

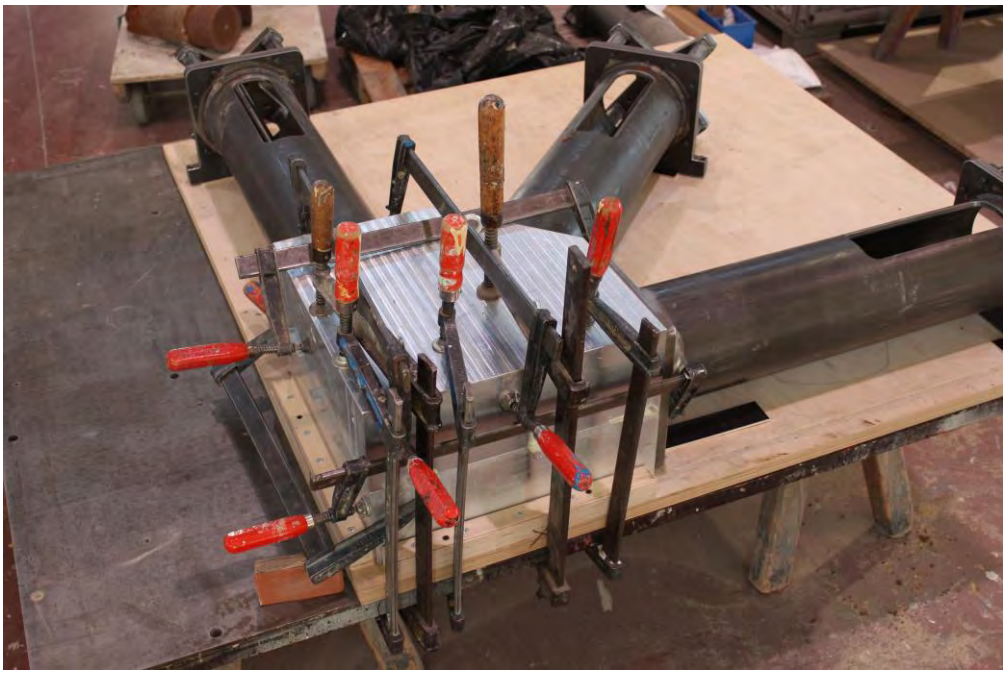

Fig. 5-45 Vacuum pressed fabrication of WFC joints (Prototype)

Fig. 5-46 shows first fabrication approaches of the moulded joints. Polymer concrete (Fig. 5-46a) and WFC (Fig. 5-46, b-d) were both used as moulded materials. The structural performance of the moulded joint might be improved with the use of WFC, but a homogenous distribution of filler (wood fibres) and binder (epoxy resin) was difficult to achieve for the fabrication process as shown in Fig. 5-44 and 5-45.

Fig. 5-46 Evolution of joint prototype fabrication composed of PC (a) and WFR (b-d)

The fabrication process was modified in the last step in order to reach a homogenous distribution of filler and binder, by a variation of the wood fibre and epoxy resin ratio, a modification of the compressive load of the internal stamps, the installation of a vacuum port in the casting mould and by prefilling pre-impregnated wood fibres in the critical region around the side opening (see also Fig. 5-46c).

Fig. 5-47 shows the last fabricated prototype in the framework of this thesis with a clearly identifiable improved distribution of material components, especially around the side opening. Further test must be planned in further studies to optimize the fabrication process.

In addition to the use of renewable raw materials and the improved material properties, the texture or architectural appearance is very different from existing moulding materials in the building sector (Fig. 5-47). This could create an incentive for architects to build with WFC in the lightweight construction sector. Along with the material aspects, the improved environmental footprint of the overall technology should be underlined at this point. In contrast to rectangular sawn timber solutions for 2D trusses, the new construction has a much higher degree of natural sources.

Fig. 5-47 Optimized joint prototype fabrication composed of WFR

The prototype fabrication of the other joint types, including the fabrication and assembly of the full truss structure, falls outside of the scope of the thesis. However, the results on the numerical investigations, material testing and prototype fabrication underlined the potential of the new joining technology, but also restrictions, which need to be investigated for the practical application.

Chapter 6 summarises the achievements of this thesis with an outlook for future research requirements.

6 SUMMARY AND OUTLOOK

This doctoral thesis focused on the development of a new joining technology for modular 2D trusses for structural roundwood and investigated the connection configuration (i) in roundwood with modified bonded-in rods and (ii) in the nodes of the trusses with digital fabricated moulded joints. The main achievements and prospective research requirements of both main focus areas are presented in the following paragraphs.

Part one of this thesis dealt with the connection configuration in roundwood with experimental investigations on the pull-out strength of grouted threaded rods, bonded parallel to grain into timber. Objective of the investigations was the structural assessment of this new technique under different service conditions for structural roundwood. The design load of the connection capacity for service class 1 and 2 of ~150 kN has been calculated from the test results and triples the connection capacity on the design level of standardised glued-in rods, which can be calculated to ~46 kN (for the same steel rod diameter, strength class and bonding length). Further research studies need to focus on increasing the connection capacity either by a modification of the joint geometry or by attached steel sleeves for confining the roundwood members and to take over the tensile loads in tangential direction analogous to the structural function of ring reinforcements. This modified approach might be the solution for further increasing the tensile load bearing capacity.

Referring to the application to different climate conditions, no softening of the timber properties was observed for service class 2 specimens. The variation in failure modes for service class 3 specimens showed the complexity of timber structures exposed to direct climate conditions. In direct comparison, 'classic' glued-in rods are only allowed for service class 1 conditions.

Natural pre-cracks in roundwood for service class 1 and 2 specimens did not affect the functionality or the load-carrying capacity under tensile loading. A visual inspection of each specimen should be done before grouting with (i) natural pre-cracks in roundwood limited according to the variations presented in Fig.4-18 and (ii) a heartwood location within the drill hole area.

The research results and achievements on modified bonded-in rods in roundwood have been published in the framework of the *16th World Conference on Timber Engineering 2021*, Santiago, Chile [SCH 2021].

Part two of this thesis focused on the development of digital fabricated moulded joints to connect roundwood members with grouted threaded rods in the nodes of modular 2D trusses. The developed algorithm for the moulded joint and truss design helped to analyse different truss variations and to automate the design process for the digital fabrication. The algorithm in combination with the advantages of roundwood truss structures and the developed joining technology form the basis for a competitive, ecological and economic position in the building sector. The analysis of the 25 truss variations showed that the circular cross-section and roof load introduction into the joints (with no bending in the upper chord) resulted in improved strength to weight ratios compared to common truss systems composed of sawn timber. Here should be noted, that the total mass of the truss structures with wood-fibre composite as outer moulded joint material did not exceed 1026 kg for truss spans up to 15 m (Tab. 5-5) with an enormous impact of the moulded material density on the overall performance of the trusses. On the other hand, the span to depth ratios of the trusses were not able to compete with common truss systems composed of sawn timber, mainly because of the limited load bearing capacity in the modified bonded-in rods for tension (150 kN).

The Structural Analysis of the moulded joints proved the structural functionality for the inner cast-steel frame structure (G18NiMoCr3-6) and outer joint for applied moulded materials with a low MoE, around 2.5 GPa. Polymer or cement based concretes were found to be unsuitable because of their high MoE and resulting high tensile stresses in the moulded material.

Wood-fibre composite specimens were fabricated and tested to optimise the structural performance of the moulded joints (also with reduced mass for improving the truss strength to weight ratio and good appearance). Pre-impregnation of the wood fibres and compaction of filler and binder by pressing under vacuum helped to achieve high material strengths of the wood-fibre composite. Specimens were fabricated and tested under compression and bending with additional investigations on the density (1.1 g/cm^3) and water saturation (~2%). The results confirmed the use of wood-fibre composite as moulded material from a structural point of view due to the low MoE of 2.6 GPa, high strengths for compression (design value of 26.5 MPa), bending (design value of 24.2 MPa) and tension (design value of 17.6 MPa). The investigations highlighted the potential of the wood-fibre composite for the lightweight construction sector. Despite the advantages, prospective research needs to focus on an optimisation or reduction of the resin content in wood-fibre composite and on test series with an increased number of specimens. The fabrication process of the moulded joint prototype underlined the problem of producing complex 3D solid bodies with an inhomogeneous distribution of filler and binder. Prospective research studies need to focus on an optimisation of the fabrication process.

The research results and achievements on the design algorithm, Structural Analysis and wood-fibre composite have been published in the *Proceedings of the Institution of Civil Engineers - Structure and Buildings* [CHA 2022b] and in the framework of the *16th World Conference on Timber Engineering 2021*, Santiago, Chile [CHA 2021].

In regard to the development specifications, defined in section 3.1, grouted rods ensure a simple roundwood fabrication with no modification of the circular cross-section and no computer aided support. The connection requires only one drill hole in the timber end grain with the additional benefit of using either cylindrical milled roundwood (constant diameter along the strut axis) or natural grown roundwood (only removed bark and bast layers) as strut members. The easy fabrication enables an access for traditional craft businesses, even without Computer Aided competences.

The moulded joints are specially developed for structural roundwood. The joints have an aesthetically pleasing appearance, providing an incentive for architects to adopt it in modern timber building design. The moulded joint ensures only compressive and tensile loads in the roundwood fibre direction, as in ideal trusses. The modularity of the truss system is defined by an adaptation of nine different joint types to 25 modular truss variations and by simple pre-assembly, assembly and deconstruction, thus leading to reductions in construction time. The technology can also be adapted to permanent and temporary buildings and individual components of the trusses are exchangeable, with no impact on the functionality of the structure. In contrast to rectangular sawn timber solutions for 2D trusses, the new construction has a much higher degree of natural sources.

REFERENCES 7

7.1 REFERENCES, STANDARDS AND DATA SHEETS

AIC 2003 Aicher, S. (2003) 'Structural adhesive joints including glued-in bolts', *In: Thelandersson, S.:Timber Engineering* , Wiley, Chichester, 2003, pp. 333-363.

AZI 2018 Azinović, B., Serrano, E., Kramar, M.. Pazlar, T. (2018) 'Experimental investigation of the axial strength of glued-in rods in cross laminated timber', *Material and Structures*, 51(6), p. 369.

BEC 2016a Becker, W., Schober, K.U. (2016) 'Holz-Beton-Verbund im Knotensystem von Rundholzbrücken'. (Timber-concrete-composites in roundwood bridge joints), *Proceedings of the 4. Internationale Holzbrückentage 2016.* Stuttgart, Germany (in German).

BEC 2016b Becker, W., Schober, K.U., Weber, J. (2016) ‚Vergussknotenlösungen im Ingenieurholzbau'. (Moulded joints in timber engineering), *Bautechnik*, 93(6), pp. 371-379 (in German).

BEC 2018 Becker, W., Weber, J. (2018) 'W*ooden strut construction comprising a first strut support member and at least one second strut support member, said members being force locked together at a node point'*, European Patent 2 954 124 B1.

BENG 2002 Bengtsson, C., Johannson, C.J. (2002) 'GIROD - Glued-in Rods for timber structures', *Research report of the Swedish national testing and research institute (SR REPORT 2002:26)*. Borås, Sweden.

BENN 1978 Bennett, J.A. (1978) 'Automated design of truss and frame geometry', *Computers & Structures*, 8(6), pp. 717–721.

BLA 2012 Blaß, H. J., Enders-Comberg, M. (2012) 'Fachwerkträger für den industriellen Holzbau'. (Trusses for industrial timber constructions), *Forschung für die Praxis Karlsruher Tage 2012,* pp. 1-14 (in German).

BRI 2012 Brito, L., Junior, C. (2012) 'Types of connections for structural elements roundwood used in brazil', *Proceedings of the World Conference on Timber Engineering 2012.* Auckland, New Zealand.

CHA 2018 Chahade, T., Schober, K.U., Morillas, L. (2018) 'Structural design optimization of multidimensional gridshells: Parametric interaction of architecture, engineering and manufacturing', *Proceedings of the World Conference on Timber Engineering 2018.* Seoul, Republic of Korea.

CHA 2021 Chahade, T., Schober, K.U., Morillas, L., Schäfer, P. (2021) 'Large scale roundwood trusses: Part 2 - the parametric BIM Tool for integrated design', *Proceedings of the 16th World Conference on Timber Engineering 2021.* Santiago, Chile.

CHA 2022a Chahade, T., Schober, K.-U., Morillas, L. (2022) 'Interactive structural design of hyperbolic grid shells', *Proceedings of the Institution of Civil Engineers - Structures and Buildings*, 175(2), pp. 141–152.

CHA 2022b Chahade, T., Schober, K.-U. (2022) 'Wood-fibre composite moulded connectors for roundwood trusses Part 1: Structural and material design', *Proceedings of the Institution of Civil Engineers - Structures and Buildings*, pp. 1–32.

DAH 2019 Dahy, H. (2019) 'Natural Fibre-Reinforced Polymer Composites (NFRP) Fabricated from Lignocellulosic Fibres for Future Sustainable Architectural Applications, Case Studies: Segmented-Shell Construction, Acoustic Panels, and Furniture', *Sensors (Basel, Switzerland)*, 19(3).

DRA 2014 Drass, M., Schober, K.U., Kuechler, M. (2014) 'Advancement of glued-in rods using polymer concrete as composite material', *Proceedings of the 13th World Conference on Timber Engineering 2014.* Quebec, QC, Canada.

ECK 1995 Eckelman, C., Senft, J. (1995) 'Truss system for developing countries using small diameter roundwood and dowel nut construction', *Forest Products Journal*, 45(10), pp. 77-80.

GAR 2022 Gartner, B., Yadama, V. and Smith, L. (2022) 'Resin Transfer Molding of Wood Strand Composite Panels', *Forests,* 13(2), p. 278.

GEN 2013 Gengnagel, C., Hernández, E.L., Bäumer, R. (2013) 'Natural-fibre-reinforced plastics in actively bent structures', *Proceedings of the Institution of Civil Engineers - Construction Materials*, 166(6), pp. 365–377.

GOR 2012 Gorman, M., Kretschmann, D. (2012) 'Assessing the capacity of three types of round-wood connections', *Proceedings of the World Conference on Timber Engineering 2012 (WCTE 2012). Auckland, New Zealand*.

HAR 2000 Harvey K., Ansell M. P. (2000) 'Improved timber connections using bonded in GFRP rods', *Proceedings of the 6th World Conference on Timber Engineering 2000*. Whistler Resort, Canada.

HER 2006 Barrios Hernandez, C.R. (2006) 'Thinking parametric design: introducing parametric Gaudi', *Design Studies*, 27(3), pp. 309–324.

HUN 2016 Hunger, F., Stepinac, M., Rajčić, V., van de Kuilen, J.-W.G. (2016) 'Pull-compression tests on glued-in metric thread rods parallel to grain in glulam and laminated veneer lumber of different timber species', *European Journal of Wood and Wood Products*, 74(3), pp. 379-391.

JAH 2018 Jahreis, M.(2018) 'Zur Entwicklung von Polymerverguss-Kopplungselementen für den Holzbau'. (Development of polymer concrete coupling elements in timber constructions), PhD thesis, Bauhaus-Universität Weimar, Germany (in German).

KAW 2002 Kawamura, H., Ohmori, H. and Kito, N. (2002) 'Truss topology optimization by a modified genetic algorithm', *Structural and Multidisciplinary Optimization*, 23(6), pp. 467–473.

LAM 2021 Lambert, T., Bender, M., Becker, W. (2021) 'Experimentelle Untersuchungen zum Materialverhalten von Polymerbeton'. (Experimental investigations on the material properties of polymer concrete), *Beton- und Stahlbetonbau, 116*(7), pp. 528-538 (in German).

LAU 2018 Lau, K.-t., Hung, P.-y., Zhu, M.-H., Hui, D. (2018) 'Properties of natural fibre composites for structural engineering applications', *Composites Part B: Engineering*, 136(2), pp. 222–233.

LET 2006 Lettow, S. (2006) 'Ein Verbundelement für nichtlineare Finite Elemente Analysen - Anwendung auf Übergreifungsstöße'.(A composite element for non-linear Finite-Element analyses - applied to overlapping joints), PhD thesis, University of Stuttgart, Germany (in German).

LEU 2008 Leutbecher, T. (2008) ‚Rissbildung und Zugtragverhalten von mit Stabstahl und Fasern bewehrtem ultrahochfesten Beton (UHPC)'. (Crack formation and tensile structural behaviour for reinforced UHPC with steel bars and fibres), PhD thesis, University of Kassel, Germany (in German).

LIN 2015 Ling, Z., Liu, W. (2015) 'Bond behavior between softwood glulam and epoxy bonded-in threaded steel rod", *Journal of Materials in Civil Engineering, 28*(3), p. 06015011.

LIP 2002 Lippert, P. (2002) 'Rahmenecke aus Holz mit eingeklebten Gewindestangen'. (Wooden frame corner with glued-in threaded rods), PhD thesis, University of Stuttgart, Germany (in German).

LOK 2014a Lokaj, A., Klajmonová, K. (2014) 'Selected Problems in Using Round Timber in Building Structures', *Advanced Engineering Forum*, 12, pp. 101–106.

LOK 2014b Lokaj A, Klaymonova K. (2014) 'Round Timber bolted joints exposed to static and dynamic loading', *Wood Research, 59*(3), pp. 439-448.

LOK 2016 Lokaj, A., Klaymonova, K. (2016) 'Behavior of round timber bolted joints under tension load', *Wood Research,* 61(5), pp. 819-830.

MOR 2013 Morgado, T.F.M., Dias, A.M.P.G., Machado, J.S. and Negrão, J.H. (2013) 'Structural Connections for Small- Diameter Poles', *Journal of Structural Engineering*, 139(11), pp. 2003-2009.

MOE 1978 Möhler, K., Lautenschläger, R. (1978) 'Großflächige Queranschlüsse bei Brettschichtholz'. (Large scale transverse connectors for glued laminated timber), *Research report of the department of timber engineering and building construction.* University of Karlsruhe, Germany (in German).

MOE 1981 Moers, F. (1981) 'Anschluss mit eingeleimten Gewindestäben'. (Joints with glued-in threaded rods), *Bauen mit Holz* 4, pp. 228-231 (in German).

OPP 2017 Oppel, M., Jahreis, M., Rautenstrauch, K. (2017) 'Numerische Modellbildung für Anschlüsse im Holzbau'. (Numerical modeling of timber joints), *Bautechnik*, 94(11), pp. 743–750 (in German).

RAN 1999 Ranta-Maunus, A. (1999) 'Round small-diameter timber for construction', *Final report of project FAIR CT 95-0091.* (VTT publications, 383). Espoo: Technical Research Centre of Finland.

RIB 1988 Riberholt, H. (1988) 'Glued bolts in glulam - Proposals for CIB code, Paper 21-7-2', *Proceedings of the International Council for Research and Innovation in Building and Innovation in Building Construction, Working Commission W18 Timber Structures*, pp. 1-18.

RIC 2012 Richardson, J.N., Adriaenssens, S., Bouillard, P., Filomeno Coelho, R. (2012) 'Multiobjective topology optimization of truss structures with kinematic stability repair', *Structural and Multidisciplinary Optimization*, 46(4), pp. 513-532.

RUG 1990 Rug, W. (1990) 'Komplexe Werkstoffausnutzung im Ingenieurholzbau', (Complex material utilisation in timber engineering), *Holztechnologie Leipzig,* 30(4), pp. 195-199 (in German).

RUG 1995 Rug, W. (1995) 'Beispiele der Holzverwendung'. (Examples of timber use), *Bautechnik,* 72(10), pp. 698-705 (in German).

SCH 2008 Schober K.U. (2008) 'Untersuchungen zum Tragverhalten hybrider Verbund-konstruktionen aus Polymerbeton, faserverstärkten Kunststoffen und Holz'. (Investigations on the structural behavior of hybrid composite structures, based on polymer concrete, fiber-reinforced plastics and wood), PhD thesis, Bauhaus-Universität Weimar, Germany (in German).

SCH 2012 Schober, K.U., Becker, W., Drass, M. (2012) 'Advanced interface interaction in timber engineering joints with dowel-type fasteners embedded in high-performance ceramic fillers', *Proceedings of the 12th World Conference on Timber Engineering 2012*. Auckland, New Zealand.

SCH 2013 Schober, K.U., Drass, M., Becker, W. (2013) 'Adhesive strength of timber joints with unconventional glued-in steel rods', *Proceedings of the International Conference on Wood Adhesives 2013*. Toronto, ON, Canada.

SCH 2014a Schober, K.U. (2014) 'New jointing techniques for large-scale timber structures', *Proceedings of the 2nd Annual International Conference on Architecture and Civil Engineering 2014.* Singapore.

SCH 2014b Schober, K.U., Becker, W., Drass, M., Weber, J. (2014) ‚High-performance timber composite joints for spatial round wood truss structures', *Proceedings of the 13th World Conference on Timber Engineering 2014.* Quebec, QC, Canada.

SCH 2016a Schober, K.U., Tannert, T. (2016) 'Hybrid connections for timber structures', *European Journal of Wood and Wood Products*, 74(3), pp. 369-377.

SCH 2016b Schober, K.U., Becker, W., Weber, J. (2016) 'Grouted joints in timber engineering', *Proceedings of the 14th World Conference on Timber Engineering 2016.* Vienna, Austria.

SCH 2018 Schober, K.U., Chahade, T., Becker, W. (2018) 'Experimental investigations of grouted timber joints exposed to different climate conditions', *Proceedings of the 15th World Conference on Timber Engineering 2018.* Seoul, Republic of Korea.

SCH 2021 Schober, K.U., Chahade, T., Schäfer, P, Morillas, L. (2021) 'Large scale roundwood trusses: Part 1 - economic connection design with grouted joints', *Proceedings of the 16th World Conference on Timber Engineering 2021.* Santiago, Chile.

SER 2001 Serrano, E. (2001) 'Glued-in rods for timber structures – An experimental study of softening behaviour', *Materials and structures*, 34(4), pp. 228-234.

STA 2008 Staiger, M.P., Tucker, N. (2008) 'Natural-fibre composites in structural applications', *Properties and Performance of Natural-Fibre Composites: Elsevier*, pp. 269–300.

STE 2015 Steiger, R., Serrano, E. (2015) 'Reinforcement with glued-in rods', *Final report of the European cooperation program in science and technology 2011-2015*, COST Action Report FP1101. Aachen, Germany.

SUM 2005 Summerscales, J., Searle, T.J. (2005) 'Low-pressure (vacuum infusion) techniques for moulding large composite structures', *Proceedings of the Institution of Mechanical Engineers, Part L: Journal of Materials: Design and Applications*, 219(1), pp. 45–58.

THE 2018 Thelin, A., Feldt, P. (2018) 'Glued-in Rods in Timber Structures - Finite Element Analyses of Adhesive Failure', Master thesis, Chalmers University of Technology, Sweden.

TLU 2011 Tlustochiwicz, G., Serrano, E., Steiger, R. (2011) 'State-of-the-art review on timber connections with glued-in steel rods', *Materials and Structures*, 44(5), pp. 997-1020.

WAD 2020 Wada, T., Ogura, D., Sano, C., Hokoi, S. and Iba, C. (2020) 'Study of the conservation and exhibition of burned wall paintings in the main hall of the treasure house at Horyu-ji Temple', *E3S Web of Conferences*, 172, p. 15005.

WEB 2016 Weber, J., Kjølsrud, E., Schober, K.-U. (2016) 'Kraftflussoptimierte Verbindungen im Ingenieurbau'. (Force flow optimized joints in timber engineering), *Bautechnik*, 93(11), pp. 834–838 (in German).

WIL 2011 Williams, C.J.K. (2011) 'Patterns on a Surface: The Reconciliation of the Circle and the Square', *Nexus Network Journal*, 13(2), pp. 281–295.

DIN 13-1 *DIN 13-1:1999-11, ISO general purpose metric screw threads - Part 1: Nominal sizes for coarse pitch threads; nominal diameter from 1 mm to 68 mm*. Berlin: Beuth Verlag GmbH.

DIN 976-1 *DIN 976-1:2016-09, Fasteners - Stud bolts - Part 1: Metric thread*. Berlin: Beuth Verlag GmbH.

DIN 1052 *DIN 1052-1:1988-04, Structural use of timber; design and construction, German version DIN 1052-1:1988.* Berlin: Beuth Verlag GmbH.

DIN 4074-1 *DIN 4074-1:2012-06, Strength grading of wood - Part 1: Coniferous sawn timber*. Berlin: Beuth Verlag GmbH.

DIN 8075 *DIN 8075:2018-08, Polyethylene (PE) pipes - PE 80, PE 100 - General quality requirements, testing; Text in German and English*. Berlin: Beuth Verlag GmbH.

EN ISO 7089	*DIN EN ISO 7089:2000-11, Plain washers - Normal series, Product grade A (ISO 7089:2000); German version EN ISO 7089:2000*. Berlin: Beuth Verlag GmbH.
EN ISO 4032	*DIN EN ISO 4032:2013-04, Hexagon regular nuts (style 1) - Product grades A and B (ISO 4032:2012); German version EN ISO 4032:2012*. Berlin: Beuth Verlag GmbH.
EN 206	*DIN EN 206:2021-06, Concrete - Specification, performance, production and conformity; German version EN 206:2013+A2:2021*. Berlin: Beuth Verlag GmbH.
EN 338	*DIN EN 338:2016-07, Structural timber - Strength classes; German version EN 338:2016.* Berlin: Beuth Verlag GmbH.
EN 1380	*DIN EN 1380:2009-07, Timber structures - Test methods - Load bearing nails, screws, dowels and bolts; German version EN 1380:2009*. Berlin: Beuth Verlag GmbH.
EN 1912	*DIN EN 1912:2013-10, Structural timber - Strength classes - Assignment of visual grades and species; German version EN 1912:2012 + AC:2013.* Berlin: Beuth Verlag GmbH.
EN 1990	*DIN EN 1990:2021-10, Eurocode: Basis of structural design; German version EN 1990:2002 + A1:2005 + A1:2005/AC:2010.* Berlin: Beuth Verlag GmbH.
EN 1993-1-8	*DIN EN 1993-1-8:2010-12, Eurocode 3: Design of steel structures - Part 1-8: Design of joints; German version EN 1993-1-8:2005 + AC:2009*. Berlin: Beuth Verlag GmbH.
EN 1995-1-1	*DIN EN 1995-1-1:2010-12, Eurocode 5: Design of timber structures - Part 1-1: General - Common rules and rules for buildings; German version EN 1995-1-1:2004 + AC:2006 + A1:2008*. Berlin: Beuth Verlag GmbH.
EN 1995-1-1/NA	*DIN EN 1995-1-1/NA, National Annex - Nationally determined parameters - Eurocode 5: Design of timber structures - Part 1-1: General - Common rules and rules for buildings; German version EN 1995-1-1 /NA:2013-08.* Berlin: Beuth Verlag GmbH.
EN 10034	*DIN EN 10034:1994-03, Structural steel I and H sections; tolerances on shape and dimensions; German version EN 10034:1993*. Berlin: Beuth Verlag GmbH.
EN 10279	*DIN EN 10279:2000-03, Hot rolled steel channels - Tolerances on shape, dimensions and mass; German version EN 10279:2000*. Berlin: Beuth Verlag GmbH.
EN 10340	*DIN EN 10340:2008-01, Steel castings for structural uses; German version EN 10340:2007*. Berlin: Beuth Verlag GmbH.
EN 14080	*DIN EN 14080:2013-09, Timber structures - Glued laminated timber and glued solid timber - Requirements; German version EN 14080:2013*. Berlin: Beuth Verlag GmbH.

EN 14081-1	*DIN EN 14081-1:2019-10, Timber structures - Strength graded structural timber with rectangular cross section - Part 1: General requirements; German version EN 14081-1:2016+A1:2019*. Berlin: Beuth Verlag GmbH.
DIBt Z-10.7-282	*German technical approval (DIBt) no. Z-10.7-282: Polymer concrete grouting for the reinforcement of wooden components; German version DIBt Z-10.7-282: 2021.*
BIR 2016	*Sika Deutschland GmbH, Product Data Sheet Biresin® LS Laminating and Multi-purpose resin; 2016.*
EPU 2007	*Epucret Mineralgusstechnik GmbH and Co.KG, Product data sheet Epument 140/5AR Lavor - Rev.-Status: 008 - 2007/08/03; 2007.*

7.2 LIST OF FIGURES

7.3 LIST OF TABLES

APPENDIX A

A.1 MODIFIED BONDED-IN RODS

A.1.1 Overview

Tab. A-1 summarises all relevant data related to the experimental investigations on modified bonded-in rods, such as the test date, room temperature, air humidity, moisture content of wood before testing, load level for cracks, final failure and so on.

Fig. A1-5 show the test specimens before grouting, before testing and after testing with additional information on the failure load.

Approximate models on the degree of pre-cracks in roundwood before testing are added in Fig. A6-7 for service class 2 and 3 specimens.

Tab. A-1 Overview test results

						Polymer concrete				Roundwood
Service class	Sample no.	Test date	Room temperature before testing (°)	Relative humidity before testing (%)	Moisture content in wood before testing (%)	Loading for crack 1 (kN)	Loading for crack 2 (kN)	Loading for crack 3 (kN)	Failure load (kN)	Start of load transmission measured from end-grain (mm)
1	1	27.11.2017	21.0	50.0	10.0	-	154.7	-	230.1	-
	2	28.11.2017	18.0	55.0	12.0	-	147.2	-	204.5	-
	3	29.11.2017	18.0	51.0	12.0	-	150.1	-	217.6	-
	4	29.11.2017	19.0	50.0	11.0	-	149.9	-	218.4	-
	5	30.11.2017	19.0	50.0	11.0	-	150.1	-	209.3	-
	6	30.11.2017	19.0	51.0	12.0	-	146.3	-	208.5	-
	7	01.12.2017	17.0	41.0	10.0	-	137.3	-	191.0	-
	8	02.12.2017	19.0	43.0	10.0	-	150.1	-	206.0	-
	9	04.12.2017	18.0	47.0	10.0	-	150.0	-	230.0	-
Average sc 1							148.4		212.8	
2	1	22.01.2020	19.4	35.9	14.0	-	-	-	210.0	-
	2	14.04.2020	21.0	28.9	15.0	-	-	-	240.0	-
	3	22.04.2020	21.8	33.7	13.0	143.1	149.1	212.1	232.0	80.0
	4	23.04.2020	21.0	32.8	16.0	136.5	136.5	162.3	240.0	60.0
	5	07.05.2020	19.5	40.3	15.0	119.8	134.3	178.1	240.0	-
	6	08.05.2020	20.0	41.2	15.0	136.9	138.2	144.8	236.0	-
	7	08.05.2020	21.0	41.2	12.0	150.2	156.5	165.2	237.0	80.0
	8	08.05.2020	22.3	38.7	16.0	-	-	-	215.0	50.0
	9	11.05.2020	20.0	50.9	17.0	-	-	-	240.0	-
Average sc 2						137.3	142.9	172.5	232.2	67.5
3	1	15.05.2020	21.1	38.9	19.0	-	-	-	217.0	60.0
	2	15.05.2020	21.0	37.7	21.0	143.5	160.1	183.3	240.0	70.0
	3	18.05.2020	20.8	40.1	20.0	126.1	131.6	143.9	231.0	-
	4	22.05.2020	22.4	53.4	20.0	110.9	123.8	133.1	227.0	70.0
	5	22.05.2020	23.1	53.6	21.0	-	-	-	231.0	60.0
	6	22.05.2020	20.8	50.8	22.0	-	-	-	236.0	-
	7	29.05.2020	21.5	38.3	22.0	128.2	133.4	137.0	216.0	-
	8	29.05.2020	21.8	36.6	18.0	122.1	131.4	143.1	239.0	60.0
	9	04.06.2020	21.8	58.0	19.0	-	-	-	223.0	60.0
Average sc 3						126.2	136.1	148.1	228.9	63.3
Average service class 1, 2 and 3						131.7	142.5	160.3	224.6	65.4

Fig. A-1 Test specimens at failure - service class 1

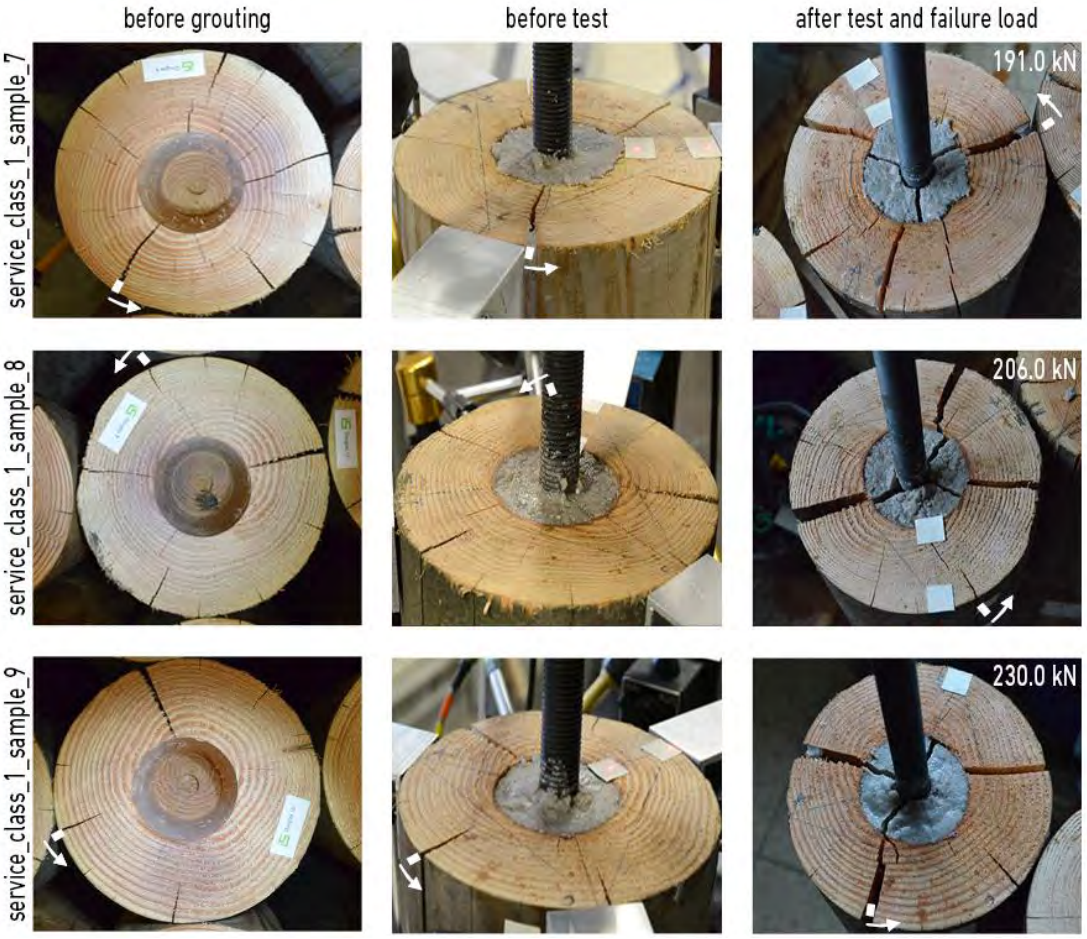

Fig. A-2 Test specimens at failure - service class 1 (cont.)

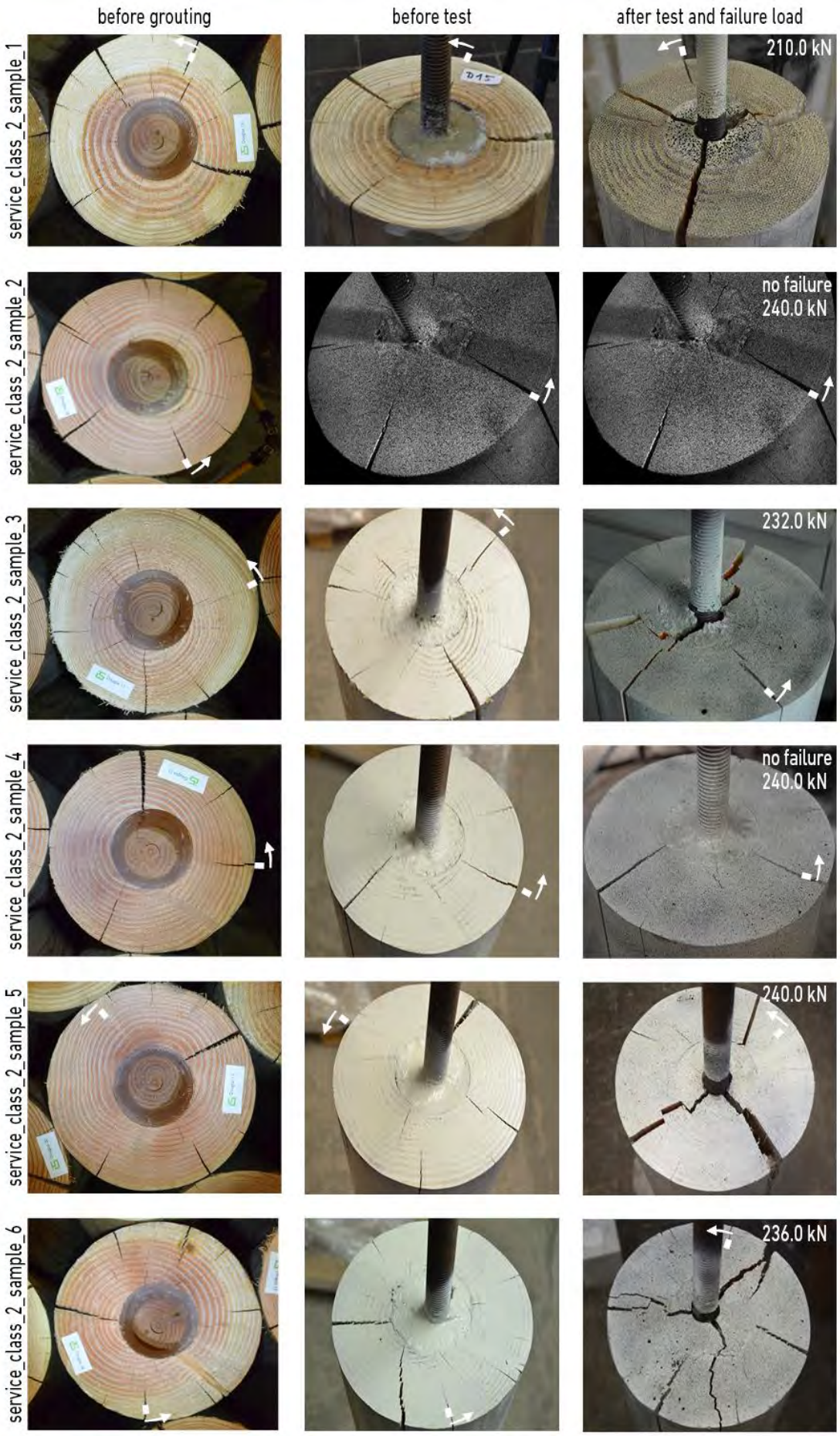

Fig. A-3 Test specimens at failure - service class 2

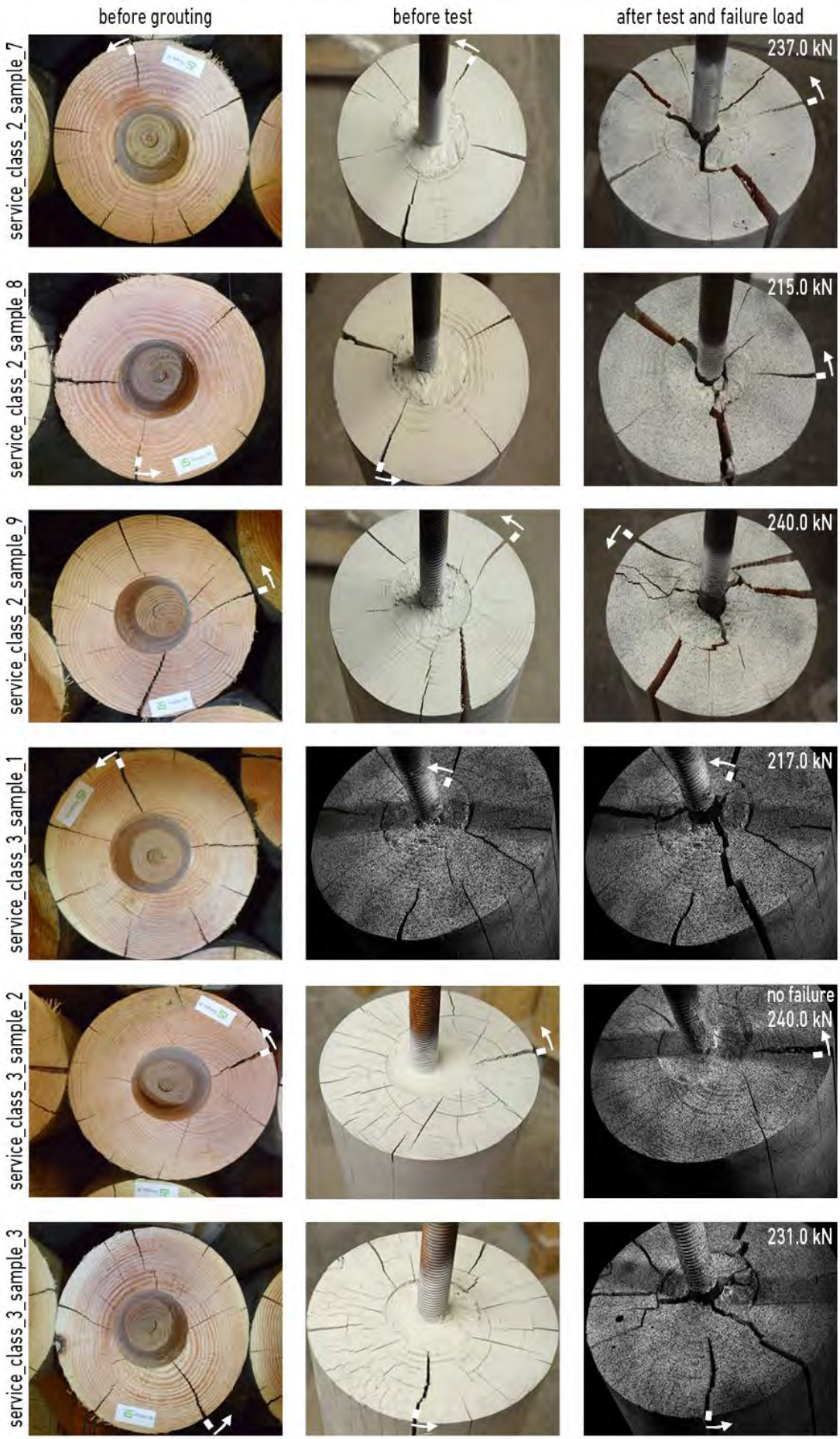

Fig. A-4 Test specimens at failure - service class 2 (cont.) and 3

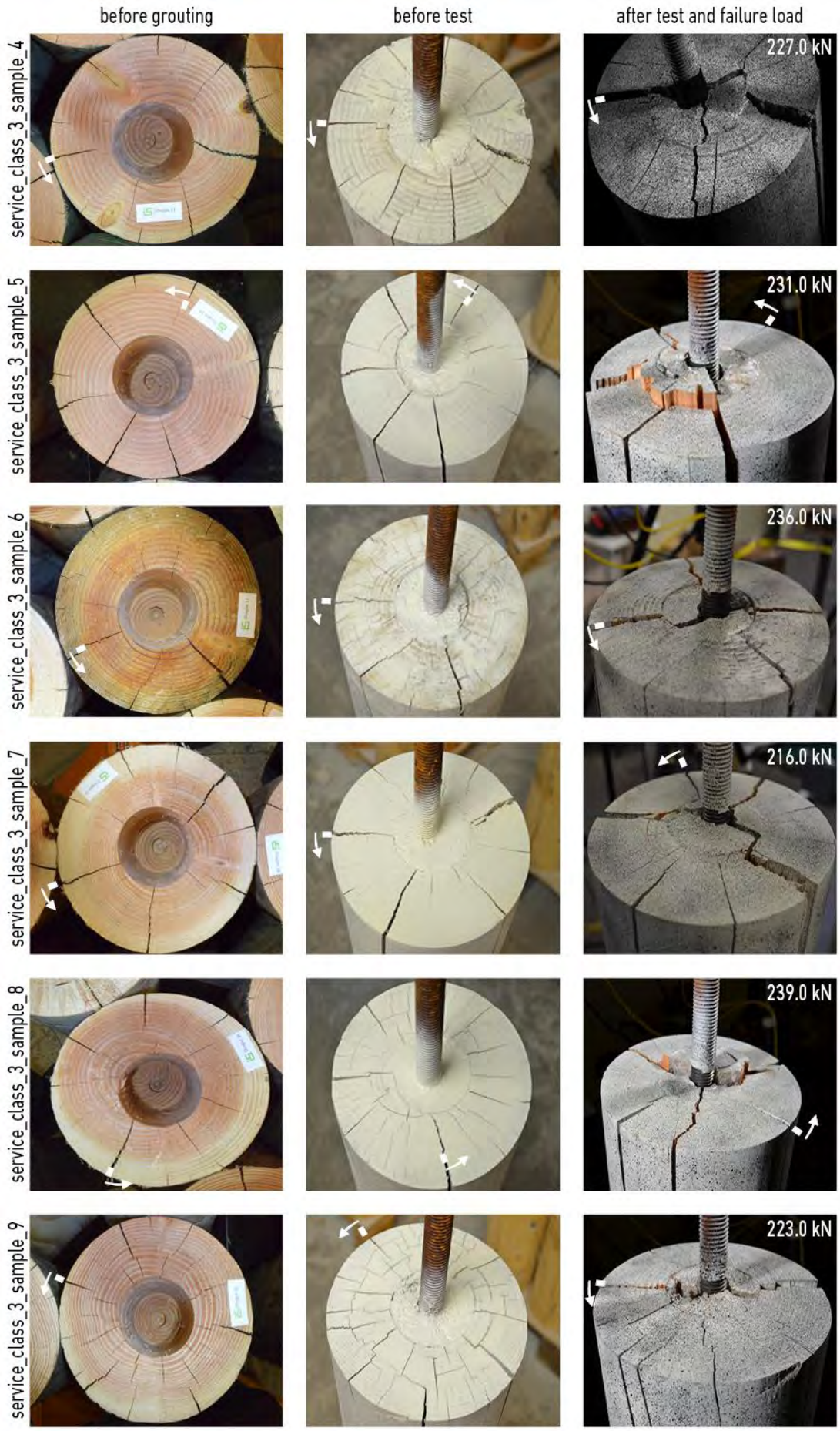

Fig. A-5 Test specimens at failure - service class 3 (cont.)

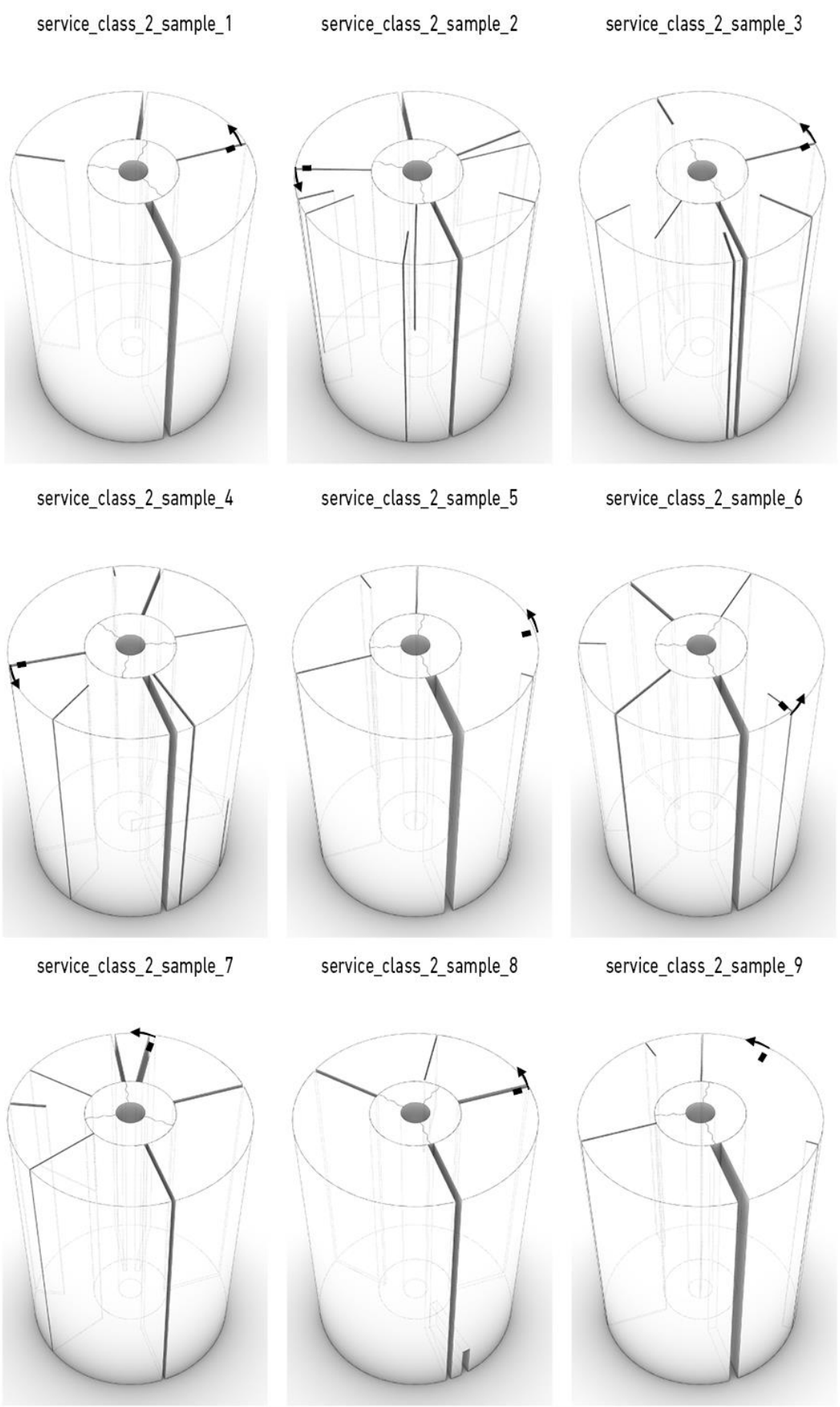

Fig. A-6 Natural pre cracks in roundwood

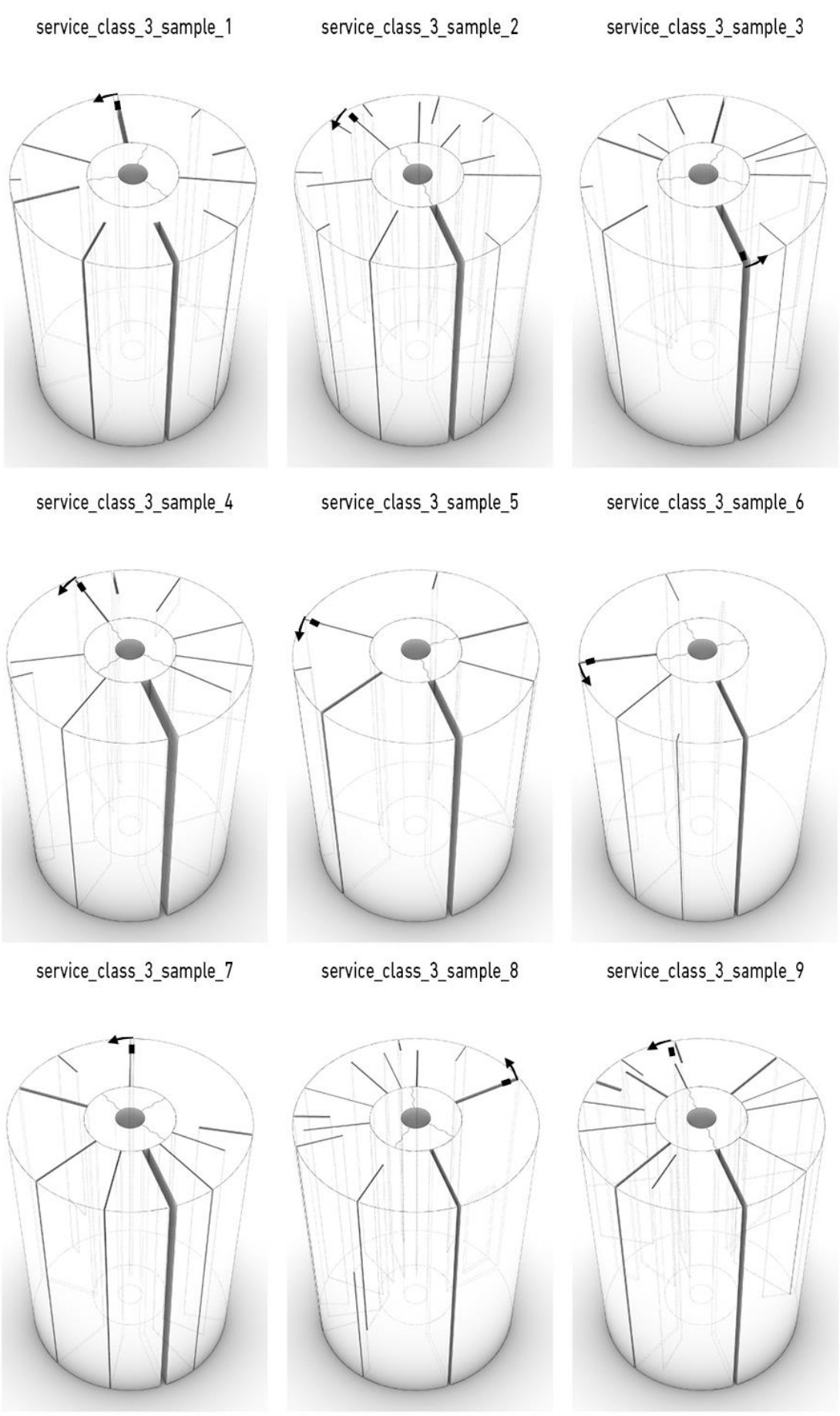

Fig. A-7 Natural pre cracks in roundwood (cont.)

A.1.2 Crack arrangement in polymer concrete

This section serves for the evaluation of tangential strains in the polymer concrete surface covered by camera system 1 and 2 of the DIC system. The data helped to determine load levels for different cracks in PC, to define the crack arrangement and to rate the influence of different service climate conditions.

The distribution of the measuring points or axes along the polymer concrete surface is explained in section 4.1.3 (data processing). Tangential strains were evaluated for

- SC2, sample 3 (pp. 164-165),
- SC2, sample 4 (pp. 166-167),
- SC2, sample 5 (pp. 168-169),
- SC2, sample 6 (pp. 170-171),
- SC2, sample 7 (pp. 172-173),
- SC3, sample 2 (pp. 174-175),
- SC3, sample 3 (pp. 176-177),
- SC3, sample 4 (pp. 178-179),
- SC3, sample 7 (pp. 180-181),
- SC3, sample 8 (pp. 182-183).

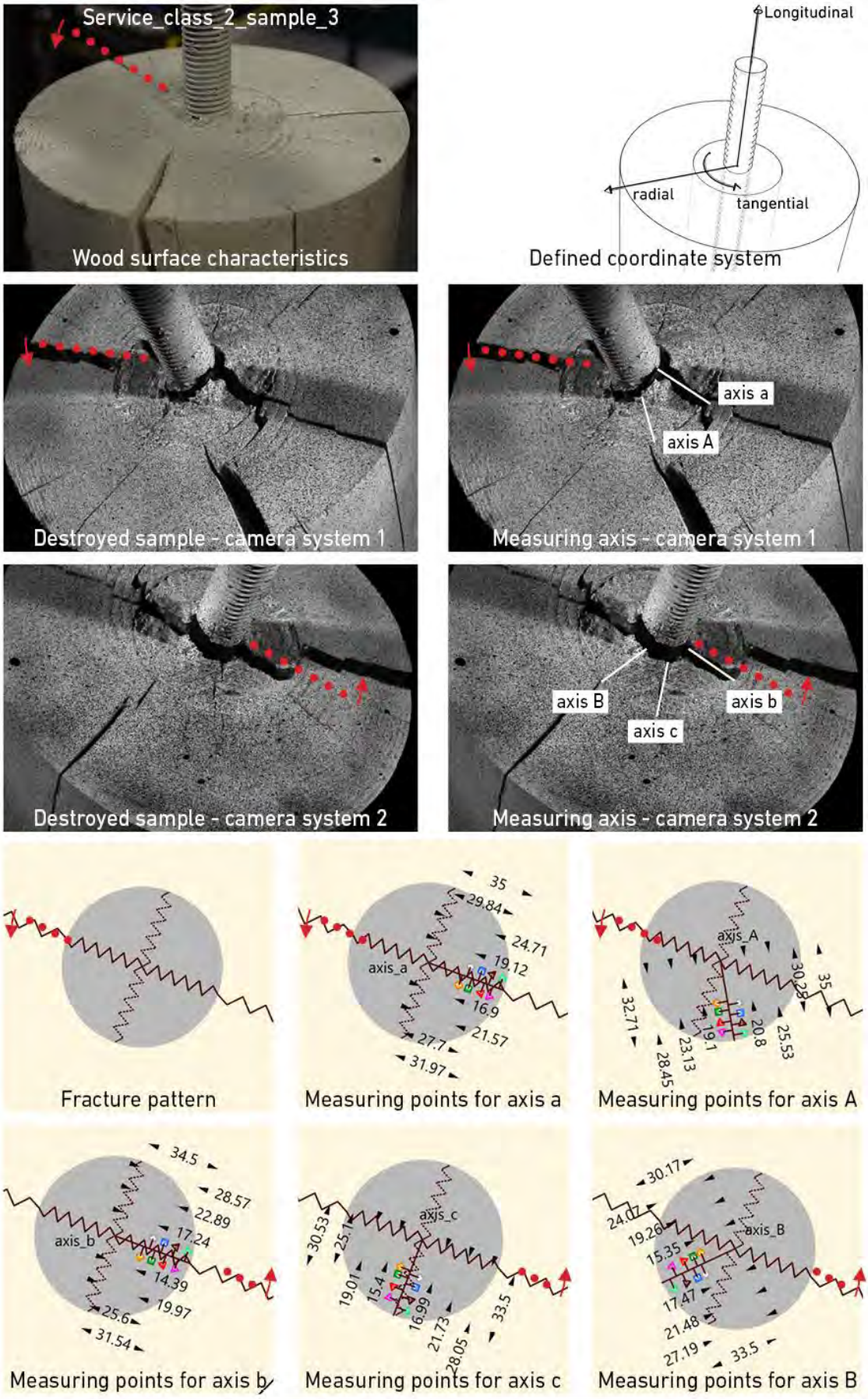

The tangential strains for the defined axis in polymer concrete are shown in the following page

Fig. A-8 Evaluation polymer concrete service class 2, sample 3

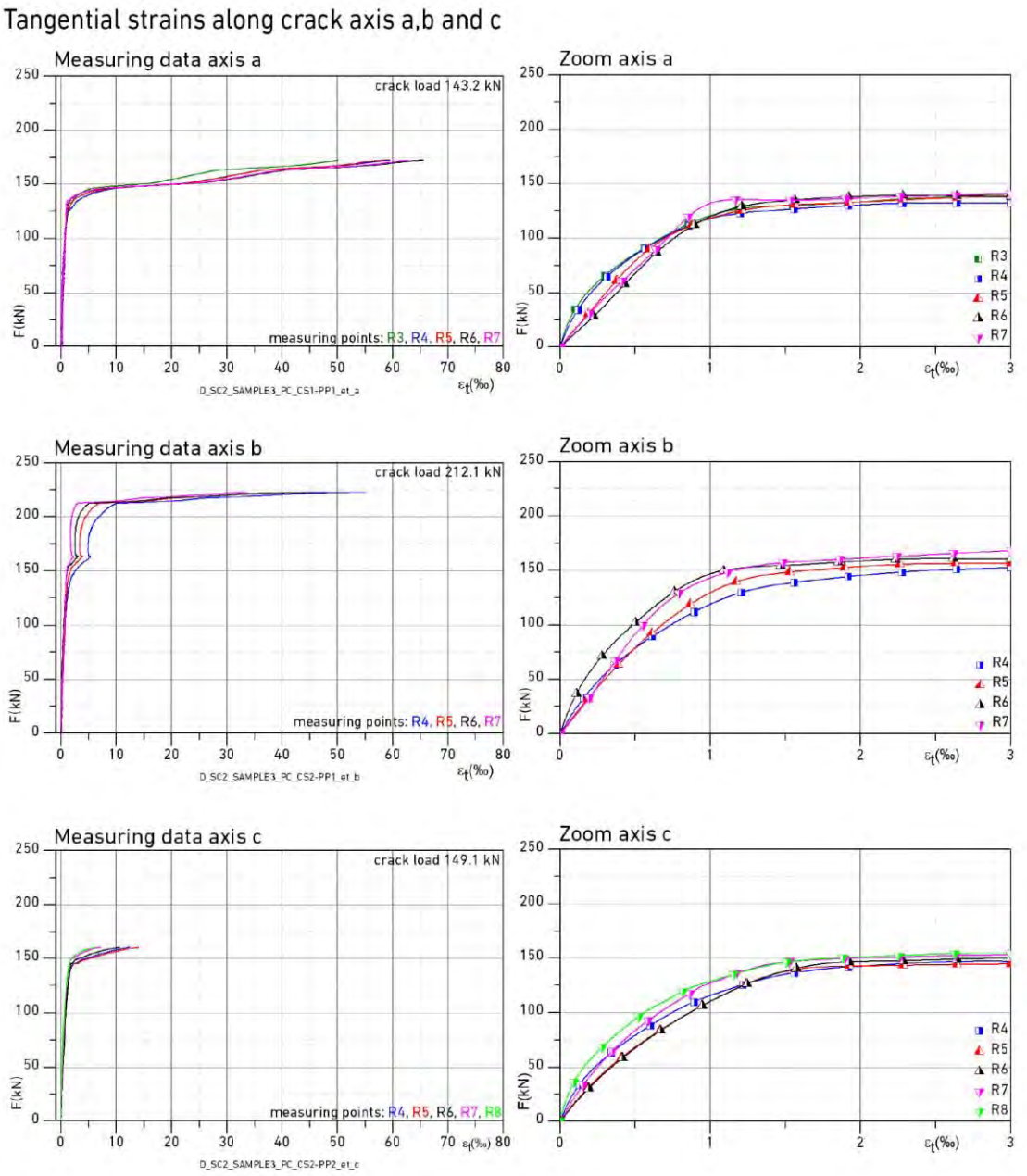

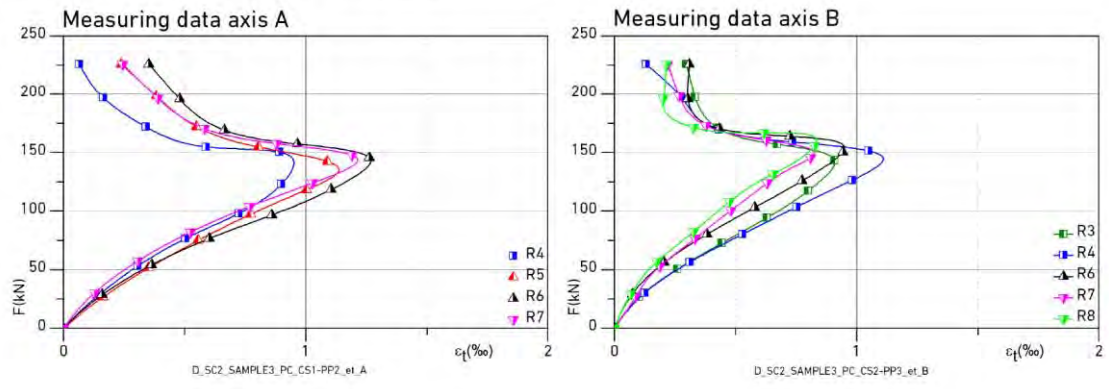

The measuring axis and points in polymer concrete are defined in the previous page

Fig. A-9 Evaluation polymer concrete service class 2, sample 3 (cont.)

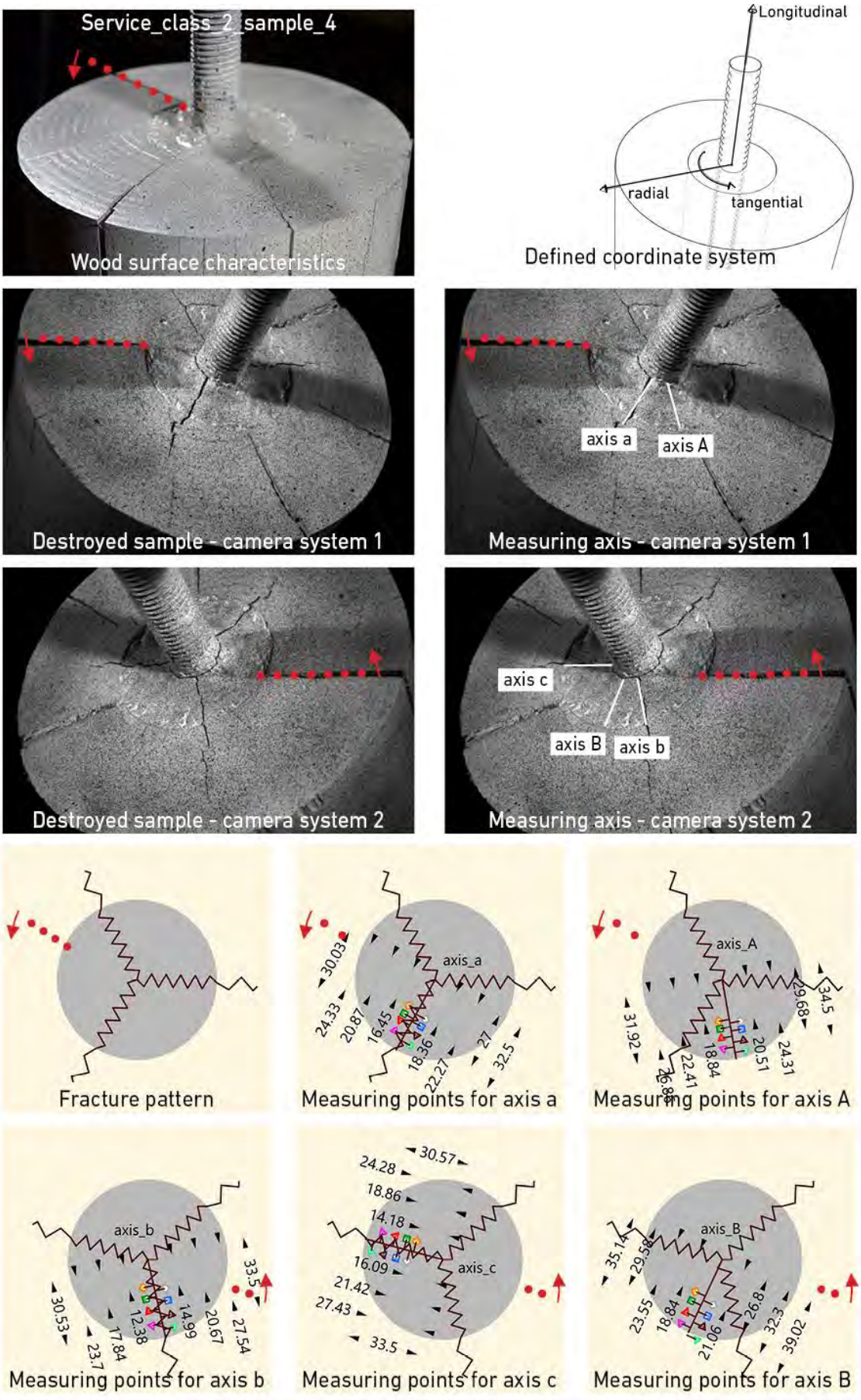

Fig. A-10 Evaluation polymer concrete service class 2, sample 4

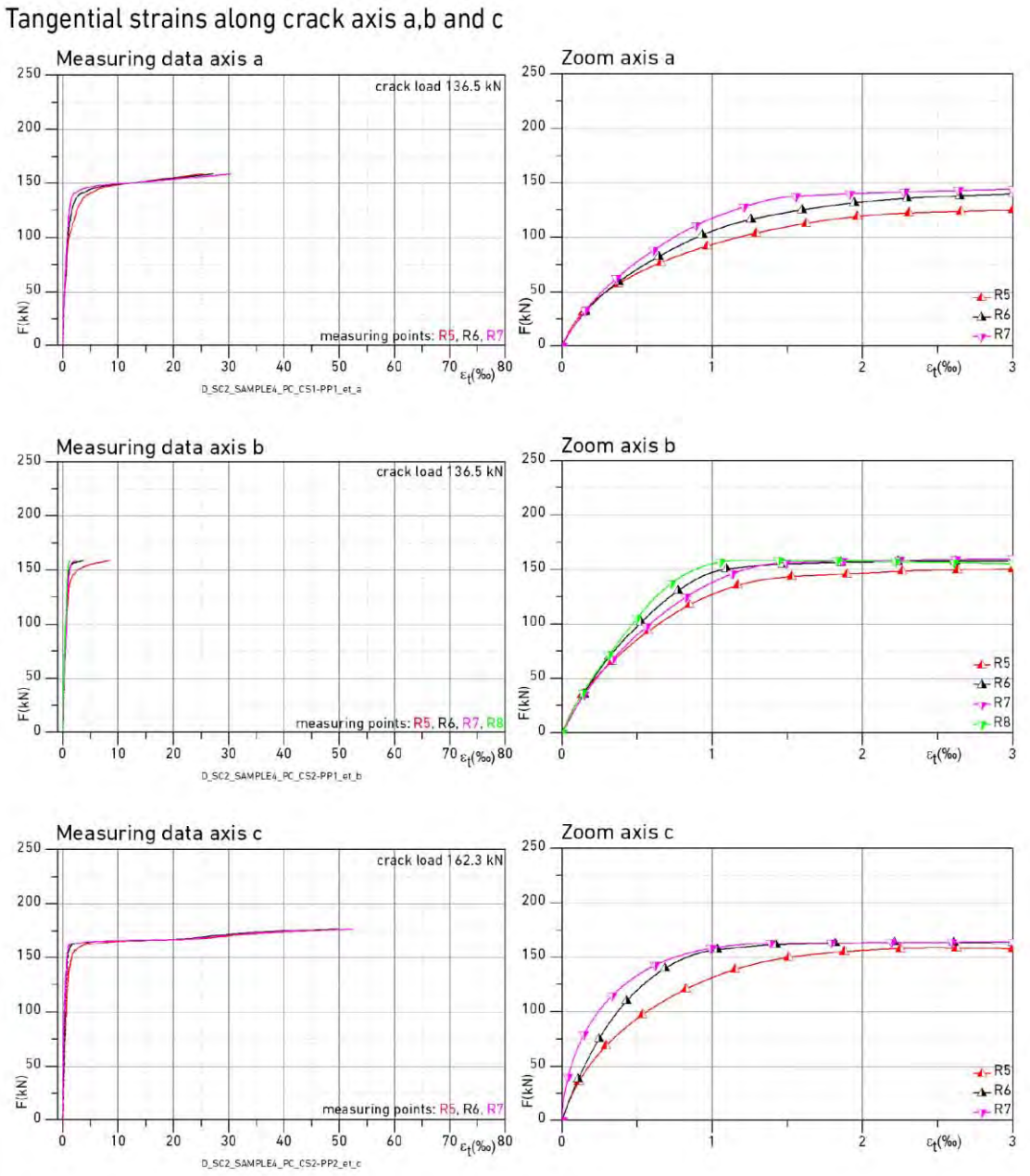

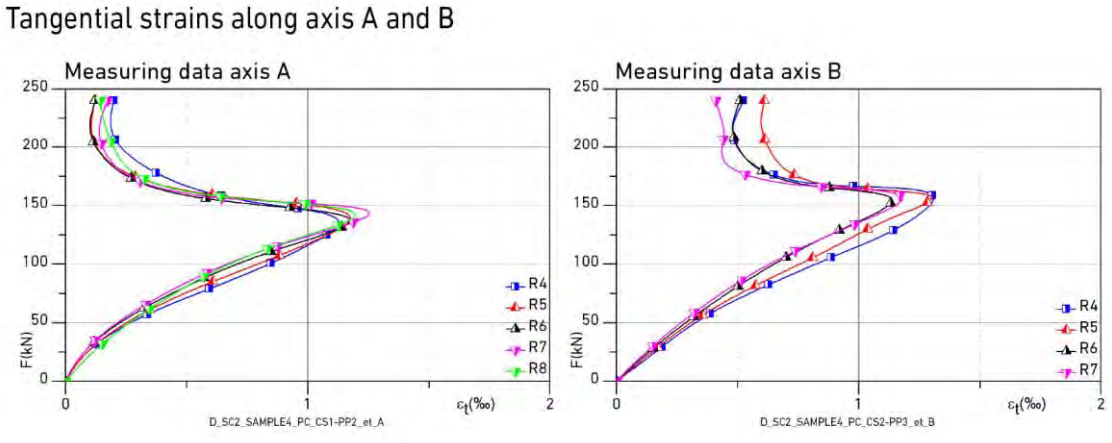

The measuring axis and points in polymer concrete are defined in the previous page

Fig. A-11 Evaluation polymer concrete service class 2, sample 4 (cont.)

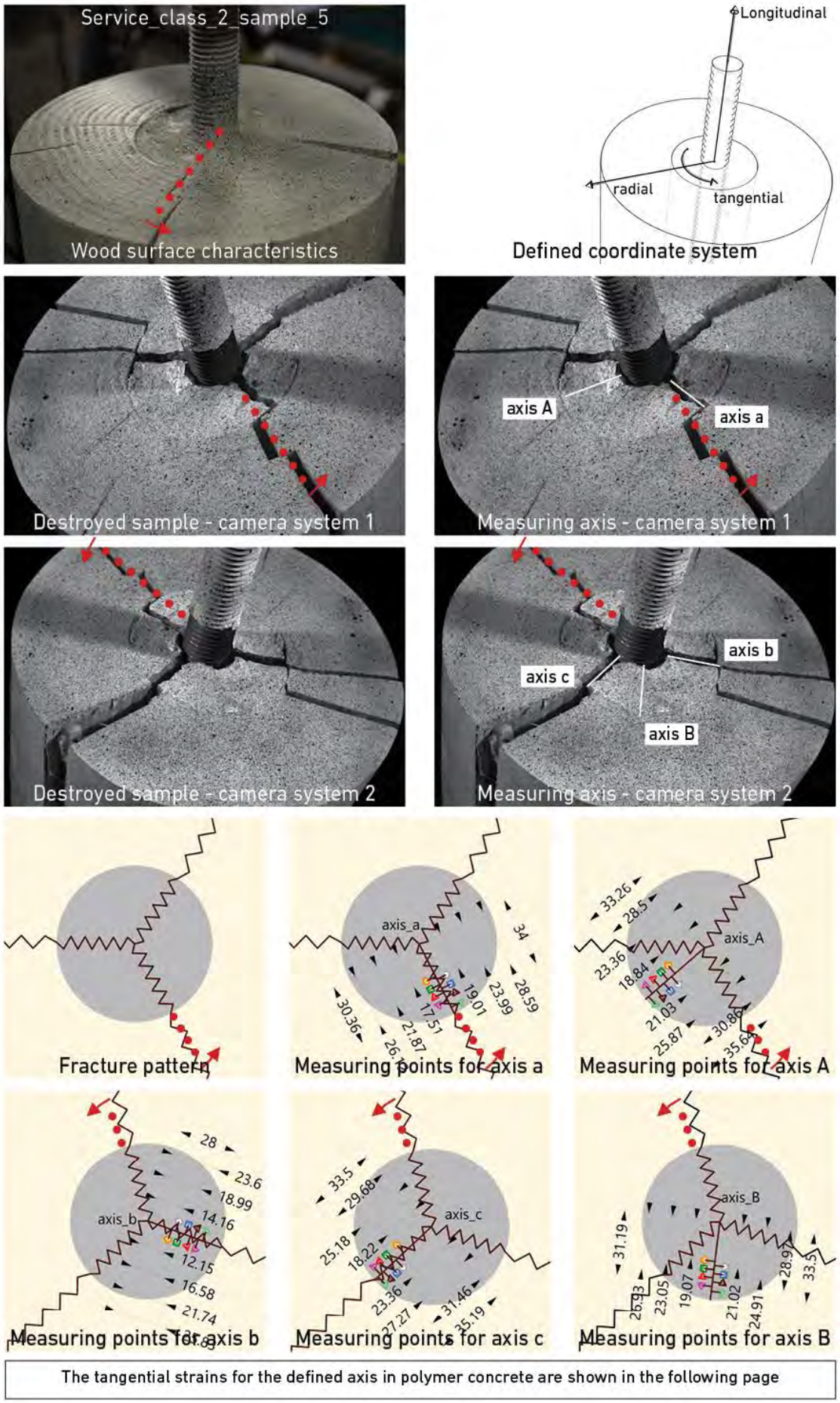

Fig. A-12 Evaluation polymer concrete service class 2, sample 5

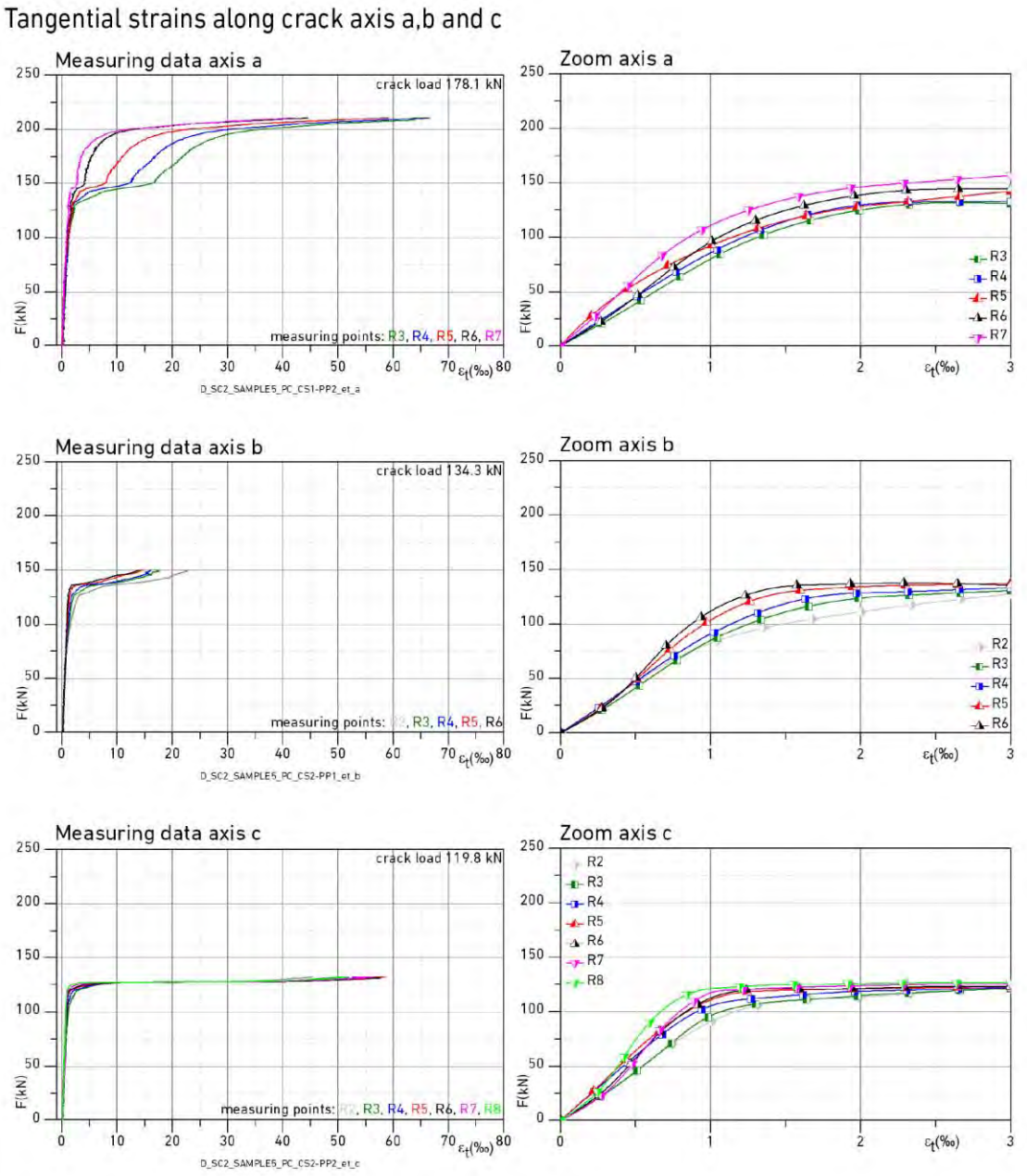

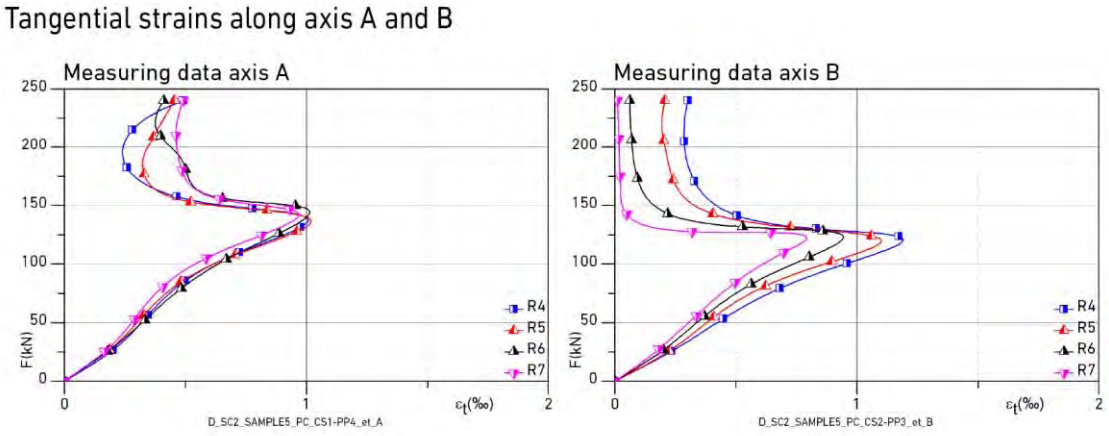

The measuring axis and points in polymer concrete are defined in the previous page

Fig. A-13 Evaluation polymer concrete service class 2, sample 5 (cont.)

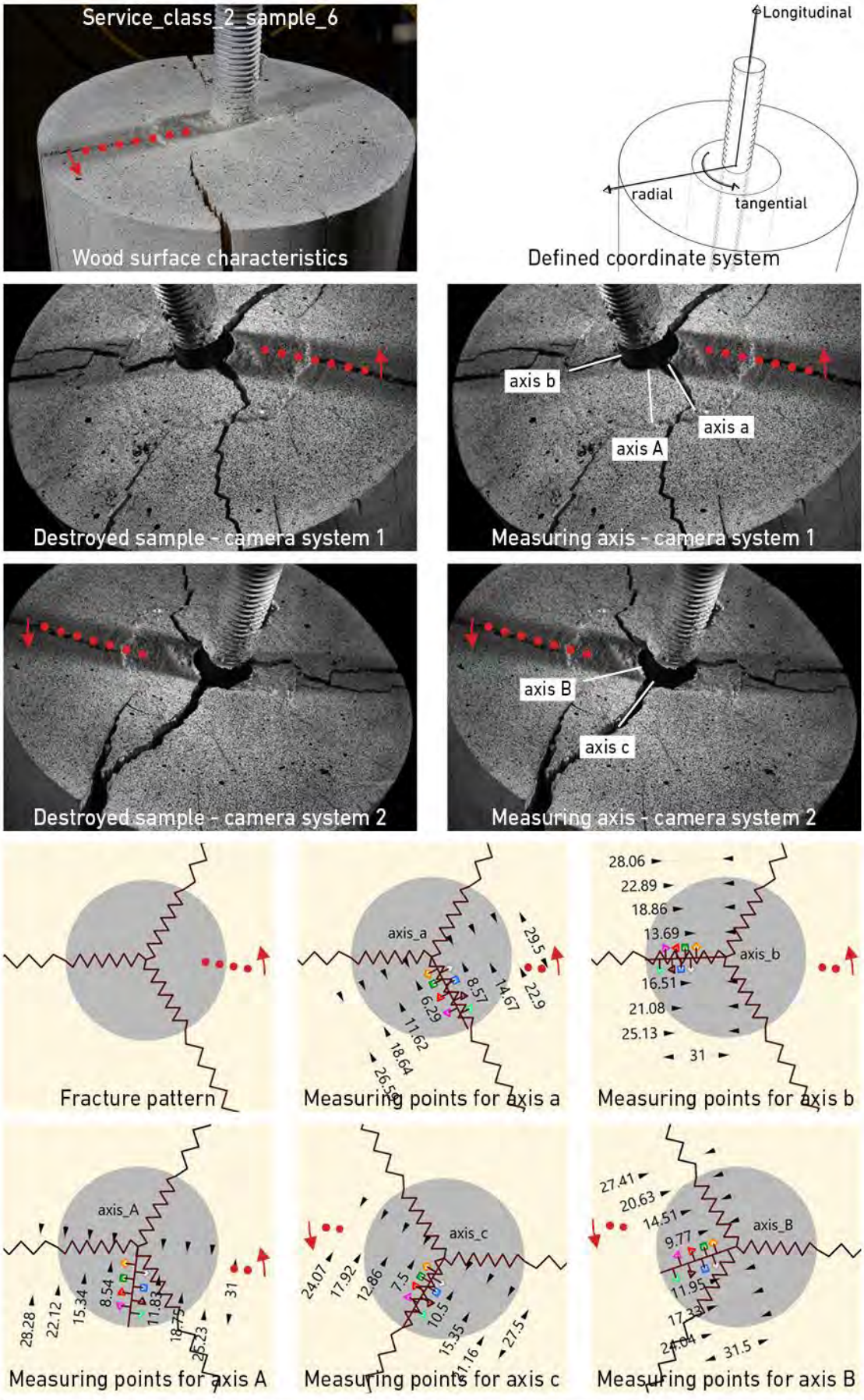

Fig. A-14 Evaluation polymer concrete service class 2, sample 6

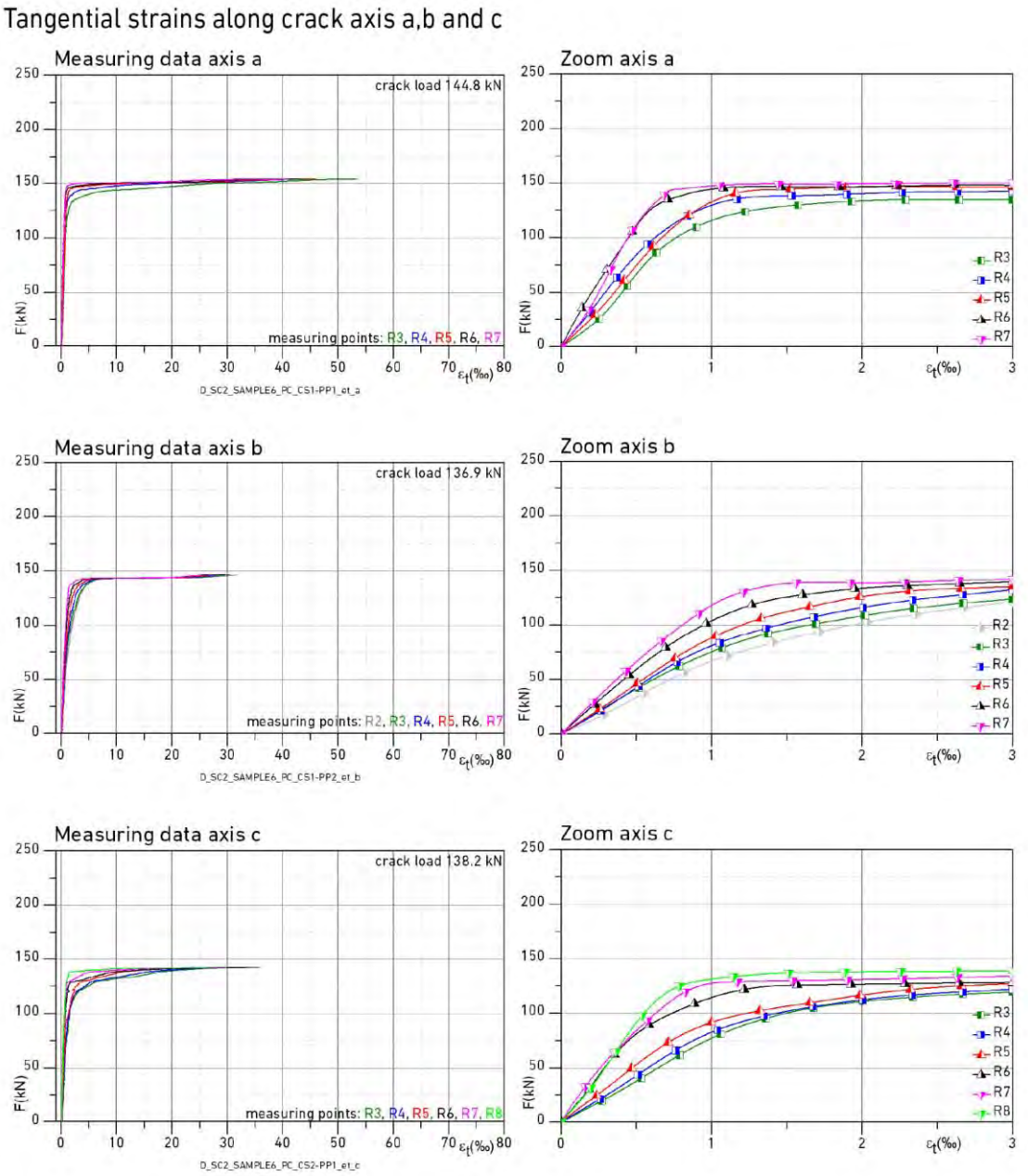

The measuring axis and points in polymer concrete are defined in the previous page

Fig. A-15 Evaluation polymer concrete service class 2, sample 6 (cont.)

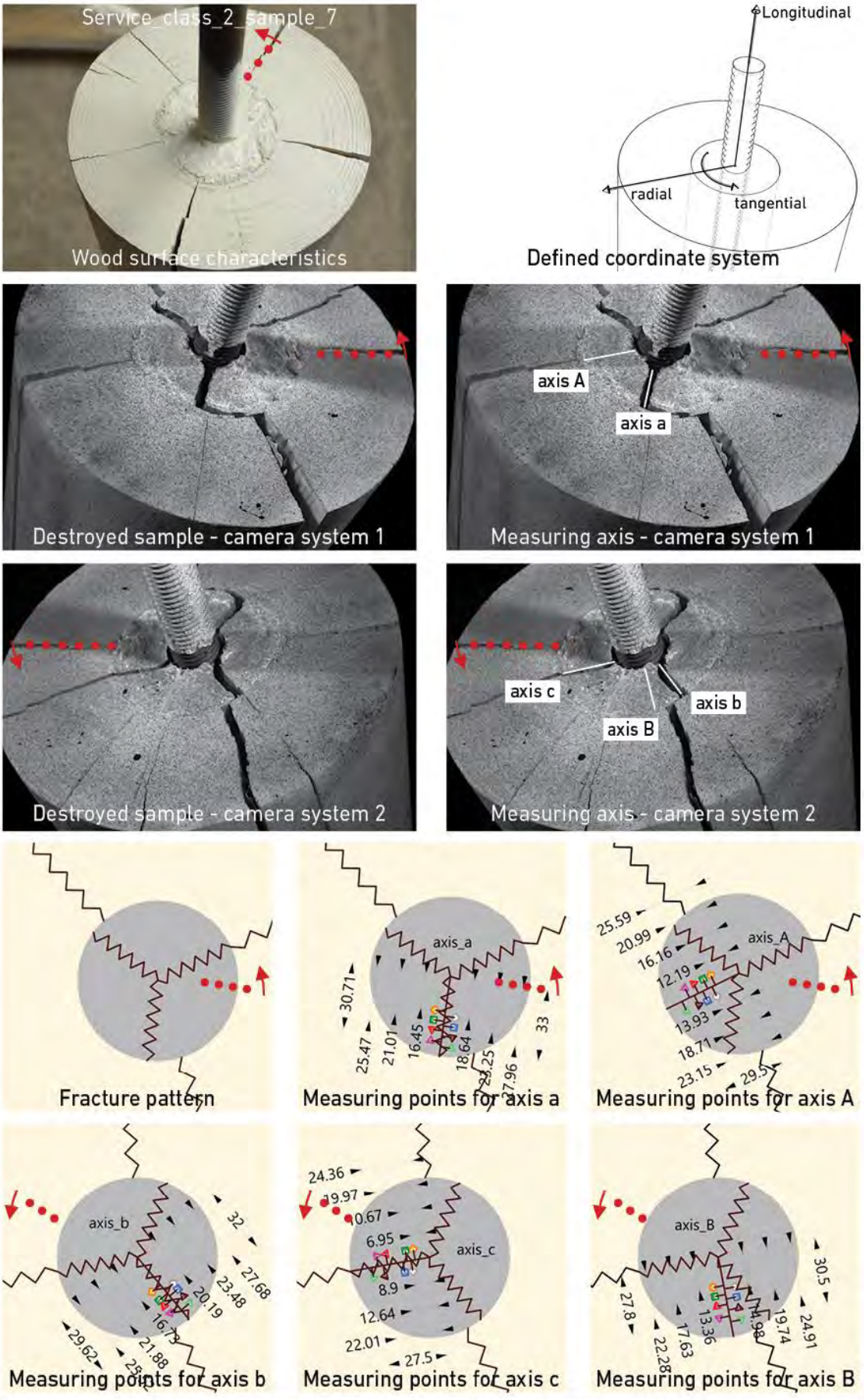

Fig. A-16 Evaluation polymer concrete service class 2, sample 7

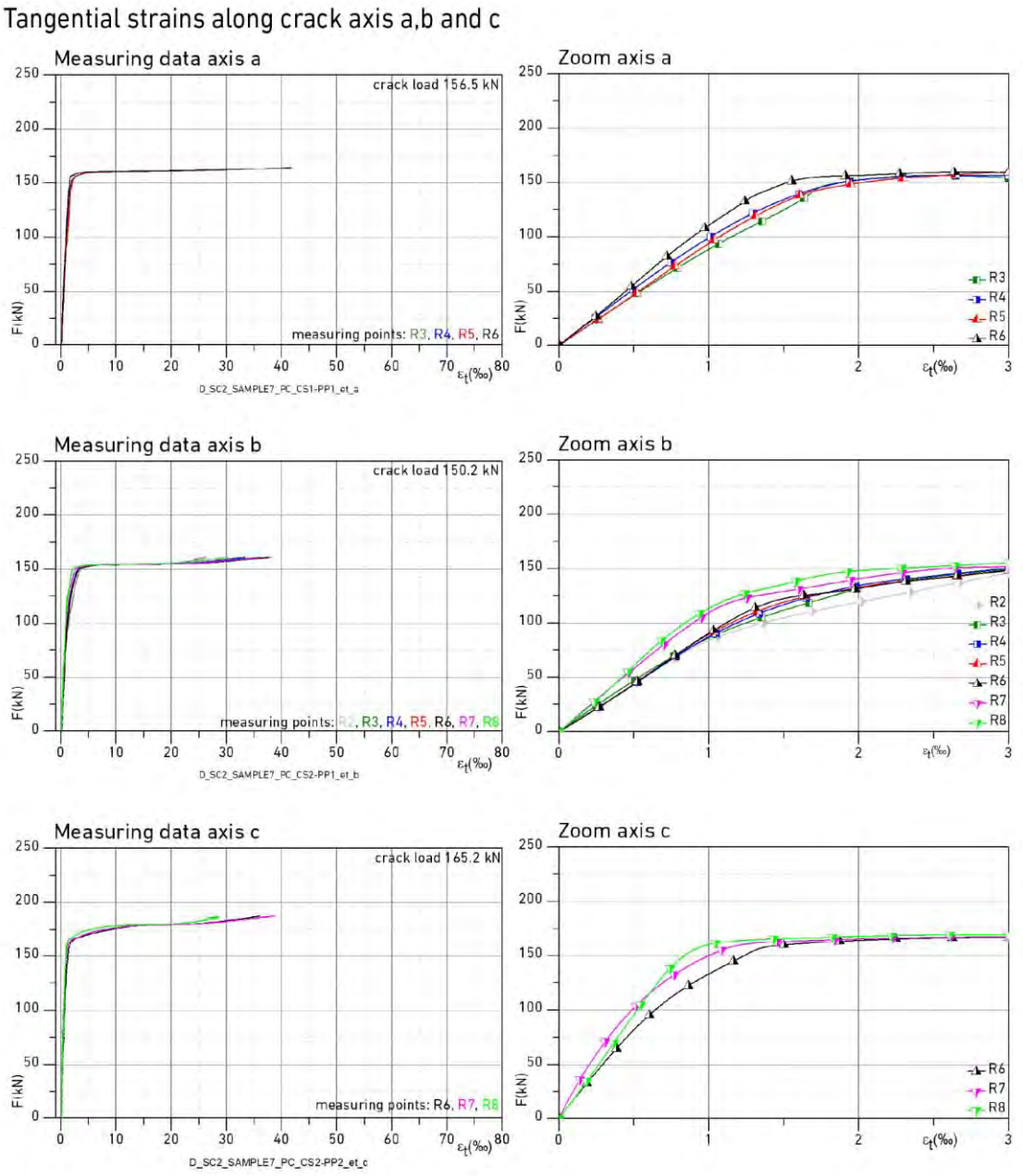

The measuring axis and points in polymer concrete are defined in the previous page

Fig. A-17 Evaluation polymer concrete service class 2, sample 7 (cont.)

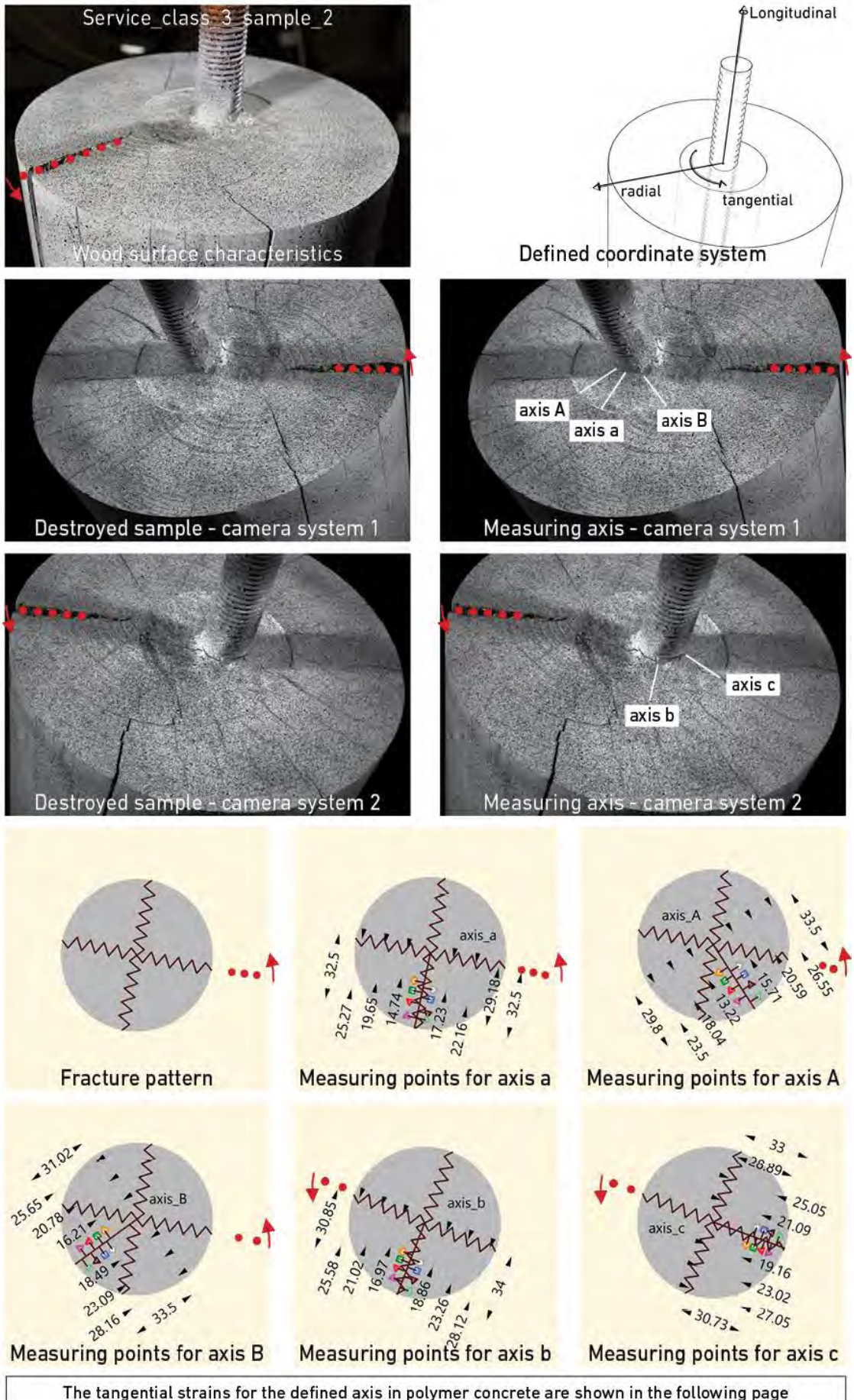

Fig. A-18 Evaluation polymer concrete service class 3, sample 2

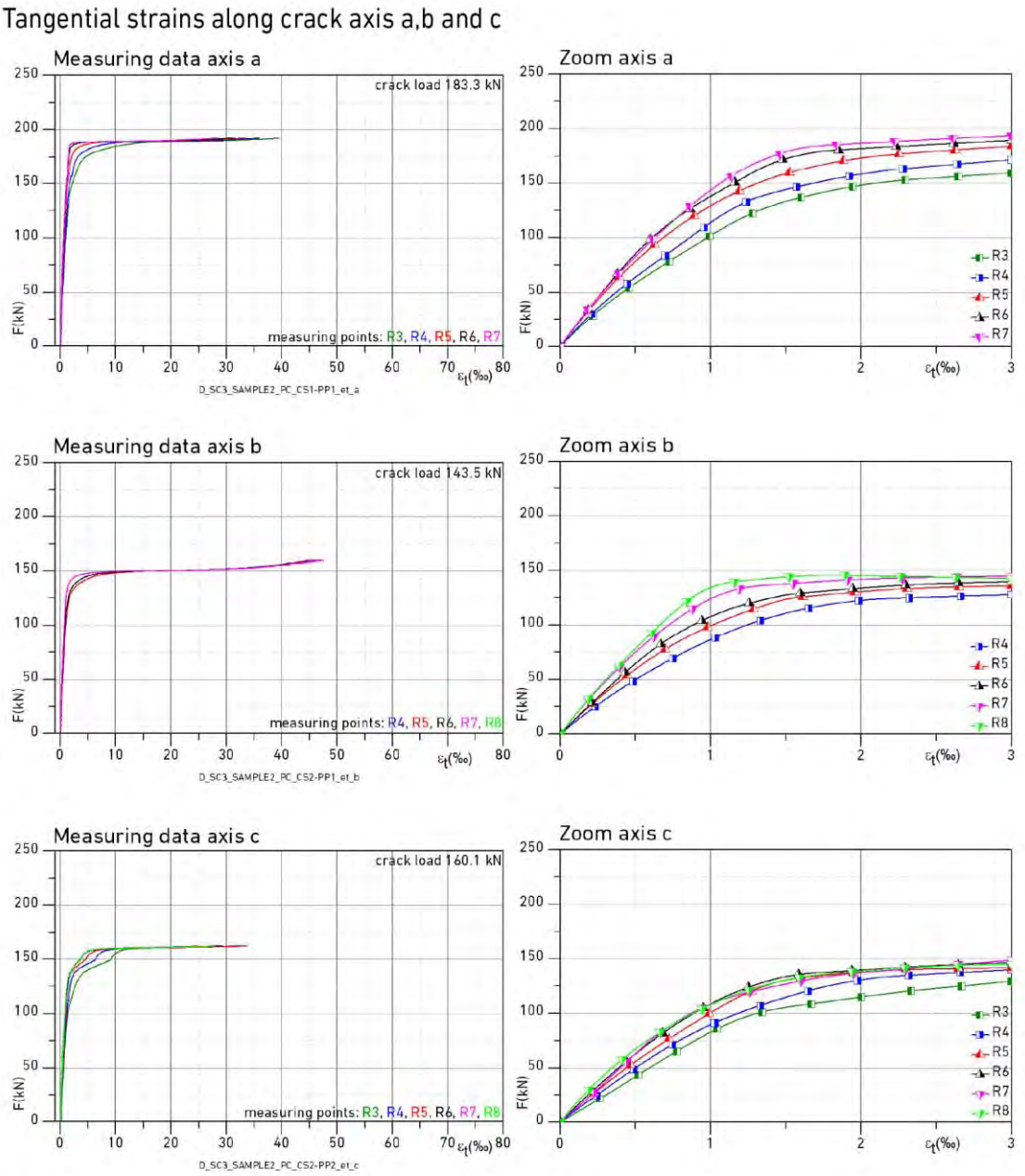

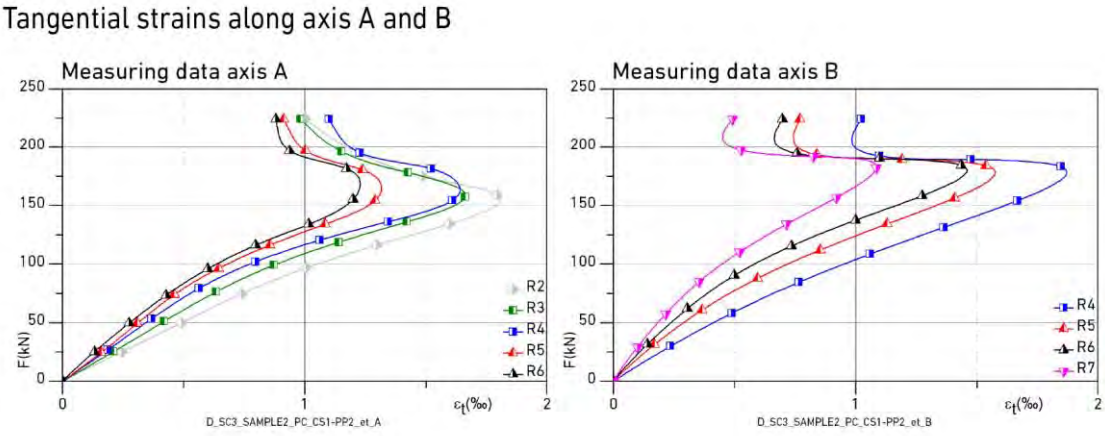

The measuring axis and points in polymer concrete are defined in the previous page

Fig. A-19 Evaluation polymer concrete service class 3, sample 2 (cont.)

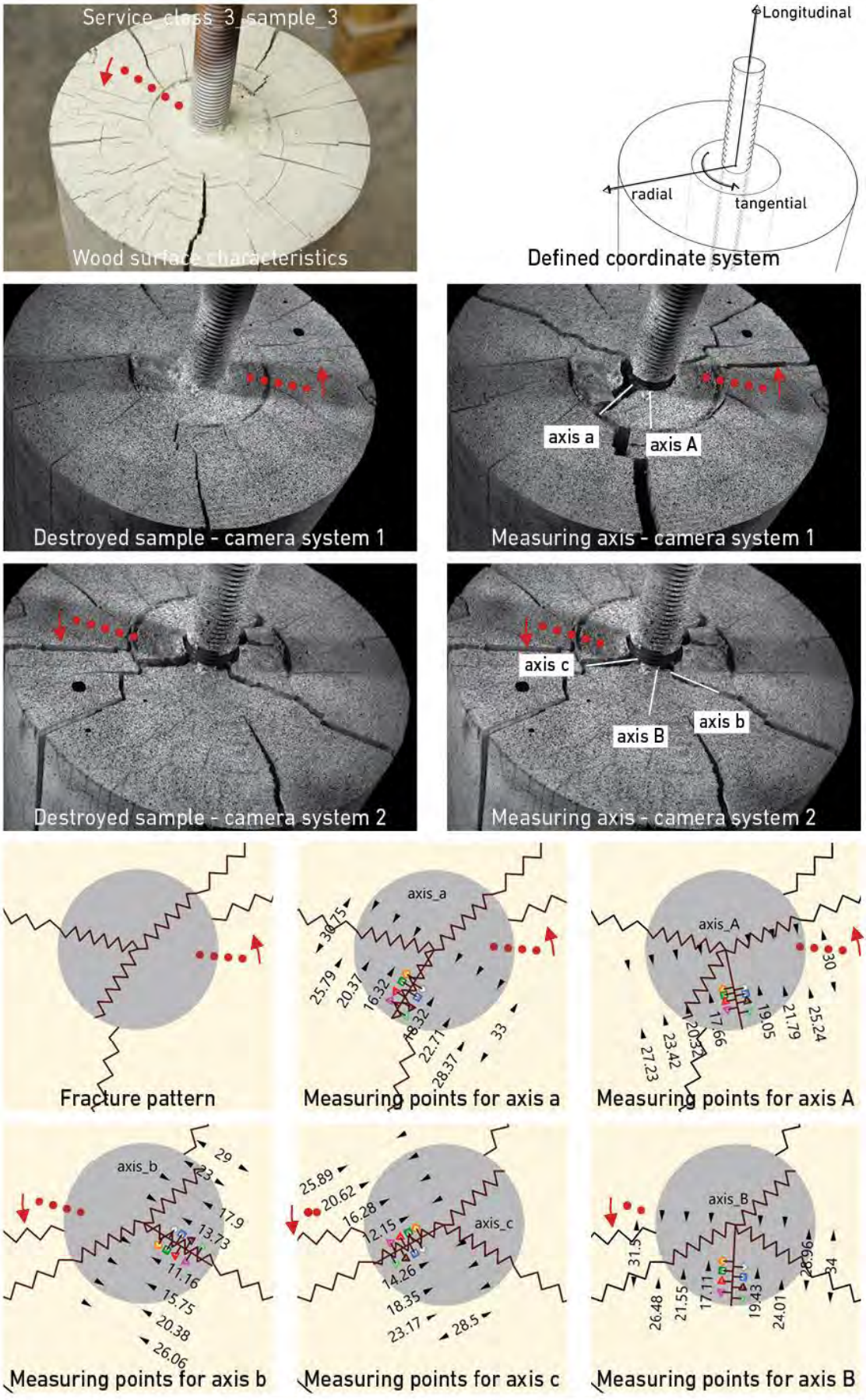

Fig. A-20 Evaluation polymer concrete service class 3, sample 3

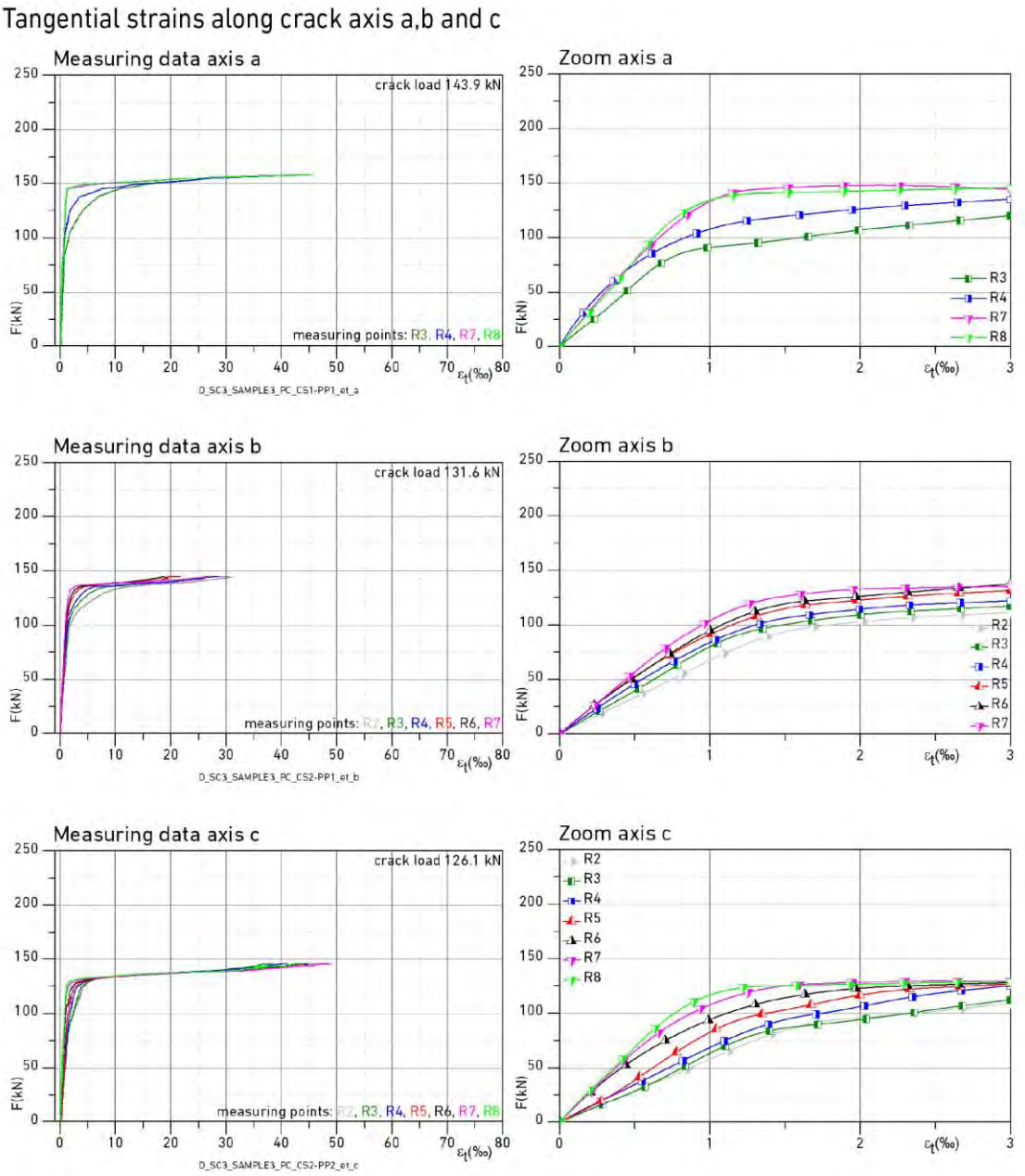

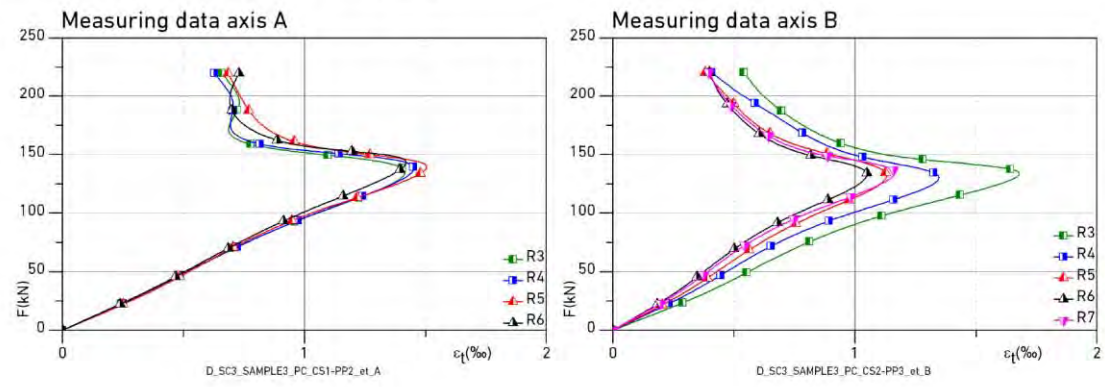

The measuring axis and points in polymer concrete are defined in the previous page

Fig. A-21 Evaluation polymer concrete service class 3, sample 3 (cont.)

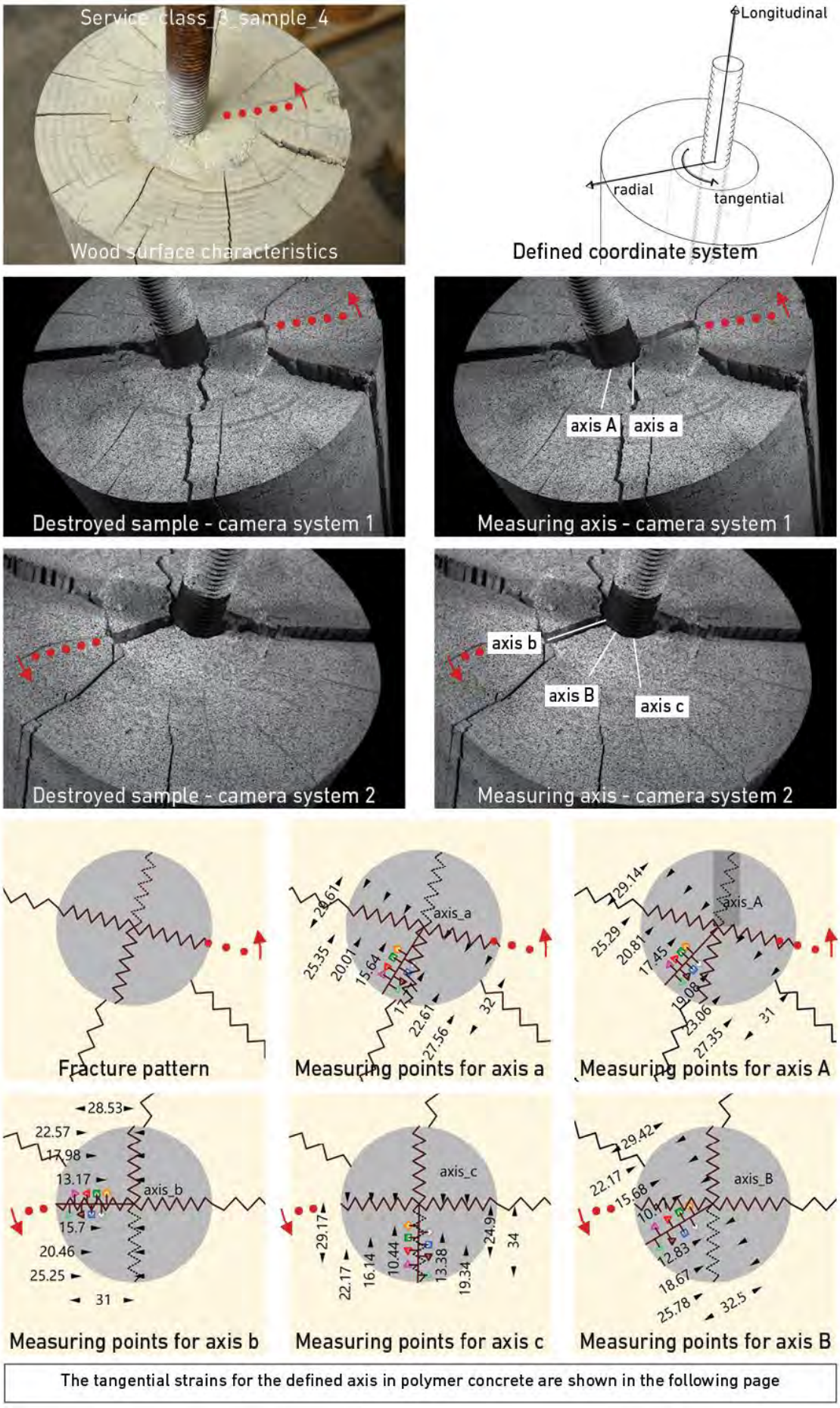

Fig. A-22 Evaluation polymer concrete service class 3, sample 4

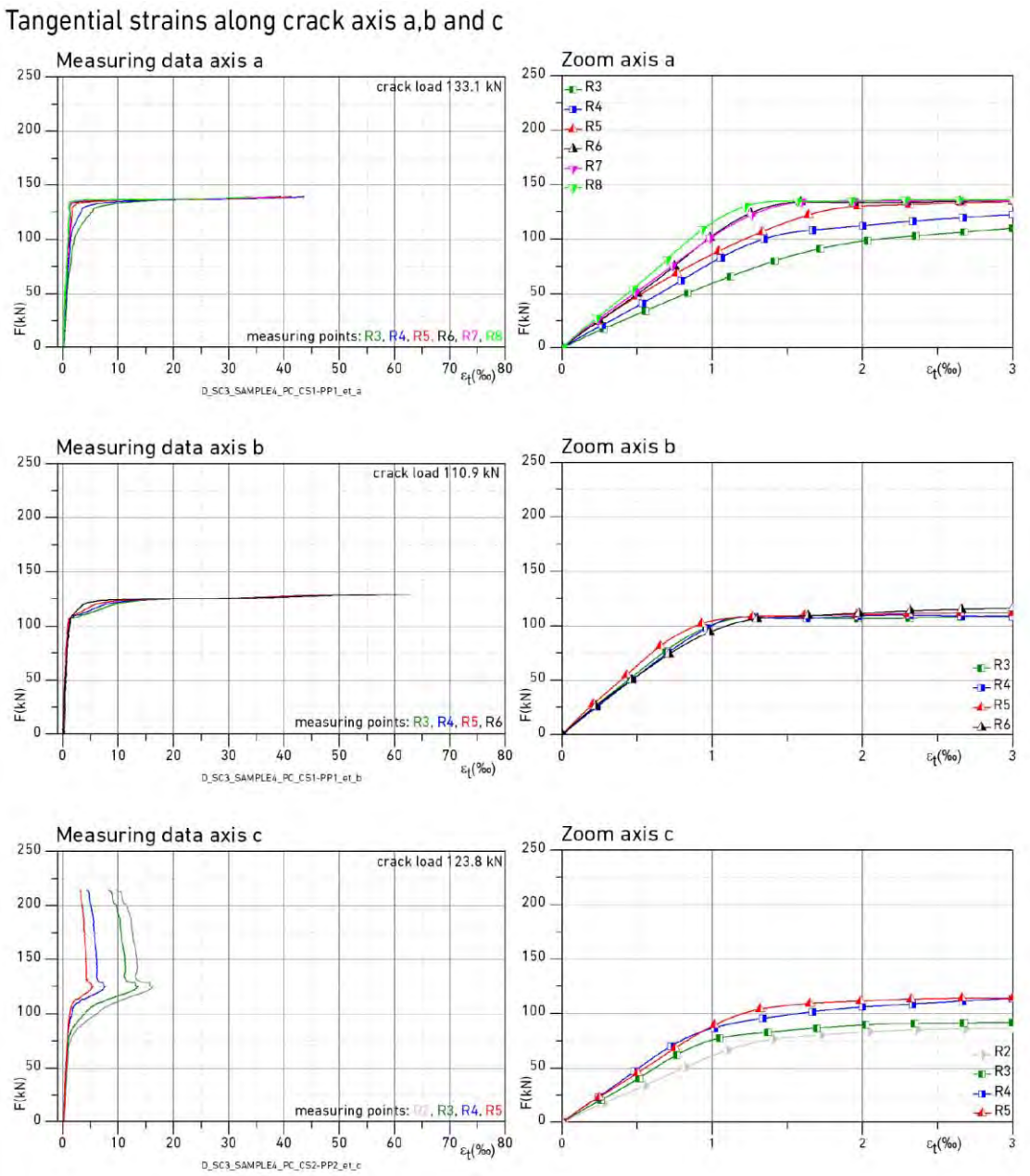

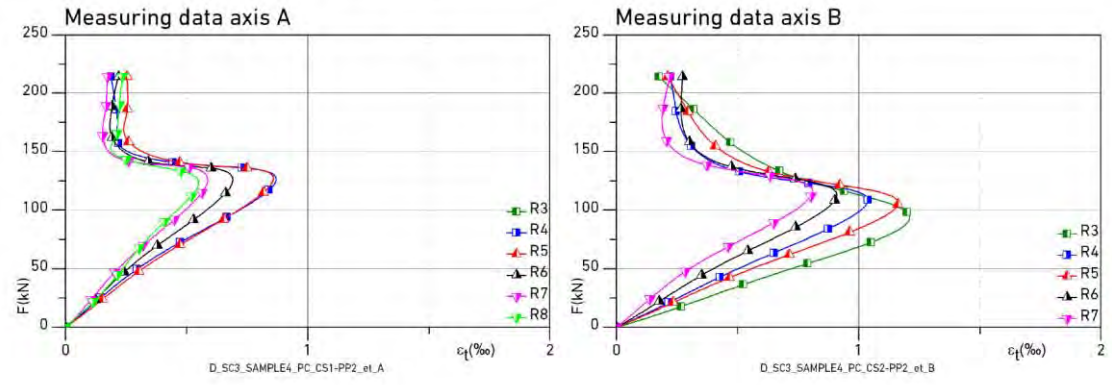

The measuring axis and points in polymer concrete are defined in the previous page

Fig. A-23 Evaluation polymer concrete service class 3, sample 4 (cont.)

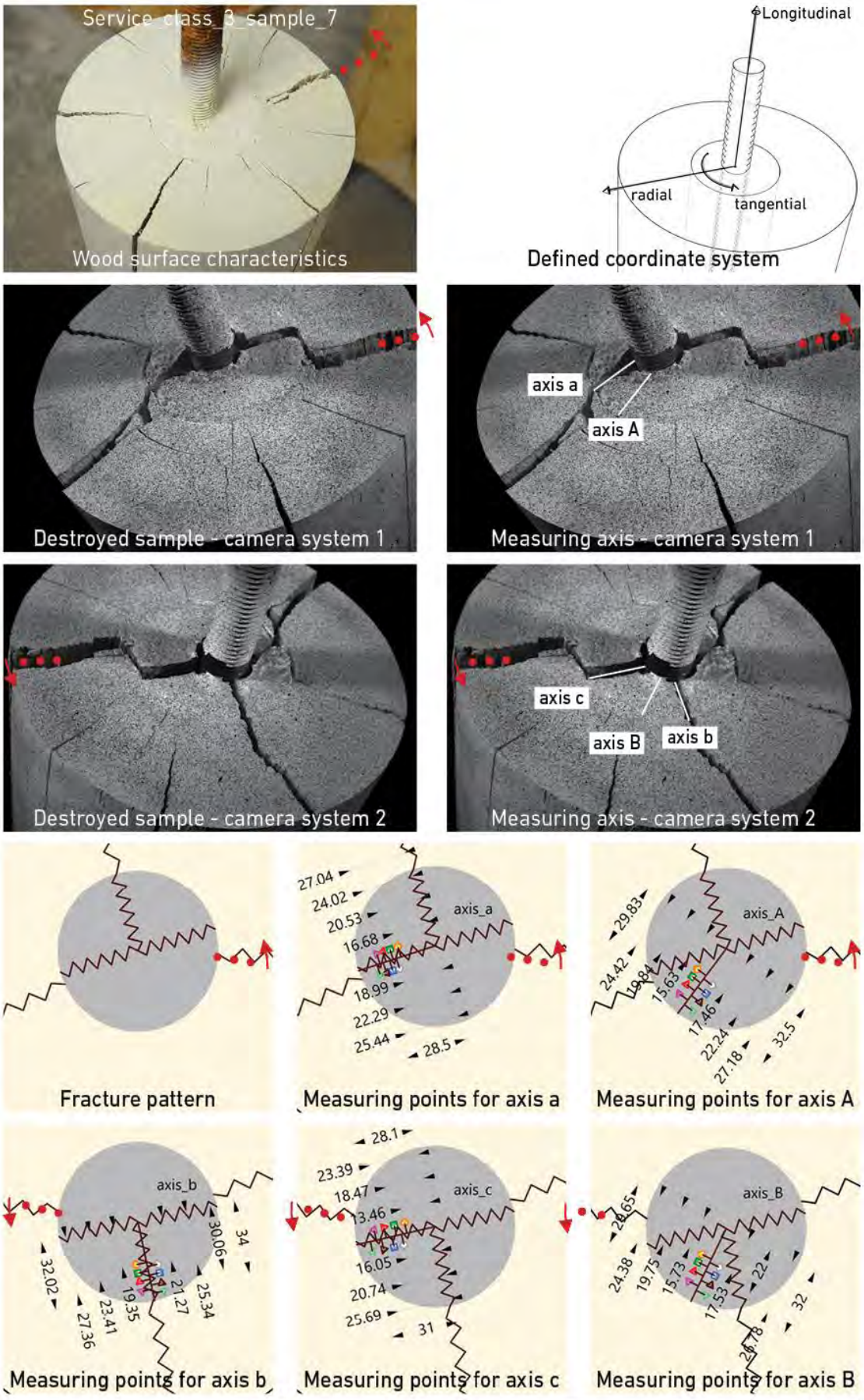

Fig. A-24 Evaluation polymer concrete service class 3, sample 7

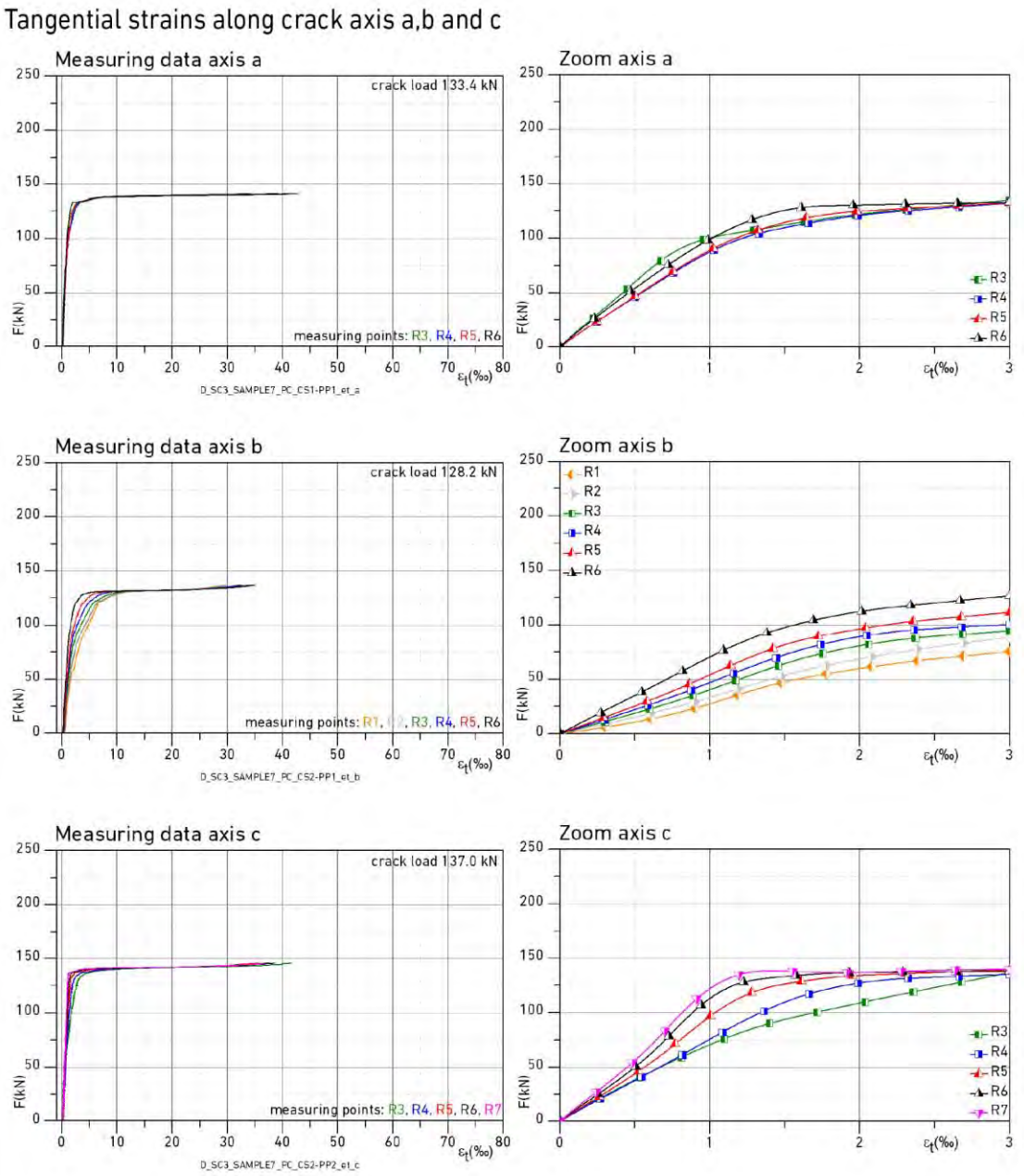

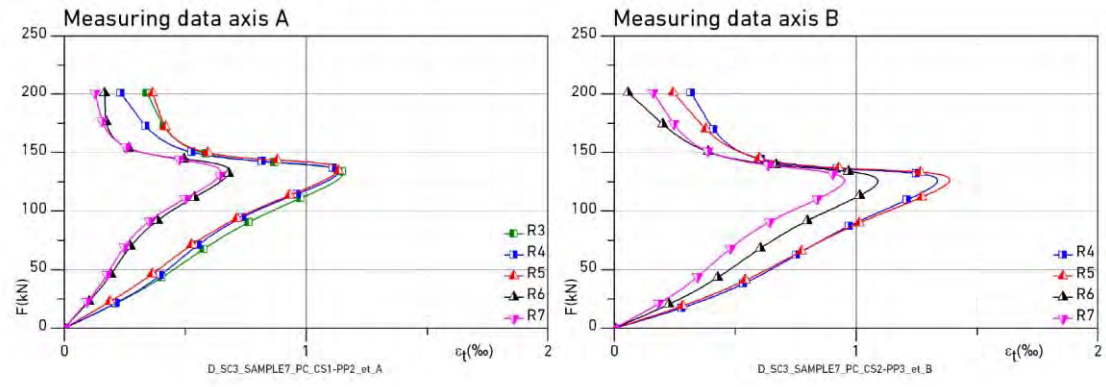

The measuring axis and points in polymer concrete are defined in the previous page

Fig. A-25 Evaluation polymer concrete service class 3, sample 7 (cont.)

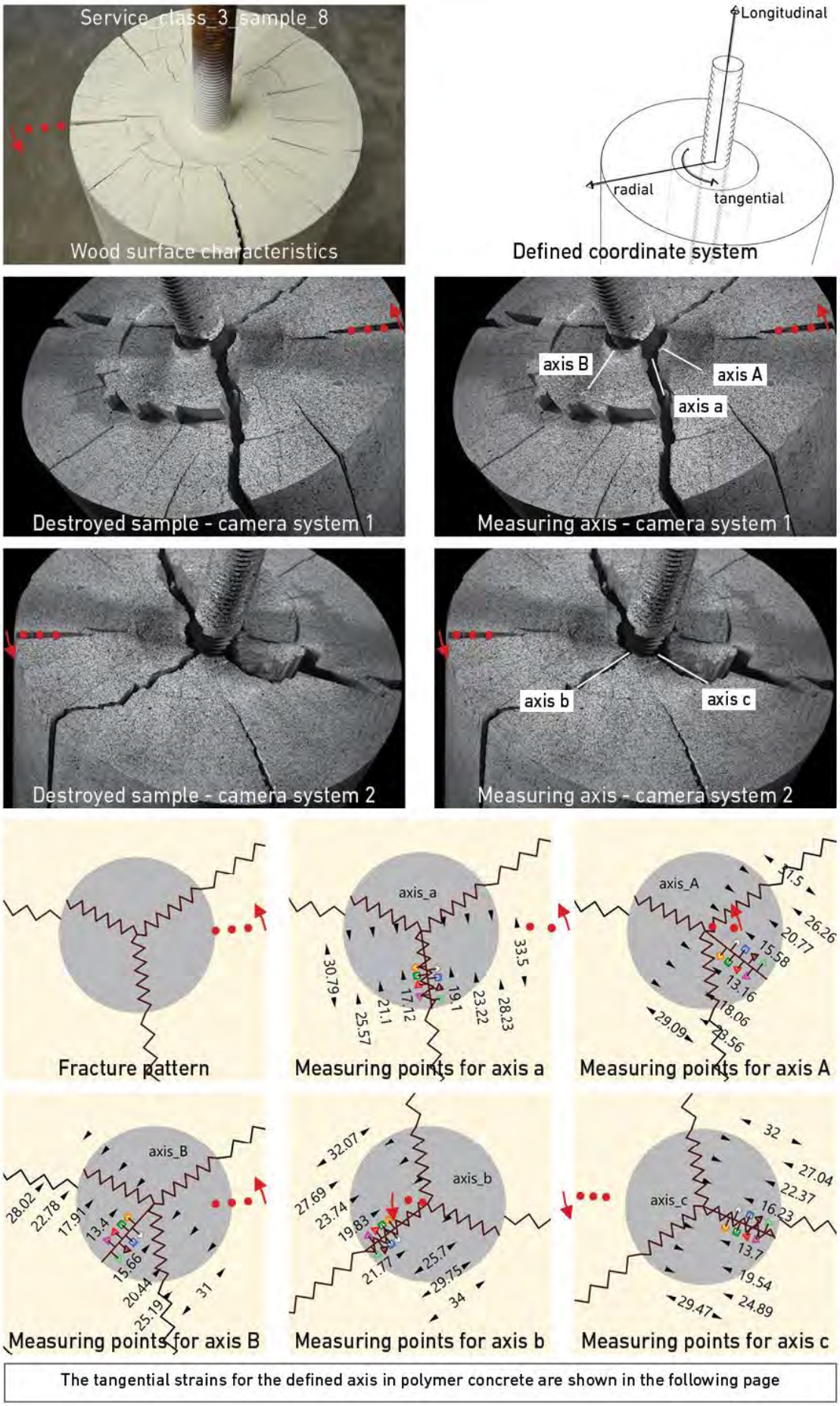

Fig. A-26 Evaluation polymer concrete service class 3, sample 8

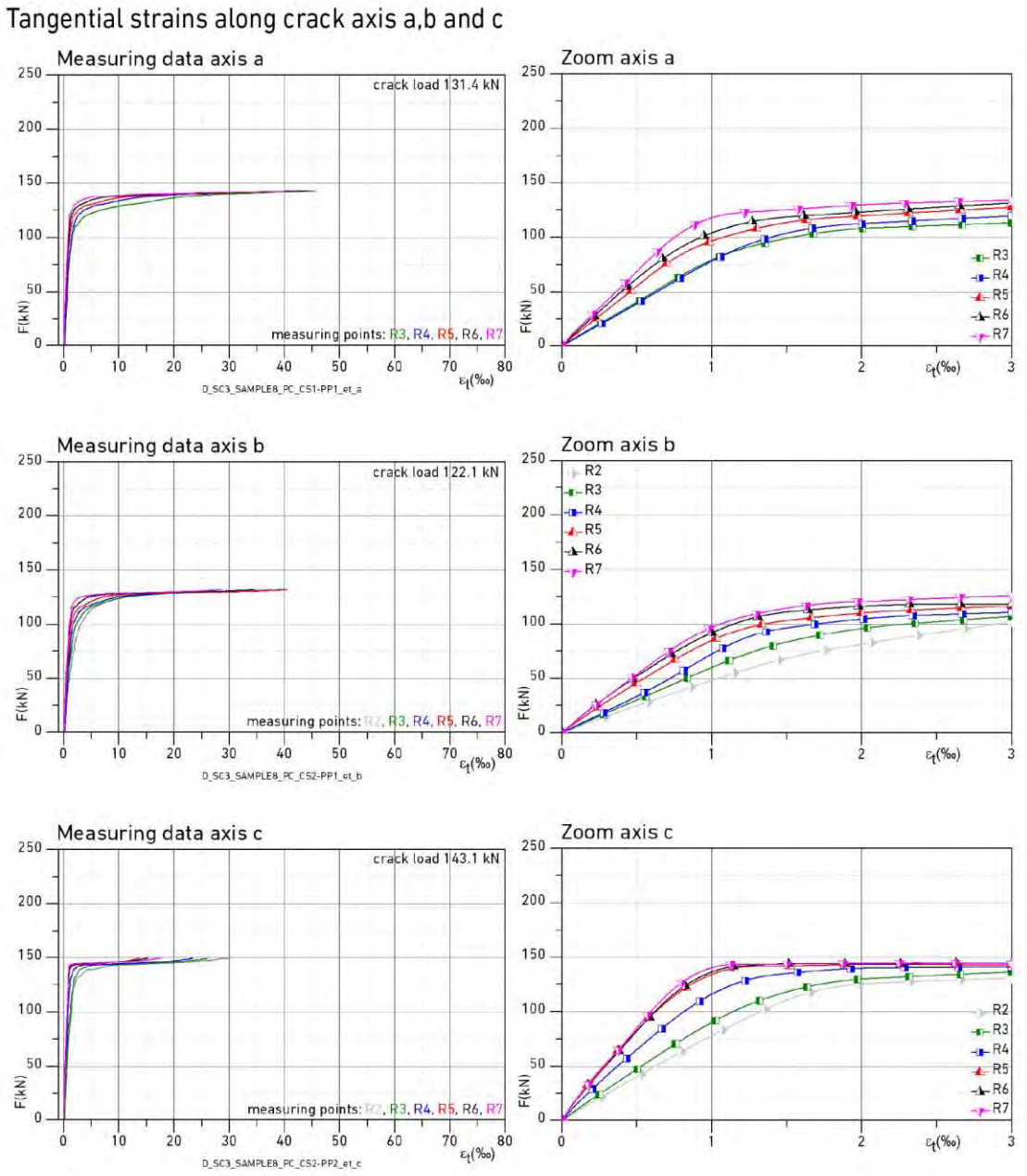

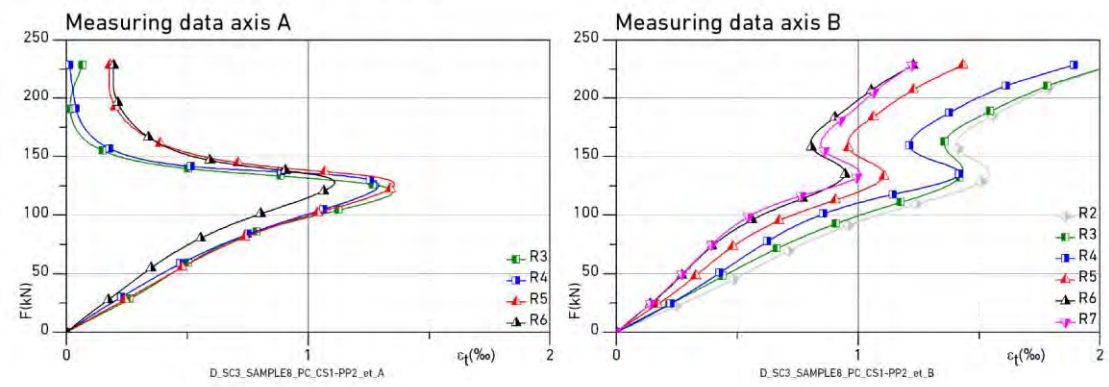

The measuring axis and points in polymer concrete are defined in the previous page

Fig. A-27 Evaluation polymer concrete service class 3, sample 8 (cont.)

A.1.3 Structural behaviour along bond line

This section serves for the evaluation of longitudinal strains in the outer roundwood surface covered by camera system 3 of the DIC system. The data helped to identify high-stressed regions along the bondline or embedment length of modified bonded-in rods.

The distribution of the measuring points or axes along the roundwood outer surface is explained in section 4.1.3 (data processing).

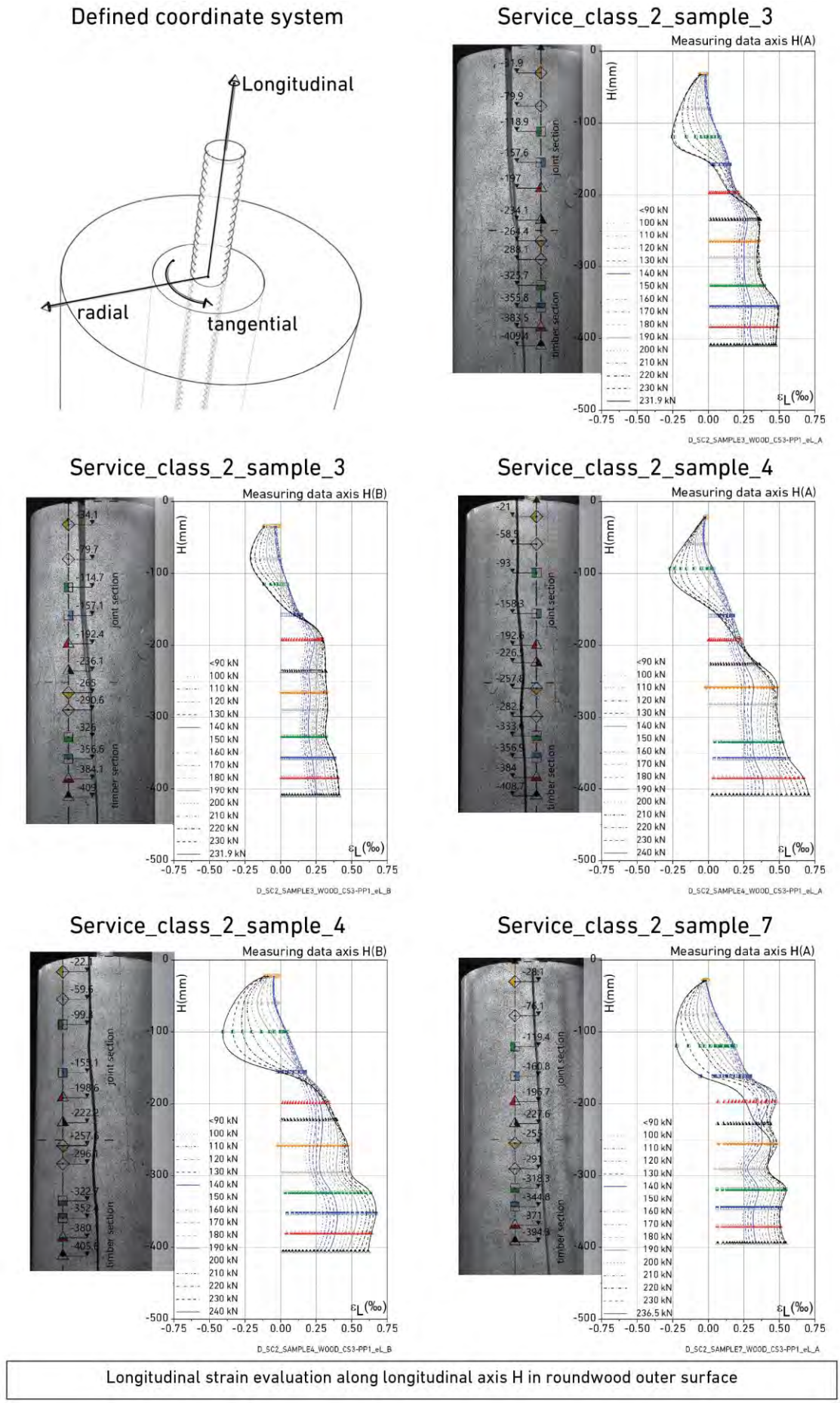

Fig. A-28 Evaluation roundwood outer surface service class 2

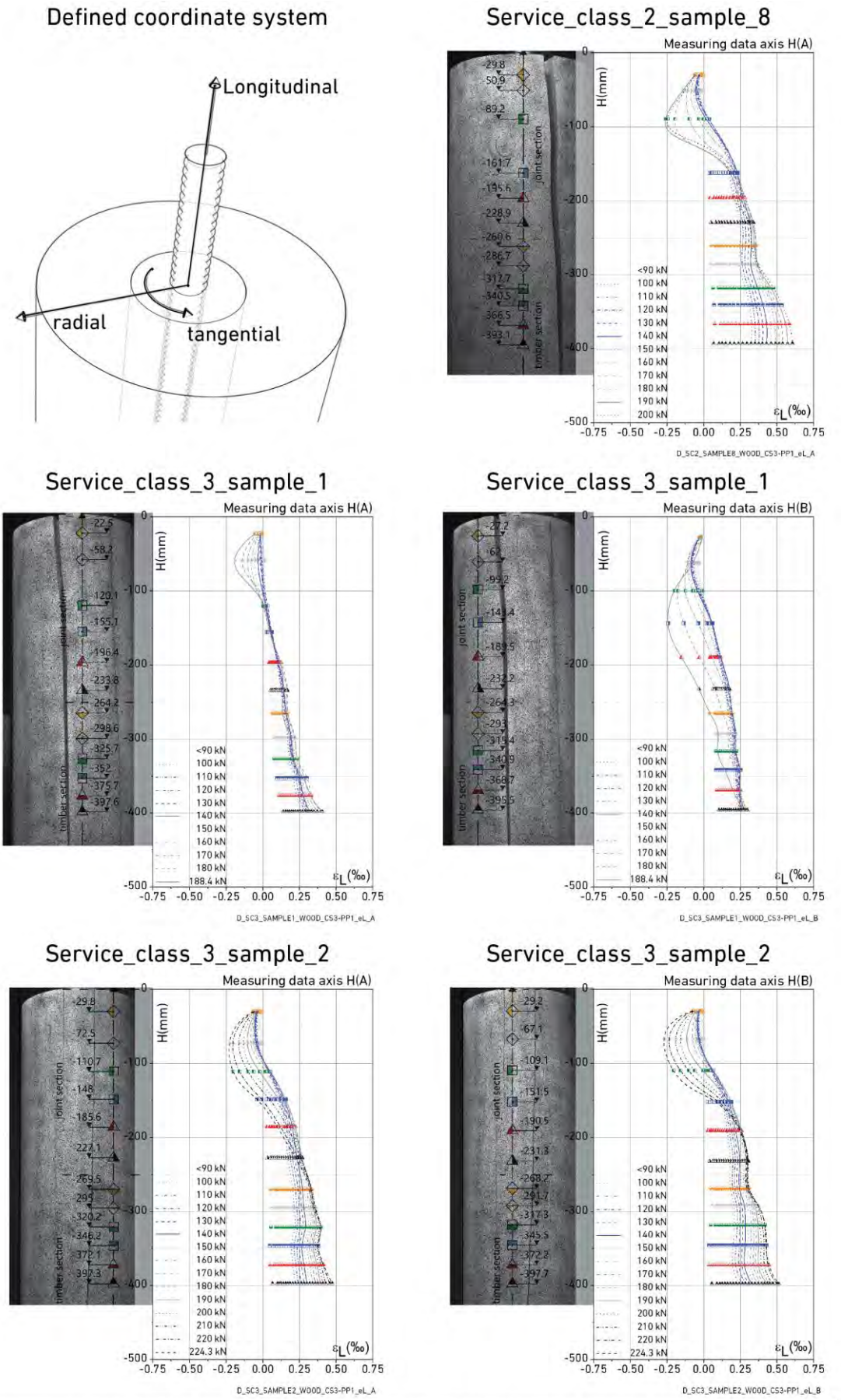

Longitudinal strain evaluation along longitudinal axis H in roundwood outer surface

Fig. A-29 Evaluation roundwood outer surface service class 2 and 3

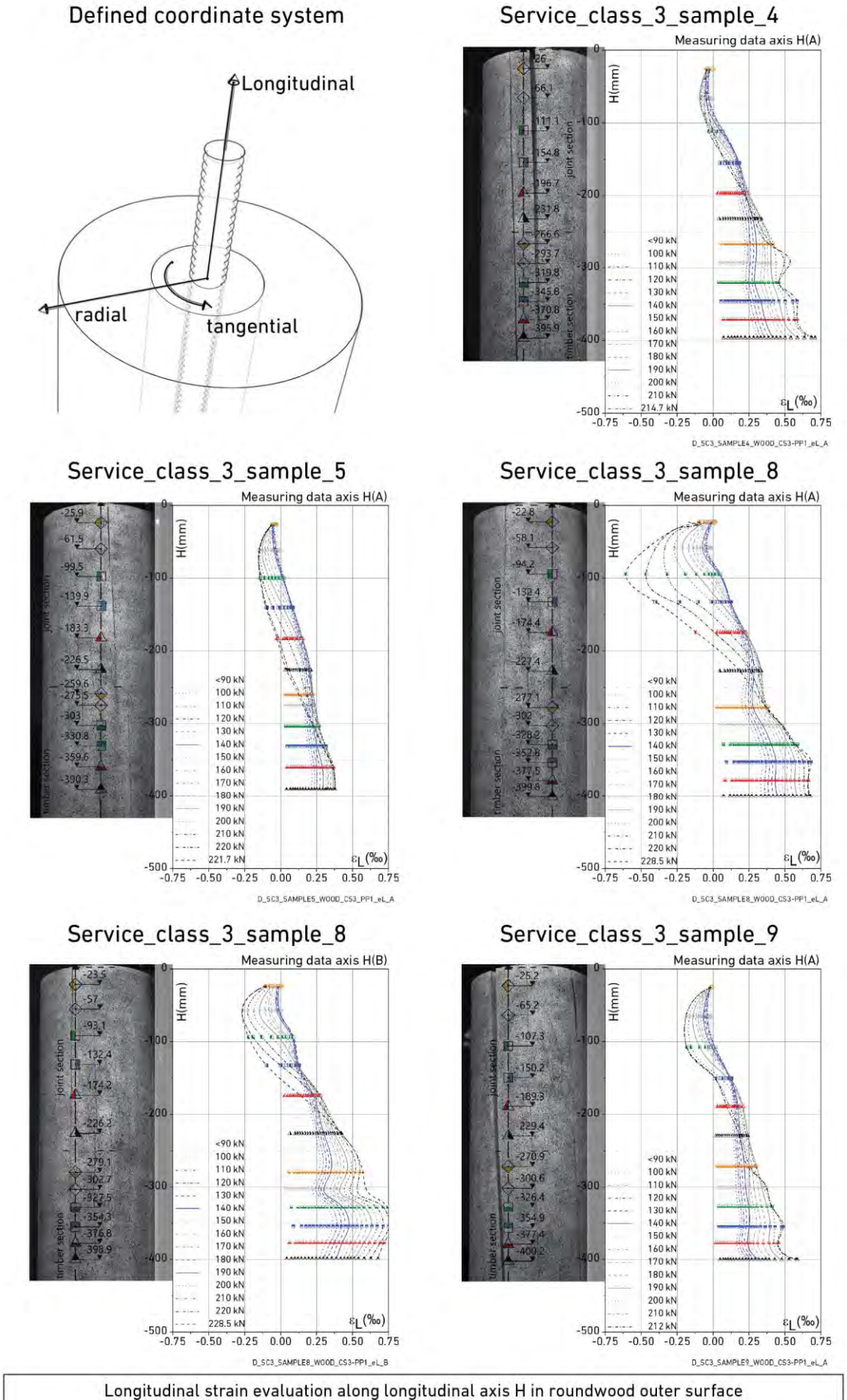

Longitudinal strain evaluation along longitudinal axis H in roundwood outer surface

Fig. A-30 Evaluation roundwood outer surface service class 3

A.1.4 Relative displacement in bond line region

Fig. A31-32 show the relative displacement in the bonded region covered by camera systems 1 and 2 of the DIC system. This relative displacement describes the slip in the contact surface between steel rod and PC, and PC and wood. Furthermore, the central load introduction of the applied tensile forces into the roundwood specimens led to a warping deformation of the timber end grain. The determined relative displacement in experimental tests covered all this effects and was further processed to calculate the slip modulus of the connection (see also section 4.2.8).

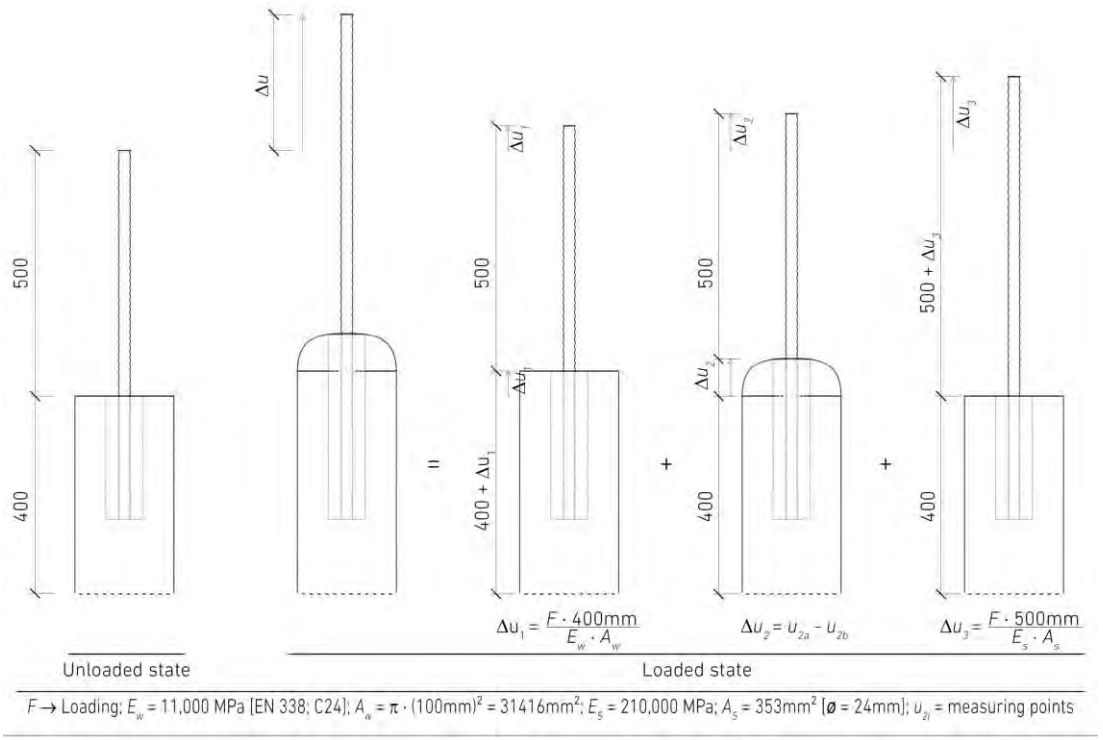

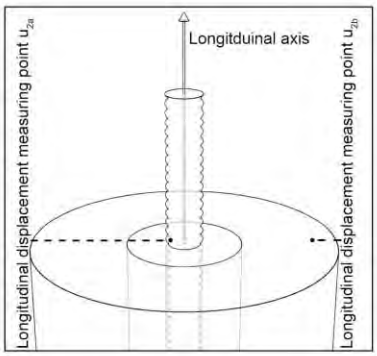

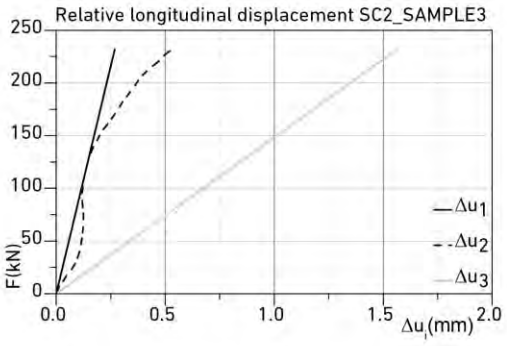

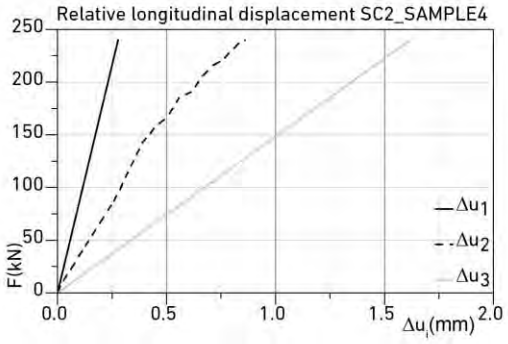

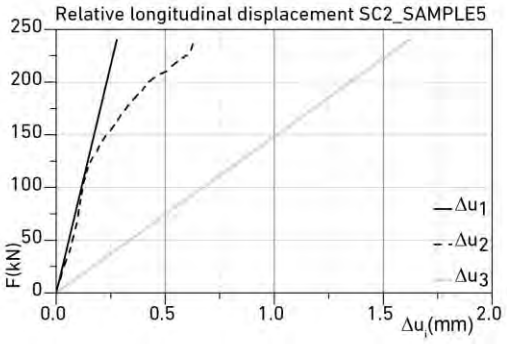

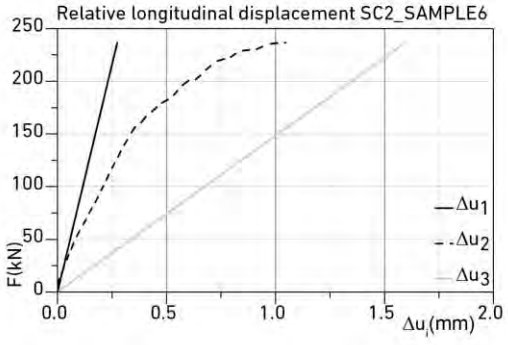

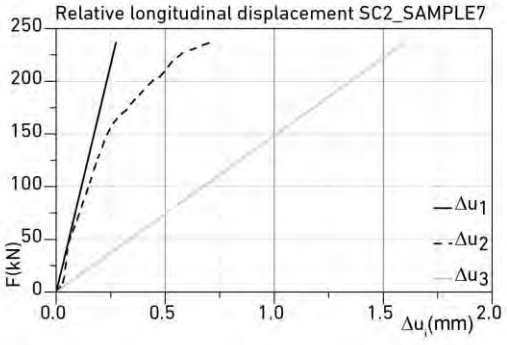

Fig. A-31 Slip deformation (relative displacement) for service class 2 specimens

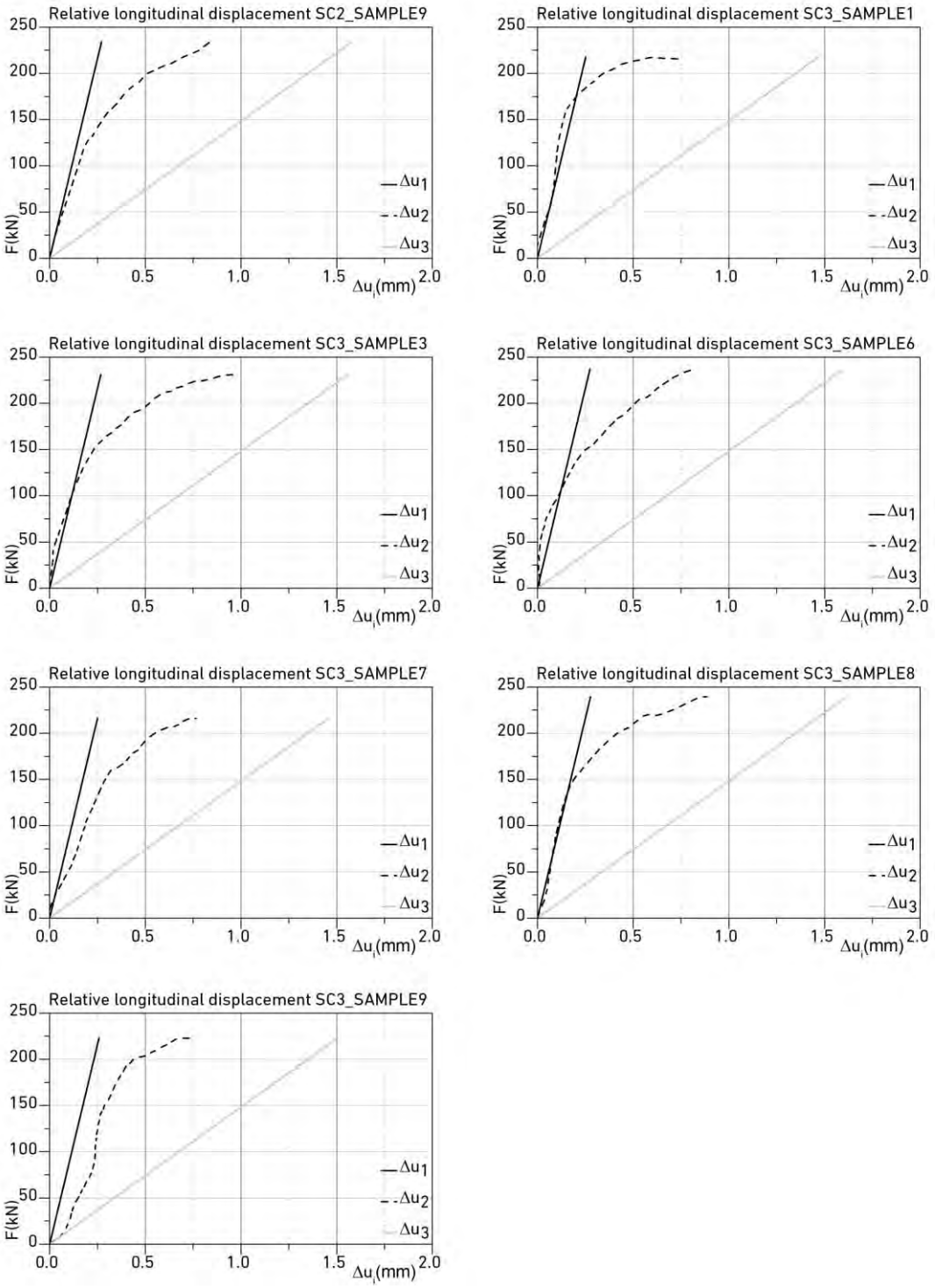

Fig. A-32 Slip deformation (relative displacement) for service class 2 and 3 specimens

A.2 MOULDED JOINING TECHNOLOGY IN 2D TRUSSES

A.2.1 Architectural and structural truss design

This section summarises the architectural and structural design of the 25 modular truss variations in roundwood, developed and design for the moulded joining technologies presented in section A.2.2.

The first illustration covers the truss typology of the trusses.

The inner normal forces in roundwood and applied line load in ULS on the upper chord for each case is presented in the second illustration.

The last figure serves with information on the stress utilisation for the ULS design of each roundwood strut member according to EN 1995-1-1.

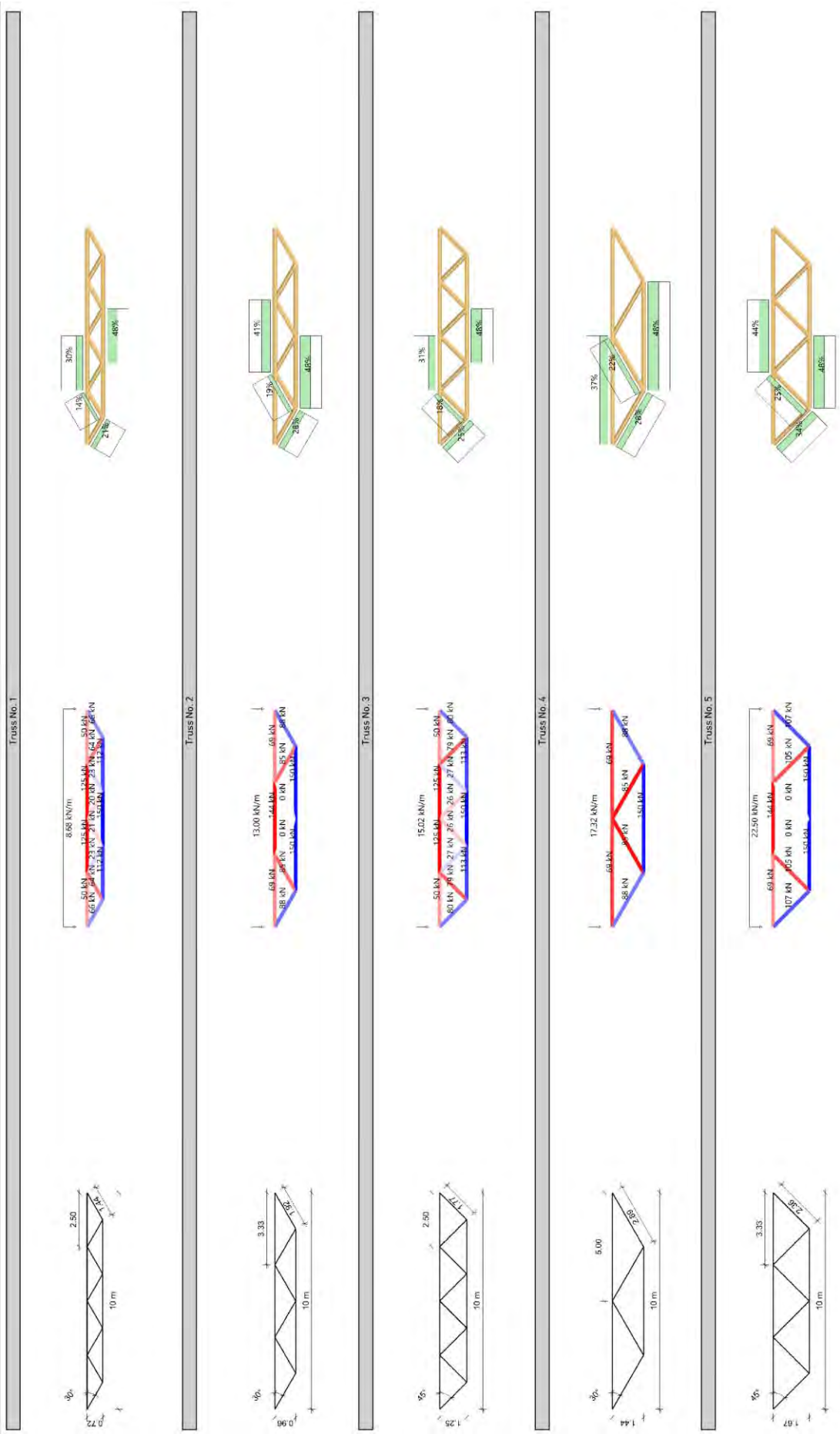

Fig. A-33 Truss types 1 - 5 (typologies, inner normal forces and stress utilisation)

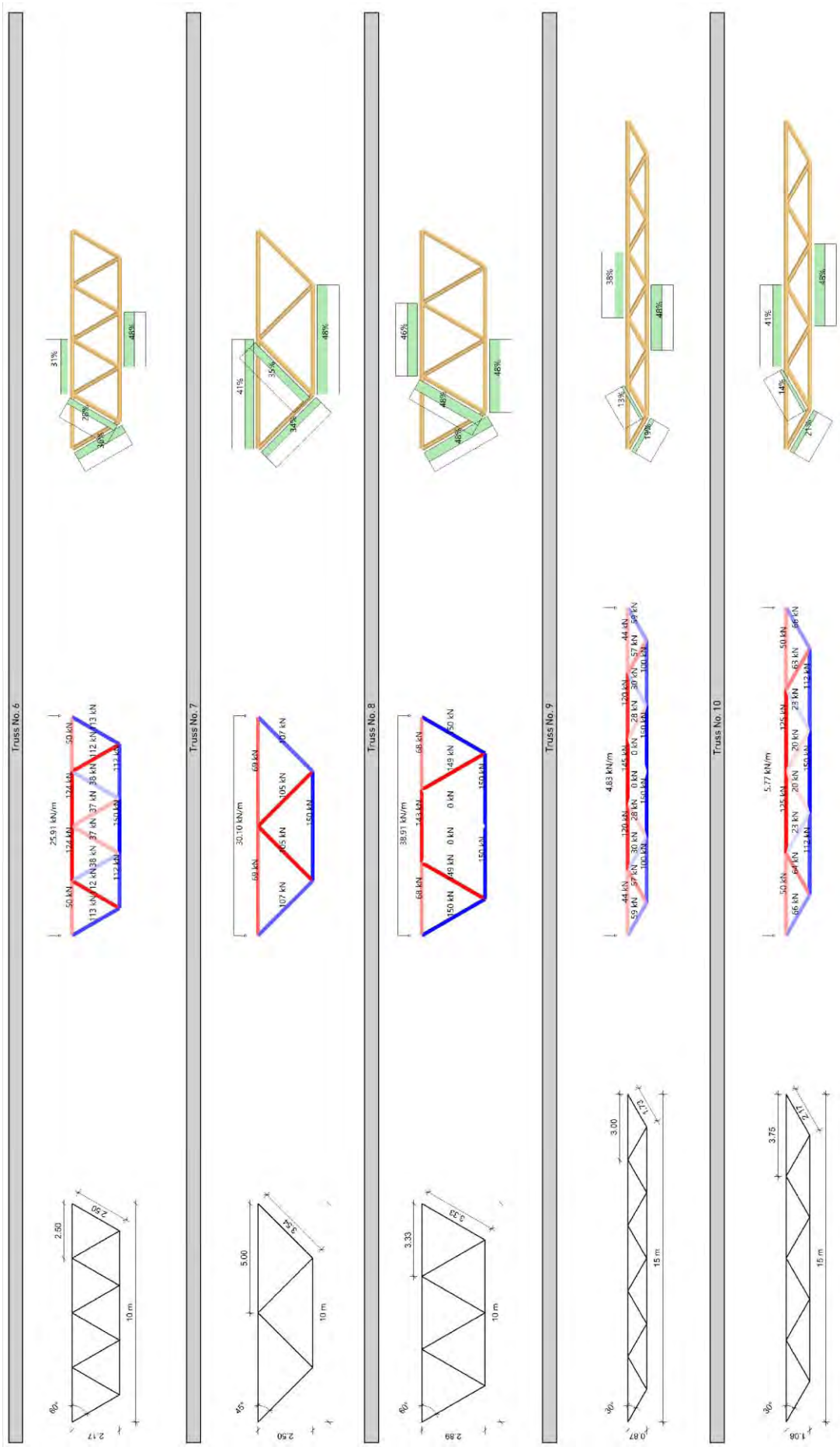

Fig. A-34 Truss types 6 - 10 (typologies, inner normal forces and stress utilisation)

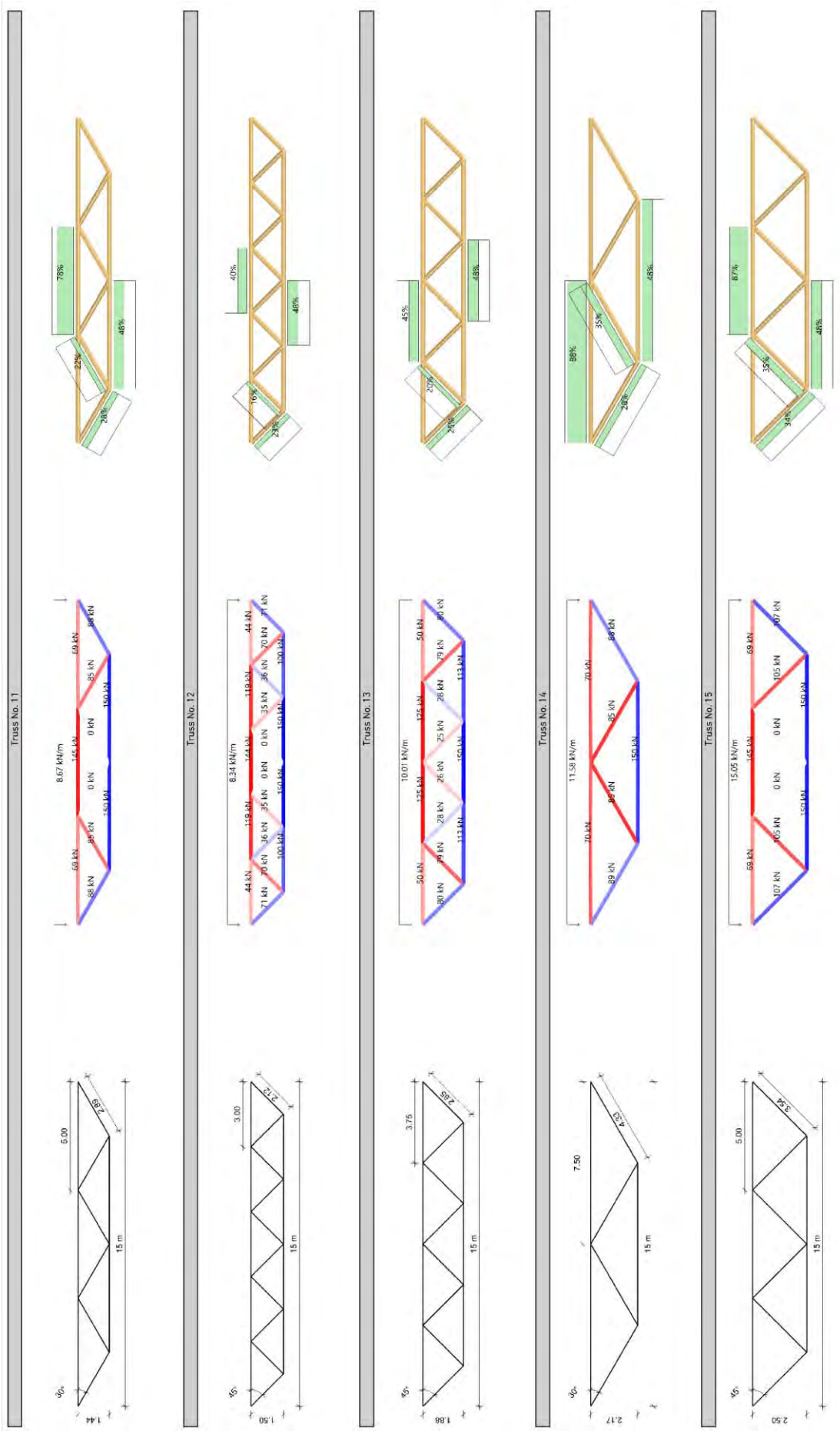

Fig. A-35 Truss types 11 - 15 (typologies, inner normal forces and stress utilisation)

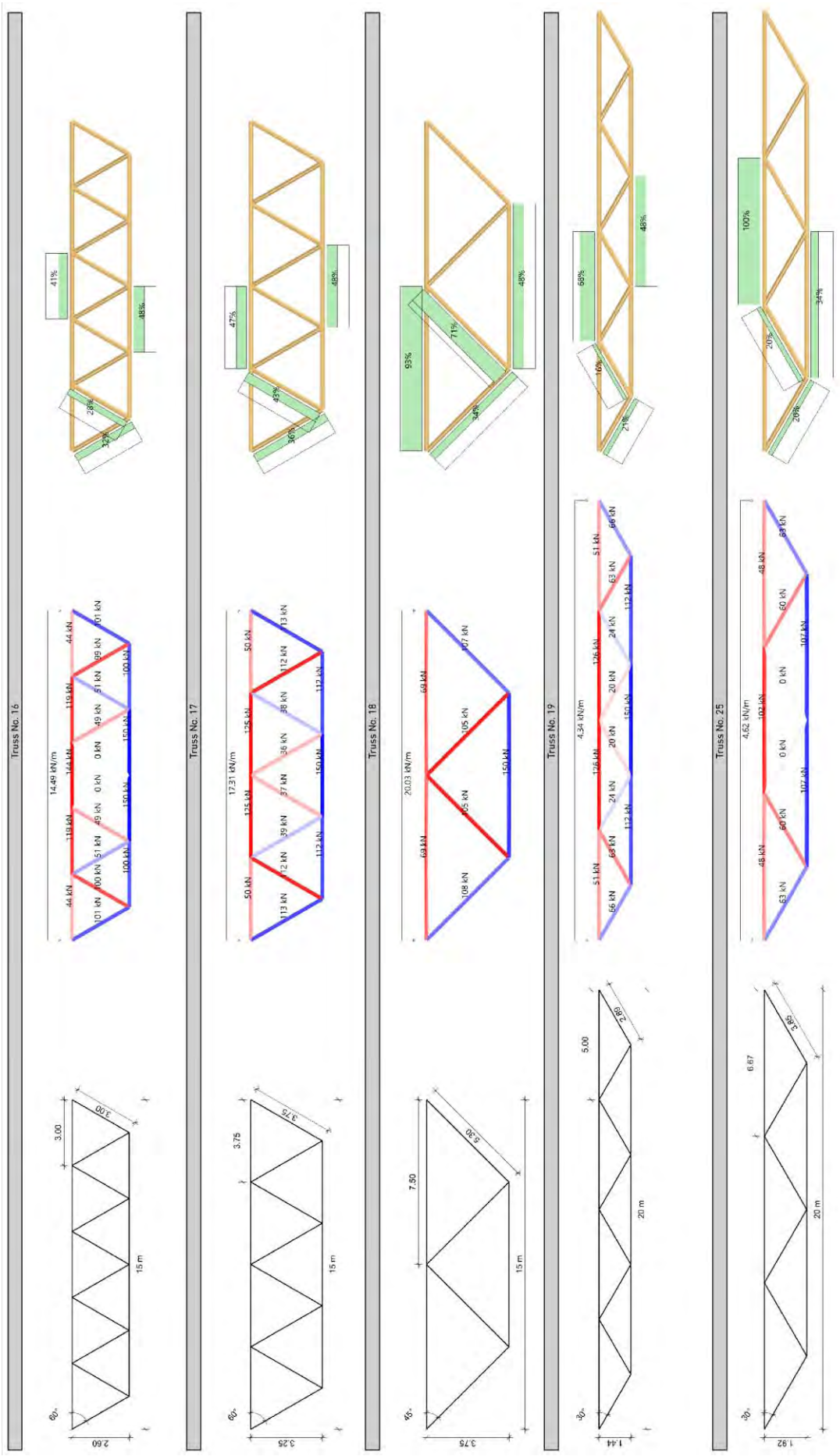

Fig. A-36 Truss types 16 - 20 (typologies, inner normal forces and stress utilisation)

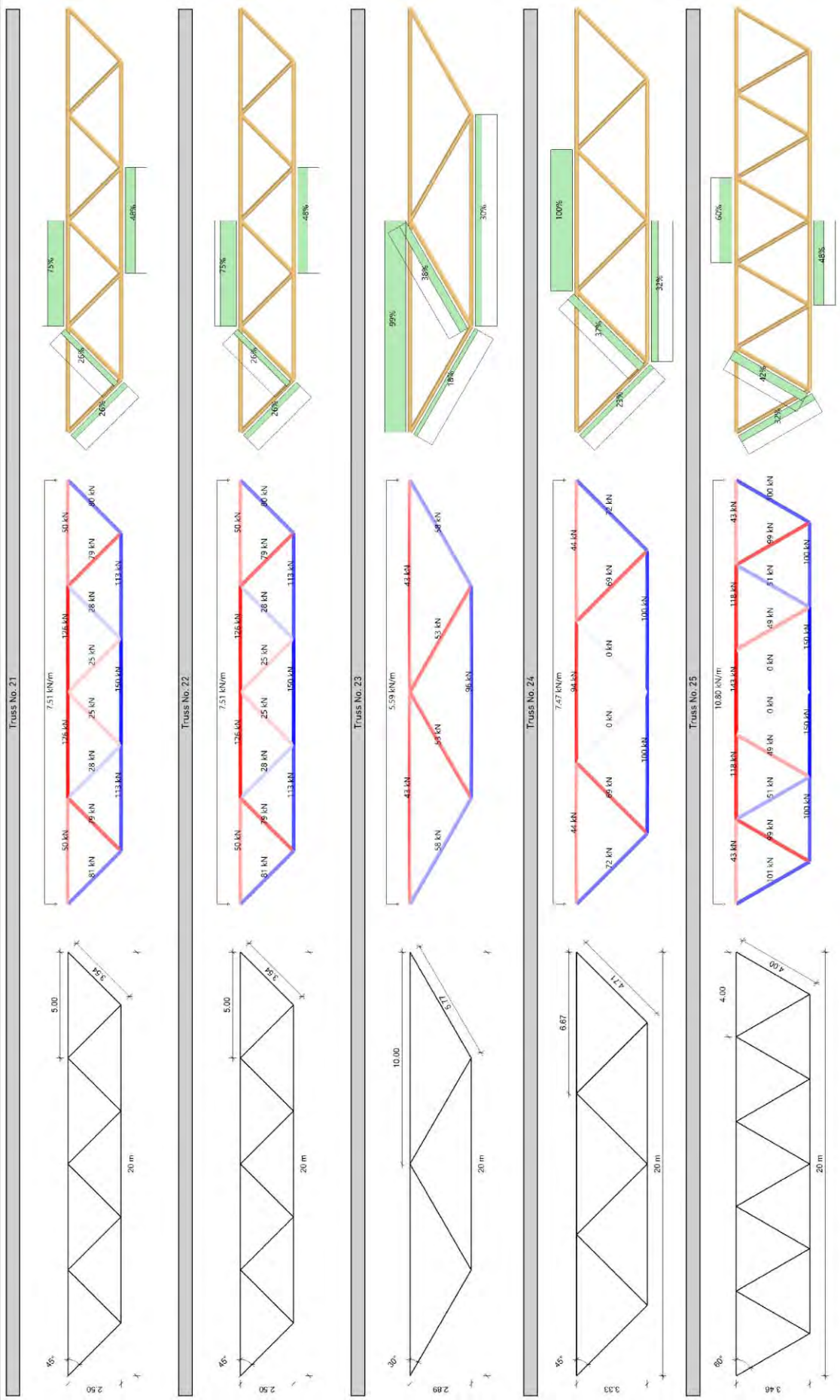

Fig. A-37 Truss types 21 - 25 (typologies, inner normal forces and stress utilisation)

A.2.2 Joint design

The developed moulded joining technologies are presented in this section, covering the field, edge and support joint for chord-diagonal strut angles of 30°, 45° and 60°. The illustrations serve with information on the dimensions, assembly space and joining configuration for second structural components, such as purlins.

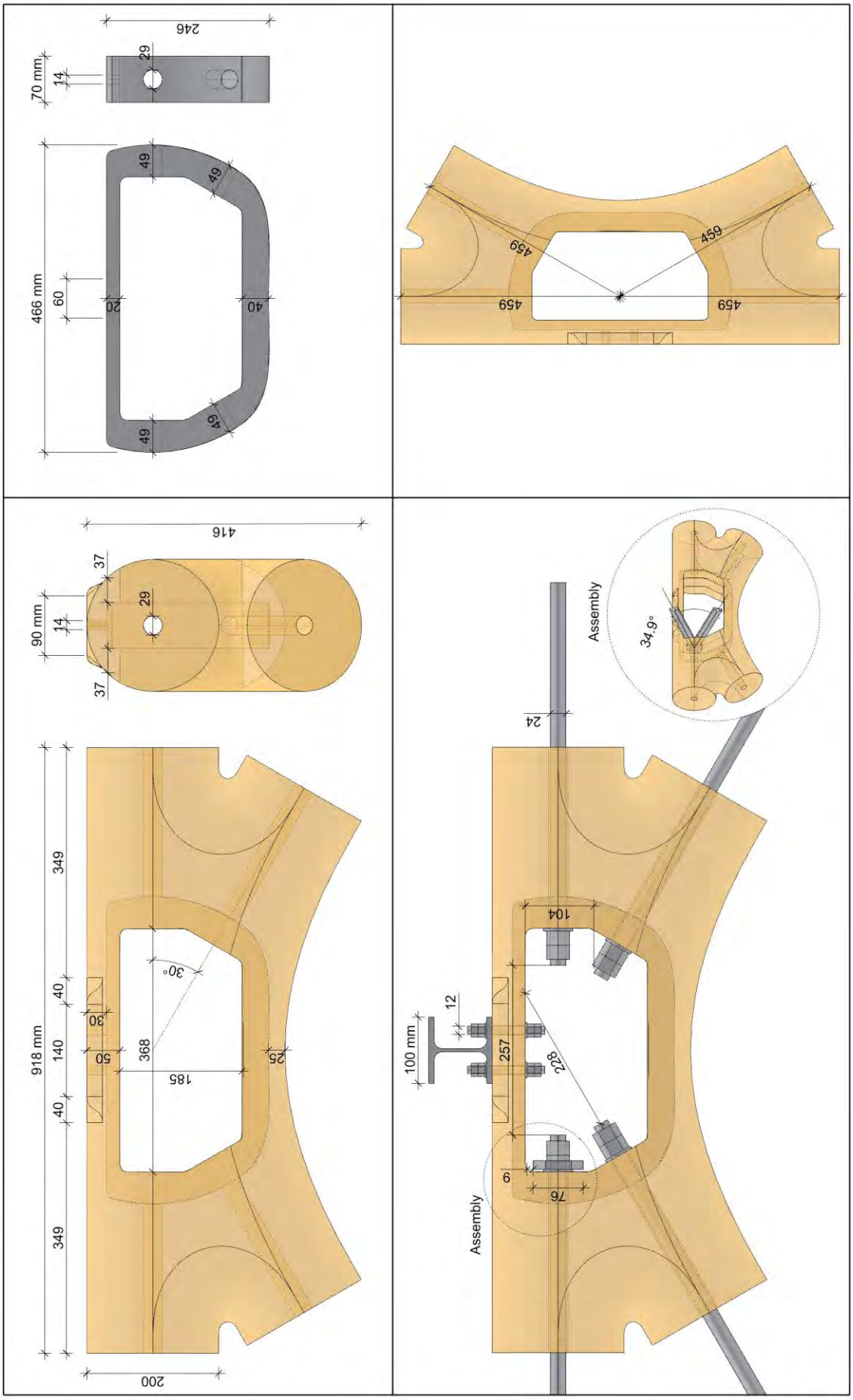

Fig. A-38 Field joint 30°

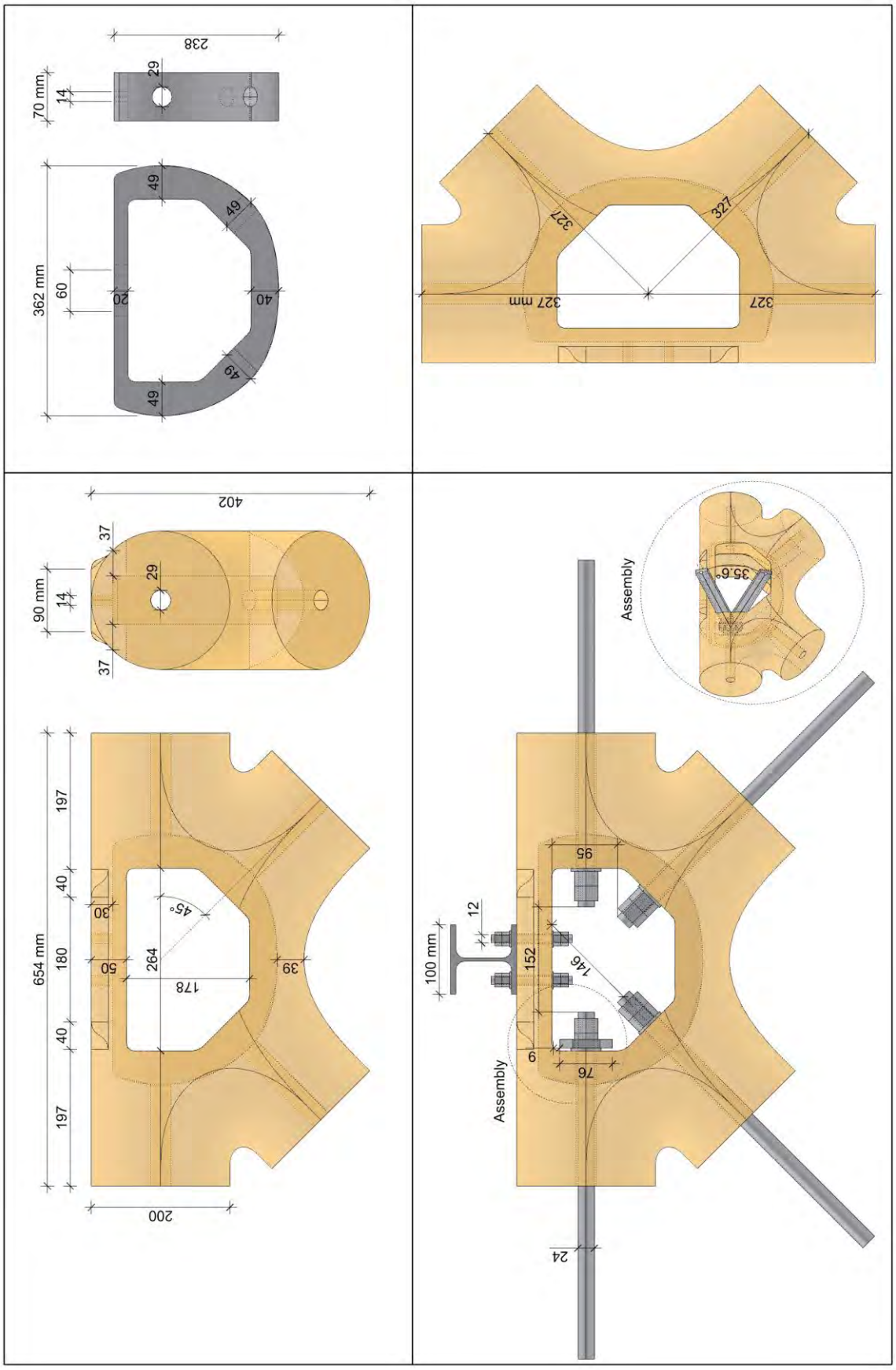

Fig. A-39 Field joint 45°

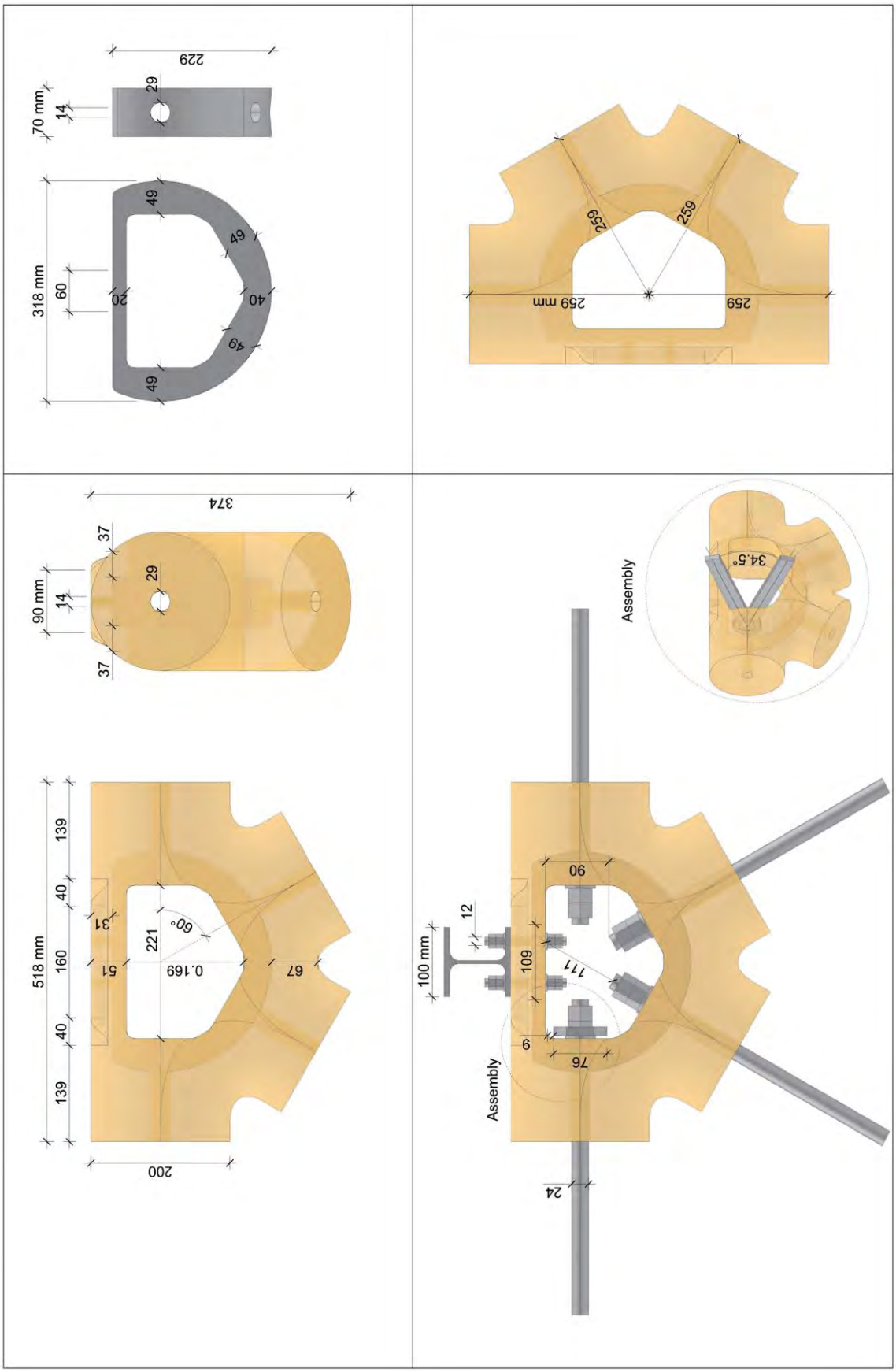

Fig. A-40 Field joint 60°

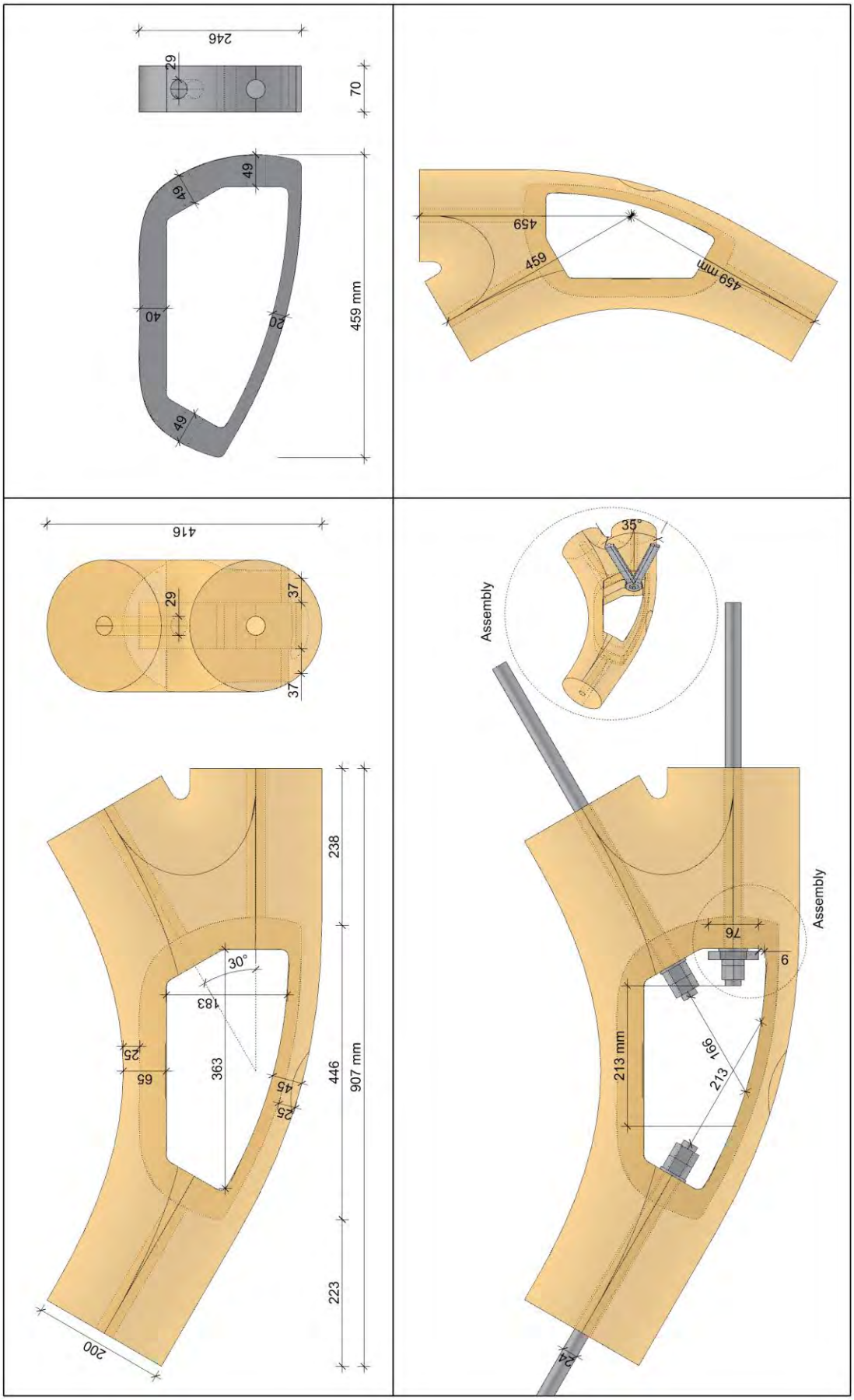

Fig. A-41 Edge joint 30°

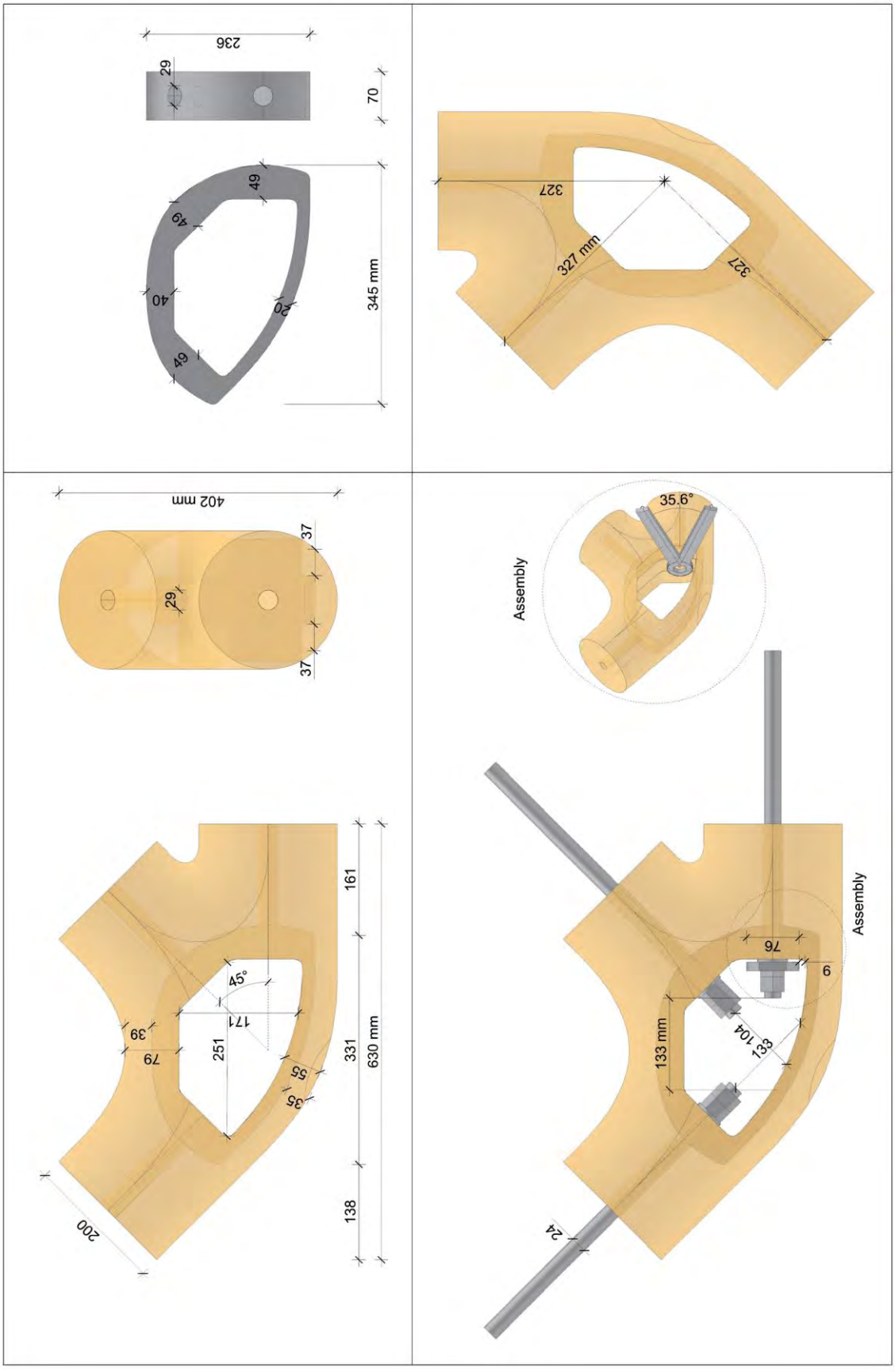

Fig. A-42 Edge joint 45°

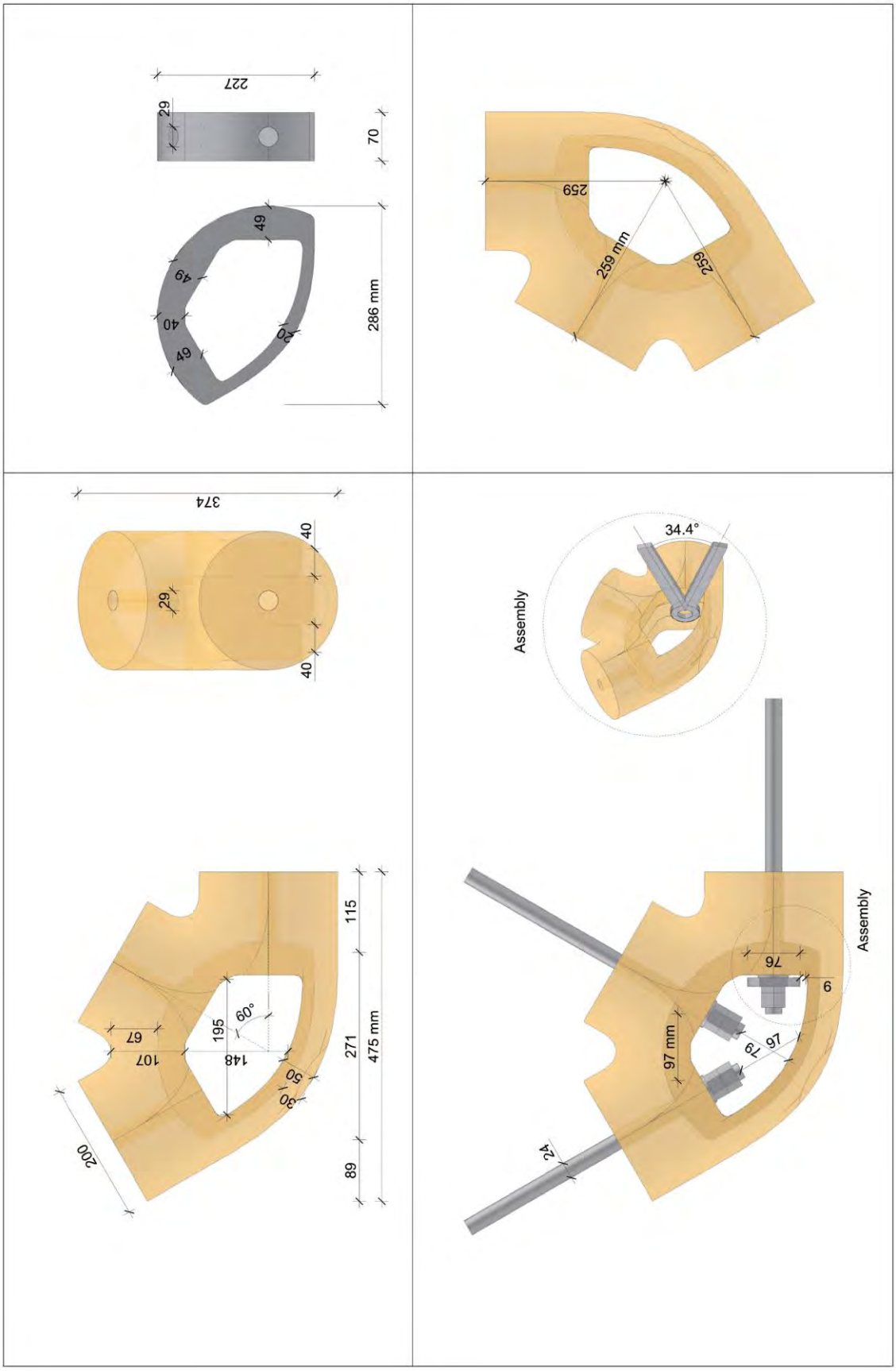

Fig. A-43 Edge joint 60°

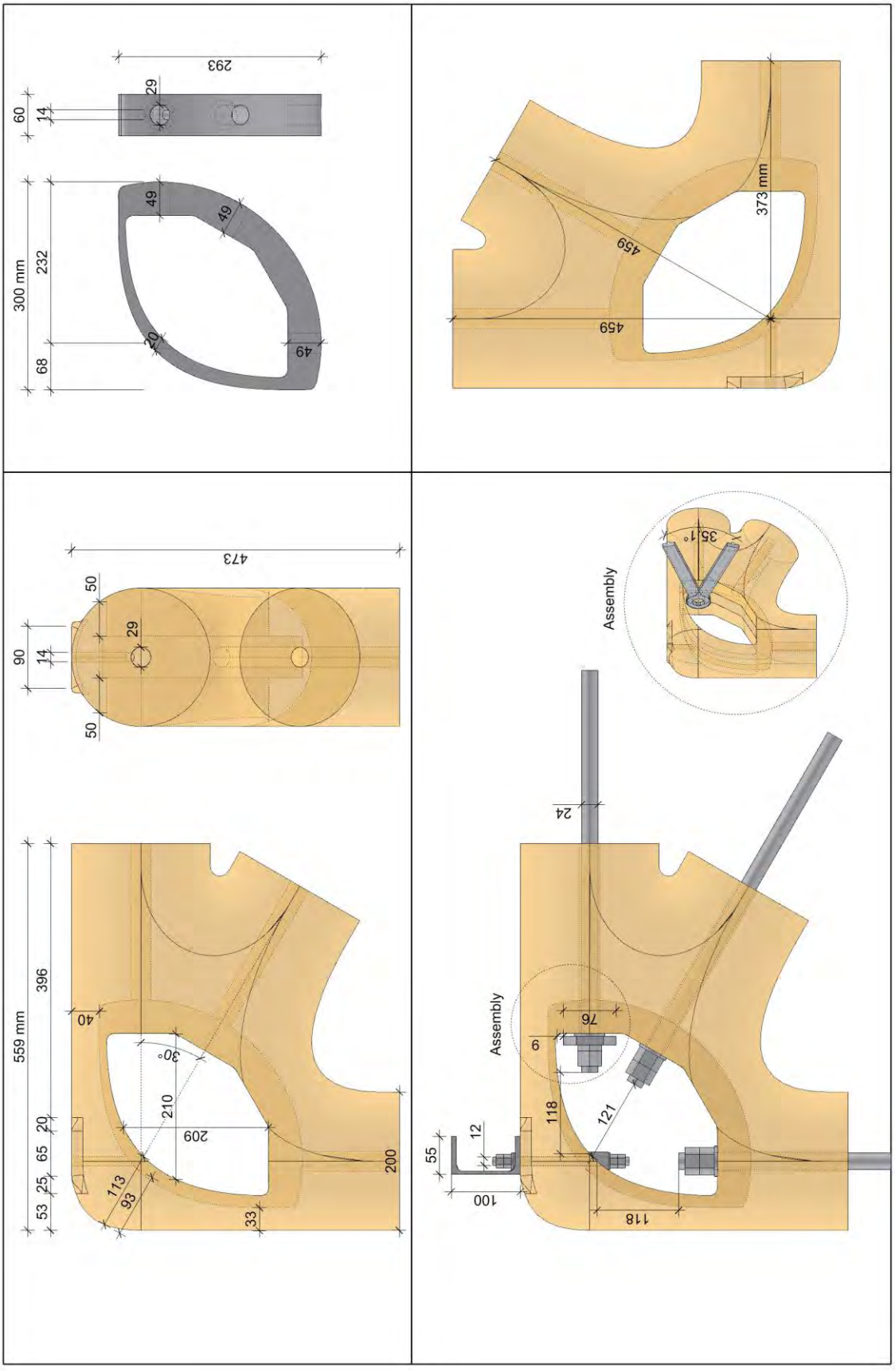

Fig. A-44 Support joint 30°

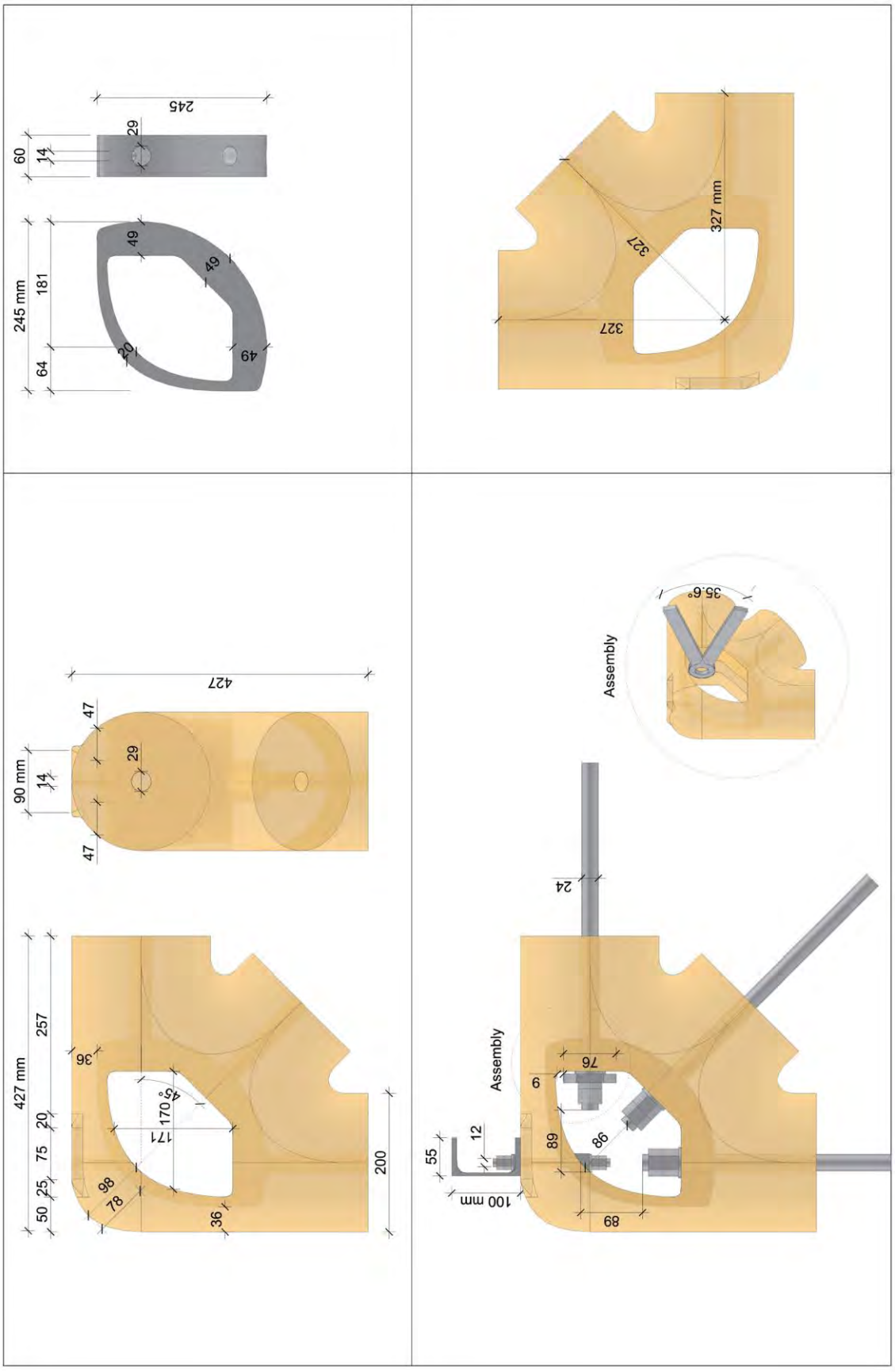

Fig. A-45 Support joint 45°

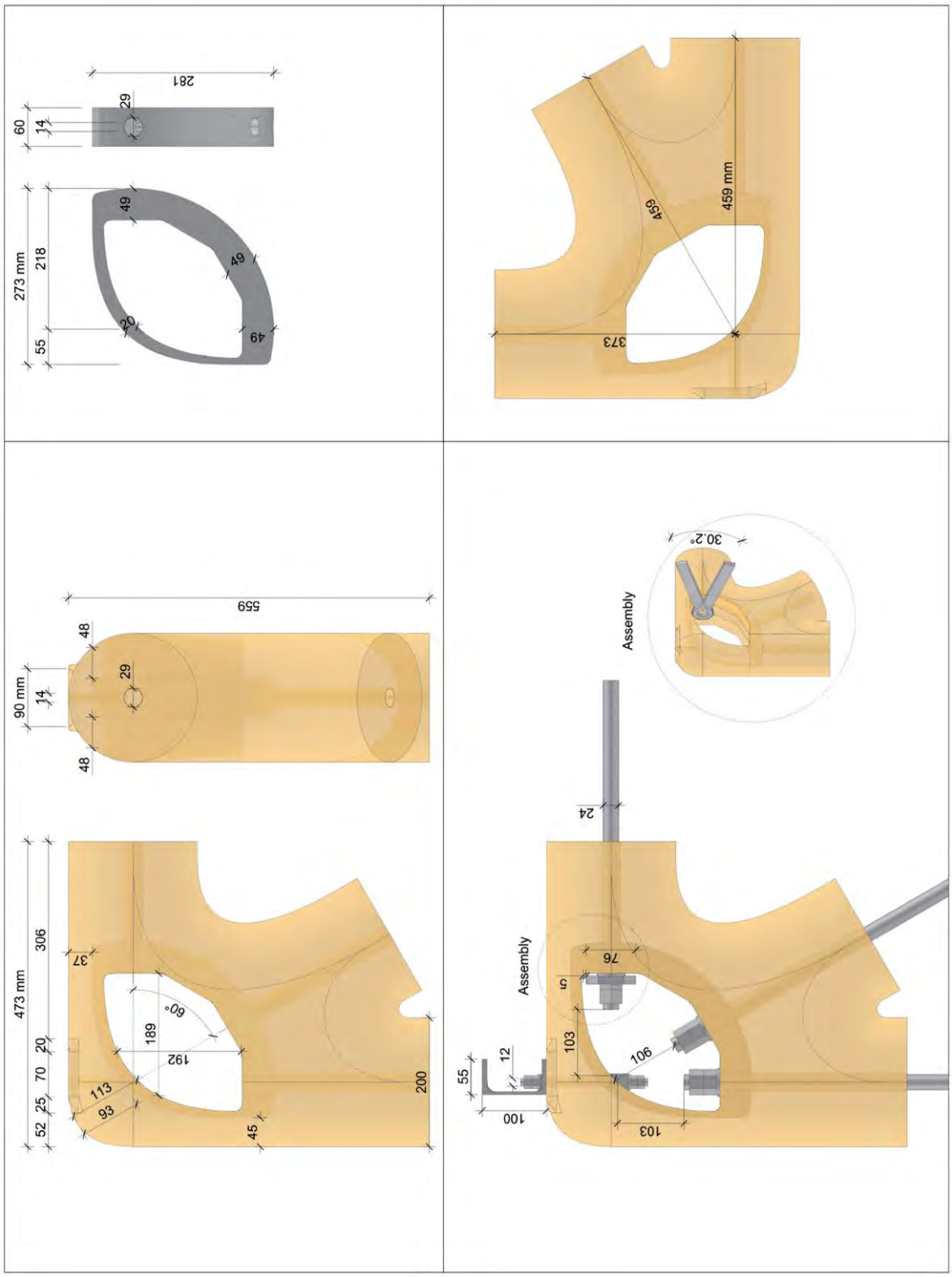

Fig. A-46 Support joint 60°

A.2.3 Modular 2D trusses

This section summarises the 25 modular truss variations in roundwood, developed and design for the moulded joining technologies presented in section A.2.2.

The first illustration covers the front view of the 3D models with information on the roundwood axis lengths with and without modified bonded-in rods.

The second illustration shows the final visualisation of the truss variations.

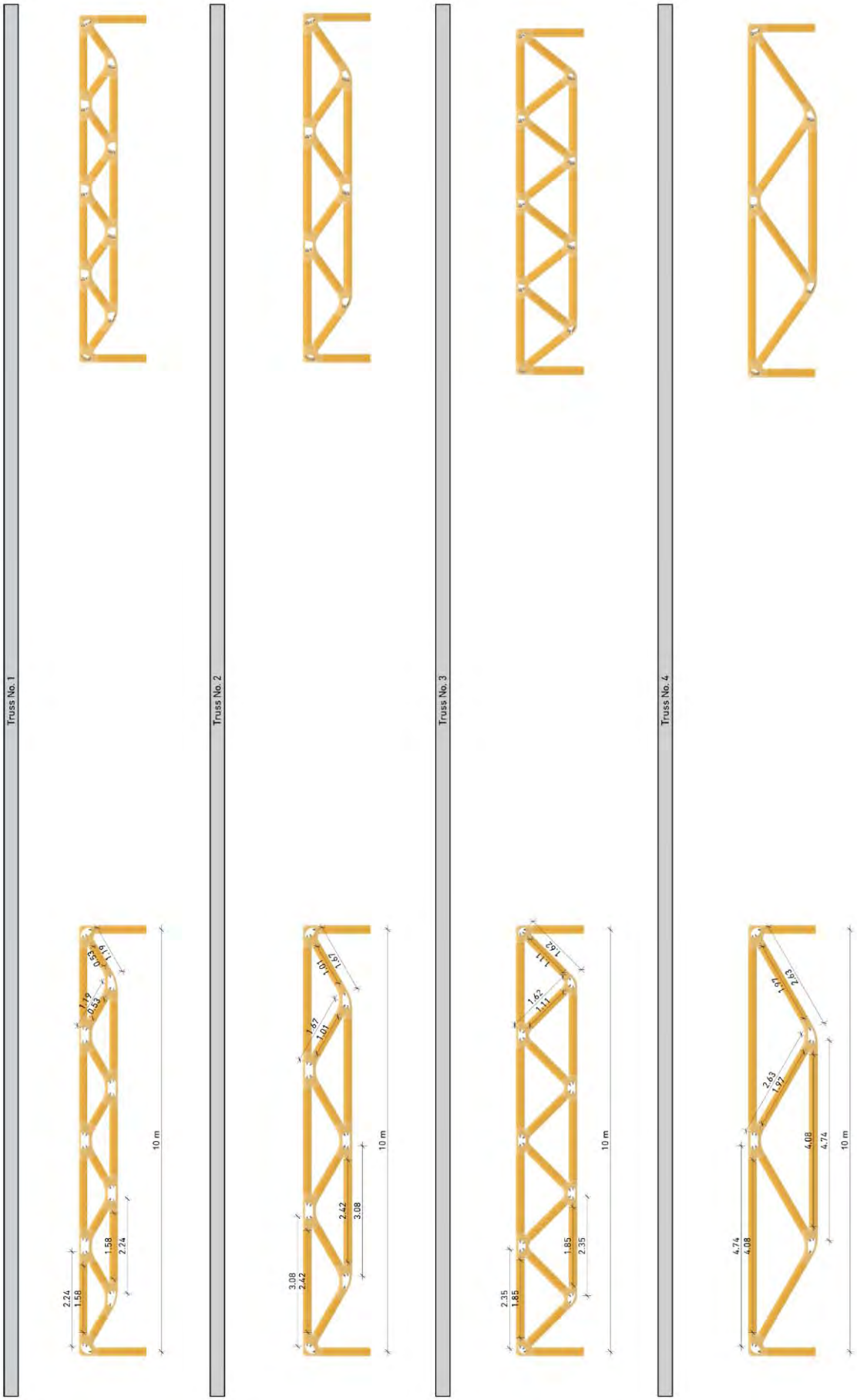

Fig. A-47 Truss types 1 - 4 (strut member lengths and perspective)

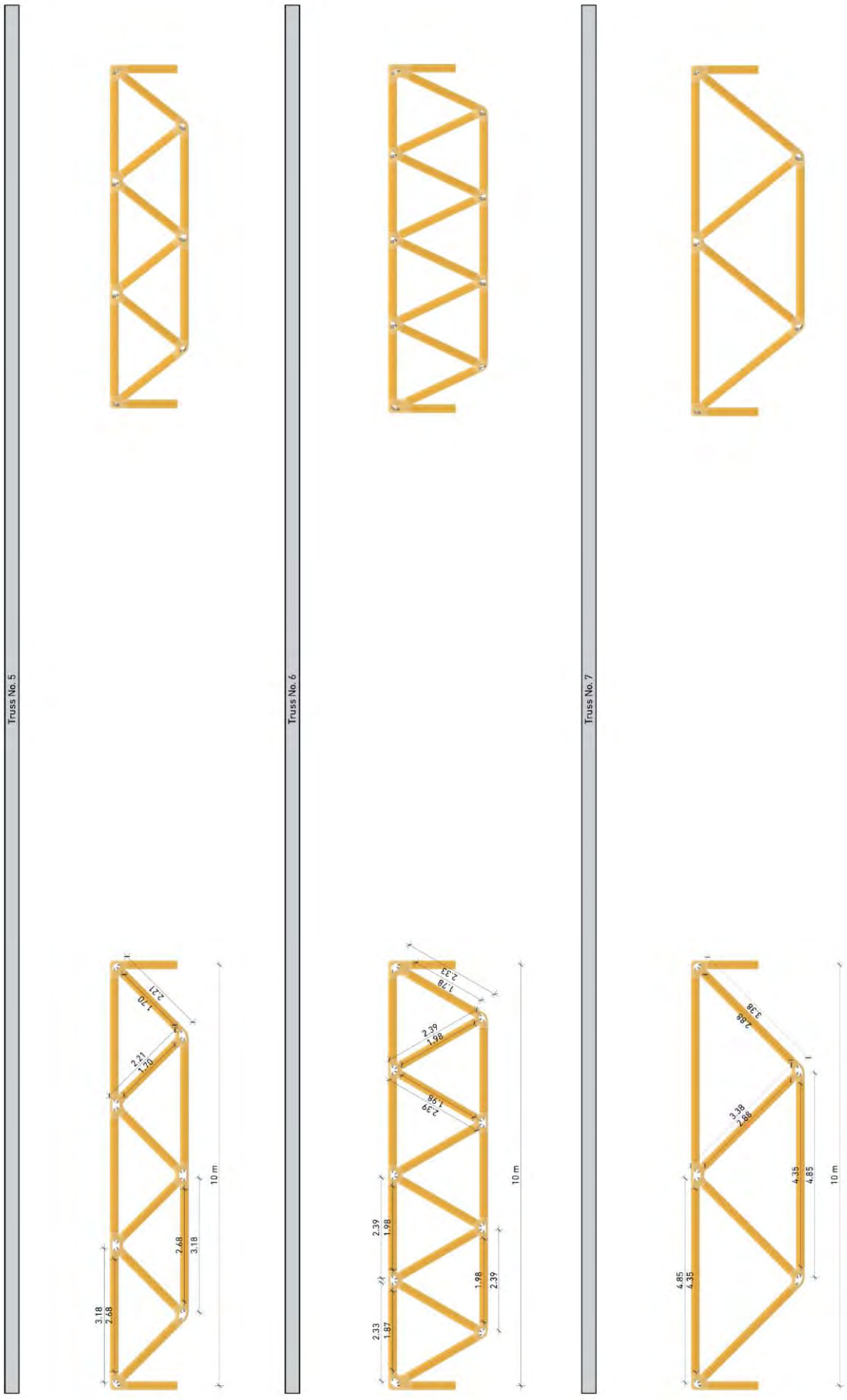

Fig. A-48 Truss types 5 - 7 (strut member lengths and perspective)

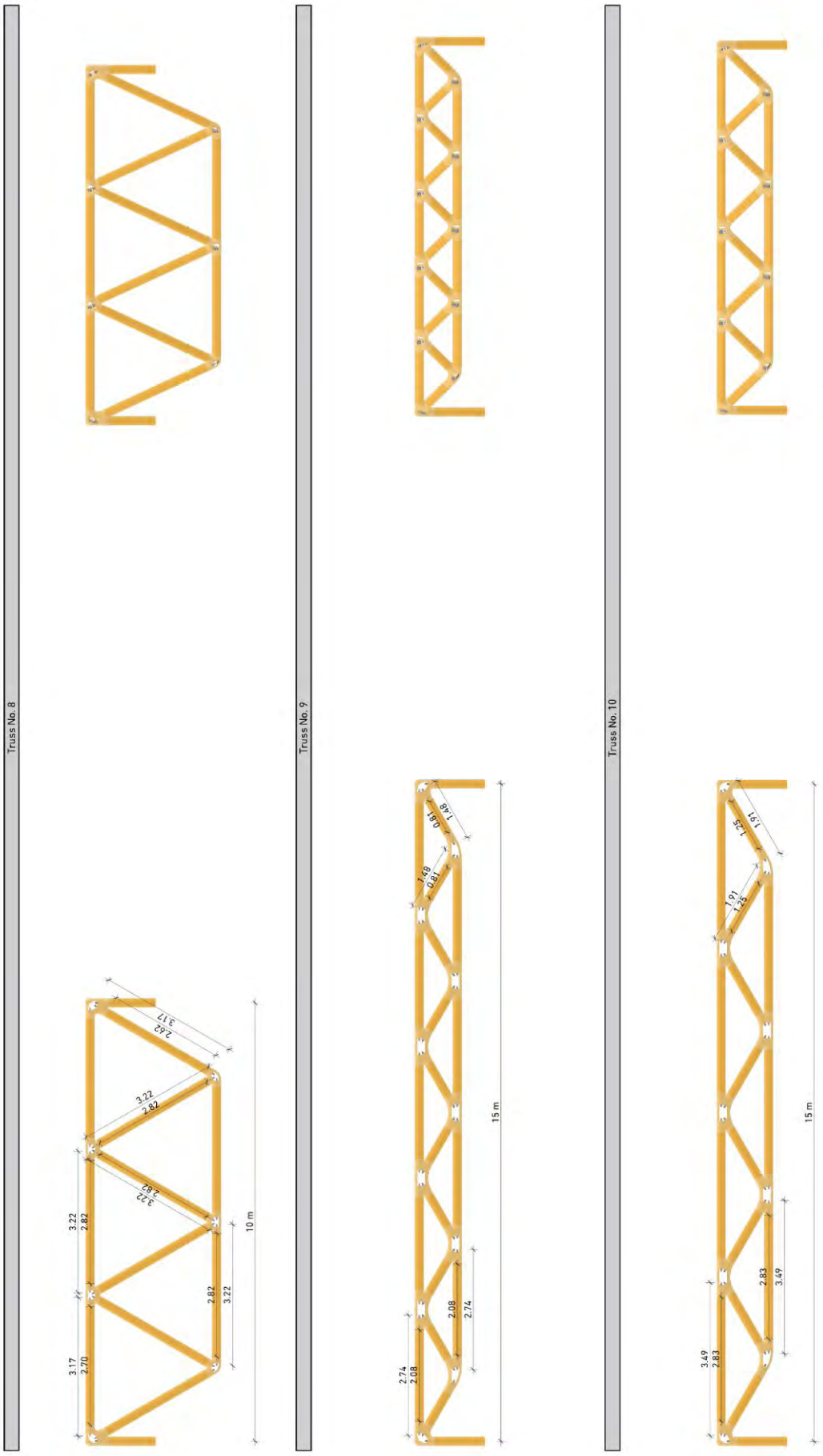

Fig. A-49 Truss types 8 - 10 (strut member lengths and perspective)

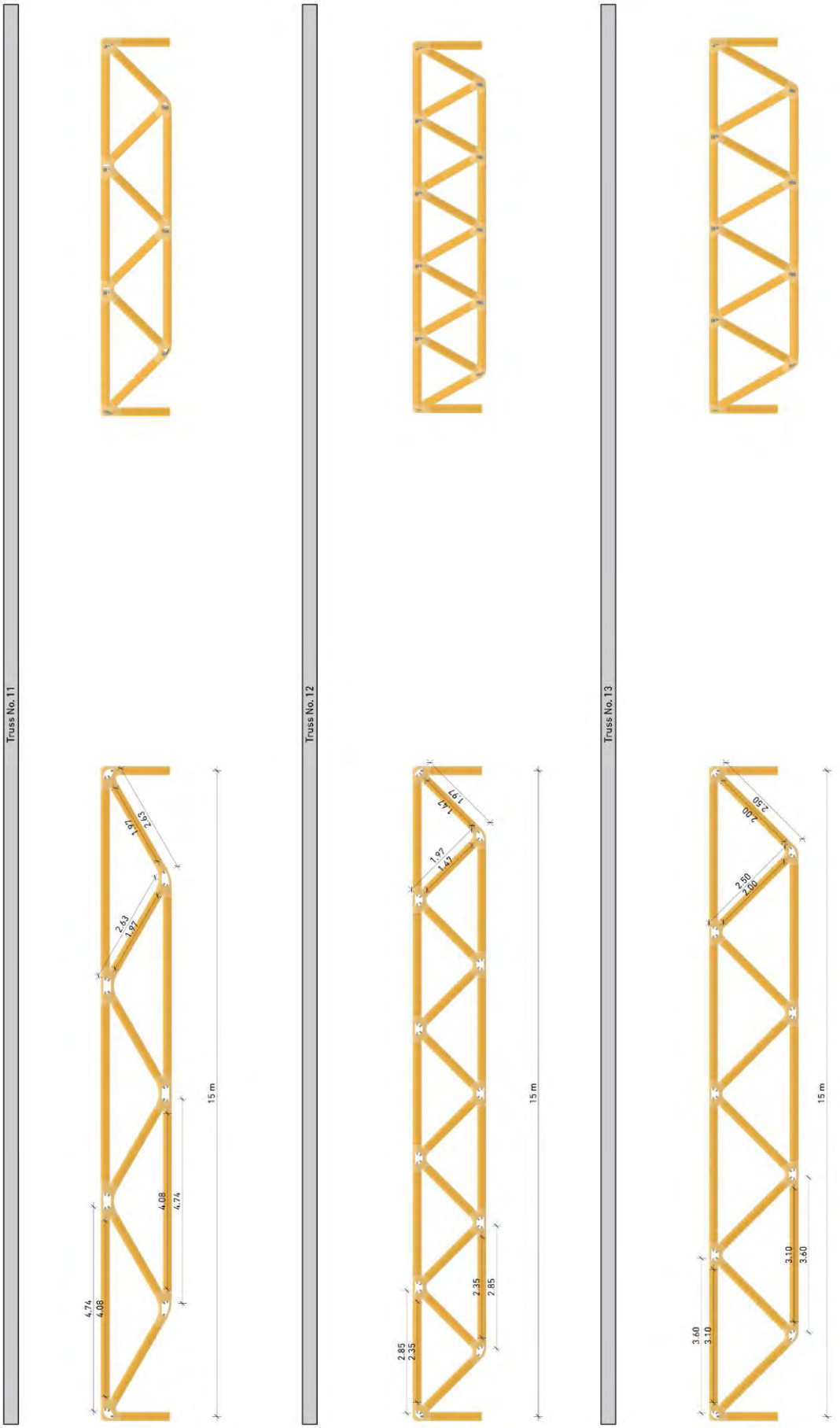

Fig. A-50 Truss types 11 - 13 (strut member lengths and perspective)

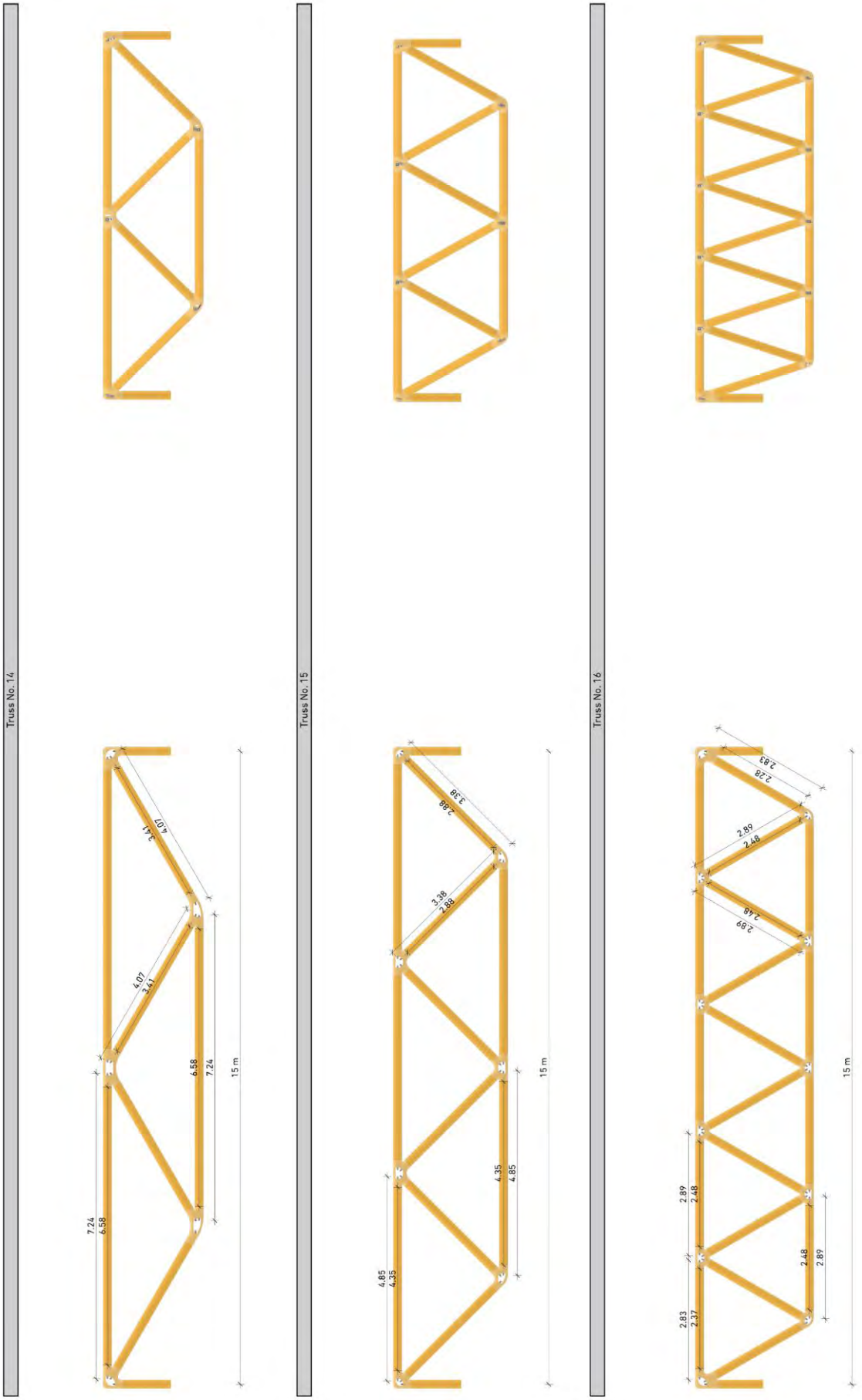

Fig. A-51 Truss types 14 - 16 (strut member lengths and perspective)

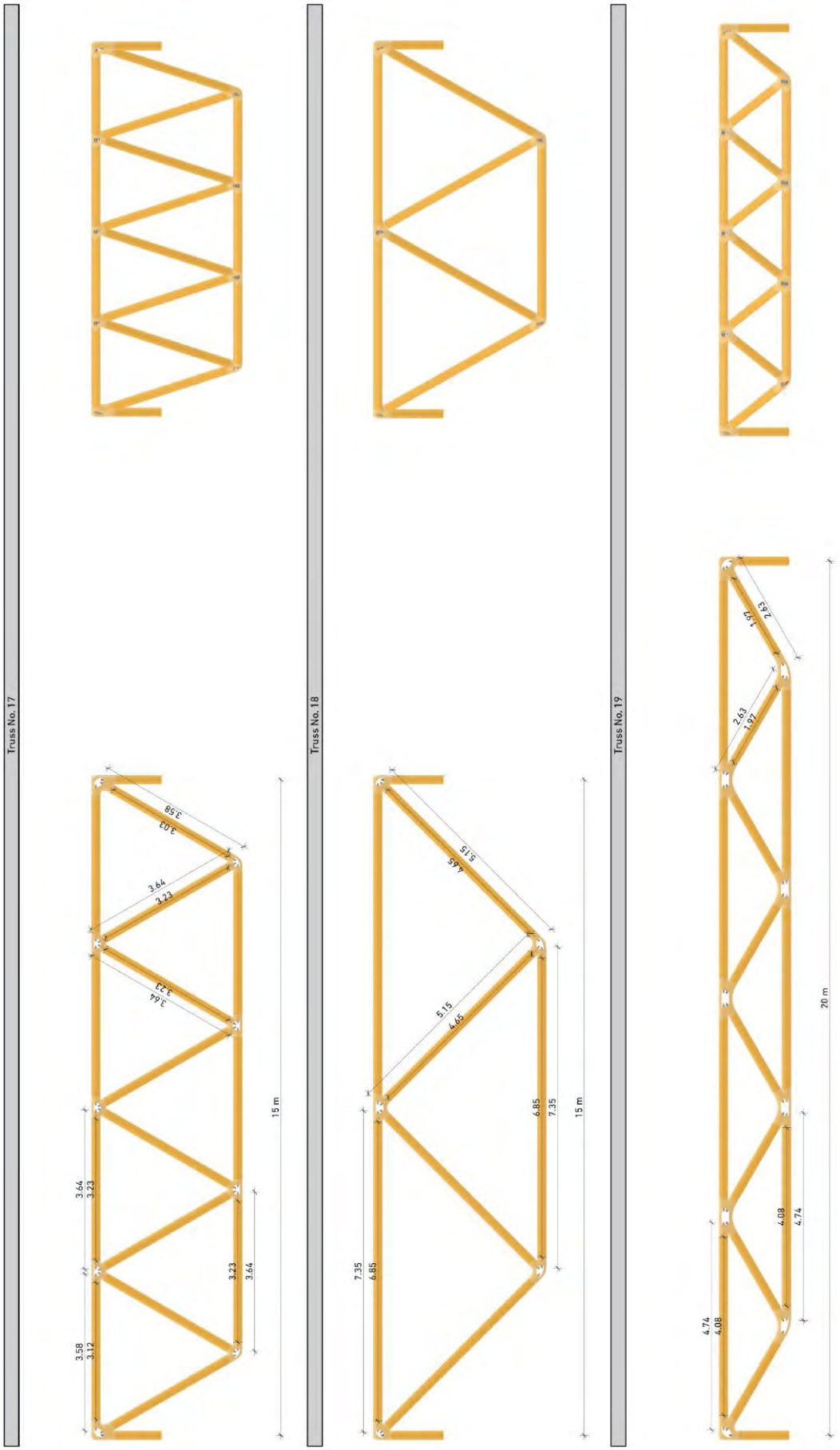

Fig. A-52 Truss types 17 - 19 (strut member lengths and perspective)

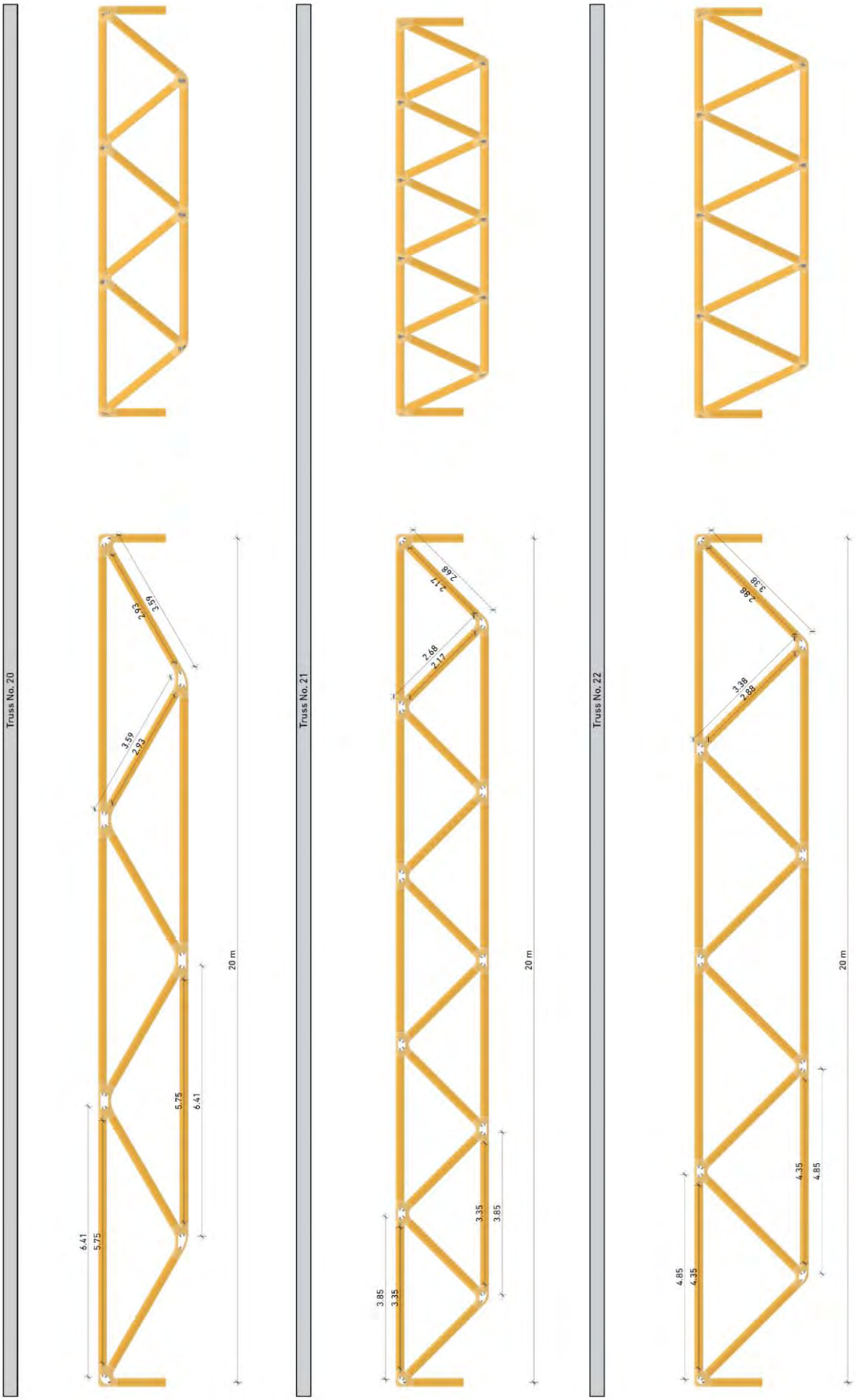

Fig. A-53 Truss types 20 - 22 (strut member lengths and perspective)

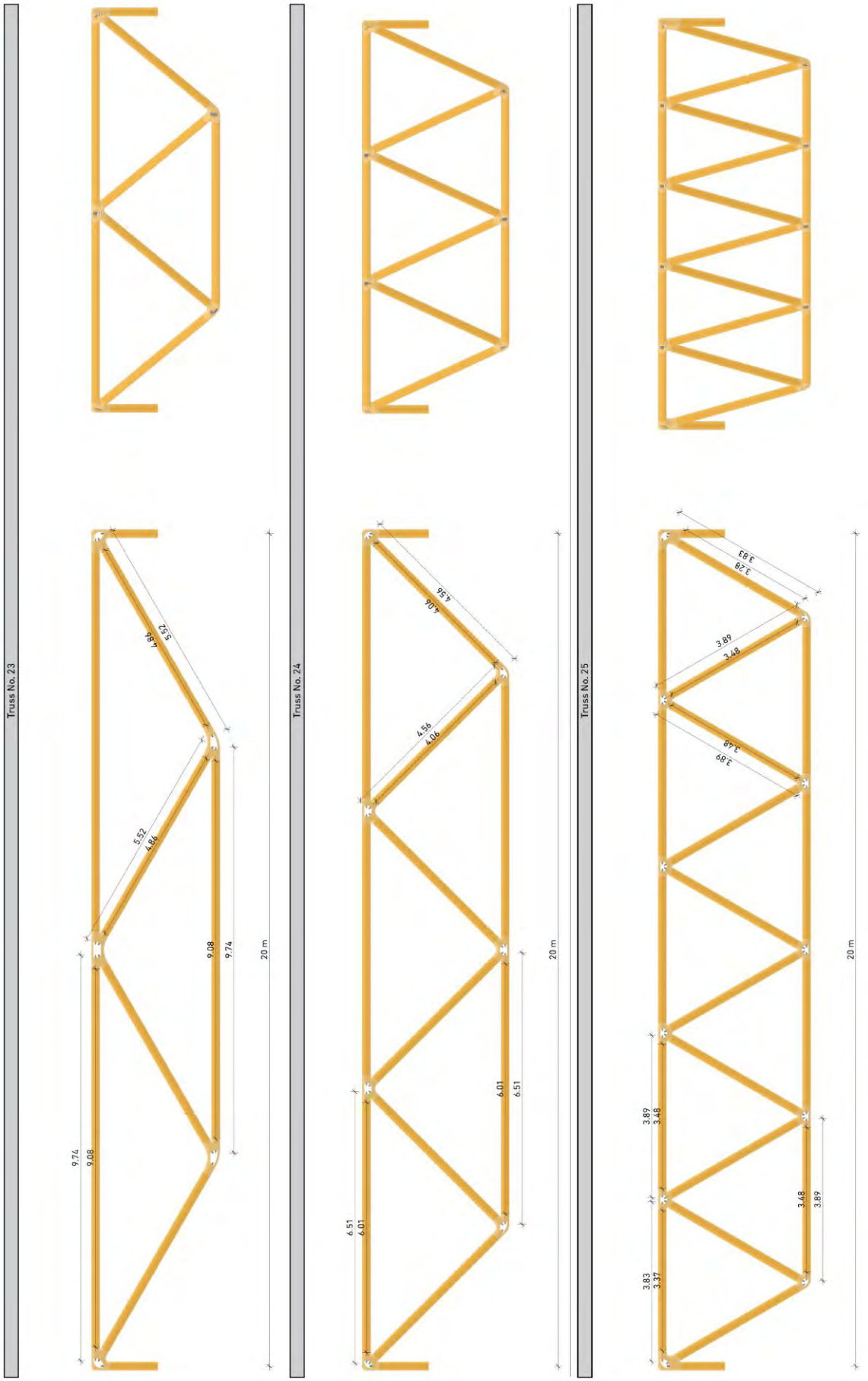

Fig. A-54 Truss types 23 - 25 (strut member lengths and perspective)

A.2.4 Joint analysis

This section summarises the results of the moulded joint Structural Analysis according to section 5.2 and provides information on each calculated sub-model. The data helped to determine the influence of the outer moulded material MoE on the structural behaviour of the joint. Based on the evaluation, suitable materials for the inner cast-steel frame structure and outer moulded joint were chosen and further investigated.

This chapter includes

Product Data Sheet
Version 11 / 2016

Biresin® LS
Laminating and Multi-purpose resin

Areas of Application

- Manufacture of precise, robust laminates with glass and/or carbon fibres
- Manufacture of laminated foam and compression moulds
- Backstampings of moulds, models, negatives and tools
- Also used for coupling layers

Product Benefits

- Multi-purpose application with different hardeners
- Good soaking and wetting properties
- For high addition of fillers
- With **Biresin® F4 (B)** for longer potlife and lower viscosity
- With **Biresin® S10** (B) for shorter potlife and thinner layers
- Additional hardeners: see separate leaflet

Description

Basis	Two component epoxy system
Component A	**Biresin® LS**, epoxy resin, yellowish-transparent, unfilled
Component B	**Biresin® LS**, standard hardener, amine, colourless-transparent, unfilled
Component B	**Biresin® F4**, amine, colourless, unfilled
Component B	**Biresin® S10**, amine, amber, unfilled
Component B	**Biresin® S12**, amine, amber, unfilled

Processing Data		**Component A**	**Component B**			
Individual components		**Biresin® LS**	**Biresin® LS**	**Biresin® F4**	**Biresin® S10**	**Biresin® S12**
Viscosity, 23°C	mPa.s	~ 1,250	~ 40	< 10	~ 3,500	~180
Density, 25°C	g/ml	1.14	0.98	0.87	1.05	1.0
Mixing ratio A : B	in pbw	100	12	18	22	16
		Mixtures				
Mixed viscosity, 23°C	mPa.s		~ 580	~ 350	~ 3,500	~1200
Potlife, 500 g, RT	min		55	80	10	60
Demoulding time, RT	h		12	16	8	12

Physical Data (approx. values)

Biresin® LS (A) with component B			**Biresin® LS**		**Biresin® F4**		**Biresin® S10**		**Biresin® S12**	
Density	ISO 1183	g/cm³	1.2		1.2		1.2		1.2	
Curing conditions	time / temperature		14 d RT	2 h 80°C	14 d RT	2 h 80°C	14 d RT	2 h 80°C	14 d RT	2 h 80°C
Shore hardness	ISO 868	-	D 83	D 83	D 80	D 82	D 83	D 84	D 82	D 84
E-Modulus	ISO 178	MPa	2,420	2,630	2,440	2,570	2,900	2,900	2,500	2,500
Flexural strength	ISO 178	MPa	95	107	88	94	108	117	96	103
Compressive strength	ISO 604	MPa	104	106	91	94	110	112	102	98
Tensile strength	ISO 527	MPa	69	74	67	69	69	74	71	74
Impact resistance	ISO 179	kJ/m²	10	14	18	44	16	21	19	16
Heat distortion temp.	ISO 75B	°C	51	70	46	53	53	82	52	72

Packaging

Individual components	**Biresin® LS** (A)	220 kg; 50 kg; 20 kg net
	Biresin® LS (B)	2.4 kg net
	Biresin® F4 (B)	2.5 kg net
	Biresin® S10 (B)	2.5 kg net
	Biresin® S12(B)	15 kg; 2.5 kg net;

Biresin® LS 1 / 2

Axson

BUILDING TRUST

Sika®

Fig. A-55 Product data sheet Biresin® LS [BIR 2016]

Allgemeine bauaufsichtliche Zulassung/
Allgemeine Bauartgenehmigung
Nr. Z-10.7-282 vom 7. Januar 2021

Deutsches Institut für Bautechnik DIBt

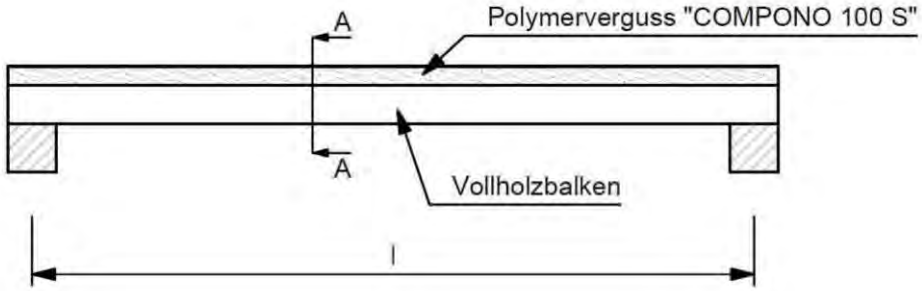

Schnitt A-A

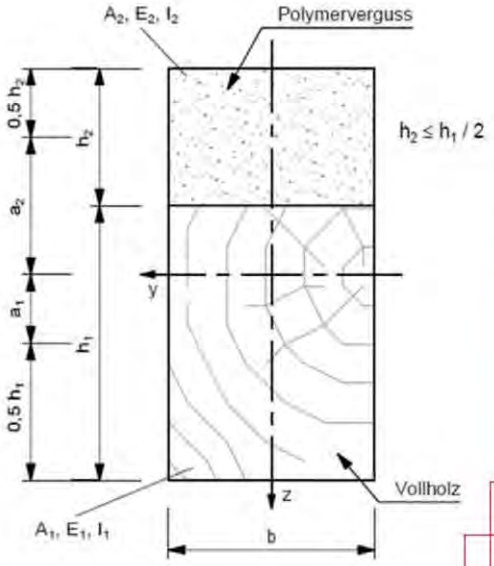

Verformungsbeiwerte k_{def} Modifikationsbeiwerte k_{mod}	Polymerverguss	
Lasteinwirkungsdauer	k_{def}	k_{mod}
ständig	1,05	0,43
lang	0,90	0,45
mittel	0,50	0,55
kurz	0,15	0,65

Festigkeitskennwerte [N/mm²]		Polymerverguss
Druck jede Richtung	$f_{c,k}$	81,0
Schub und Torsion	$f_{v,k}$	... (1)

(1) Bei Schub und Torsion sind die Holzwerte maßgeblich

Steifigkeitskennwerte [N/mm²]		Polymerverguss
Elastizitätsmodul Druck jede Richtung	E_{mean}	18000
	E_{05}	14500
Rohdichte [kg/m³]	ρ	1960

Compression strength
(characterstic value)

Modulus of elasticity for compression
(mean value and 5%-fractile)

Density
(mean value)

Polymerverguss zur Verstärkung von Holzbauteilen	Anlage 1
Verbundträger aus Holz und Polymerverguss Querschnittsabmessungen und Kennwerte für den Polymerverguss	

Further parameter are adressed to in Tab. 4-1 according to SCHOBER [SCH 2008]

Fig. A-56 Product data sheet Compono® 100 S [DIBt Z-10.7-282]

www.rampf-gruppe.de

EPUCRET
discover the future

Technisches Merkblatt
EPUMENT 140/5A3

Labor - Rev.-Status: 008 – 2007/08/03 Seite 1 von 2

Produktbeschreibung	EPUMENT 140/5A3 Reaktionsharzbeton ist eine 3-komponentige Ausgießmasse auf Epoxidharzbasis mit spezieller Füllstoffkombination auf quarzitischer Basis, welche höchsten Ansprüchen gerecht wird:
Eigenschaften	• Bestes Dämpfungsverhalten • Gute Steifigkeit • Geringe Wärmeleitfähigkeit • Thermischer Ausdehnungskoeffizient annähernd angepasst an Stahl • Niedrigstes Kriechverhalten unter Lasteinwirkung
Anwendung	Füllen von Stahlschweiß- oder Gusskonstruktionen z.B. Maschinenteile (Ständer, Maschinengestelle und Maschinenbetten) sowie Unterbauten für schwingungsbelastete Baugruppen wie z.B. Motoren, Getriebe, Turbinen, Zentrifugen, Versuchs- und Prüfstände zur Erhöhung der statischen und dynamischen Steifigkeit.
Gebindegröße	30 kg (andere Gebindegrößen auf Anfrage)

Kenndaten

• **Dichte**	ca. 2,3 g/cm³	Density (mean value)
• **Druckfestigkeit ***	140 -160 N/mm²	Compressive strength (mean value)
• **Biegezugfestigkeit ***	35 - 45 N/mm²	Flexural strength (mean value)
• **E-Modul ***	30 -35 kN/mm²	Modulus of elasticity for compression (mean value)
• **Therm. Ausdehnungskoeffizient**	ca. 19,5 10^{-6} K^{-1}	bei 20 °C
• **Wärmeleitfähigkeit**	2,3 W/m K	bei 25 °C
• **Spez. Wärmekapazität**	ca. 0,8 J/g K	bei 25 °C
• **Temperaturleitfähigkeit**	ca. 1,3 mm^2/s	bei 25 °C
• **Maximale Körnung**	5 mm (Wandstärke Ausgießmasse > 40 mm)	
• **Logarithmisches Dekrement**	0,035	
• **Mischungsverhältnis**	A : B : C = 2,06 : 0,74 : 27,2	(Gew.teile)
• **Verarbeitungszeit**	2,5 - 4 Stunden	bei 20°C
• **Verarbeitungstemperatur**	15-25 °C	
• **Aushärtung**	ca. 24 Stunden	

Vorbereitung der zu fül-	- Dichte Schweißnähte - Innenflächen sandgestrahlt, frei von Fett, Farbe, Zunder, Rost und Restsand

EPUCRET Mineralgusstechnik GmbH & Co.KG
Daimlerstraße 18-26 • D-73117 Wangen bei Göppingen• T +49 (0) 7161 95889-0 • F +49 (0) 7161 95889-29
E info@epucret.de • http://www.epucret.de

Fig. A-57 Product data sheet Epument® 140/5AR [EPU 2007]

DIN EN 10340:2008-01
EN 10340:2007 (D)

Tabelle 2 *(fortgesetzt)*

Bezeichnung		Wärmebehandlung [a]		Dicke	Zugversuch bei Raumtemperatur			Kerbschlagbiegeversuch [b]	
Kurzname	Werkstoffnummer	Symbol [c]	Normalglühen oder Austenitisieren °C	Anlassen °C	t mm	$R_{p0,2}$ MPa [d] min.	R_m MPa [d]	A % min.	KV [e] J min.	Temperatur °C
G18NiMoCr3-6	1.6759	+ QT1	900 bis 980 [g]	580 bis 620	$t \leq 80$	700	830 bis 980	12	27	– 40
		+QT2	900 bis 980 [g]	590 bis 630	$t \leq 150$	630	780 bis 930	12	27	– 40
GX4CrNi13-4	1.4317	+QT	1 000 bis 1 050	590 bis 620	$t \leq 300$	570	760 bis 960	15	50	RT [f]
GXCrNiMo16-5-1	1.4405	+QT	1 020 bis 1 070	580 bis 630	$t \leq 300$	540	760 bis 960	15	60	RT [f]
GX2CrNi19-11	1.4309	+ AT [h]	1 050 bis 1 150	–	$t \leq 150$	185	440 bis 640	30	80	RT [f]
GX2CrNiMo19-11-2	1.4409	+AT [h]	1 080 bis 1 150	–	$t \leq 150$	195	440 bis 640	30	80	RT [f]
GX2CrNiMoN25-6-3	1.4468	+AT [h]	1 120 bis 1 150	–	$t \leq 150$	480	650 bis 850	22	50	RT [f]

a Temperatur und Abkühlungsmittel (nur zur Information).

b Wenn zwei Kerbschlagarbeitswerte angegeben sind, siehe 7.2.2.3.

c + N bedeutet Normalglühen, + QT oder + QT1 oder + QT2 oder + QT3 bedeutet Vergüten (Härten + Anlassen); +AT bedeutet Lösungsglühen.

d 1 MPa = 1N/mm².

e Abkühlung in Luft (nur zur Information).

f RT bedeutet Raumtemperatur.

g Abkühlung in Flüssigkeit (nur zur Information).

h Lösungsglühen mit Abschrecken in Wasser.

Fig. A-58 Steel cast material properties according to EN 10340

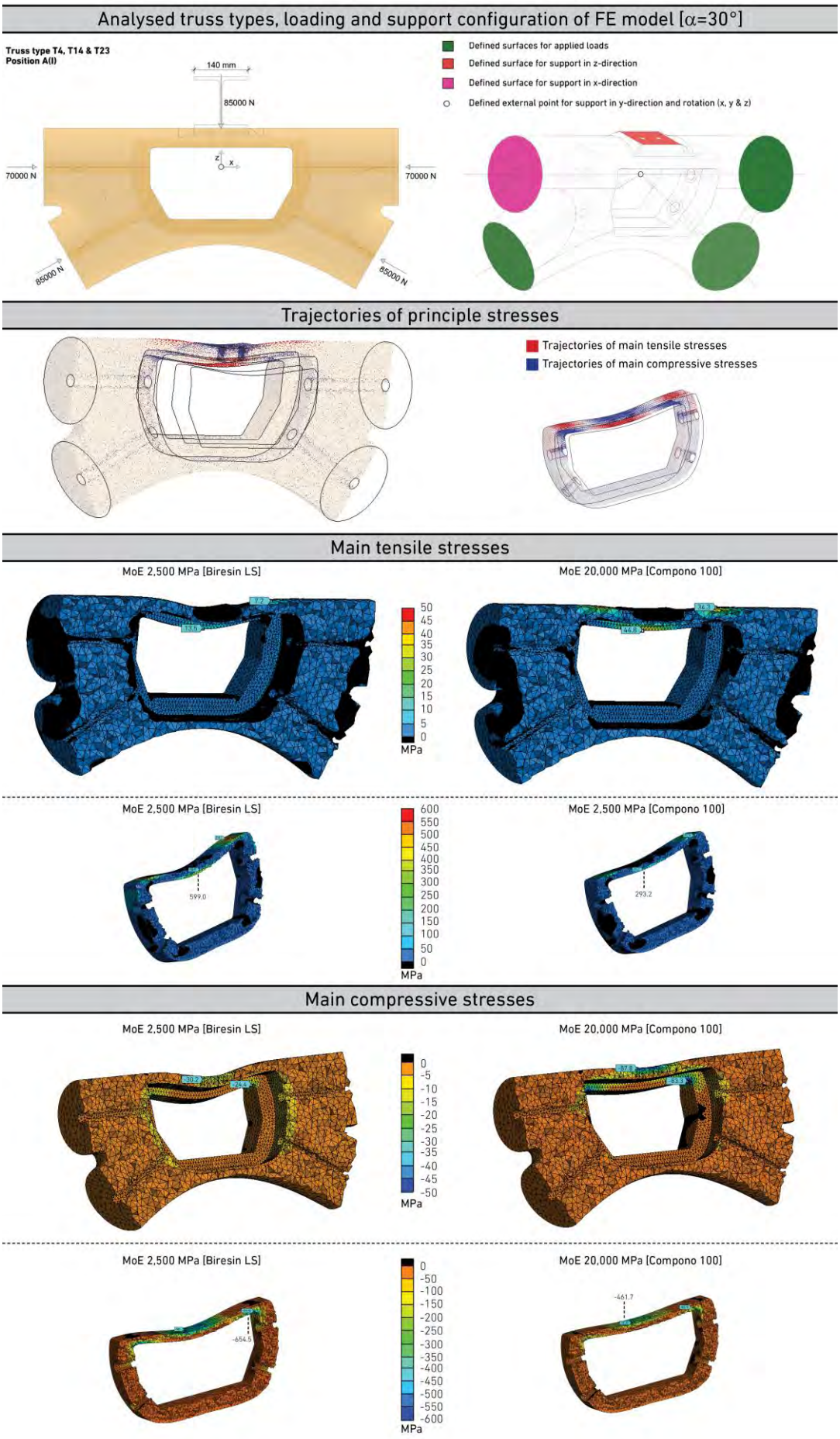

Fig. A-59 Field joint analysis 30° - Sub-model A(I)

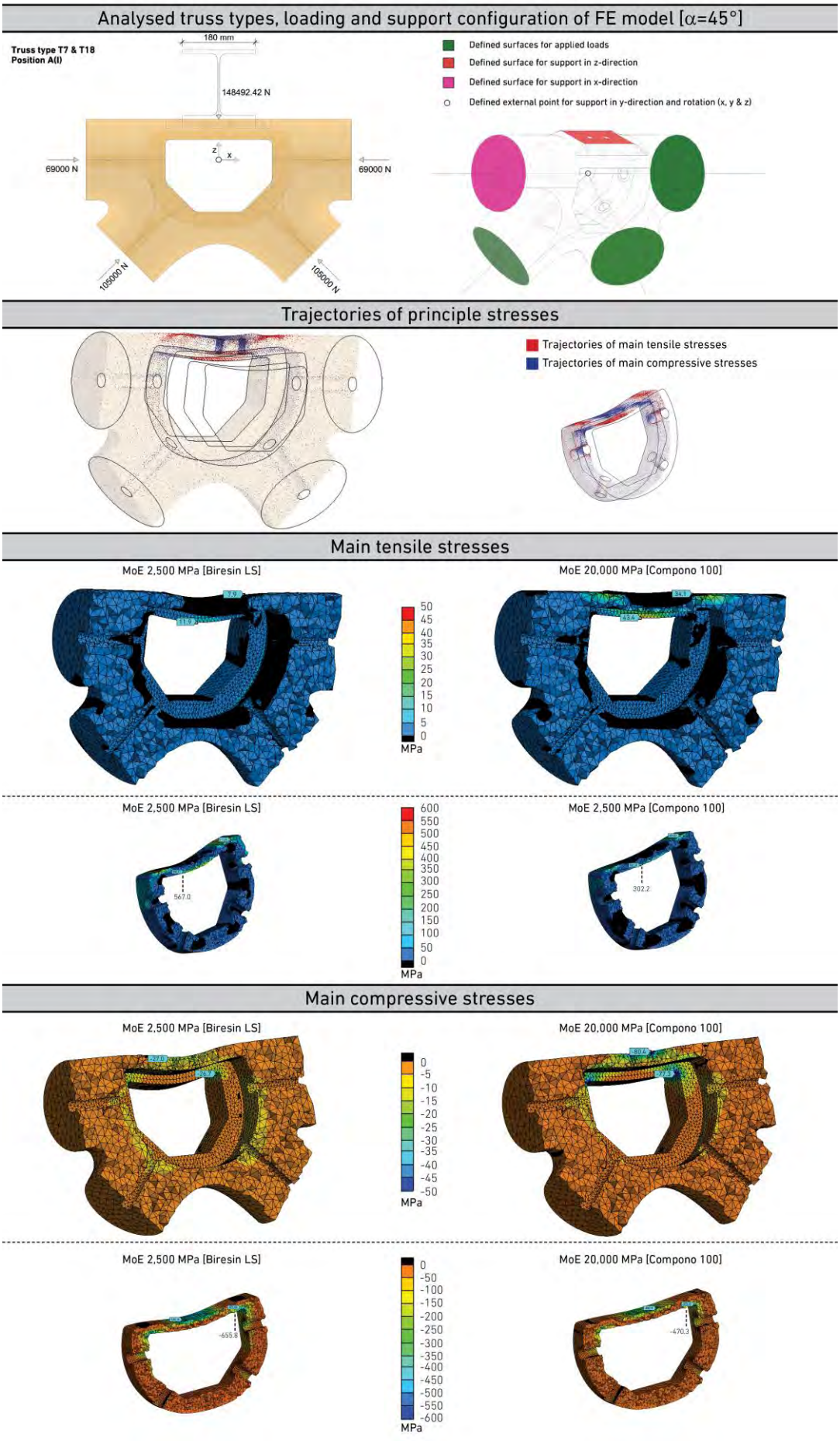

Fig. A-60 Field joint analysis 45° - Sub-model A(I)

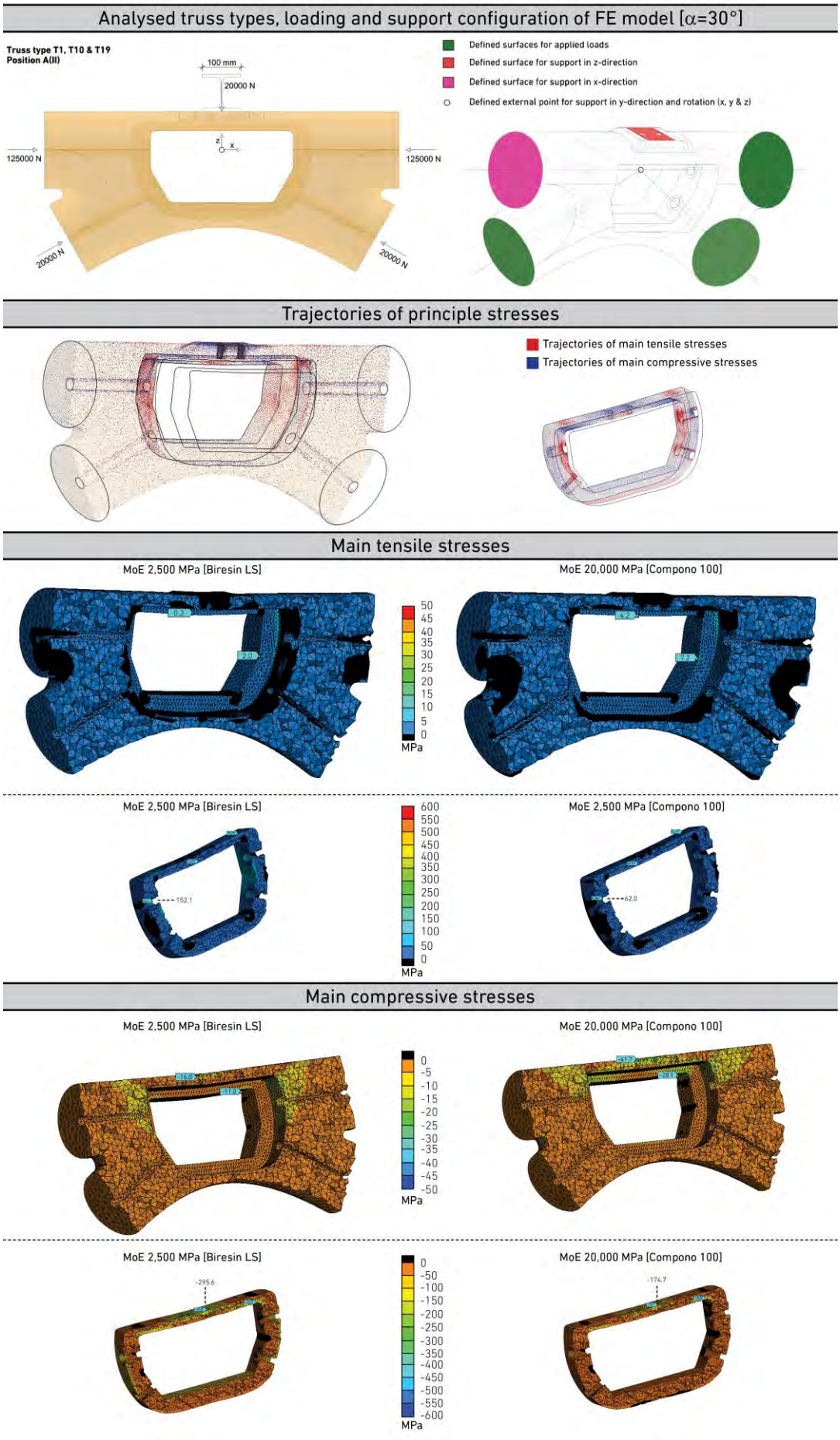

Fig. A-61 Field joint analysis 30° - Sub-model A(II)

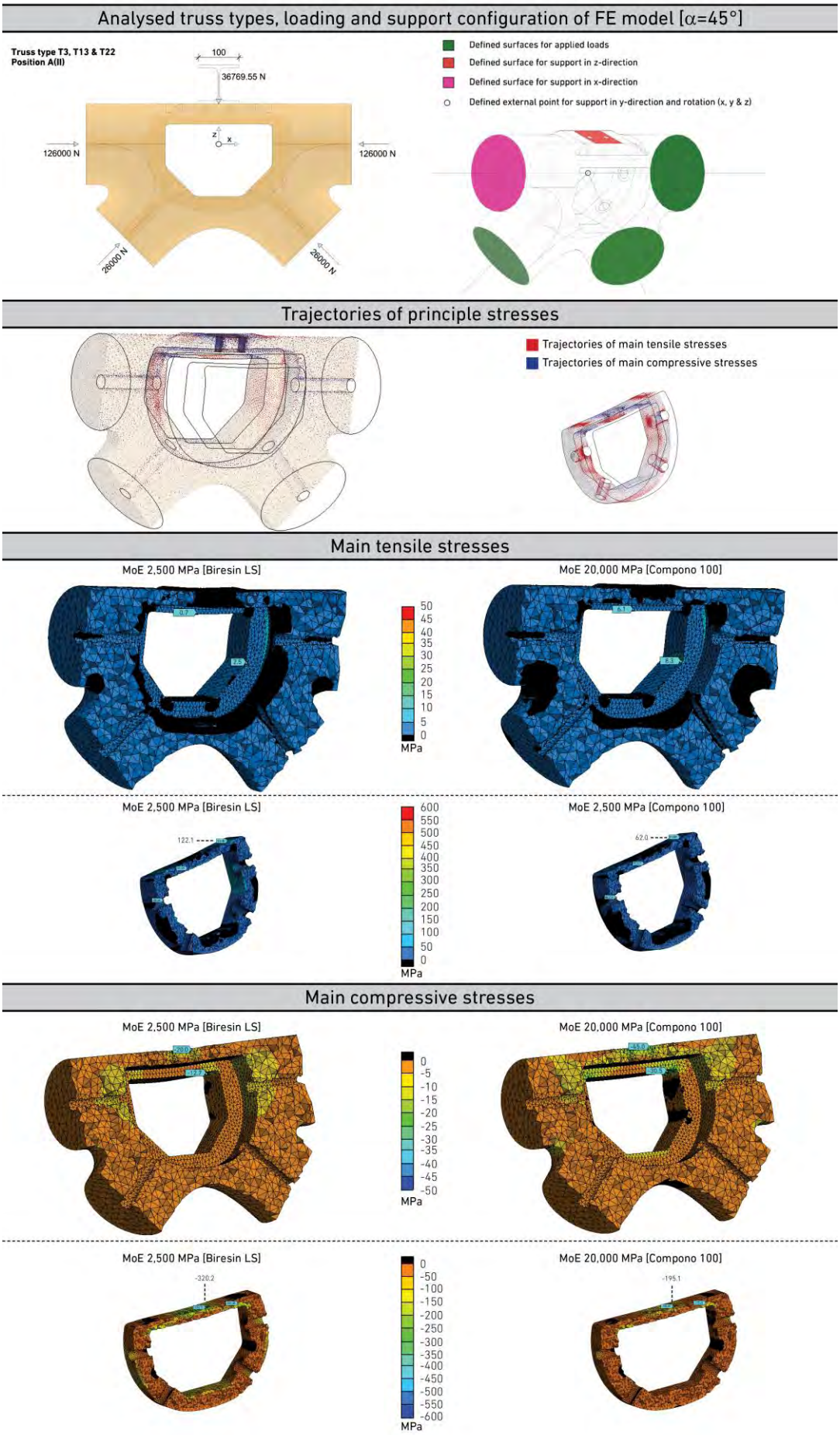

Fig. A-62 Field joint analysis 45° - Sub-model A(II)

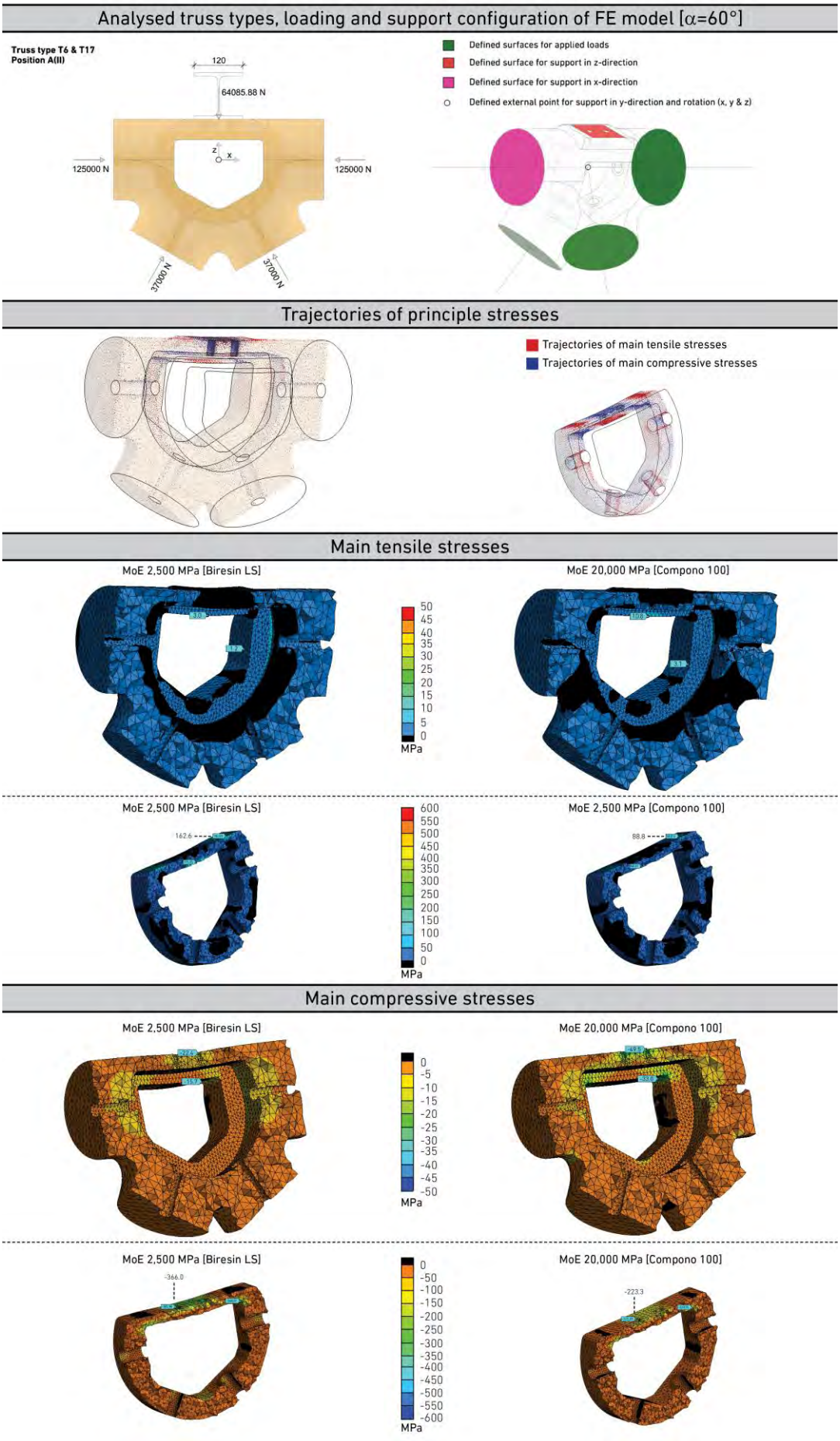

Fig. A-63 Field joint analysis 60° - Sub-model A(II)

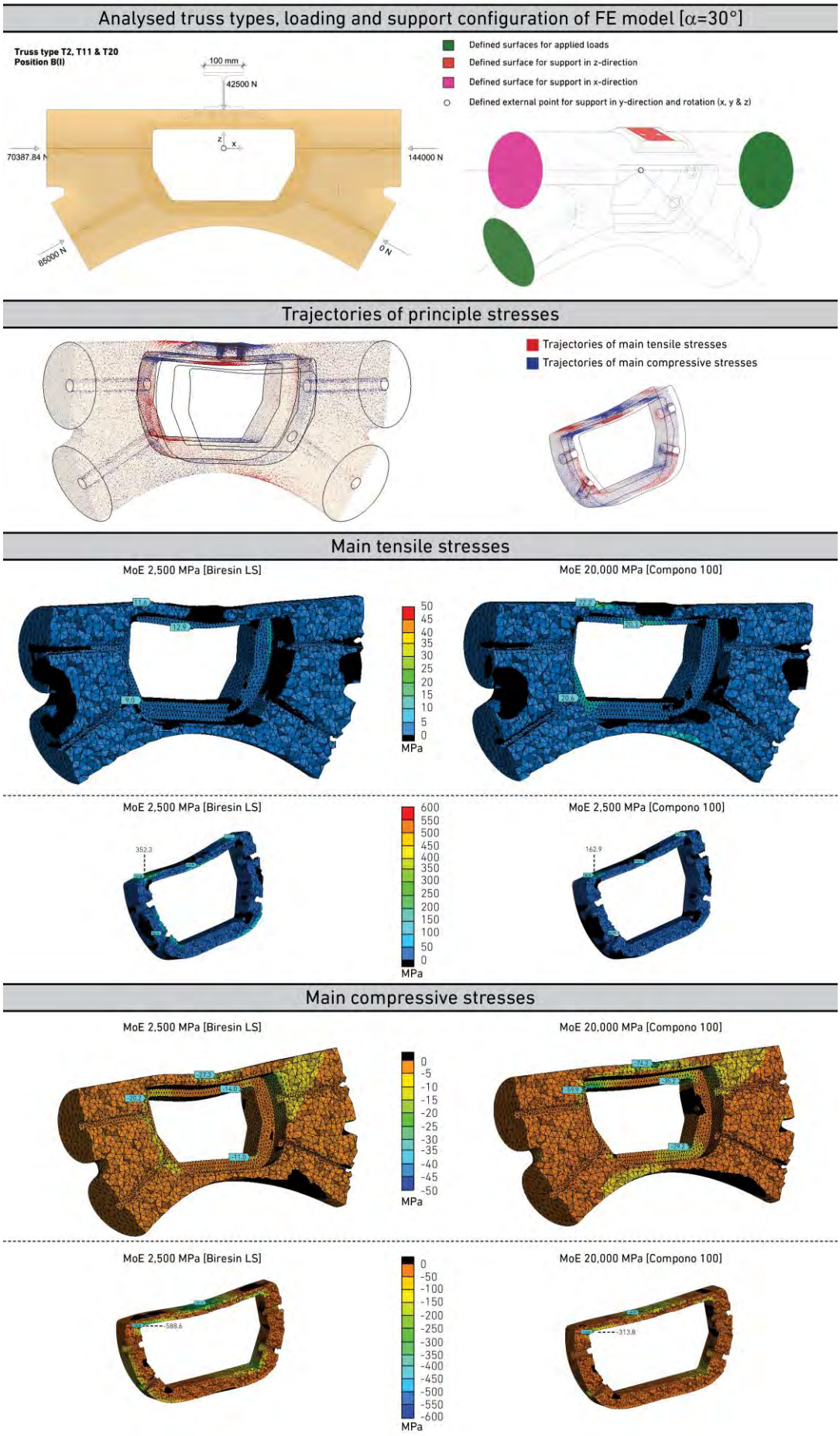

Fig. A-64 Field joint analysis 30° - Sub-model B(I)

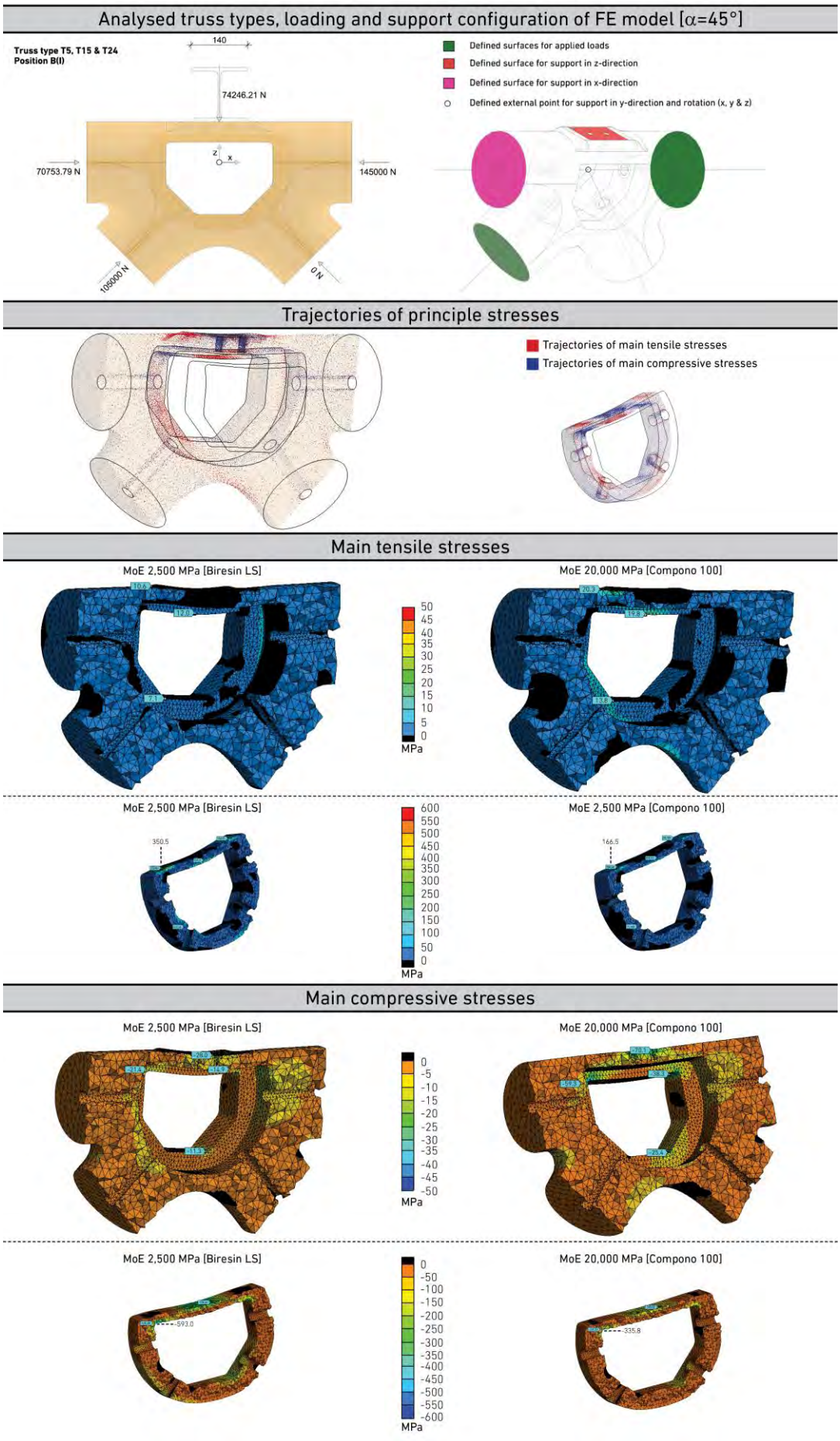

Fig. A-65 Field joint analysis 45° - Sub-model B(I)

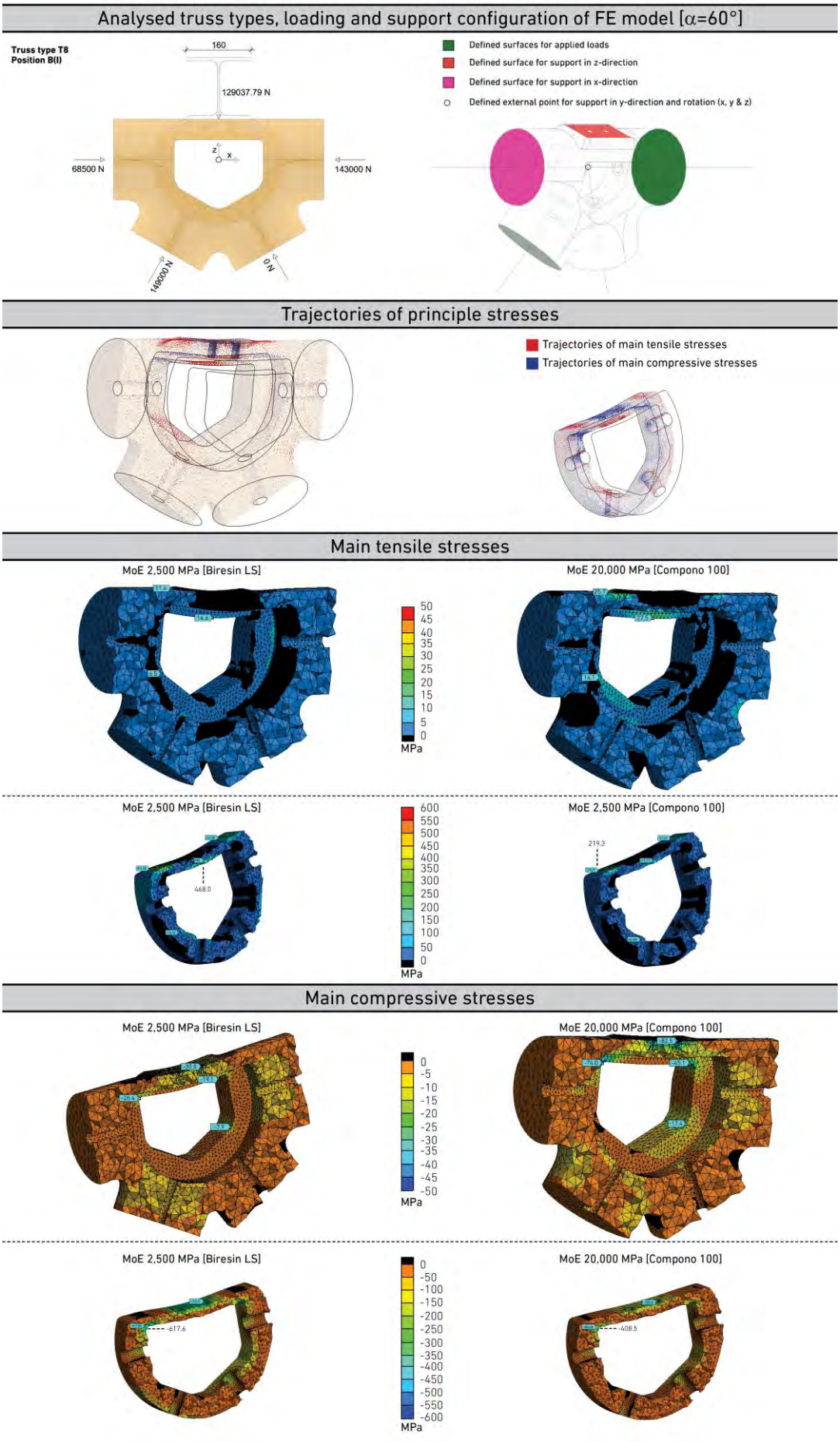

Fig. A-66 Field joint analysis 60° - Sub-model B(I)

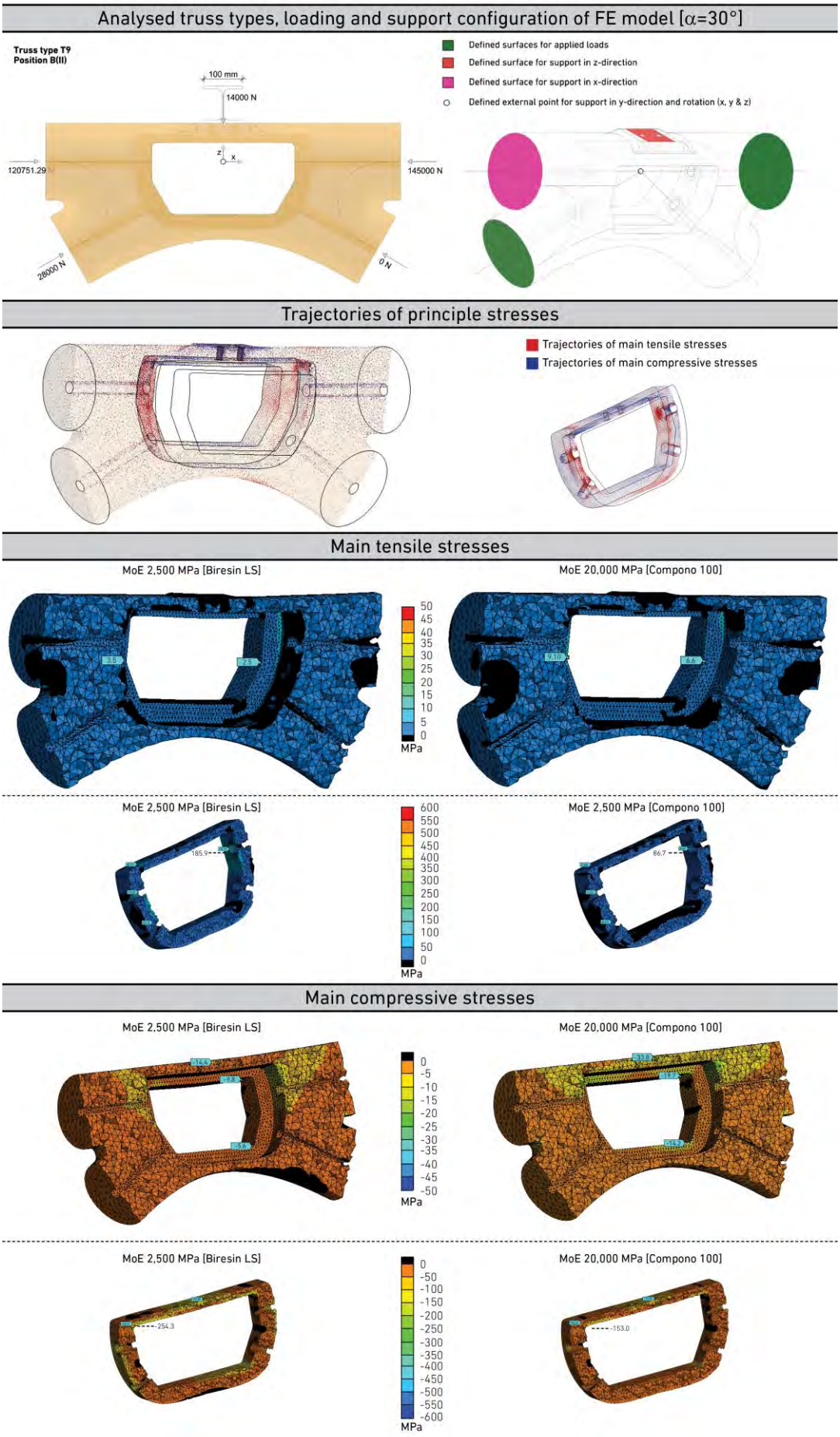

Fig. A-67 Field joint analysis 30° - Sub model B(II)

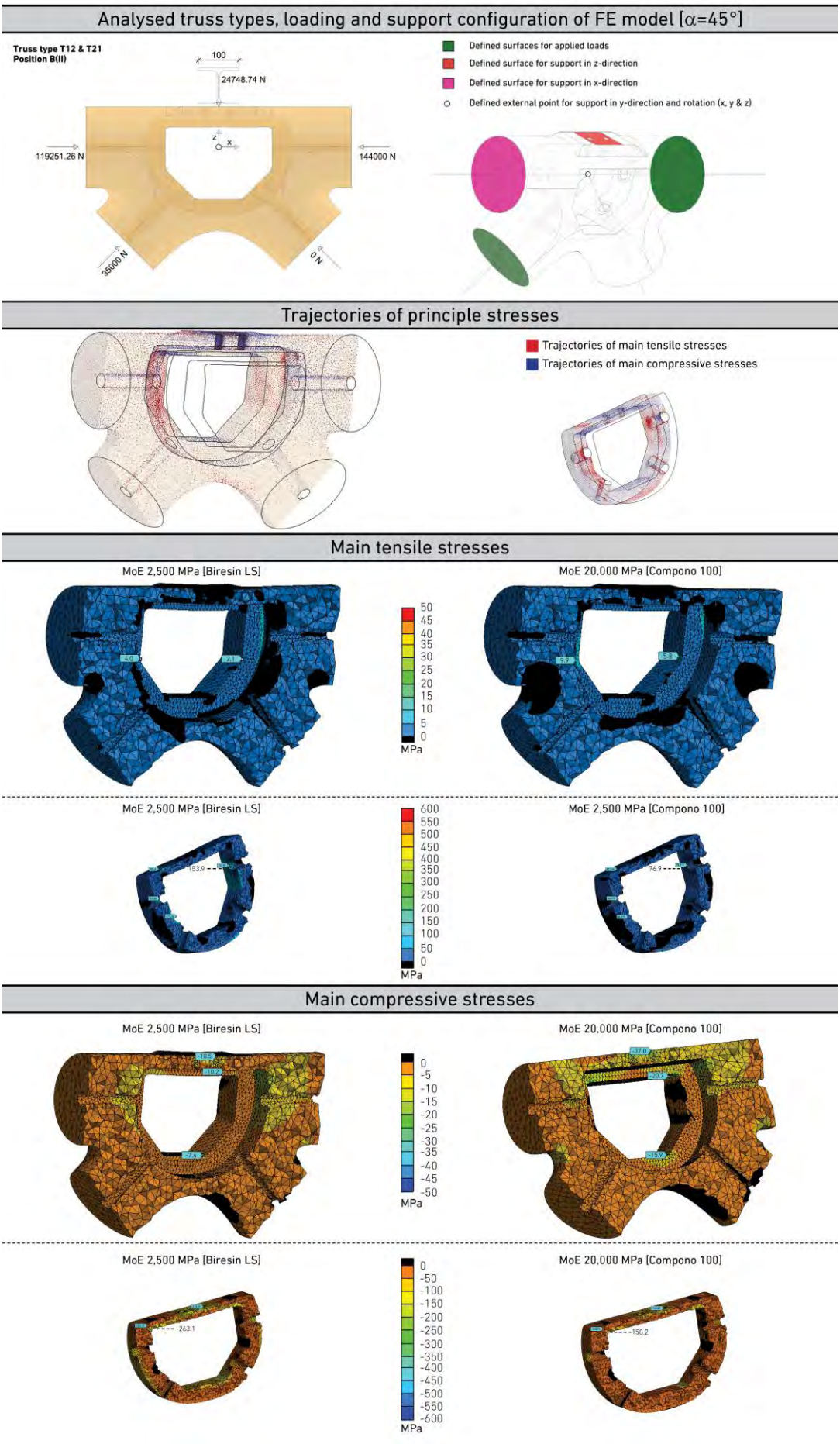

Fig. A-68 Field joint analysis 45° - Sub-model B(II)

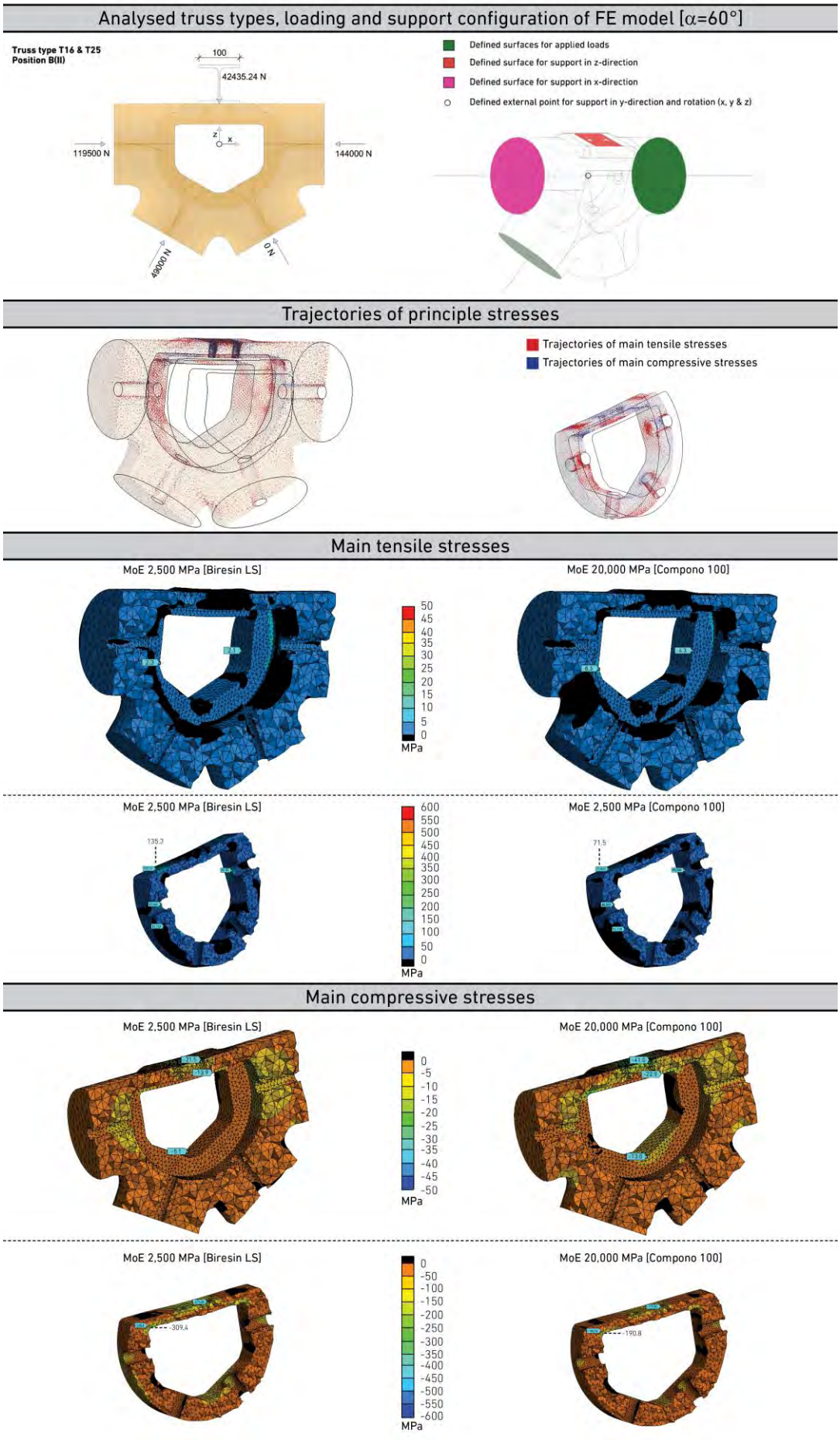

Fig. A-69 Field joint analysis 60° - Sub-model B(II)

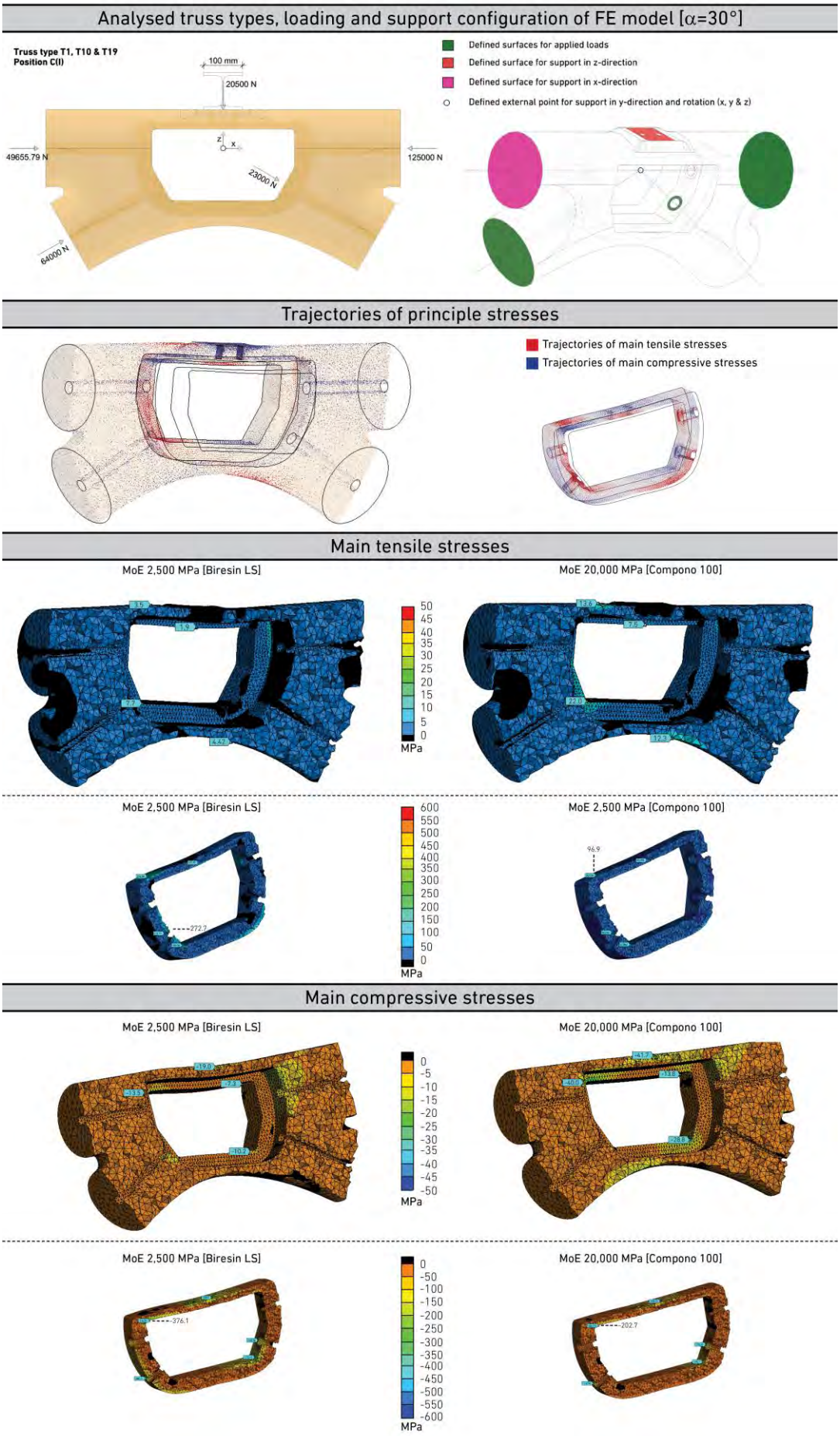

Fig. A-70 Field joint analysis 30° - Sub-model C(I)

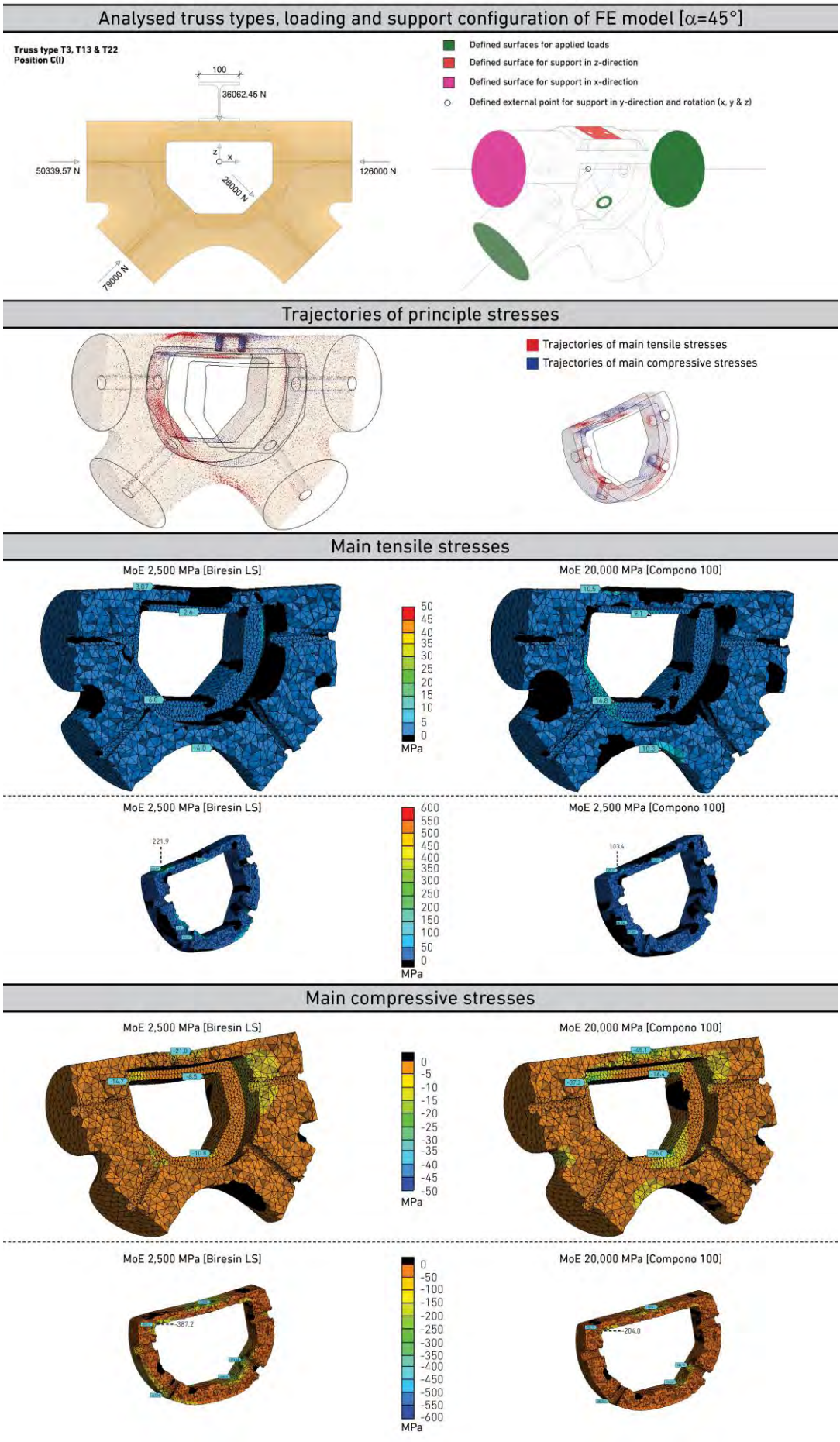

Fig. A-71 Field joint analysis 45° - Sub-model C(I)

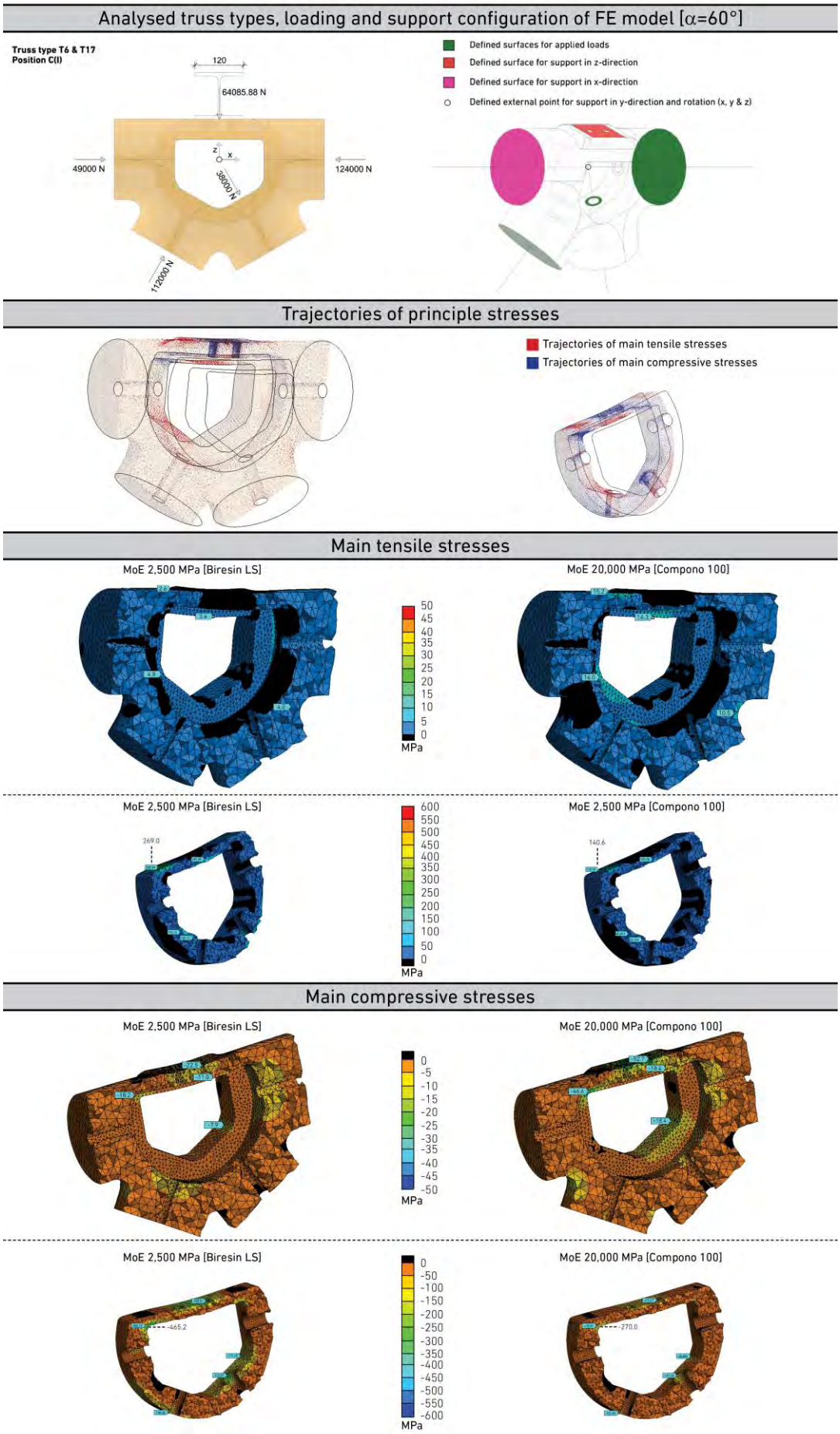

Fig. A-72 Field joint analysis 60° - Sub model C(I)

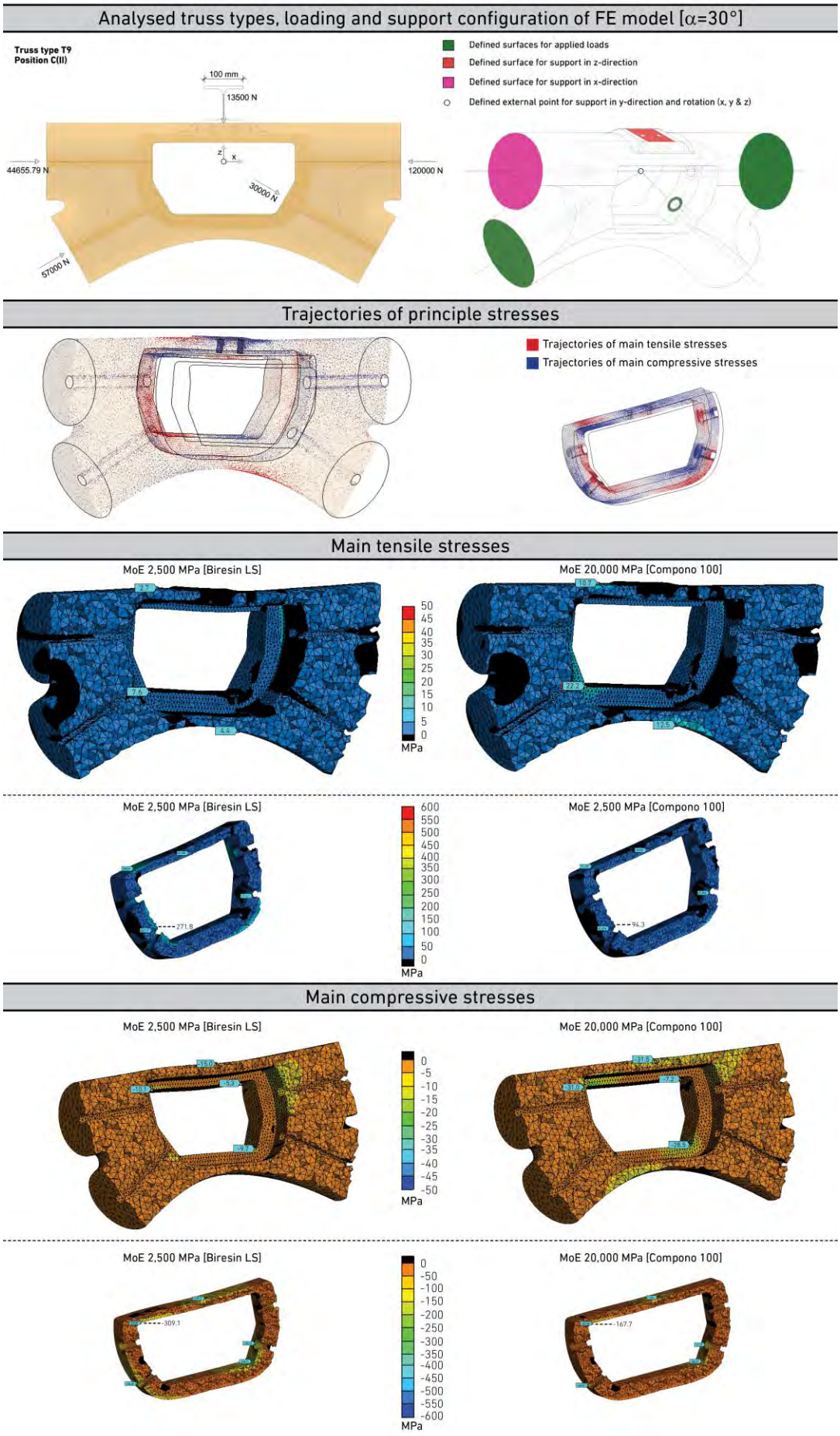

Fig. A-73 Field joint analysis 30° - Sub-model C(II)

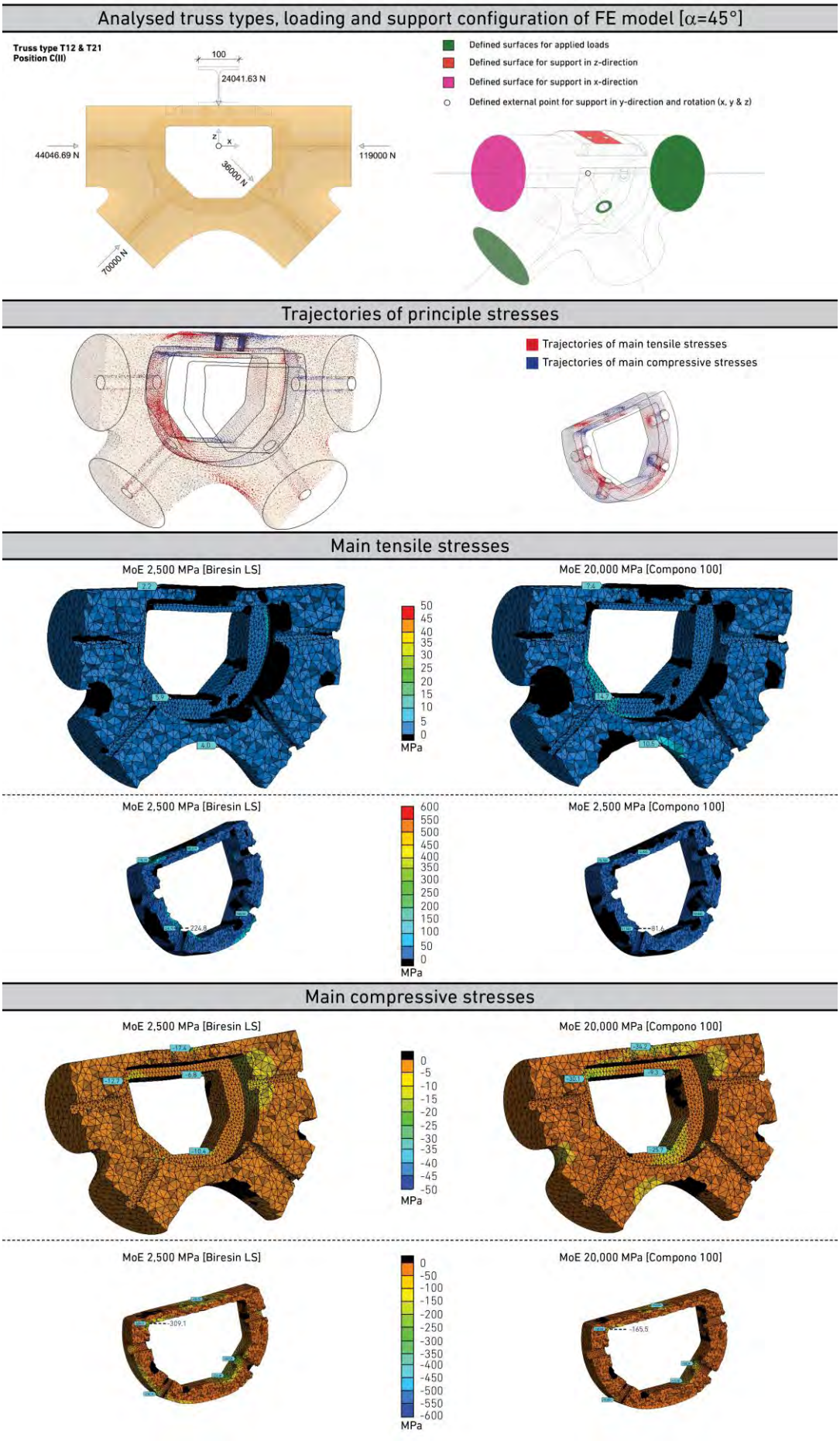

Fig. A-74 Field joint analysis 45° - Sub-model C(II)

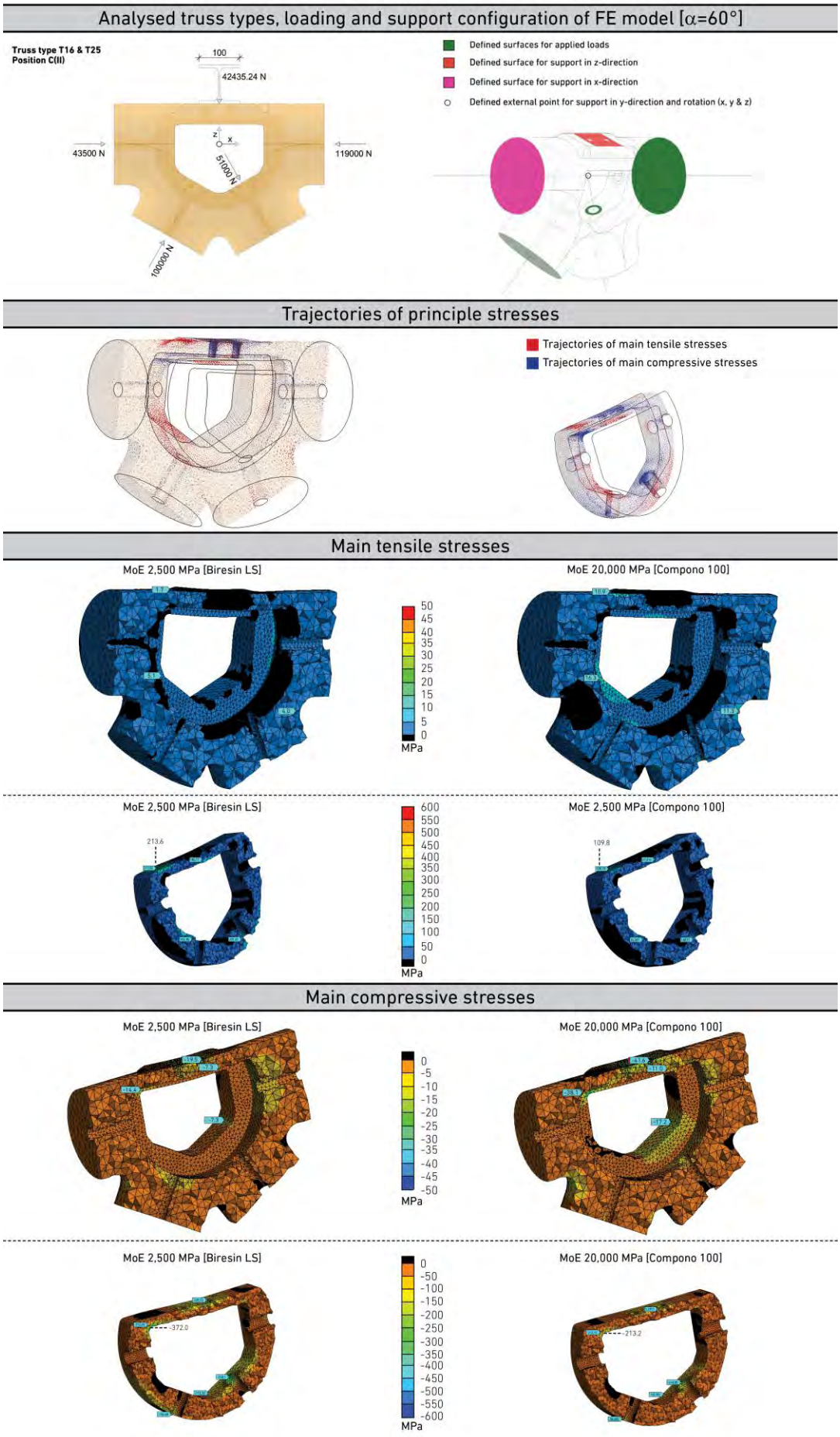

Fig. A-75 Field joint analysis 60° - Sub-model C(II)

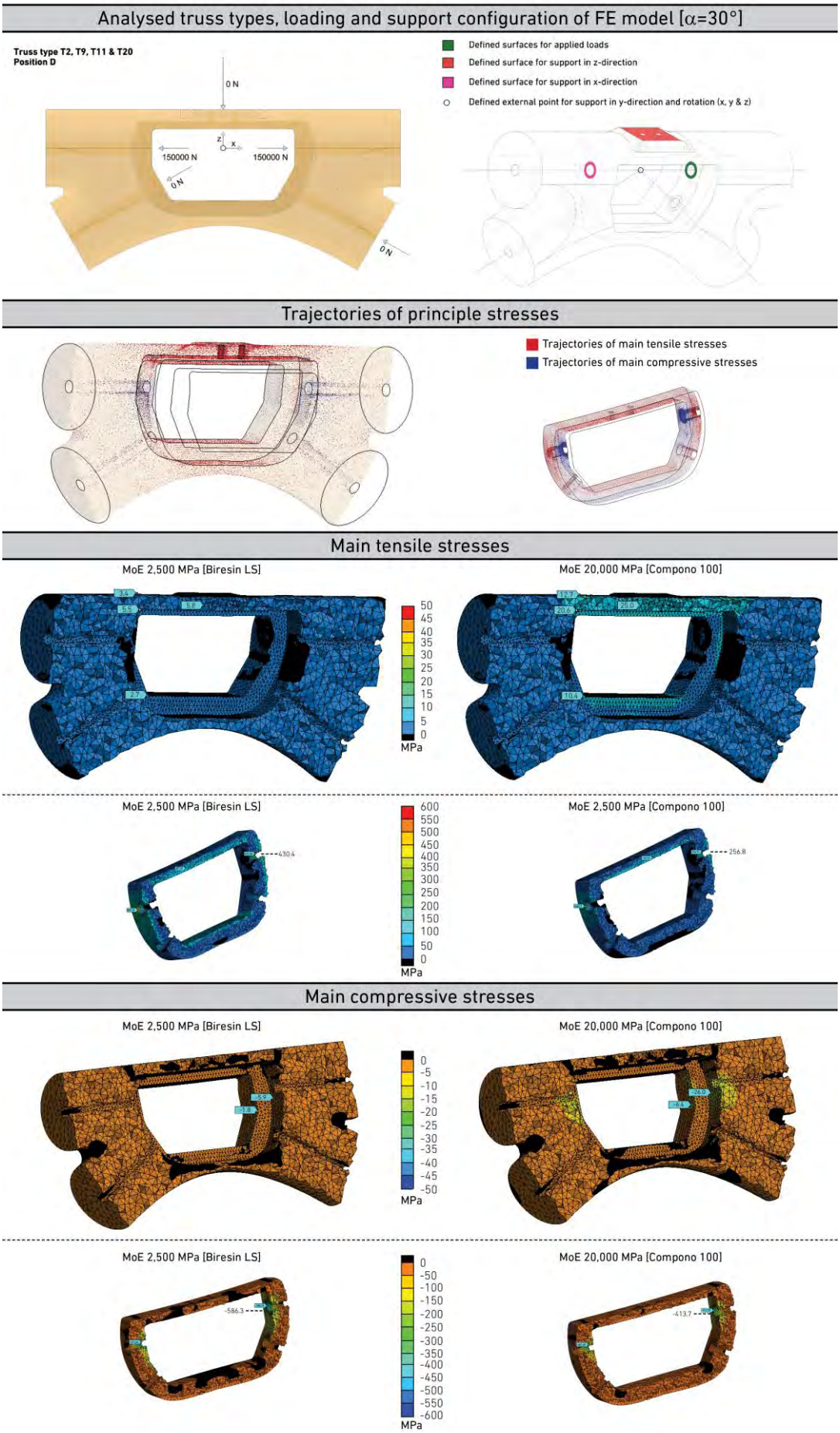

Fig. A-76 Field joint analysis 30° - Sub-model D

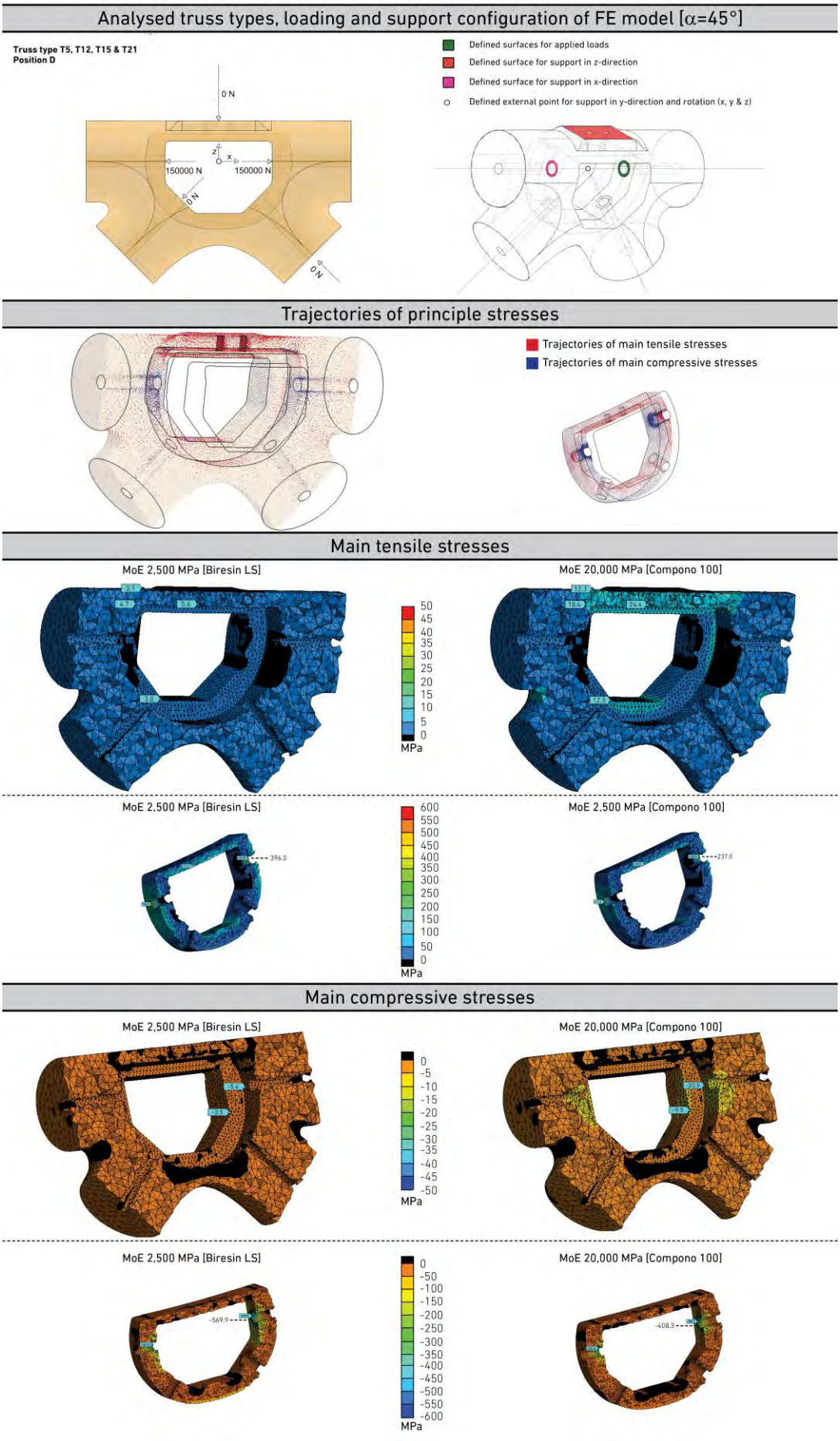

Fig. A-77 Field joint analysis 45° - Sub-model D

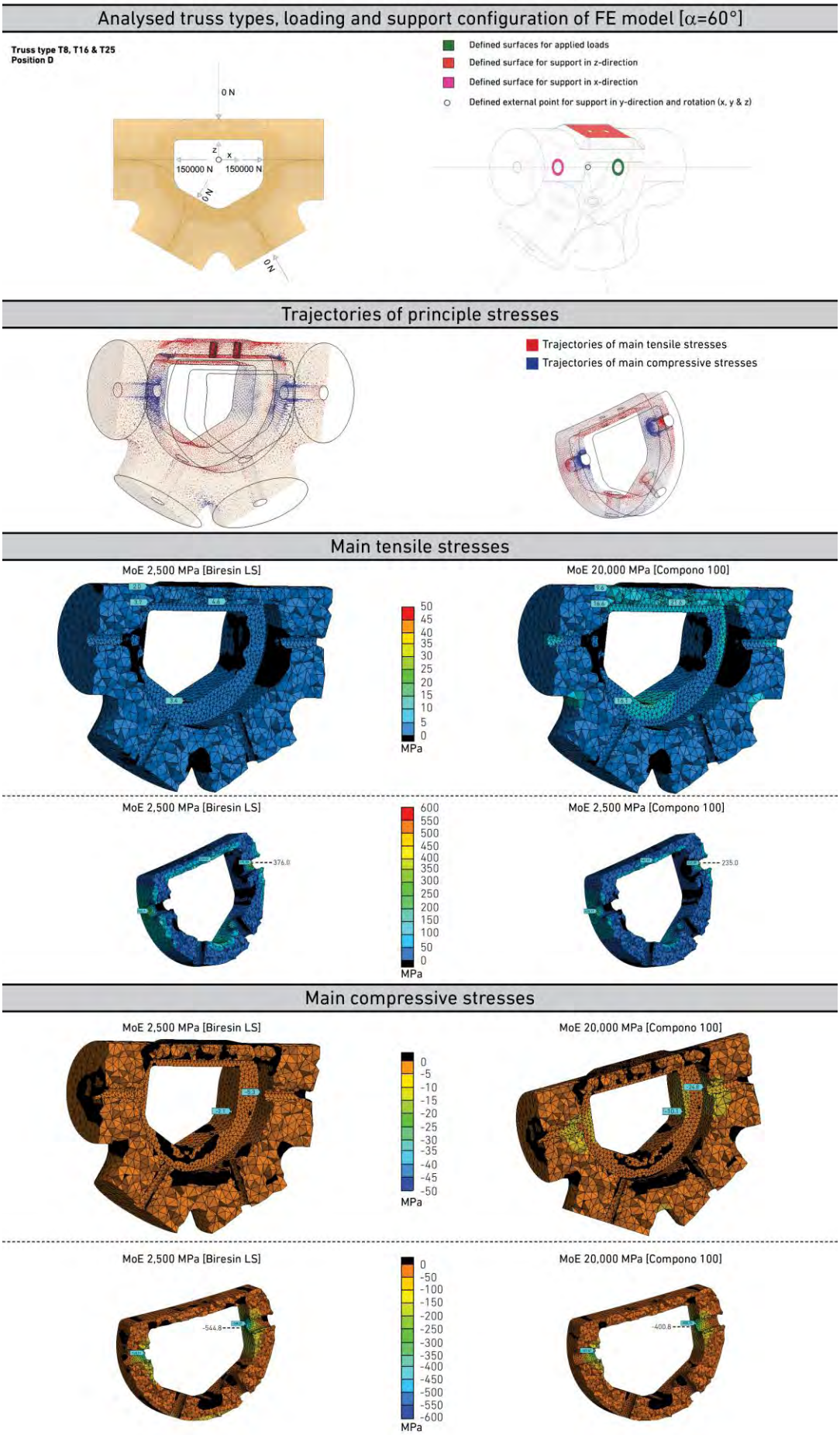

Fig. A-78 Field joint analysis 60° - Sub-model D

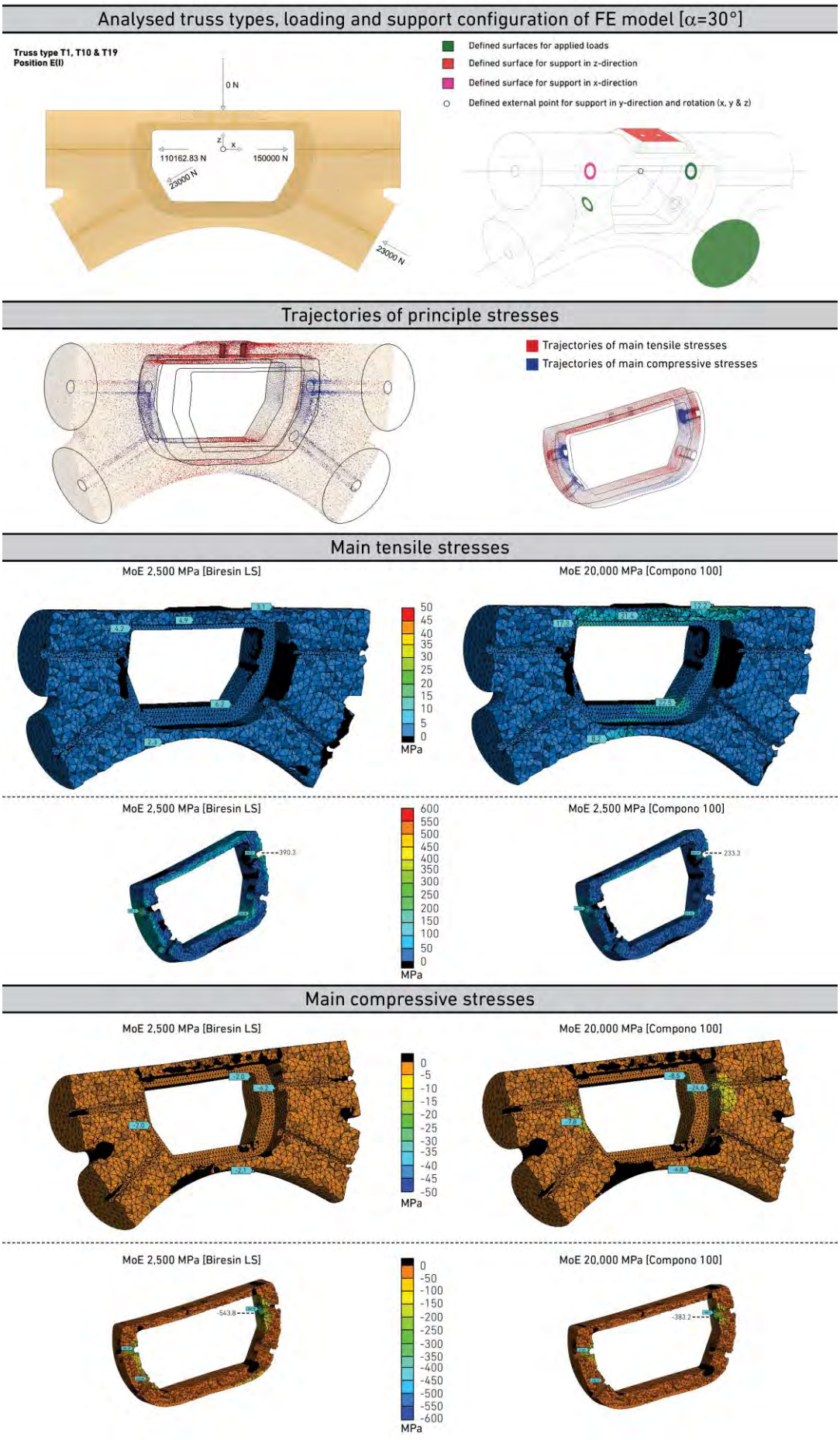

Fig. A-79 Field joint analysis 30° - Sub-model $E^{(I)}$

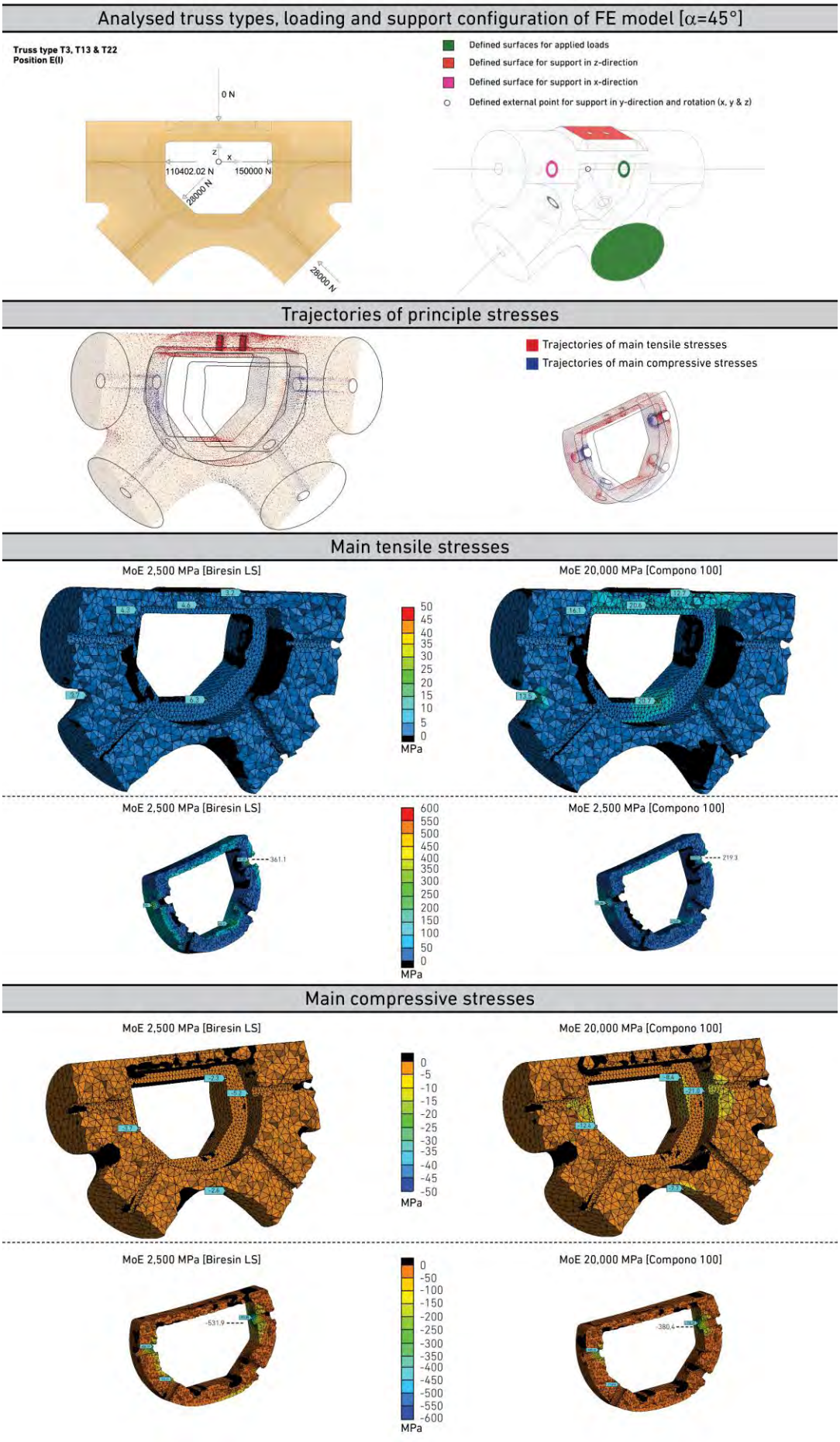

Fig. A-80 Field joint analysis 45° - Sub-model $E^{(I)}$

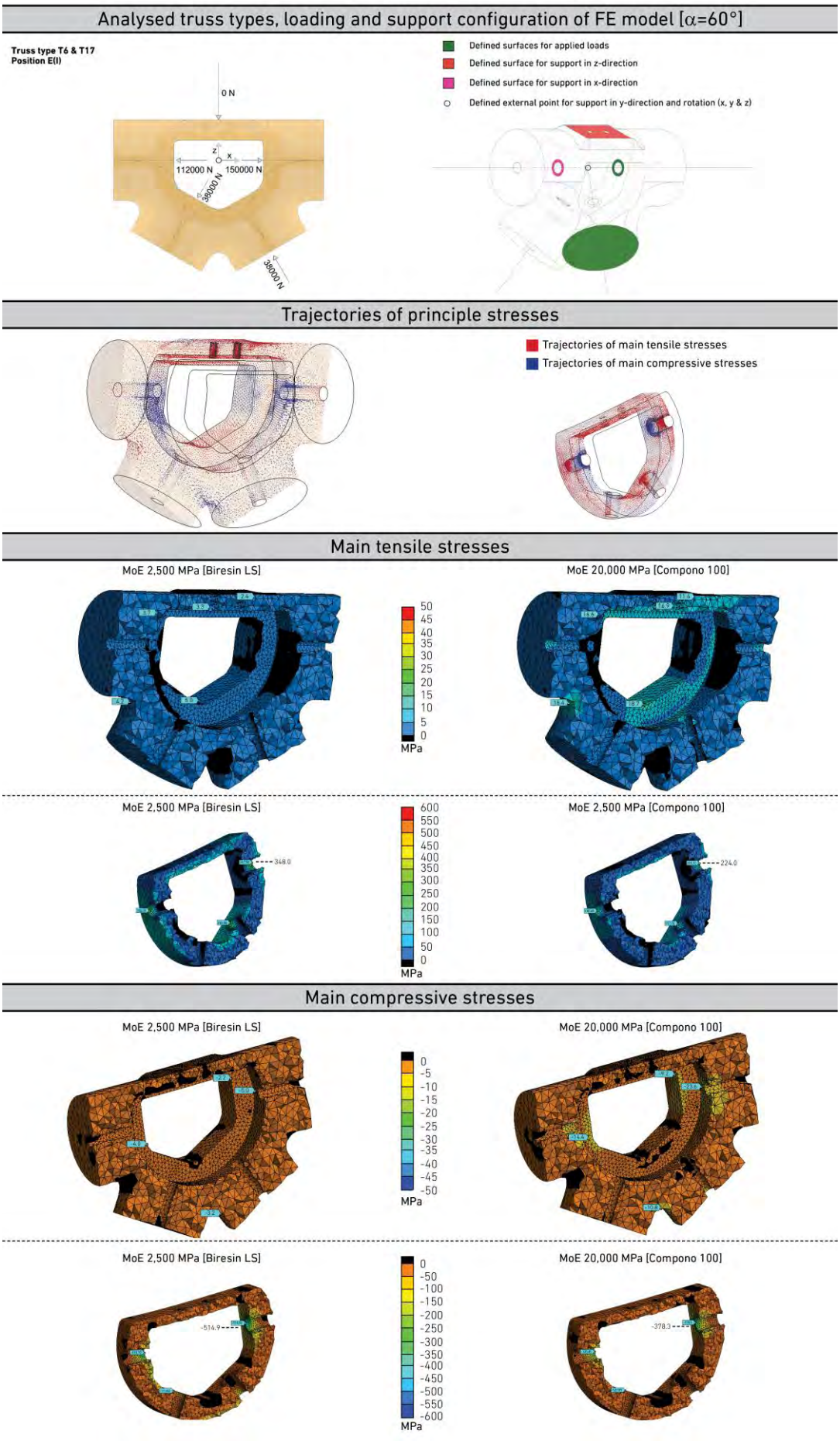

Fig. A-81 Field joint analysis 60° - Sub-model E(I)

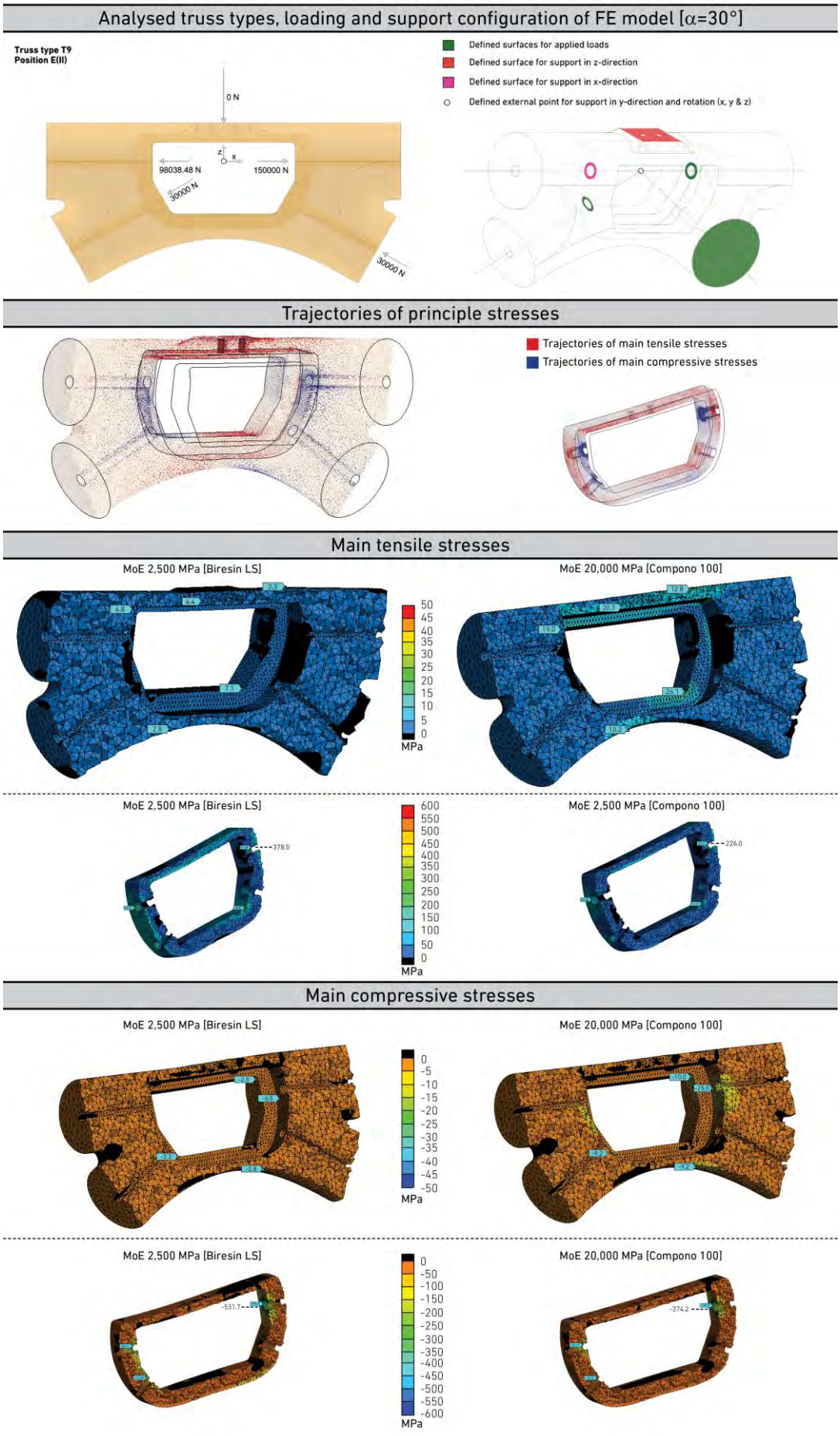

Fig. A-82 Field joint analysis 30° - Sub-model $E^{(II)}$

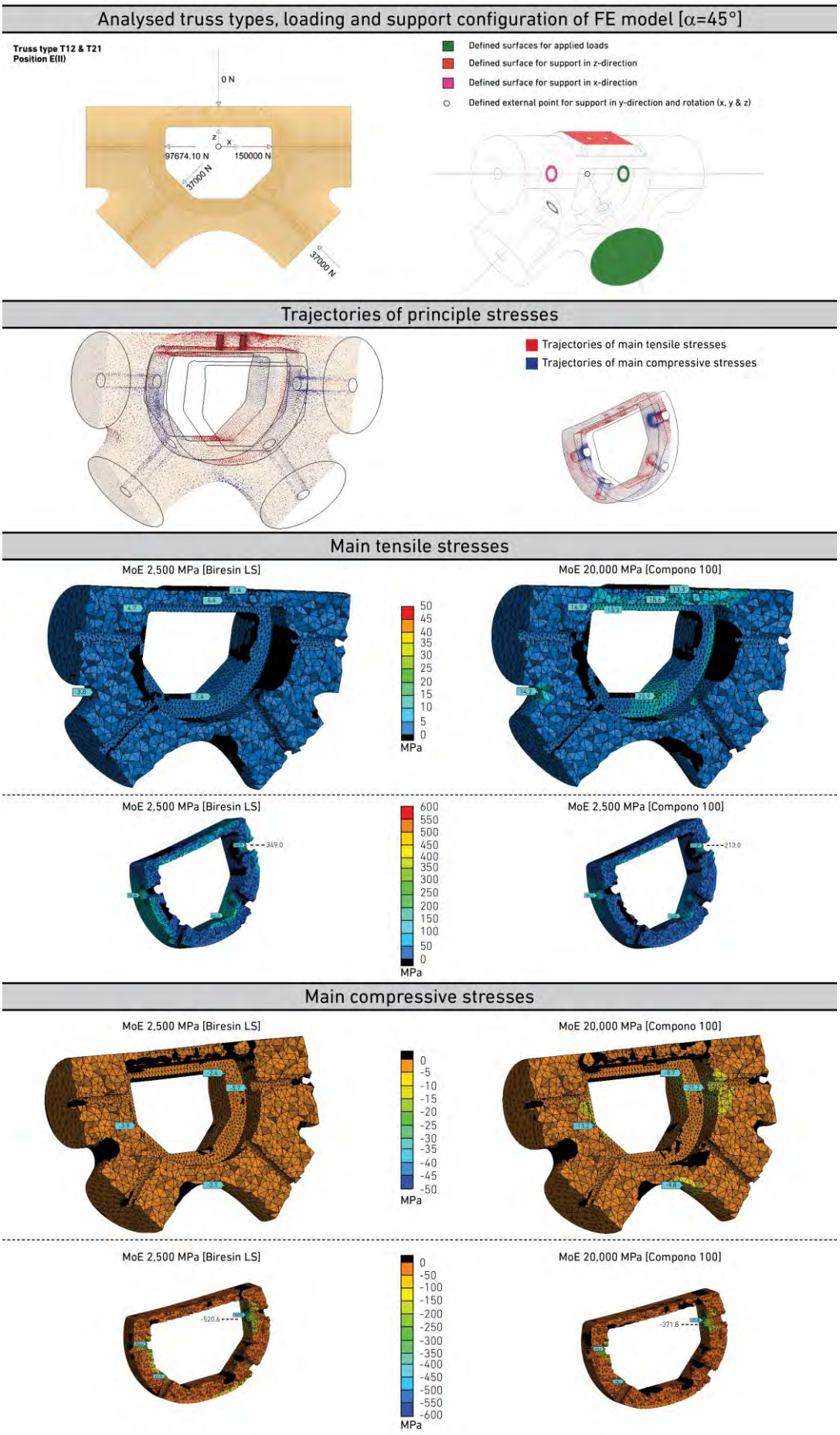

Fig. A-83 Field joint analysis 45° - Sub-model E(II)

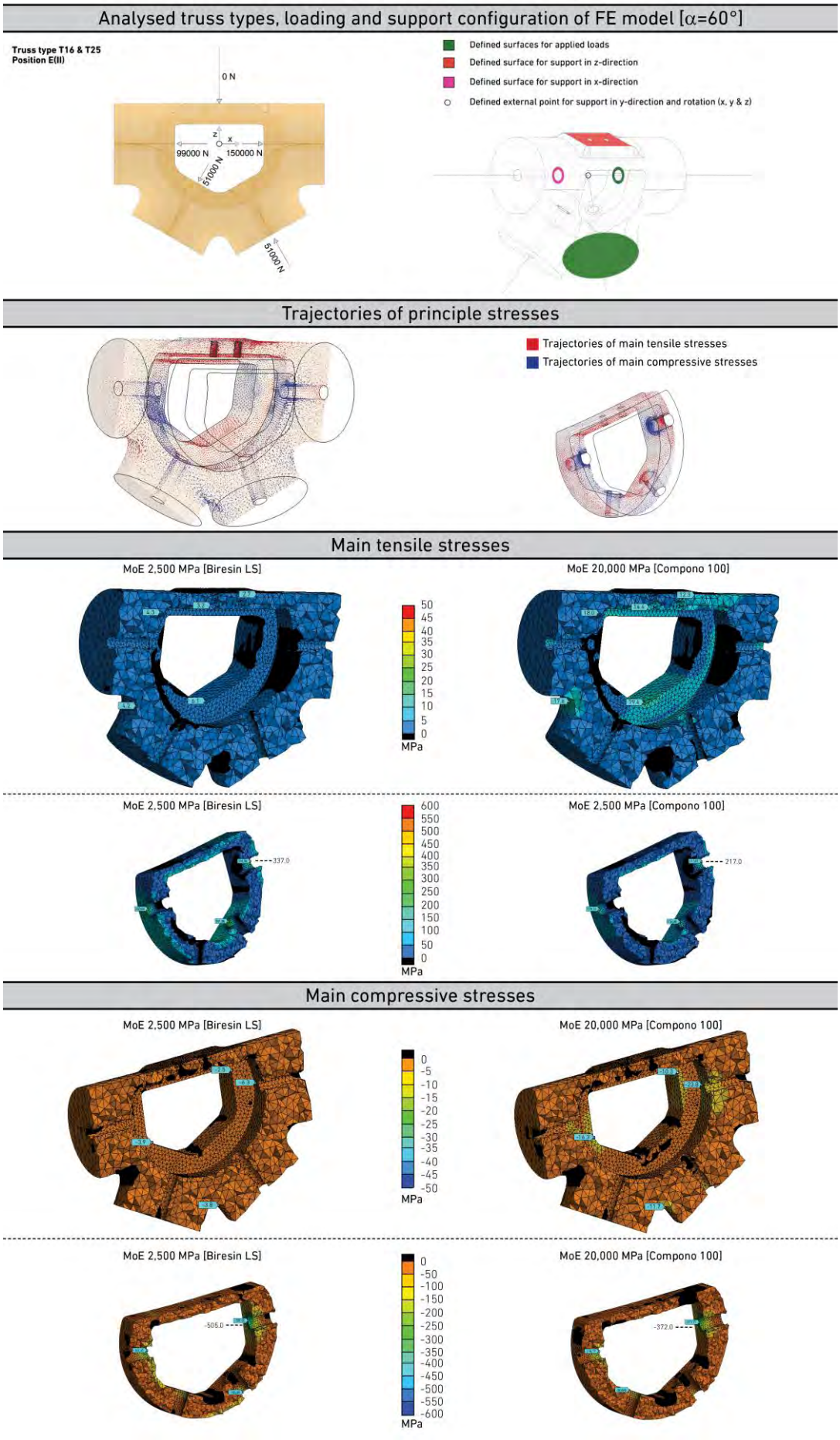

Fig. A-84 Field joint analysis 60° - Sub-model $E^{(II)}$

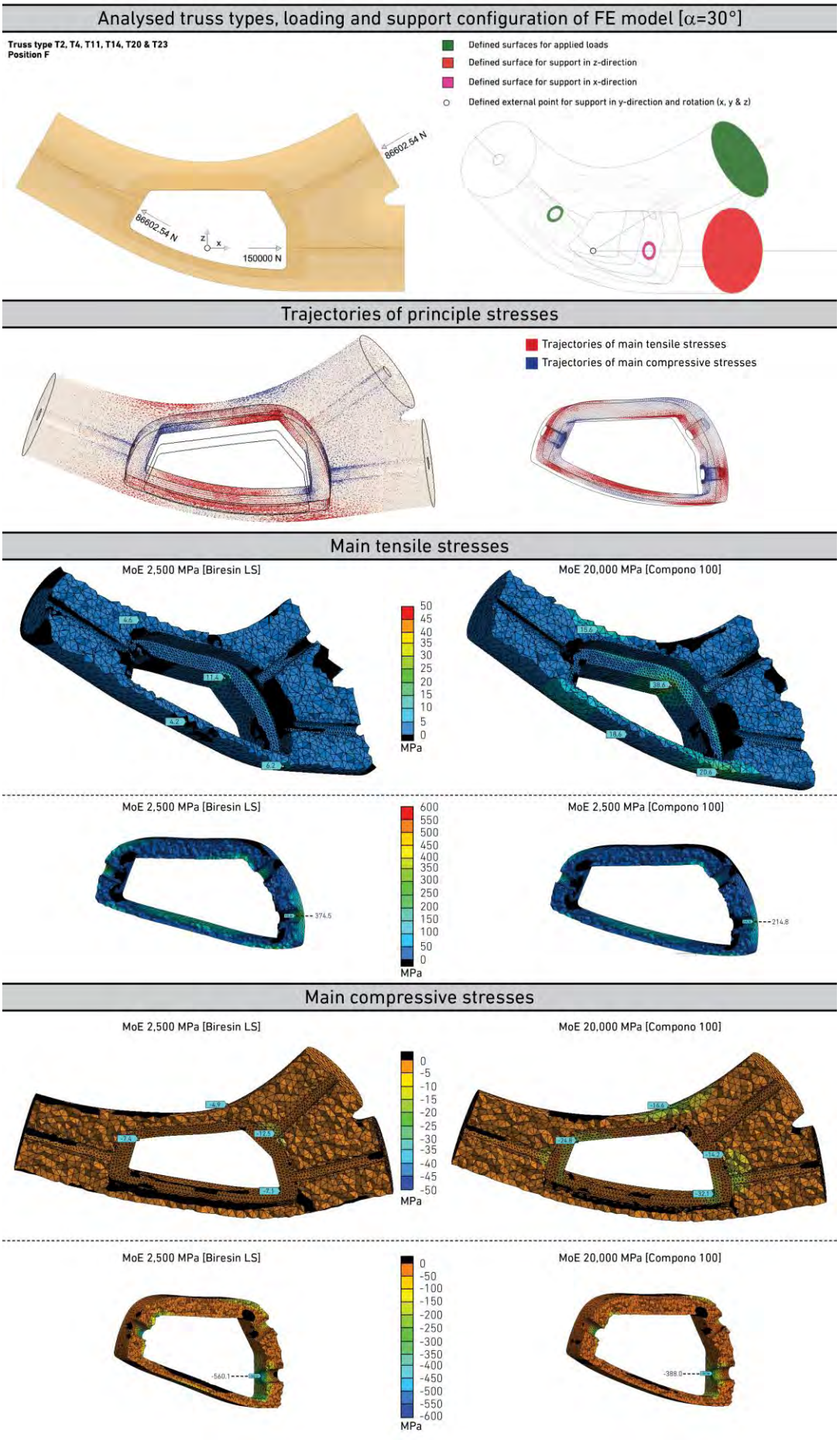

Fig. A-85 Edge joint analysis 30° - Sub-model F

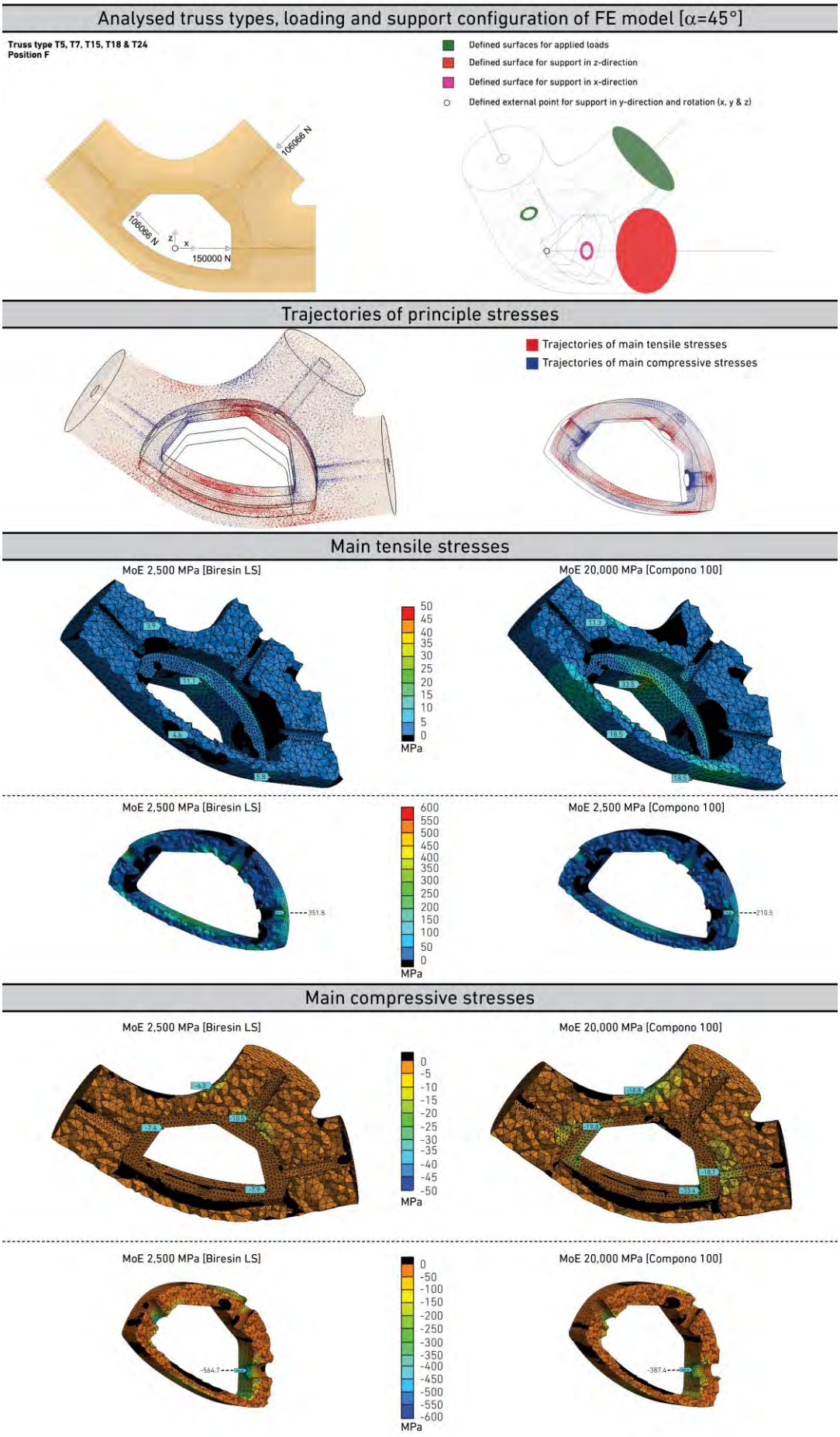

Fig. A-86 Edge joint analysis 45° - Sub-model F

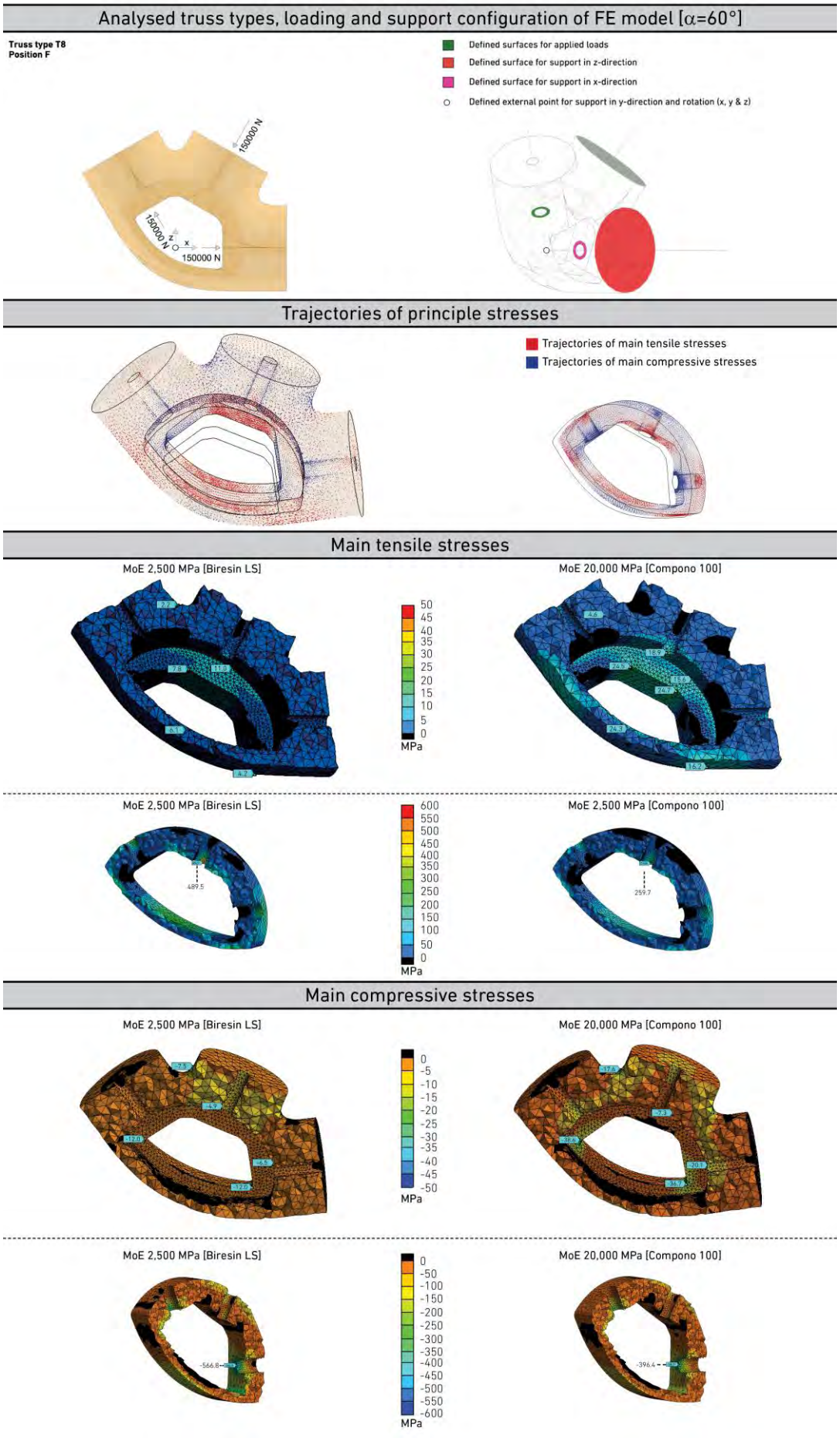

Fig. A-87 Edge joint analysis 60° - Sub-model F

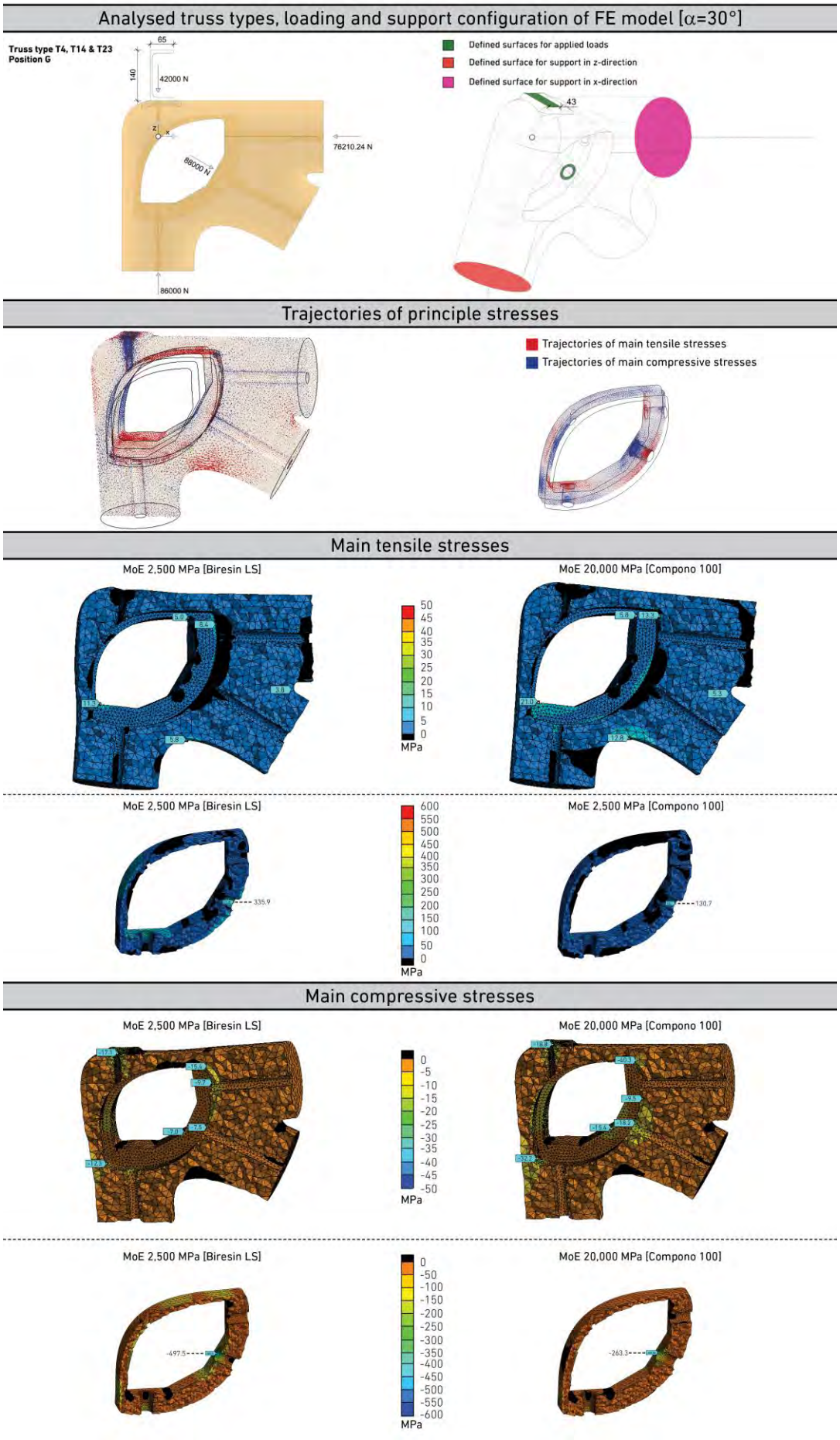

Fig. A-88 Support joint analysis 30° - Sub-model G

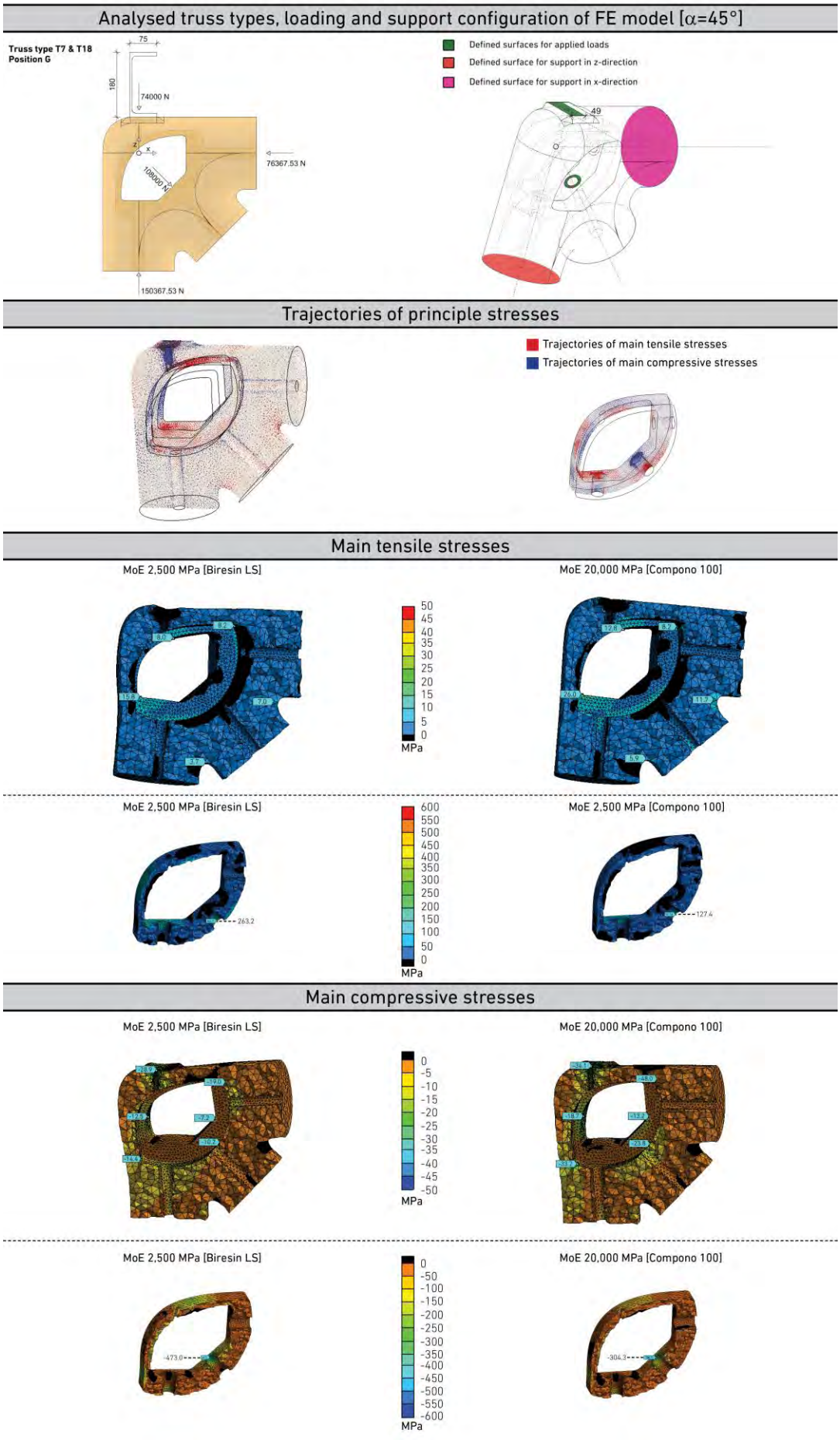

Fig. A-89 Support joint analysis 45° - Sub-model G

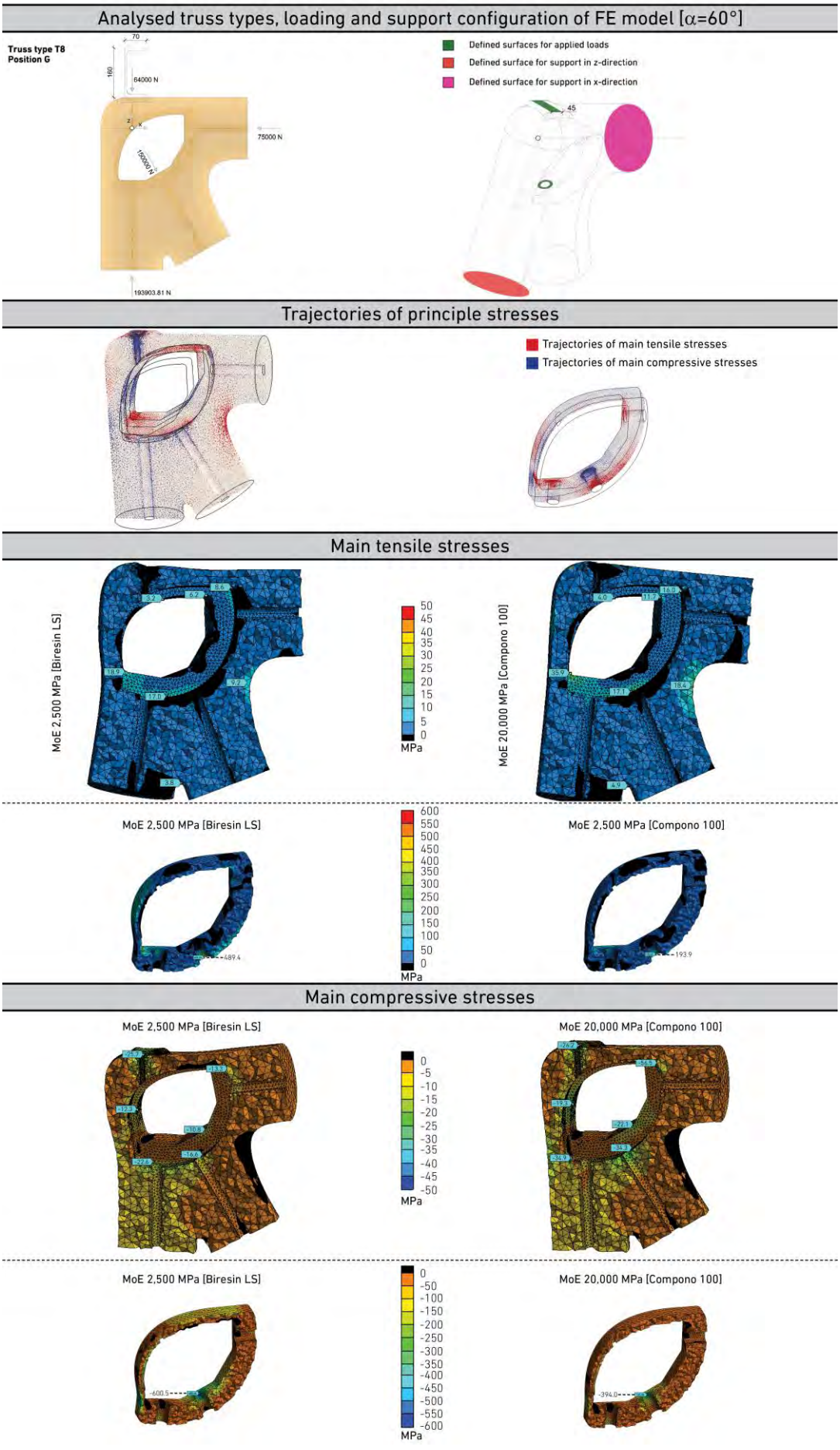

Fig. A-90 Support joint analysis 60° - Sub-model G